CANADA – UNITED STATES
Transboundary PM Science Assessment

The report was undertaken by the Canada-U.S.
Subcommittee on Scientific Co-operation, in support of the
Canada-U.S. Air Quality Agreement

This report is available electronically at:
http://www.msc-smc.ec.gc.ca/saib
http://www.epa.gov/airmarkt/usca/index.html

Additional hard copies may be obtained from:

Science Assessment and Integration Branch
Atmospheric and Climate Science Directorate
Meteorological Service of Canada
4905 Dufferin Street
Toronto, Ontario CANADA M3H 5T4
(416) 739-4433

© Minister, Public Works and Government Services, 2004
ISBN: 0-662-38678-7
Catalogue No. En56-203/2004E

CANADA – UNITED STATES
TRANSBOUNDARY PARTICULATE MATTER
SCIENCE ASSESSMENT

A REPORT BY THE
CANADA-U.S. AIR QUALITY COMMITTEE
SUBCOMMITTEE 2: SCIENTIFIC COOPERATION

DECEMBER 2004

ACKNOWLEDGMENTS

The following individuals have contributed to the preparation of this report:

CANADA	UNITED STATES OF AMERICA
Keith Puckett, Co-chair of SC2	William Russo, Co-chair of SC2
Heather Morrison, Secretariat of SC2	Laurel Schultz, USEPA
Carrie Lillyman, Environment Canada	Fred Dimmick, USEPA
Bob Vet, Environment Canada	Tom Braverman, USEPA
Jeff Brook, Environment Canada	Joe Tikvart, USEPA
Chul-Un Ro, Environment Canada	Bill Kuykendal, USEPA
Louis-Philippe Crevier, Environment Canada	Neil Frank, USEPA
Sophie Cousineau, Environment Canada	Rich Poirot, VTDEC
Mike Moran, Environment Canada	Nash Gerald, USEPA
Paul Makar, Environment Canada	John Bachmann, USEPA
Véronique Bouchet, Environment Canada	Donna Kenski, Lake Michigan Air Directors Consortium
David Niemi, Environment Canada	Rob Wilson, USEPA
Marc Deslauriers, Environment Canada	Alan Rush, USEPA
Tom Dann, Environment Canada	Mark Schmidt, USEPA
Julie Dion, Environment Canada	Jeff West, USEPA
David Waugh, Environment Canada	
Colin di Cenzo, Environment Canada	
Ann McMillan, Environment Canada	
Harry Hirvonen, Canadian Forest Service	

In March, 2003, this report underwent an external scientific peer review. The following individuals reviewed the report:

DR. PRAVEEN AMAR
Director, Science and Policy
NESCAUM, Boston, USA.

DR. WEIMIN JIANG
Research Officer, National Research Council of Canada
Ottawa, Canada

DR. JACK McCONNELL
Professor, Department of Earth and Space Science and Engineering
York University, Toronto, Canada

DR. ARMISTEAD RUSSELL
Professor, Environmental Engineering
Georgia Institute of Technology, Atlanta, USA.

DR. BRET SCHICHTEL
National Park Service, Air Resource Division
Denver, USA.

TABLE OF CONTENTS

Summary xv

1. Introduction 1

2. Foundation for the Transboundary PM Issue in North America 3
- 2.1. PM is recognized as an important health concern 3
- 2.2. High ambient levels of PM and its precursors are observed in North America 4
- 2.3. Precursors of PM generally contribute to the acidification of ecosystems 4
- 2.4. PM and its precursors are a significant cause of visibility impairment 5
- 2.5. PM and its precursors can be transported long distances 6
- 2.6. PM and its precursors are transported between the United States and Canada 6
- 2.7. Reductions in SO_2 are likely to result in reductions in $PM_{2.5}$, visibility impairment and acid deposition 7

3. Ambient Observations in Border Regions 9
- 3.1. Levels of and Trends in $PM_{2.5}$ 9
  - 3.1.1. Integrated Observations between Canada and the United States 9
  - 3.1.2. Canada 13
  - 3.1.3. United States 14
    - 3.1.3.1. Spatial Variations in Annual Average $PM_{2.5}$ Concentrations across the United States 14
    - 3.1.3.2. Annual Means of $PM_{2.5}$ at U.S. FRM Sites by Region 15
    - 3.1.3.3. Annual Means of $PM_{2.5}$ at U.S. FRM Sites within 300 km of Border by Region 15
    - 3.1.3.4. Annual Means of $PM_{2.5}$ at U.S. IMPROVE Sites by Region 16
    - 3.1.3.5. Three year Annual Means and 98th Percentiles (2000-2002) of $PM_{2.5}$ for U.S. Sites (FRM & IMPROVE) within 200 km of the Canadian Border 16
    - 3.1.3.6. Long-term Trends in $PM_{2.5}$ 17
- 3.2. Ambient Characterization of $PM_{2.5}$ 18
  - 3.2.1. Canada 18
    - 3.2.1.1. Chemical Composition of the Organic Fraction of $PM_{2.5}$ 19
  - 3.2.2. United States 20
- 3.3. Levels of Sulphate and Nitrate Deposition 23
  - 3.3.1. Wet Sulphate Deposition and Critical Load Exceedances 23
  - 3.3.2. Wet Nitrate Deposition 24
- 3.4 Key Science Messages 25

4. Emissions 27
- 4.1. Development of Emission Inventories 27
  - 4.1.1. Development of Canadian and U.S. Emission Inventories for REMSAD and AURAMS 27
    - 4.1.1.1. Base Year Inventories 27
    - 4.1.1.2. Base Case Inventories for 2010 and 2020 27
    - 4.1.1.3. Control Case Inventories for 2010 and 2020 28
  - 4.1.2. Processing of Canadian and U.S. Emission Inventories for REMSAD and AURAMS 29
    - 4.1.2.1. Processing of Emission Inventories for REMSAD 29
    - 4.1.2.2. Processing of Emission Inventories for AURAMS 29
  - 4.1.3. Development and Processing of Emission Inventories used for CMAQ 30

4.2. Description of Emissions in the United States and Canada 30
4.2.1. Emissions used in AURAMS and REMSAD 30
4.3 Key Science Messages 40

5. Air Quality Model Applications 41
5.1. Results of REMSAD Control Strategy Modelling 41
5.1.1. REMSAD Results 42
5.1.2. Conclusions 57
5.2. Results of AURAMS Control Strategy Modelling 57
5.2.1. Model Set-up, Emission Files and Post-Processing 58
5.2.2. Evaluation of Emission Reduction Impacts 59
5.2.2.1. Winter Period 59
5.2.2.2. Summer Period 65
5.2.3. Comparison with REMSAD results 66
5.2.4. Summary and Conclusions 71
5.3. Results of CMAQ Modelling in the Georgia Basin – Puget Sound Region 72
5.3.1. Qualitative Analysis of Simulations for the 2000 Base Case 73
5.3.1.1. Summer $PM_{2.5}$ 73
5.3.1.2. Winter $PM_{2.5}$ 73
5.3.2. Significance of Transboundary Transport 74
5.3.2.1. Qualitative Analysis of the No-U.S. Anthropogenic Emissions Scenarios 74
5.3.2.2. Qualitative Analysis of the No-Canadian Anthropogenic Emissions Scenarios 74
5.3.2.3. Summary and Conclusions 75
5.3.3. Impacts of Forecast Emissions for 2010 and 2020 75
5.3.3.1. Qualitative Analysis of Simulations for the 2010 Forecast 75
5.3.3.2. Qualitative Analysis of Simulations for the 2020 Forecast 76
5.3.3.3. Summary and Conclusions 76
5.4 Co-benefits of Emission Reductions 76
5.5 Key Science Messages 79

6. Relationships between Sources and Ambient Levels of PM 81
6.1. Attributing Sources to Ambient Levels of $PM_{2.5}$ 81
6.1.1. Observational Receptor-Oriented Analyses 81
6.1.1.1. Quantifying the Transboundary Transport of $PM_{2.5}$ using a Geographic Information System 81
6.1.1.2. Sources of $PM_{2.5}$ to Urban Areas in the United States 83
6.1.1.3. Sources of $PM_{2.5}$ to Eastern North America 84
6.1.1.4. Back Trajectory Analysis of $PM_{2.5}$ Transport to Eastern Canada 84
6.1.1.5. Sources of PM to Glacier National Park, Montana 85
6.1.1.6. Sources of PM and Acid Rain Precursors to Southwestern Ontario: Study 1 85
6.1.1.7. Sources of PM and Acid Rain Precursors to Southwestern Ontario: Study 2 89
6.1.1.8. Sources of $PM_{2.5}$ to Southern Quebec 89
6.1.1.9. Sources of $PM_{2.5}$ to Nova Scotia and New Brunswick 89
6.1.2. Positive Matrix Factorization 91
6.1.2.1. Sources of PM to Toronto, Ontario and Vancouver, British Columbia 91
6.1.2.2. Comparability of Receptor Model Results on $PM_{2.5}$ Sources in Toronto 92
6.1.2.3. PMF and Back Trajectory Analysis at Eight U.S. Cities 96
6.1.2.4. Compilation of $PM_{2.5}$ Source Apportionment Studies from the United States 97
6.1.2.5. Source Locations and Time Series Analyses of PM in U.S. Cities 98
6.1.3. Satellite Observations 99
6.1.3.1. Impact of PM from Forest Fires to Eastern North America 99
6.2 Key Science Messages 99

7. Conclusions 101

8. References 105

Appendix: REMSAD and AURAMS Model Performance 111

LIST OF TABLES

Table 2.1: Ambient Air Quality Objectives and Standards for $PM_{2.5}$ 4
Table 4.1: Country-total anthropogenic emissions for PM and PM precursors on the REMSAD domain for the 2010 base, 2010 control, 2020 base, and 2020 control inventory scenarios used as REMSAD input. 31
Table 4.2: Country-total anthropogenic emissions for PM and PM precursors on the AURAMS domain for the 1996, 2010 base, 2010 control, 2020 base, and 2020 control inventory scenarios used as AURAMS input. 31
Table 5.1: Characteristics of ten AURAMS simulations. 59
Table 5.2: Percent differences between scenario emissions of primary $PM_{2.5}$ and PM precursors on the AURAMS domain for three pairs of scenarios. 59
Table 6.1: Average concentration and percent mass selected State contributions to Class I areas. 83
Table 6.2: Proportions (percent) of $PM_{2.5}$ mass with respect to 3-day back-trajectory at 950hPa (1999-2002). 89

LIST OF FIGURES

Figure 2.1: Average $PM_{2.5}$ concentrations 5
Figure 2.2: 3-day back-trajectories arriving at Simcoe, Ontario, for the warm season (May–September), 1998 and 1999 6
Figure 3.1: Mean annual concentration of $PM_{2.5}$ at Canadian dichot and U.S. FRM monitors in the border region for the data years 2000-2003 9
Figure 3.2: 98th percentile $PM_{2.5}$ concentrations at Canadian TEOM and U.S. FRM sites for the data years 2000-2002 10
Figure 3.3: Long-term trends in the precursor gases SO_2 and particulate $SO_4^=$ at rural CAPMoN and CASTNet sites, 1989–2002 11
Figure 3.4: Trends in total nitrate (gaseous HNO_3 and particulate NO_3^-) and particulate NH_4^+ at rural CAPMoN and CASTNet sites, 1989–2002 12
Figure 3.5: Trend in annual median $PM_{2.5}$, 1984–2002 (median, 75th, 25th percentile) 13
Figure 3.6: Three year mean, 10th and 98th percentile $PM_{2.5}$ concentrations, 1997–1999 13
Figure 3.7: The 98th percentile of Canadian 24-hour $PM_{2.5}$ concentrations in 2001 14
Figure 3.8: U.S. regions used for data analysis purposes 14
Figure 3.9: County-level maximum annual mean $PM_{2.5}$ concentrations, averaged over three years, 2000-2002 15
Figure 3.10: Annual $PM_{2.5}$ means at U.S. FRM sites by region, over three years, 2000-2002 15
Figure 3.11: Annual means of $PM_{2.5}$ at U.S. FRM sites within 300 km of the Canadian border by region, over three years, 2000-2002 16
Figure 3.12: Annual $PM_{2.5}$ means at rural U.S. IMPROVE sites by region 16
Figure 3.13: 3-year annual means and 98th percentiles (2000-2002) for U.S. sites within 200 km of the border (FRM) 17
Figure 3.14: Average measured annual $PM_{2.5}$ concentration trend at IMPROVE sites, 1992-2001 17
Figure 3.15: The fractional chemical composition of $PM_{2.5}$ at various urban sites based on 1995-98 NAPS dichot data 18
Figure 3.16: $PM_{2.5}$ speciation data for NAPS network sites in Canada September 2001-August 2002 19
Figure 3.17: The relative composition of $PM_{2.5}$ mass at Egbert (ON) during (a) a wintertime $PM_{2.5}$ episode December 30, 1995, and (b) a summertime episode June 11, 1999 20
Figure 3.18: Annual average composition of $PM_{2.5}$ in the United States by region 21
Figure 3.19: Summary of urban speciation data for $PM_{2.5}$ in the United States (EPA Speciation Network) 22
Figure 3.20: Summary of rural speciation data (IMPROVE network) 22
Figure 3.21: Seasonal variation in PM species for selected urban areas in the United States 23
Figure 3.22: Spatial distribution of wet $SO_4^=$ deposition (kg/ha/yr) in eastern North America, 1996-2001 24
Figure 3.23: Five-year (1996-2000) mean wet deposition exceedance of critical $SO_4^=$ loads (kg $SO_4^=$ /ha/yr) for 95% lake protection level 24
Figure 3.24: Spatial distribution of wet NO_3^- deposition (kg/ha/yr) in eastern North America, 1996-2001 25
Figure 4.1a: 1996 Summer weekday SO_2 emissions for Canada and the United States 32
Figure 4.1b: 2010 Summer weekday base case SO_2 emissions for Canada and the United States 33
Figure 4.1c: 2010 Summer weekday reductions in SO_2 emissions for Canada and the United States 33
Figure 4.2a: 2020 Summer weekday base case SO_2 emissions for Canada and the United States 34
Figure 4.2b: 2020 Summer weekday reductions in SO_2 emissions for Canada and the United States 34
Figure 4.3a: 1996 Winter weekday NO_x emissions for Canada and the United States 35
Figure 4.3b: 2010 Winter weekday base case NO_x emissions for Canada and the United States 35

Figure 4.3c: 2010 Winter weekday reductions in NO_x emissions for Canada and the United States. 36
Figure 4.4a: 2020 Winter weekday base case NO_x emissions for Canada and the United States. 36
Figure 4.4b: 2020 Winter weekday reductions in NO_x emissions for Canada and the United States. 37
Figure 4.5a: 1996 Summer weekday NH_3 emissions for Canada and the United States. 37
Figure 4.5b: 1996 Winter weekday NH_3 emissions for Canada and the United States. 38
Figure 4.6a: 2010 Summer weekday base case NH_3 emissions for Canada and the United States. 38
Figure 4.6b: 2010 Winter weekday base case NH_3 emissions for Canada and the United States. 39
Figure 4.7a: 2020 Summer weekday base case NH_3 emissions for Canada and the United States. 39
Figure 4.7b: 2020 Winter weekday base case NH_3 emissions for Canada and the United States. 40
Figure 5.1: REMSAD modelling domain (~36x36 km^2). 42
Figure 5.2a: Annual average $PM_{2.5}$ concentrations 2010 base case. 44
Figure 5.2b: Reductions in annual $PM_{2.5}$ concentrations from controls in 2010. 44
Figure 5.3a: Annual average $PM_{2.5}$ concentrations 2020 base case. 45
Figure 5.3b: Reductions in annual $PM_{2.5}$ concentrations from controls in 2020. 45
Figure 5.4a: January average $PM_{2.5}$ concentrations 2020 base case. 46
Figure 5.4b: Reductions in January $PM_{2.5}$ concentrations from controls in 2020. 46
Figure 5.5a: July average $PM_{2.5}$ concentrations 2020 base case. 47
Figure 5.5b: Reductions in July $PM_{2.5}$ concentrations from controls in 2020. 47
Figure 5.6a: Annual average $SO_4^=$ concentrations 2020 base case. 48
Figure 5.6b: Reductions in annual $SO_4^=$ concentrations from controls in 2020. 48
Figure 5.7a: January average $SO_4^=$ concentrations 2020 base case. 49
Figure 5.7b: Reductions in January $SO_4^=$ concentrations from controls in 2020. 49
Figure 5.8a: July average $SO_4^=$ concentrations 2020 base case. 50
Figure 5.8b: Reductions in July $SO_4^=$ concentrations from controls in 2020. 50
Figure 5.9a: Annual average NO_3^- concentrations 2020 base case. 51
Figure 5.9b: Reductions in annual NO_3^- concentrations from controls in 2020. 51
Figure 5.10a: January average NO_3^- concentrations 2020 base case. 52
Figure 5.10b: Reductions in January NO_3^- concentrations from controls in 2020. 52
Figure 5.11a: July average NO_3^- concentrations 2020 base case. 53
Figure 5.11b: Reductions in July NO_3^- concentrations from controls in 2020. 53
Figure 5.12a: Annual average NH_4^+ concentrations 2020 base case. 54
Figure 5.12b: Reductions in annual NH_4^+ concentrations from controls in 2020. 54
Figure 5.13a: January average NH_4^+ concentrations 2020 base case. 55
Figure 5.13b: Reductions in January NH_4^+ concentrations from controls in 2020. 55
Figure 5.14a: January average NH_4^+ concentrations 2020 base case. 56
Figure 5.14b: Reductions in January NH_4^+ concentrations from controls in 2020. 56
Figure 5.15: AURAMS domain for all simulations (85x105 grid points, Δx=42 km). 58
Figure 5.16: Nine-day-average $PM_{2.5}$ mass concentration field and $PM_{2.5}$ inorganic chemical component concentration fields predicted by AURAMS for the Feb. 7-15, 1998 winter period for the "2010 base" case emissions. 61
Figure 5.17: Nine-day-average $PM_{2.5}$ mass concentration difference field and $PM_{2.5}$ inorganic chemical component concentration difference fields predicted by AURAMS for the Feb. 7-15, 1998 winter period for the "2010 control" case minus the "2010 base" case. 62

Figure 5.18: Same as Figure 5.16 but for the "2020 base" case emissions 63
Figure 5.19: Same as Figure 5.17 but for the "2020 control" case minus the "2020 base" case 64
Figure 5.20: Eleven-day-average $PM_{2.5}$ mass concentration field and $PM_{2.5}$ inorganic chemical component concentration fields predicted by AURAMS for the July 8-18, 1995 summer period for the "2010 base" case emissions 67
Figure 5.21: Eleven-day-average $PM_{2.5}$ mass concentration difference field and $PM_{2.5}$ inorganic chemical component concentration difference fields predicted by AURAMS for the July 8-18, 1995 summer period for the "2010 control" case minus the "2010 base" case 68
Figure 5.22: Same as Figure 5.20 but for the "2020 base" case emissions 69
Figure 5.23: Same as Figure 5.21 but for the "2020 control" case minus the "2020 base" case 70
Figure 5.24: Geographical references and domain extents for the CMAQ model 72
Figure 5.25: $PM_{2.5}$ concentrations for the August, 2001 summer base case, predicted over the CMAQ domain on a 4x4 km^2 grid 73
Figure 5.26: Peak ozone concentration difference field at 15 m height for the July 12-15, 1995 summer period for the "2020 control" case minus the "2020 base" case 77
Figure 5.27: Annual reduction in $SO_4^=$ wet deposition from additional U.S. and Canadian controls (2020 control vs. base) 77
Figure 5.28: Annual reduction in NO_3^- wet deposition from additional U.S. and Canadian controls (2020 control vs. base) 78
Figure 5.29: Aerosol light extinction (in Mm^{-1}) for the haziest 20 percent days and contribution by individual particulate matter constituents, based on1997-1999 IMPROVE data 78
Figure 6.1: Average concentrations of $PM_{2.5}$ and components ($\mu g/m^3$) by state and province 82
Figure 6.2: Urban Excess Analysis for $SO_4^=$, NH_4^+, NO_3^-, TCM and crustal material for 13 urban areas in the United States 84
Figure 6.3: Combined QTBA plot derived using 2000 and 2001 TEOM $PM_{2.5}$ measurements for the warm months (May-September) 85
Figure 6.4: Sectors used to categorize 3-day back-trajectories of air masses at Longwoods, Ontario 86
Figure 6.5: Long-term trends and median concentrations of SO_2, particle $SO_4^=$ and particle NO_3^- in air at Longwoods, Ontario associated with three-day back trajectories from Canada, the United States and "Not Attributable" (N/A) to either sector 87
Figure 6.6: Long-term trends and median concentrations of pH, $SO_4^=$ and NO_3^- in precipitation at Longwoods, Ontario associated with 72-hour back trajectories from Canada, the United States and "Not Attributable" (N/A) to either sector 88
Figure 6.7: The geometric mean concentration of SO_2, $SO_4^=$ and TNO_3^- measured in air at Longwoods, ON (1983-2000) for the particular subset of air mass trajectories that passed through that grid square 90
Figure 6.8: $PM_{2.5}$ top and bottom quartile back-trajectory climatology events (based on 1999-2001 data) 91
Figure 6.9: Percent contribution, by component, to $PM_{2.5}$ mass observed in a) Toronto and b) Vancouver as determined using PMF-MLR 92
Figure 6.10: Annual average modelled $PM_{2.5}$ contributions in Toronto, (February 2000 – February 2001) using UNMIX (a) and PMF (b) receptor modelling techniques 93
Figure 6.11: Average day of week variations in UNMIX motor vehicle sources 93
Figure 6.12: Seasonal variations in Toronto PMF & UNMIX source contributions 93
Figure 6.13: UNMIX motor vehicle and coal-related sources vs. local surface wind speed and direction 94

Figure 6.14: Incremental probability fields for coal-related sources at Toronto and other eastern sites. 94

Figure 6.15: Incremental probability fields and day-of-week patterns in Toronto NH_4NO_3 "sources." 95

Figure 6.16: Summary of major Toronto source regions and influences on daily $PM_{2.5}$ mass concentrations. 95

Figure 6.17: Sulphate source region plot for Source 1, $(NH_4)_2SO_4$, at Milwaukee, WI. 96

Figure 6.18: Pie charts of the source apportionment results for various locations in the United States. 97

Figure 6.19: The composites of MODIS-derived aerosol optical depth and cloud optical depth superimposed over continuous $PM_{2.5}$ monitors for July 6th and 7th, 2002. 98

SUMMARY

The Canada-U.S. Air Quality Agreement was established to provide "a practical and effective instrument to address shared concerns regarding transboundary air pollution". Initially, the *Agreement* was intended to address the primary pollutants responsible for acid rain. However, the *Agreement* also confirmed the commitment of the United States and Canada to consult on, and develop, the means to address other transboundary air pollution issues, including particulate matter.

The Subcommittee on Scientific Cooperation, of the Air Quality Committee, was charged to summarize and understand the current knowledge of the transboundary transport of PM and PM precursors between Canada and the United States in a scientific Assessment. The seven key objectives can be summarized as:

Objective 1: To identify whether or not there is a fine PM problem in the border region;

Objective 2: To identify the extent of the problem;

Objective 3: To describe the PM issue in terms of geographic regions;

Objective 4: To identify PM precursors of concern on a regional or sub-regional basis;

Objective 5: To describe sources (or source regions) of PM and PM precursors;

Objective 6: To describe the characteristics of the emissions of PM and PM precursors; and

Objective 7: To identify the impact of emission reduction scenarios on PM levels.

The Assessment represents a significant co-operative effort between scientists in Canada and the United States, and in several cases, the information provided is the first presentation of joint scientific results. The report contains findings on ambient levels, data analyses, and the application of modelling tools in both Canada and the United States. This Assessment will provide the initial scientific knowledge required to determine the need for a PM annex pursuant to the Air Quality Agreement.

KEY FINDINGS

THE TRANSBOUNDARY TRANSPORT OF PM CAN CONTRIBUTE TO ABOVE AVERAGE PM LEVELS IN BOTH CANADA AND THE U.S.

- Current ambient levels of $PM_{2.5}$ in the border regions exceed the standards set for $PM_{2.5}$ in several regions of both Canada and the United States. In the United States, these sites are primarily in urban areas. The eastern portion of the border domain (i.e., northeastern United States, Industrial Midwest, and the Windsor-Quebec City corridor) exhibits levels that exceed the 15 $\mu g/m^3$ annual standard in the United States and the 30 $\mu g/m^3$ 98th percentile three-year average Canadian standard for the time periods evaluated.
- $PM_{2.5}$ is transported across the border region between Canada and the United States, leading to elevated concentrations of $PM_{2.5}$ in both countries. Most of the analyses point to sulphur dioxide as a primarily regional contributor and nitrogen oxides as both a local and regional contributor to $PM_{2.5}$, while

organic/black carbon and other PM constituents tend to be more local in nature.

- Canadian provinces have been found to contribute to $PM_{2.5}$ measured at several Class I areas in the United States, while the transport of $PM_{2.5}$ and PM precursors across the border region leads to 'above average' $PM_{2.5}$ concentrations in eastern Canada.
- In the Georgia Basin - Puget Sound region, impacts from transboundary transport occur along the border (within ± 50 km) with some frequency; however, the incidence of long-range/regional transport (over 100 km) was low.

PM LEVELS VARY SIGNIFICANTLY OVER GEOGRAPHIC REGIONS

- Elevated concentrations of $PM_{2.5}$ are found more often in the following regions: northeastern United States, Industrial Midwest, southwestern Ontario and the northwestern United States. Most areas of both Canada and the United States are subject to elevated concentrations during episodic conditions.
- Urban concentrations of $PM_{2.5}$ are higher than rural concentrations in all regions of both Canada and the United States; however, rural sites can exhibit very high $PM_{2.5}$ levels during large-scale PM episodes.
- The highest particle sulphate and nitrate concentrations are found in areas with high sulphur dioxide and nitrogen oxide emissions. Such areas include the northeastern United States and southwestern Ontario.

THERE ARE MANY SOURCES OF PM AND PM PRECURSORS

- Local motor vehicle sources (and small nearby smelter or industrial sources) have a relatively constant influence on $PM_{2.5}$ concentrations in Toronto, and are most evident on the cleanest days (which also tend to occur with northerly wind flows). Coal-related sources have a substantial transboundary contribution from the United States, and are particularly important on days of high $PM_{2.5}$ concentration.
- A region of high density emissions from coal fired utilities exists in the northeastern United States, which influences $PM_{2.5}$ concentrations. A similar analysis for ammonium nitrate indicates a more widespread source region, in the northeastern United States as well as the north-central United States, a region of high agricultural ammonia emissions.
- Components and contributing sources to $PM_{2.5}$ identified in both Vancouver and Toronto include secondary nitrate, regional transport of coal combustion products, diesel motor vehicles, secondary organic acids and road dust.
- Natural sources of PM (i.e., forest fires and biogenic sources) can also influence ambient air quality. Satellite observations confirm the impact of Canadian forest fire events on U.S. aerosol optical depth.

EMISSION REDUCTION SCENARIOS FOR PM AND PM PRECURSORS WERE EVALUATED USING AIR QUALITY MODELS

- Emissions of sulphur dioxide and nitrogen oxides are projected to decrease while emissions of ammonia, volatile organic compounds and carbon monoxide are projected to increase between base case and control case scenarios. Sulphur dioxide, nitrogen oxides and ammonia emissions, and their contributions to $PM_{2.5}$ levels vary seasonally.
- Emissions of sulphur dioxide and nitrogen oxides under all considered scenarios are concentrated in the Industrial Midwest, northeastern United States and southern Ontario, while emissions of ammonia are concentrated further west in the central Midwest region.

- U.S. and Canadian controls that are expected to be implemented result in maximum annual reductions of $PM_{2.5}$ of 1.8 μg/m^3 in 2010 and 2.3 μg/m^3 in 2020. The reductions vary temporally and spatially.
- Proposed additional sulphur dioxide and nitrogen oxide emission reductions should provide additional reductions in ambient $PM_{2.5}$ levels in eastern North America. The observed $PM_{2.5}$ reductions may vary by season and depend strongly on reductions in particle sulphate mass.
- Simultaneous reductions in both sulphur dioxide and nitrogen oxides may also provide concurrent reductions in particle ammonium, due to the reduction of gaseous sulphur dioxide and nitrogen oxides available to react with gaseous ammonia.
- Reductions in sulphur dioxide emissions that are not accompanied by adequate nitrogen oxide emissions may result in nitrate increases in some areas. Reductions in nitrogen oxide emissions will correspond to decreases in particle nitrate mass in some parts of eastern North America but increases in other areas due to nitrate substitution (i.e. for sulphate reductions in ammonia-limited locations, the replacement of sulphate by nitrate in the particle phase). There is significance placed on the role of ammonia in this relationship, suggesting there may be value in investigating possible benefits due to gaseous ammonia emission reductions in conjunction with sulphur dioxide and nitrogen oxide emission reductions.

THERE ARE LINKAGES BETWEEN PM AND OTHER AIR QUALITY ISSUES

- Ambient levels of PM precursors also contribute to the wet deposition of nitrate and sulphate, and resulting ecosystem acidification. The highest levels of deposition are located in the northeastern United States and eastern Canada, particularly in the border regions.
- Co-benefits of emission reduction scenarios include reduced ground-level ozone levels, reductions in nitrate and sulphate deposition, and improved visibility.

CONCLUSION

The results of the Canada-United States Transboundary PM Assessment indicate that there is a significant relationship between the emissions of PM and PM precursors and elevated PM levels in both Canada and the United States. The transboundary transport of PM and PM precursors can be significant enough in some regions to potentially compromise the attainment of national standards. The information presented in this Assessment provides the scientific foundation to support the future development of joint strategies under a PM Annex pursuant to the *Agreement*.

CHAPTER 1

INTRODUCTION

On March 13, 1991, the President of the United States and the Prime Minister of Canada signed the Canada-U.S. Air Quality Agreement (hereafter referred to as the *Agreement*). The purpose of the *Agreement* was to establish "a practical and effective instrument to address shared concerns regarding transboundary air pollution". At the time of inception, the *Agreement* was intended to address the primary pollutants responsible for acid rain. However, the *Agreement* also confirmed the commitment of the United States and Canada to consult on, and develop, the means to address other transboundary air pollution issues.

In 1997, in response to shared concerns over the transboundary transport of ozone and fine particulate matter (PM), Canada and the United States signed a "Commitment to Develop a Joint Plan of Action for Addressing Transboundary Air Pollution." The commitment articulated the intent of the Parties to jointly address the shared problems of ground-level ozone and PM within the framework of the *Agreement*.

Stemming from this Commitment, the Parties signed a Joint Work Plan for Transboundary Fine Inhalable Particles in June 1998. The Joint Work Plan described the steps necessary to institute "comparable and harmonized analytical tools to enable the assessment of transboundary transport, trends and analysis regarding fine inhalable particles in the transboundary region". To facilitate this process, the Subcommittee on Scientific Cooperation, or Subcommittee 2 (SC2), of the Air Quality Committee held three bi-national workshops between 1999 and 2003. In addition to facilitating the institution of comparable and harmonized analytical tools, SC2 sought to understand the scientific information needs of the bi-national policy community, as articulated by the Subcommittee on Program Monitoring and Reporting, or Subcommittee 1 (SC1), and plan and deliver a scientific assessment of the transboundary transport of PM. During this process, Canada and the United States agreed to include acid rain and visibility endpoints in the Assessment where possible, in recognition of the fact that reductions in PM and ozone precursors can also affect acid rain and visibility.

As a cumulative result of the three bi-national workshops, and of discussions therein, seven key objectives were identified for the Transboundary PM Science Assessment:

Objective 1: To identify whether or not there is a fine PM problem in the border regions (ambient observations versus standards) with a focus on health, visibility and environmental endpoints;

Objective 2: To identify the extent of the problem (if standards are exceeded, by how much, where and when are they exceeded);

Objective 3: To describe the PM issue in terms of geographic regions (i.e. west, central, east);

Objective 4: To identify PM precursors of concern on a regional or sub-regional basis;

Objective 5: To describe sources (or source regions) of PM and PM precursors in the context of geographic regions (i.e., west, central, east);

Objective 6: To describe emissions of PM precursors, the spatial distribution of emissions and the transport characteristics of these emissions; and,

Objective 7: To identify the impact of current and proposed emission reduction scenarios on fine PM levels in North America.

The process undertaken for this Assessment includes an initial overview of the PM issue in North America, as determined primarily by the 2003 NARSTO PM Science Assessment. This background is then expanded by examining ambient observations and emission information, performing air quality model applications, and analyzing sources and their corresponding PM levels, specific to the transboundary region. Each of these steps concludes with a summary of the key science messages learned from the analyses; these key science messages are then applied in the conclusions in order to address the objectives listed above.

The Assessment is intended to synthesize the current state of knowledge on the transboundary transport of fine inhalable particles, in keeping with the information needs of the bi-national policy community. In fulfilling this purpose, this Assessment and its conclusions are consistent with the requirements of the 1998 Joint Work Plan for PM. The conclusions of this Assessment will provide the scientific support required to determine the need for a PM annex pursuant to the *Agreement*.

CHAPTER 2

FOUNDATION FOR THE TRANSBOUNDARY PM ISSUE IN NORTH AMERICA[1]

Seven key features of the PM issue have provided the impetus for this Transboundary PM Science Assessment. These key features are listed below and explored in greater detail in this chapter:

- PM is recognized as an important health concern.
- High ambient levels of PM and its precursors are observed in North America.
- Precursors of PM generally contribute to the acidification of ecosystems.
- PM and its precursors are a significant cause of visibility impairment.
- PM and its precursors can be transported long distances.
- PM and its precursors are transported between the United States and Canada.
- Reductions in SO_2 are likely to result in reductions in $PM_{2.5}$, acid deposition, and visibility impairment.

2.1 PM IS RECOGNIZED AS AN IMPORTANT HEALTH CONCERN

PM has been recognized as an important health concern in both the United States and Canada. Recent health studies in both countries indicate an association between adverse health outcomes, especially of the cardio-respiratory system, and short- and long-term exposures to ambient PM, particularly $PM_{2.5}$. In recognition of these health outcomes, both countries have committed to addressing the PM air-quality problem within their own territories (e.g., Canada-Wide Standard for $PM_{2.5}$, U.S. Clean Air Act). Furthermore, Canada and the United States have developed objectives and standards for ambient PM (Table 2.1).

---

[1] Unless cited as otherwise, the primary source of information for this chapter is the report by NARSTO entitled "Particulate Matter Science for Policy Makers: A NARSTO Assessment." In February 2003, NARSTO, a cooperative public-private sector organization of Canada, Mexico and the United States, produced this report. The assessment of PM science presents a concise and comprehensive discussion of the current understanding of airborne particulate matter among atmospheric scientists. The goal of the NARSTO assessment was to provide policy makers with relevant and needed scientific information and as such, the assessment focused on two primary objectives: the interpretation of complex and new atmospheric science so that it is useful for the management of PM, and, informing exposure and health scientists about the atmospheric science of PM. While meeting these primary objectives, the NARSTO assessment summarizes science relevant to the transboundary transport of PM between Canada and the United States.

Table 2.1 Ambient Air Quality Objectives and Standards for $PM_{2.5}$

	United States	**Canada**
Averaging Time	*National Ambient Air Quality Standards*	*Canada-Wide Standard*
Annual	15 µg/m³ based upon the 3-year average of the annual arithmetic mean concentration.	
24 hour	65 µg/m³ based upon the 3-year average of the 98th percentile of 24-hr average concentrations.	30 µg/m³ based upon the 98th percentile of a 24-hr average, measured over three consecutive years.
Visibility	Improve visibility on the haziest days and ensure no degradation on the clearest days, with the ultimate goal of reaching natural background conditions in 60 years.	

2.2 HIGH AMBIENT LEVELS OF PM AND ITS PRECURSORS ARE OBSERVED IN NORTH AMERICA

The highest annual-mean $PM_{2.5}$ concentrations are found in urban areas throughout North America, particularly in California, the southeastern United States, and the large urban centres of southeastern Canada (Figure 2.1).

$PM_{2.5}$ mass measurements typically exhibit concentration frequency distributions that are dominated by a large number of low values and a smaller number of high concentrations. Annual average $PM_{2.5}$ concentrations can vary by up to a factor of two across distances of 50 to 100 km in some large metropolitan regions. In California, the southeastern United States, the northeastern United States, and the Ohio River Valley-Great Lakes states, annual-mean $PM_{2.5}$ mass concentrations at about half of the urban sites exceeded the U.S. 3-year average annual-mean $PM_{2.5}$ mass standard of 15 µg/m³ in 1999 and 2000. In Canada, 24-hour average concentrations greater than 30 µg/m³ occur over most of southern Ontario and Quebec approximately 2 percent of the year.

Locally observed PM is composed of multiple chemical constituents, largely organic carbon (OC), sulphate ($SO_4^=$), black carbon (BC) and nitrate (NO_3^-) in combinations that differ by geographic region. PM composition is influenced by sources and seasonal meteorology, and has substantial regional contributions. Typically, $SO_4^=$ is a major fraction of $PM_{2.5}$ in eastern North America while NO_3^- is a major component in California. Nitrate concentrations across North America are greater in the winter compared to the summer, and urban concentrations are greater than rural concentrations in eastern North America.

2.3 PRECURSORS OF PM GENERALLY CONTRIBUTE TO THE ACIDIFICATION OF ECOSYSTEMS

Wet and dry deposition of $SO_4^=$ and NO_3^- contributes to the acidification of ecosystems. Although the most commonly used measures of

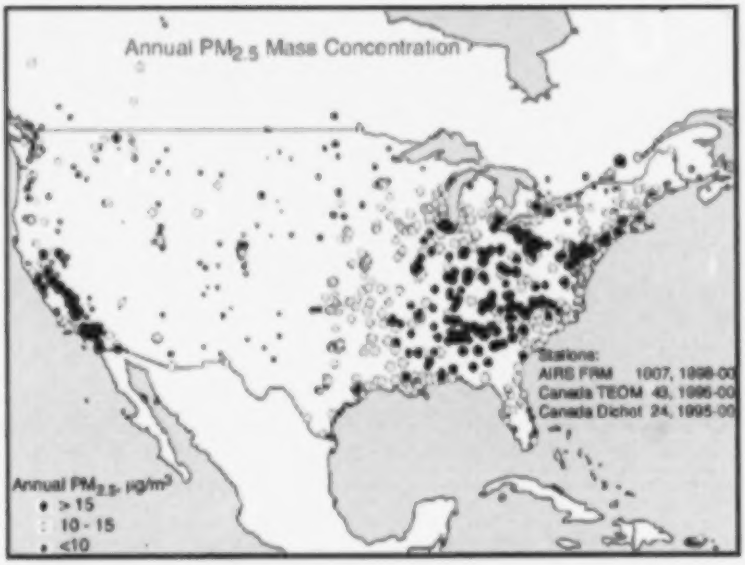

Figure 2.1 - Average $PM_{2.5}$ concentrations. The U.S. data are from FRM monitors at sites in the EPA AIRS database for July 1998 through July 2000. Canadian data are from TEOM and dichotomous samplers operating from 1995 through 2000. The currently available data from sites in Mexico represented less than one year of sampling and were excluded from the computation of annual averages. Spot diameter varies in proportion to concentration.

(Source: R. Husar, pers. comm.)

acid deposition focus on wet deposition of $SO_4^=$ and NO_3^-, research in south-central Ontario indicates that approximately 40% of the total deposition of sulphur and nitrogen occurs in the form of dry deposition (Sirois et al., 2001). These acidifying pollutants have been shown to damage terrestrial and aquatic ecosystems and susceptible materials at levels measured frequently in Canada and the northeastern United States.

The geographic region most affected by acid deposition is southeastern Canada and the northeastern United States; east of Manitoba and south of 52 degrees latitude. The relative contribution of the sources of acid deposition (local versus long-range) is area-dependent, however, the majority of acid deposition in southeastern Canada originates from long-range transport, as does a significant proportion of the deposition in the northeastern United States.

2.4 PM AND ITS PRECURSORS ARE A SIGNIFICANT CAUSE OF VISIBILITY IMPAIRMENT.

Optically, PM interferes with visibility by either absorbing or scattering visible light. Light scattering is roughly proportional to the mass concentration of fine particles, while light absorption is roughly proportional to the mass concentration of the light-absorbing species. The impairment of visibility that results from the absorption or scattering of light reduces the distance to which one can see and decreases the apparent contrast and colour of distant objects, causing a washed out or hazy appearance.

The light extinction effects of PM vary with particle size, chemical composition, and humidity. The particles with the greatest influence on visibility are fine particles of the same scale as the wavelengths of visible light (approximately 0.3 to 1 mm in diameter). These particles are generally composed of $SO_4^=$ and NO_3^- salts, OC, or BC.

2.5 PM AND ITS PRECURSORS CAN BE TRANSPORTED LONG DISTANCES.

PM can remain in the atmosphere for days to a few weeks, depending on the size and rate at which it is removed from the atmosphere (e.g., by precipitation). Particles in any given area may originate locally or from sources hundreds to thousands of kilometers away. Particles can also be formed during atmospheric transport from precursor gases originating from either local or long-range sources.

Both local and regional emissions underlie local ambient concentrations in many urban areas. Regional contributions from sources distant from eastern North American urban sites (including upwind urban areas) can account for 50 to 75 percent of the total observed $PM_{2.5}$ mass concentration within a specific urban area.

2.6 PM AND ITS PRECURSORS ARE TRANSPORTED BETWEEN THE UNITED STATES AND CANADA.

The NARSTO PM Assessment described two studies in Canada and the United States that demonstrate the transboundary transport of PM and its precursors.

Brook et al. (2002) traced 3-day back-trajectories of air masses arriving at Simcoe, ON during the warm season (May-September) of 1998 and 1999 (Figure 2.2). These back-trajectories were divided into categories based on the concentration of $PM_{2.5}$ measured at Simcoe and the directionality of the contributing air mass. This analysis resulted in three "source-receptor" categories: 1) "low" $PM_{2.5}$ (6 hour averages of 6.8 μg/m3) category, characterized by north-south airflows, 2) "high" (22.4 μg/m^3) $PM_{2.5}$ category, characterized by

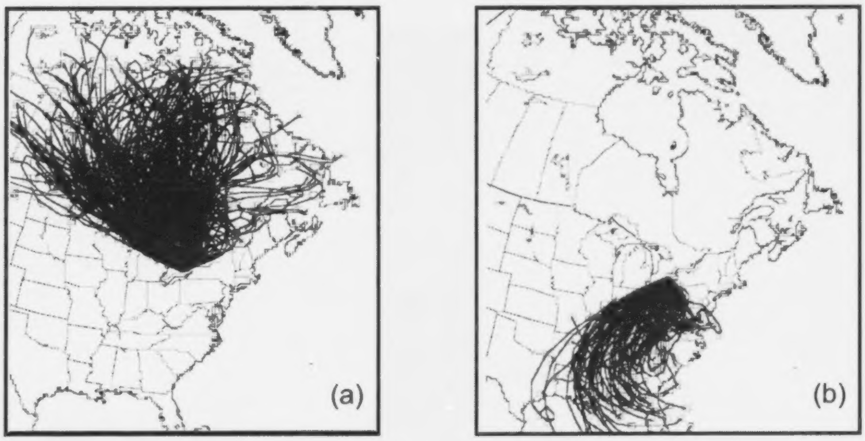

Figure 2.2 - 3-day back-trajectories arriving at Simcoe, Ontario, for the warm season (May–September), 1998 and 1999. (The sectors shown represent a) northerly flow over predominantly Canadian source regions and b) southerly flow over U.S source regions. Corresponding median $PM_{2.5}$ concentrations are a) Sector 1: 3.8 μg/m^3 and b) Sector 2: 20.3 μg/m^3).

south-north airflows, and 3) "unclassified high" (>30 µg/m^3) $PM_{2.5}$ category. Category three air masses were characterized by very short transport distances, indicating stagnant conditions in the Midwest and Great Lakes Region. Air mass trajectories associated with high levels of $PM_{2.5}$ frequently crossed the border between Canada and the United States.

During 1977-1978, a field study was conducted in eastern North America to assess the transport and fate of $SO_4^=$. The Sulphate Regional Experiment (SURE) found a correlation between air flow patterns and $SO_4^=$ aerosol concentrations. In general, regional PM episodes were characterized by the presence of a quasi-stationary high-pressure ridge oriented in an east-west direction across Virginia and North Carolina. Higher concentrations of $SO_4^=$ at locations in southern Ontario were linked to transport from the midwestern and southern United States.

2.7 REDUCTIONS IN SO_2 ARE LIKELY TO RESULT IN REDUCTIONS IN $PM_{2.5}$, VISIBILITY IMPAIRMENT AND ACID DEPOSITION.

PM, visibility impairment and acid deposition are related through common emissions and precursors, production pathways and meteorological processes. Consequently, the typical response of PM, visibility (by extension of the response of PM), and acid rain to reductions in SO_2 and other pollutants (i.e., NO_x) have been derived. These relationships indicate that a reduction in the emissions of SO_2 is likely to result in reductions in the $SO_4^=$ component of PM, total $PM_{2.5}$ mass, visibility impairment and acid deposition.

For example, in the last decade, there have been substantial reductions in emissions of SO_2 in North America. In southeastern Canada, these reductions have resulted in a general decline in $SO_4^=$ concentrations in precipitation but with a relatively smaller compensating increase in pH (often attributed to a parallel decline in base cation concentrations). Similarly, lakes in the affected regions of southeastern Canada generally exhibit declining $SO_4^=$ trends in response to emission reductions but, as yet, they are not exhibiting widespread increases in pH or alkalinity. The only exceptions to these observations are lakes located near smelters that have dramatically reduced emissions.

In the eastern United States, wet and dry sulphur deposition (and the acidity associated with sulphur deposition) has also declined with reductions of SO_2 emissions (Butler et al., 2001; Likens et al., 2001; Dutkiewicz et al., 2000; Lynch et al., 2000; Shannon, 1999). Strong correlations, near linear, between large scale SO_2 emission reductions and large reductions in $SO_4^=$ concentrations in precipitation have been noted for the northeastern United States, one of the areas most affected by acid deposition (Butler et al., 2003). Some of the greatest reductions in wet $SO_4^=$ deposition occurred in the Mid-Appalachian region, including Maryland, New York, West Virginia, Virginia, and most of Pennsylvania. Wet $SO_4^=$ deposition decreased more than 8 kilograms/hectare (kg/ha) from rates observed throughout the early 1990s in much of the Ohio River Valley and northeastern United States. Other less dramatic reductions were observed across much of New England, portions of the southern Appalachian Mountains and in the Midwest, most notably Indiana and Illinois. These reductions are primarily attributed to the reduction in $SO_4^=$ from emission sources located in the Ohio River Valley following implementation of Title IV of the 1990 Clean Air Act Amendments. Freshwater monitoring in eastern U.S. lakes and streams indicates measurable improvements in surface water chemistry (lower $SO_4^=$ concentrations and decreases in acidity) concomitant with reductions in $SO_4^=$ deposition (Stoddard et al., 2003).

In three of the five areas studied, one-quarter to one-third of lakes and streams previously affected by acid rain are no longer acidic, although they are still highly sensitive to future changes in deposition. In other areas, signs of recovery are not yet evident, suggesting that additional reductions will assist further ecosystem recovery. Increases in the Acid Neutralizing Capacity of surface waters, an indicator of aquatic ecosystem recovery, were evident in three of the regions (Adirondacks, Northern Appalachian Plateau and Upper Midwest) and was unchanged in New England and the Ridge/Blue Ridge region of the southeast U.S.

A review of the state of acid deposition science in Canada, completed in 1997, suggested that a 75 percent reduction in emissions of SO_2, beyond that agreed to in the 1991 Canada-U.S. Air Quality Agreement, is required to mitigate the effects of acid deposition on eastern Canadian ecosystems. Recent assessments of acid deposition science in the United States have concluded that further reductions of $SO_4^=$ deposition beyond levels achieved by the Title IV SO_2 emission reductions are necessary to protect aquatic ecosystems from further deterioration in the southeast and achieve ecosystem recovery in the northeast.

CHAPTER 3

AMBIENT OBSERVATIONS IN BORDER REGIONS

3.1 LEVELS OF AND TRENDS IN $PM_{2.5}$

3.1.1 Integrated Observations between Canada and the United States.

Levels of PM and PM precursors are monitored and reported across the United States and Canada. Monitoring techniques vary between the two countries, but wherever possible in this Assessment, efforts have been made to account for differences in techniques and combine monitoring results to provide a more comprehensive view of PM levels in the border regions. Figure 3.1 illustrates mean annual $PM_{2.5}$ concentrations at Canadian dichotomous (dichot) and U.S. Federal Reference Method (FRM) sites. Annual levels of $PM_{2.5}$ are as high as 18 µg/m³ in the northeastern United States, but are consistently lower than 12 µg/m³ in the mid-continental States. The bi-national map in Figure 3.1 shows few monitoring sites north of the Canada-U.S. border due to differences in sampling frequency between the two countries.

When Canadian hourly TEOM observations are included in the database, a more detailed picture of ambient levels can be achieved. The 98th percentile values for the years 2000-2002 are shown in Figure 3.2. The northeastern United States is again a region of high ambient $PM_{2.5}$ levels, with 98th percentile values in excess of 30 µg/m³ at a majority of the sites. Canadian locations exhibit generally lower levels of $PM_{2.5}$, although concentrations greater than 30 µg/m³ occur in several regions of the country for the years 2000-2002, particularly in the Windsor-Quebec City corridor.

Time trends of gaseous SO_2, particle $SO_4^=$, particle NH_4^+ and total nitrate (HNO_3 + NO_3^-) concentrations were investigated at a number of rural/remote sites in the eastern United States and Canada from 1989 to 2002 (Figures 3.3 and 3.4). Canadian measurements were made by the Canadian Air and Precipitation Monitoring Network (CAPMoN), and U.S. measurements by

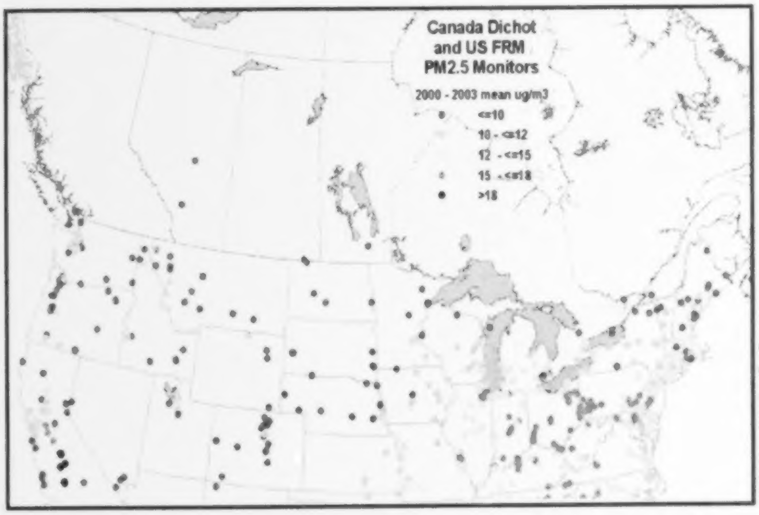

Figure 3.1 Mean annual concentration of $PM_{2.5}$ at Canadian dichot and U.S. FRM monitors in the border region for the data years 2000-2003.

(Note: Canadian sites are years 2000-2002; not all sites include three full years of data)

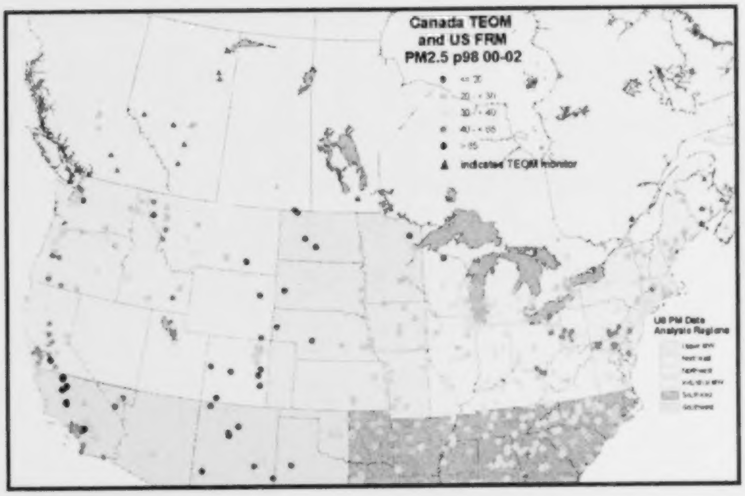

Figure 3.2 - 98th percentile $PM_{2.5}$ concentrations at Canadian TEOM and U.S. FRM sites for the data years 2000-2002.

(Note: Canadian sites do not all include three full years of data).

the Clean Air Status and Trends Network (CASTNet). The two networks use similar filter-pack sampling technology, but the Canadian measurements are 24-hour average concentrations while the U.S. measurements are weekly-average concentrations. This difference has no significant impact on the comparability of the trends. The time trends shown in the figures were produced using a Kernel smoothing technique. The Kernel smoothing technique uses a moving weighted-mean smoother. The weighting function has a maximum value at the center of the moving data window and a value of zero at the edges of the window.

Figure 3.3 shows time trends for SO_2 and particle $SO_4^=$ at seven CASTNet and six CAPMoN sites for the period 1989 to 2002. The highest SO_2 and $SO_4^=$ concentrations are observed in regions with high SO_2 emissions (i.e., Indiana, Ohio, Pennsylvania) while in contrast, the lowest concentrations occur in the northernmost and easternmost regions of Canada, at sites distant from major emission source areas. Consistent with the large decline in eastern North American SO_2 emissions during the 1990s, all of the Canadian and U.S. sites showed marked decreases in ambient SO_2 and $SO_4^=$ concentrations between the early and late 1990s. At most sites, the $SO_4^=$ and SO_2 trends lines follow each other closely, with both species beginning their downward drop around 1989-91. At some sites (Vincennes, IN; Deer Creek, OH; Prince Edward; VA), however, the decline in $SO_4^=$ concentrations occurred two or three years later than the decline in SO_2 concentrations. This may be due to the close proximity of sources with rapidly declining emissions, whereas particle $SO_4^=$ concentrations may not decline as rapidly due to relatively larger distances between the sources and receptors. The SO_2 and $SO_4^=$ trends at Canadian sites generally level off around 1998-2000 while most U.S. sites continue a downward trend, with $SO_4^=$ leveling off at only a few sites.

Particle NH_4^+ and total NO_3^- concentration trends are shown in Figure 3.4 for the same time period, 1989 to 2002. Total NO_3^- is defined here as the sum of gaseous HNO_3 and particle NO_3^-, both reaction products of NO_x. Figure 3.4 indicates that particle NH_4^+ concentrations in Canada remained roughly constant throughout the period while U.S. concentrations generally decreased between the early and late 1990s. Ammonium concentrations were considerably higher in the United States in comparison to Canada, with the exception of the site at Longwoods, which is located in a major agricultural region of southwestern Ontario, a large source of NH_3 emissions.

Total NO_3^- concentrations remained roughly constant, throughout the 1989-2002 time period at

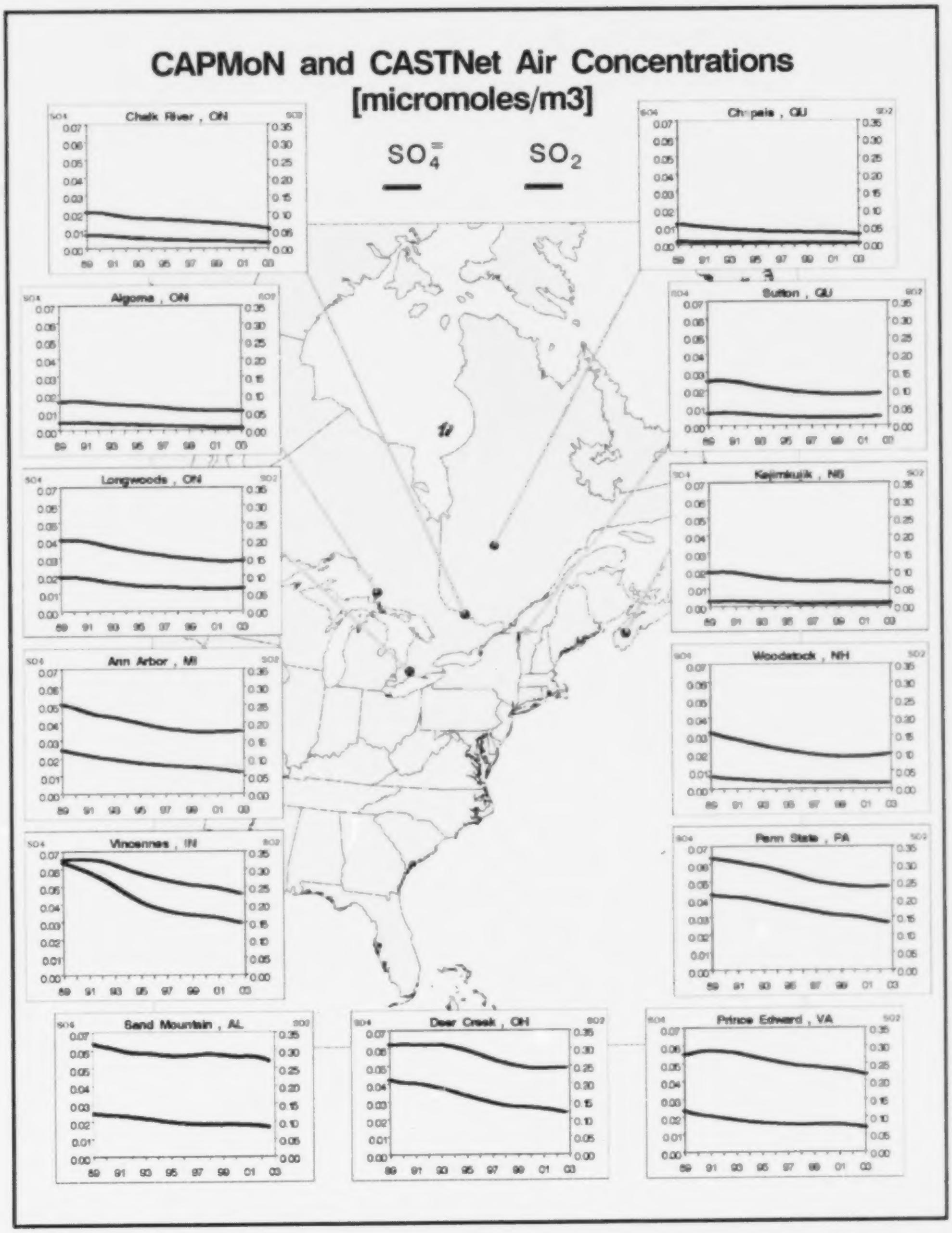

Figure 3.3 - Long-term trends in the precursor gases SO_2 (green) and particulate $SO_4^=$ (blue) at rural CAPMoN and CASTNet sites, 1989–2002.

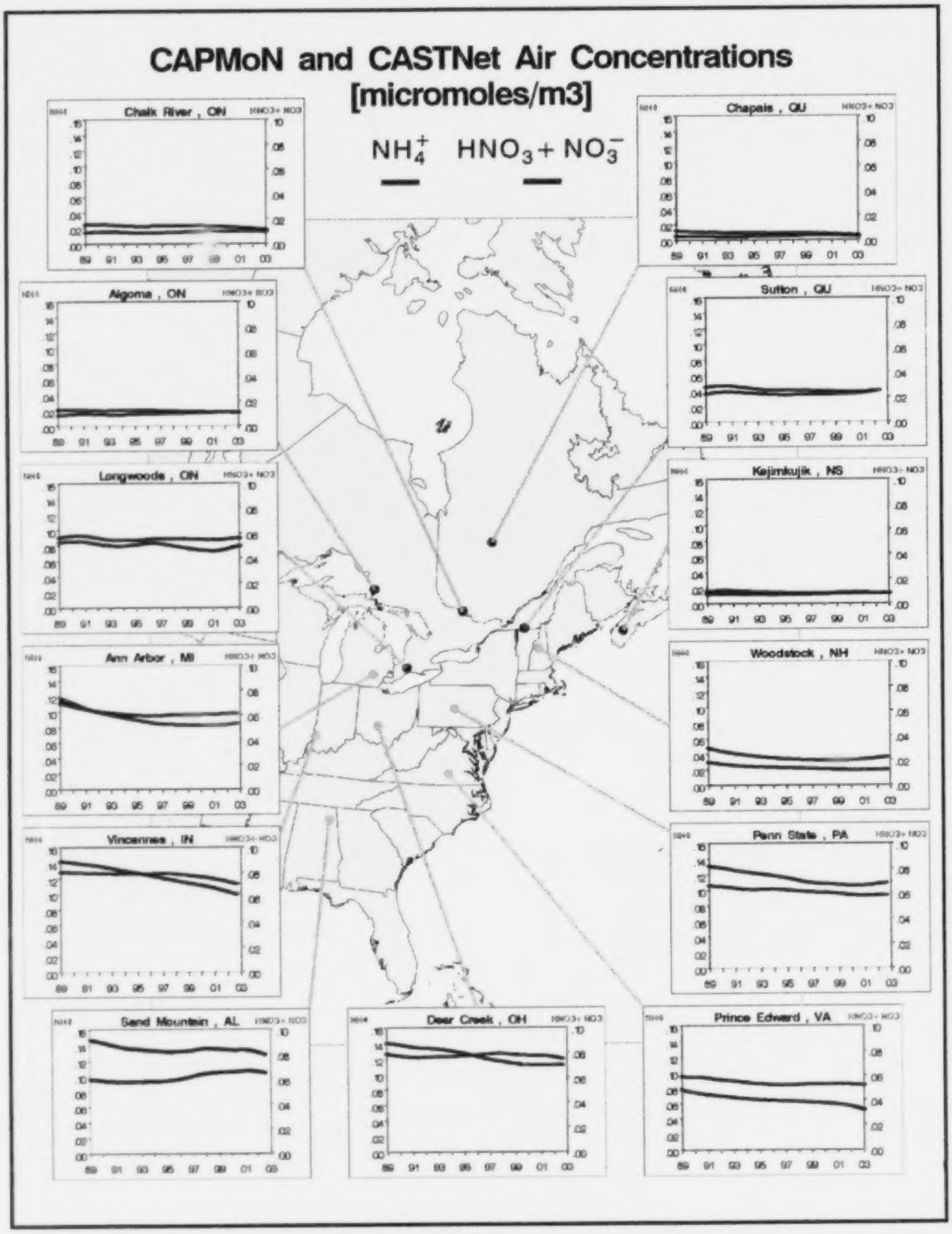

Figure 3.4 - Trends in total nitrate (gaseous HNO_3 and particulate NO_3^-) (green) and particulate NH_4^+ (blue) at rural CAPMoN and CASTNet sites, 1989–2002.

all Canadian sites. Canadian sites also had lower total NO_3^- concentrations than the U.S. locations throughout the measurement period. In contrast, trends at the U.S. sites were not consistent and varied from site to site, some showing higher concentrations in the late 1990s compared to the early 1990s, some showing decreased concentrations in the late 1990s and others showing no change. The variability in the trends at the U.S. sites is possibly a reflection of changing NO_x emissions at near- to medium-distance sources whereas the trends at the Canadian sites may reflect NO_x emissions from more distant sources.

3.1.2 Canada

$PM_{2.5}$ data typically exhibit strongly skewed frequency distributions, characterized by a large number of low values and a small number of high values. It has been shown that the accuracy of the estimated annual means and maxima decreases with decreasing sampling frequency. Hence, the mean and extreme values of $PM_{2.5}$ measurements from the NAPS (National Air Pollution Surveillance Network) dichot network will generally be biased low because of the 1-in-6-day sampling regime. Errors in the NAPS annual means have been estimated to be about 10 percent. Errors in the annual maxima have been estimated to range from 30 to 50 percent (WGAQOG, 1999). Extreme values along the tails of the frequency distributions are often of special interest because they are associated with high concentration PM episodes.

Figure 3.5 shows the trend in annual median $PM_{2.5}$ mass at 11 urban NAPS network sites across Canada from 1984 to 2002. Overall, there is a slight decreasing trend in median $PM_{2.5}$ mass over time, although the 98th percentile values have declined significantly. Data collected between 1984 to the mid-1990s show a decreasing trend, however; from the mid-1990s onward, the median mass of $PM_{2.5}$ is relatively stable. The reasons for these trends are not entirely clear, but the decrease earlier in the data record may be due to SO_2 reductions from acid rain control programs that occurred in the late 1980s and early 1990s (see Figure 3.3).

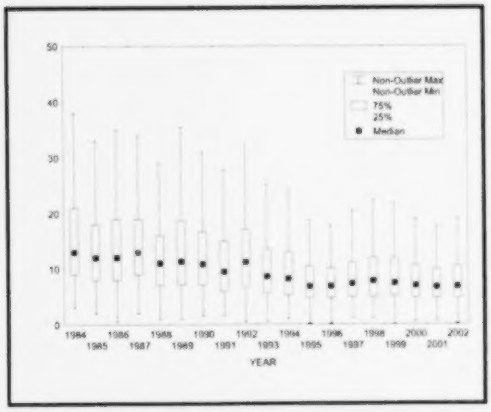

Figure 3.5 - Trend in annual median $PM_{2.5}$, 1984–2002 (median, 75th, 25th percentile). Data are from dichotomous samplers.

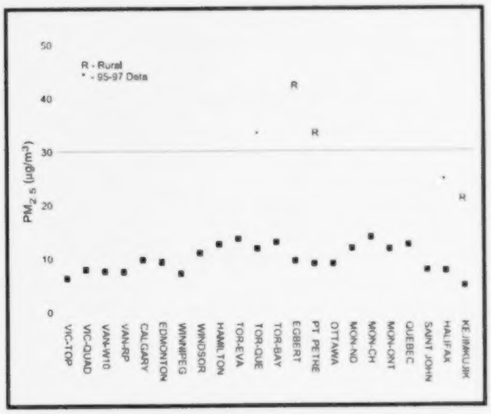

Figure 3.6 - Three-year mean, 10th and 98th percentile $PM_{2.5}$ concentrations, 1997–1999. (Except at sites marked with an *, where the period is 1995–1997. The solid line shows the current Canada-Wide Standard (CWS) for $PM_{2.5}$ of 30 µg/m^3, expressed as a three year average of 98th percentile 24-hour values. Victoria data are considered incomplete. Data are from dichotomous samplers.

Figure 3.6 shows three-year $PM_{2.5}$ averages across Canada for the years 1997 through 1999. The 98th percentile concentrations ranged from a minimum of 16.5 µg/m^3 at a site in Victoria, to a maximum of 40 µg/m^3 at Egbert, Ontario. Measurement data indicate that in eastern Canada, urban and 'point-source influenced' sites

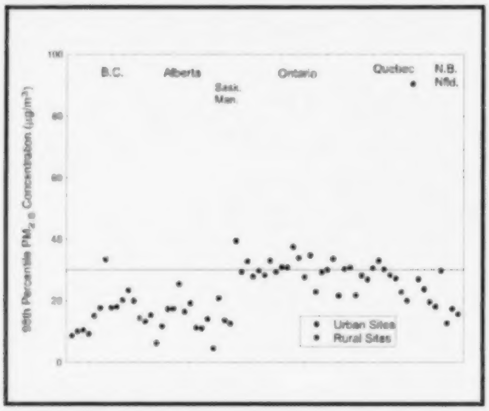

Figure 3.7 - The 98th percentile of Canadian 24-hour PM$_{2.5}$ concentrations in 2001. Sites shown are from west to east. The Canada-Wide Standard numerical target of 30 µg/m³ is shown by the solid line. Data are from continuous TEOM samplers.

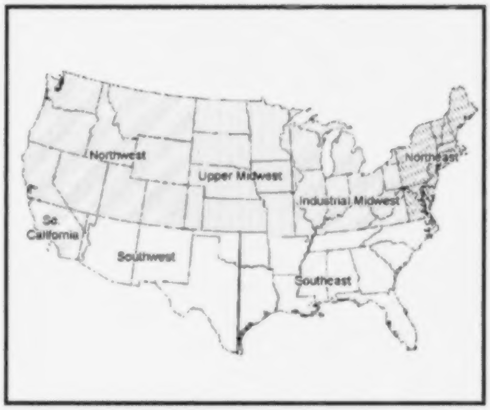

Figure 3.8 - U.S regions used for data analysis purposes.

generally experience higher PM$_{2.5}$ concentrations than do rural and remote sites. This pattern has also been observed in Alberta by Cheng et al. (2000). However, rural sites can also experience very high PM$_{2.5}$ levels during large-scale PM episodes, often comparable to levels observed at urban locations.

Figure 3.7 presents the one-year 98th percentile values of 24-hour PM$_{2.5}$ concentrations in 2001 at monitoring sites that satisfied the 75 percent NAPS data completeness criterion (or had a 98th percentile > 30 µg/m³ as per the Canada-Wide Standard Achievement document), shown by location from west to east. In 2001, 98th percentile values were greater than 30 µg/m³ (shown by the red line in Figure 3.7) at seventeen sites. All of these seventeen sites are in urban areas except for the rural site of Simcoe, Ontario. Outside of Ontario and Quebec, only Prince George recorded a 98th percentile value greater than 30 µg/m³.

3.1.3 United States

The U.S. EPA and the states have been using a national network to measure PM$_{2.5}$ concentrations since 1999. Summaries through the end of 2002, based on data publicly available from the U.S. EPA's Air Quality System (AQS) as of April 2003, are presented here. PM$_{2.5}$ data from the network for Interagency Monitoring of Protected Visual Environments (IMPROVE) are also presented. Many data summaries are presented by region, as shown in Figure 3.8, for understanding potential differences in the characteristics of PM in different parts of the United States. Four of these regions border Canada.

Following the establishment of new ambient standards for PM$_{2.5}$ in 1997, the U.S. EPA led a national effort to deploy and operate over 1000 PM$_{2.5}$ monitors. The U.S. EPA has analyzed the available data collected by this network from 2000-2002. Data from the monitors were screened for completeness with the purpose of avoiding seasonal bias. To be included in these analyses, a monitor needed to record at least a full year of data, defined as either 4, 8, or 12 consecutive quarters with eleven or more observations per quarter.

3.1.3.1 *Spatial Variations in Annual Average PM$_{2.5}$ Concentrations across the United States*

Figures 3.9 is a national map depicting county-level annual mean PM$_{2.5}$ concentrations from the U.S. FRM network. The monitor with the highest

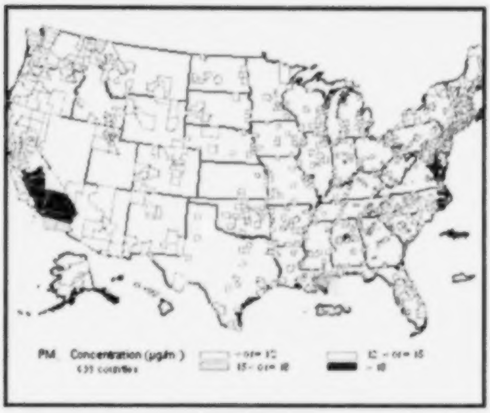

Figure 3.9 - County-level maximum annual mean $PM_{2.5}$ concentrations, averaged over three years, 2000-2002.

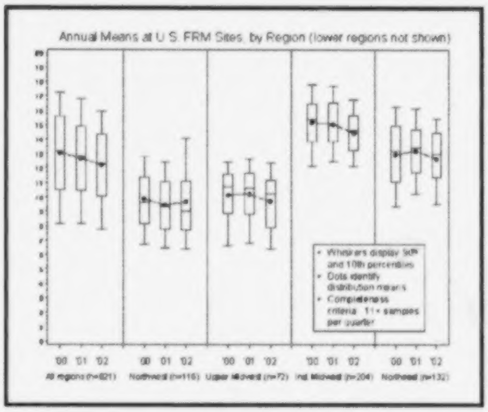

Figure 3.10 - Annual $PM_{2.5}$ means at U.S. FRM sites by region over three years, 2000-2002. The box identifies the inter-quartile range, the line in the middle shows the median, whiskers display 90th and 10th percentiles, and dots identify the distribution means.

concentration in each monitored county is used to represent the value in that county. The map and box plots show that many locations in the eastern United States and in California had annual mean $PM_{2.5}$ concentrations above 15 µg/m^3.

Annual mean $PM_{2.5}$ concentrations were above 18 µg/m^3 in several urban areas throughout the eastern United States, including Atlanta, Birmingham, Chicago, Cincinnati, Cleveland, Detroit, Indianapolis, Knoxville, Louisville, Pittsburgh, and St. Louis. Los Angeles and the central valley of California were also above 18 µg/m^3. Sites in the upper Midwest, Southwest, and Northwest regions of the United States had generally lower annual mean $PM_{2.5}$ concentrations, most below 12 µg/m^3.

3.1.3.2 *Annual Means of $PM_{2.5}$ at U.S. FRM Sites by Region*

The annual $PM_{2.5}$ mean concentrations across the northern regions of the United States range from about 6 to 18 µg/m^3, with a median of about 13 µg/m^3. The 98th percentiles of the distribution of 24-hour average concentrations range from about 8 to 94 µg/m^3, with a median of about 33 µg/m^3. Figure 3.10 shows 3 years of annual mean concentrations at FRM sites, for the data years 2000-2002. Most FRM sites are urban ('Urban and Center City' or 'Suburban') according to AQS definitions; FRM sites sample every day, every 3rd day, or every 6th day, with the predominant measurements being every 3rd day.

The left-most graph in Figure 3.10 shows the three years of data for all sites in the United States (irrespective of region) and the four other plots show the northern U.S. regions bordering Canada. $PM_{2.5}$ concentrations decreased approximately 7 percent nationwide but the northern United States did not see such a decrease. Except for the Industrial Midwest, concentrations in the northern regions have been much flatter. Average $PM_{2.5}$ levels are lower than the U.S. averages in all northern regions except for the Industrial Midwest (Detroit, Cleveland).

3.1.3.3 *Annual Means of $PM_{2.5}$ at U.S. FRM Sites within 300 km of Border by Region*

Figure 3.11 focuses on U.S. FRM sites within 300 km of the Canadian border. This boundary was recommended based on various analyses of correlation distance, back trajectories, and source attribution analysis. The left-most plot shows $PM_{2.5}$ con-

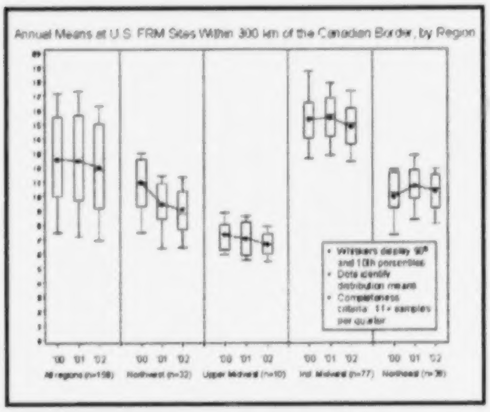

Figure 3.11 - Annual mean $PM_{2.5}$ at U.S. FRM sites within 300 km of the Canadian border by region, over three years, 2000-2002.

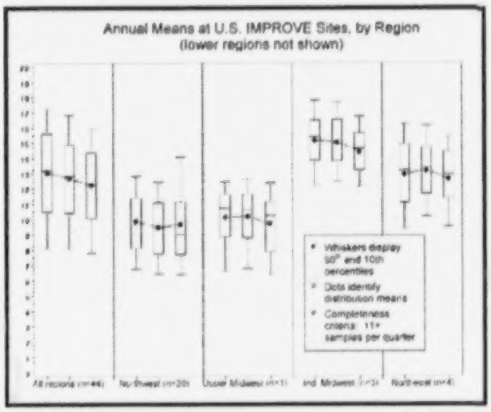

Figure 3.12 - Annual $PM_{2.5}$ means at rural U.S. IMPROVE sites by region.

centrations at all U.S. sites within 300 km of the border. This figure includes all of the sites in the 4 plots to the right (with one exception) since none of the 'southern' regions have points that close. The exception is one site (Alaska) which is not included in a region, but meets the completeness criterion. Mean $PM_{2.5}$ concentrations for all sites (within 300 km) are relatively flat with the Industrial Midwest driving the 'all regions' plot since about half of the 158 sites are located there. Sites in the Northwest show a large decline, -22 percent (in average mean $PM_{2.5}$ concentrations) from 2000 to 2002. The 10 sites closest to the Canadian border show a decline in mean $PM_{2.5}$ of 10 percent.

3.1.3.4 *Annual Means of* $PM_{2.5}$ *at* U.S. IMPROVE *Sites by Region*

Figure 3.12 shows the U.S. annual mean $PM_{2.5}$ at the rural IMPROVE network sites for the data years 2000-2002. $PM_{2.5}$ levels are relatively unchanged over the three years, with a slight increase in the middle year (with the exception of the Northwest region). Annual mean concentrations declined from 1998 to 2001 at the three sites in the Industrial Midwest. Annual mean levels of $PM_{2.5}$ at sites in the Northwest and Upper Midwest are consistent with national averages (at IMPROVE sites). The levels in the two eastern regions, particularly the Industrial Midwest, are higher on average than the other sites.

3.1.3.5 *Three year Annual Means and* 98*th* *Percentiles* (2000-2002) *of* $PM_{2.5}$ *for* U.S. *Sites* (FRM) *within* 200 *km of the Canadian Border*

Figure 3.13 shows 3-year average 98th percentile (triangle) and 3-year average annual mean (dot) concentrations of $PM_{2.5}$ at 'border' sites. The data for FRM sites are for the years 2000-2002. The distance criterion of 'within 200 km of the border' is useful to show relationships, while removing any significant clutter observed on the figures when the distance from the border is increased. Sites are shown (left to right) in a west-to-east longitude order while the vertical lines separate the regions. The first site (left-most) in the Northwest is really located in Alaska (undefined region). The dashed horizontal line at 15 $\mu g/m^3$ corresponds to the annual U.S. National Ambient Air Quality Standard for $PM_{2.5}$. Numerous FRM sites in the Industrial Midwest have annual means over the standard. Only 1 site elsewhere (Northwest; Libby, Montana) exceeds the annual standard. $PM_{2.5}$ concentrations measured at the IMPROVE sites (mean and 98th), while not displayed, are below most of the concentrations measured at the FRM sites, as expected from the rural and urban comparison.

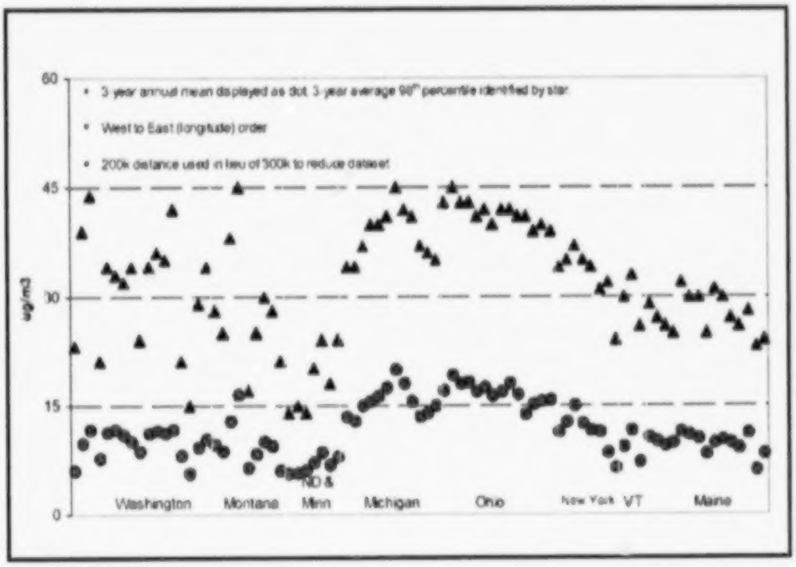

Figure 3.13 - 3-year annual means (dots) and 98th percentiles (triangles) (2000-2002) for U.S. sites within 200 km of the border (FRM)

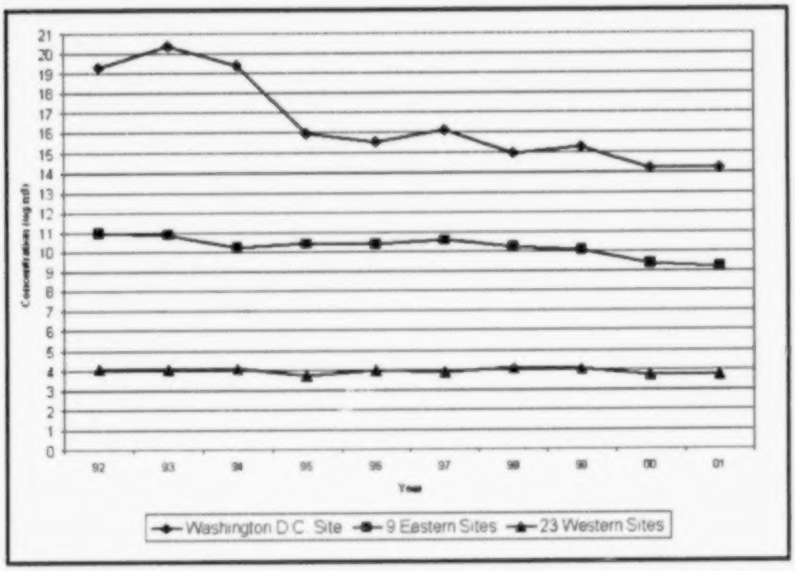

Figure 3.14 - Average measured annual $PM_{2.5}$ concentration trend at IMPROVE sites, 1992-2001. To be included sites must have 8 of 10 valid years of data; missing years are interpolated. Measured mass represents measurement from the filter.

3.1.3.6 *Long-term Trends in* $PM_{2.5}$

Figure 3.14 shows the composite long-term trend (1992-2001) at 9 eastern sites, 23 western sites, and 1 urban site in Washington, D.C. all from the IMPROVE network. At the rural eastern sites, measured $PM_{2.5}$ decreased about 16 percent from 1992 to 2001. At the rural western sites $PM_{2.5}$ decreased about 10 percent from 1992 to 2001. At the Washington, D.C. site, the annual average $PM_{2.5}$ concentration in 2001 was about 30 percent lower than the 10-year peak in 1994.

3.2 AMBIENT CHARACTERIZATION OF PM

3.2.1 Canada

There are significant differences in the chemical composition of PM across Canada, resulting from differences in contributing sources. Toward the goal of effectively managing the emission and formation of PM, recent work has sought to determine the chemical composition of PM at urban sites (Brook et al., 1997, 1999; Brook and Dann, 1999). Analyses of $PM_{2.5}$, collected at 14 cities across Canada, indicate that seven major chemical fractions are present (Figure 3.15). In approximate order of size from largest to smallest, these fractions are "undetermined" (generally assumed to be black and organic carbon), $SO_4^=$, NH_4^+, soil, NO_3^-, sodium chloride (NaCl) and "other" (thought to be major ions, metals and possibly water, not allocated to the other components).

Figure 3.16 shows the contribution of $SO_4^=$, NO_3^-, NH_4^+ and Total Carbonaceous Mass (TCM) to $PM_{2.5}$ concentrations across Canada. TCM comprises a large component of $PM_{2.5}$ in Canada, along with $SO_4^=$, NO_3^-, and NH_4^+.

In these figures, TCM is estimated as:

[Organic Carbon Mass (OCM) + Black Carbon (BC)]

OCM is estimated as measured and blank-corrected Organic Carbon (OC) multiplied by 1.40 to convert OC to OCM. Crustal concentrations are estimated using the IMPROVE method.

The composition of $PM_{2.5}$ varies seasonally and has been examined at a rural site (Egbert, Ontario) during both winter and summer "high PM" episodic conditions (Figure 3.17). In the winter episode, the seven major fractions of $PM_{2.5}$ from largest to smallest were NO_3^-, NH_4^+, $SO_4^=$, organic carbon compounds, black carbon, soil and other (major ions and metals not allocated to the other components). In the summer episode, the seven major fractions in descending order of size were $SO_4^=$, NH_4^+, organic carbon compounds, NO_3^-, soil, black carbon and other. These data suggest

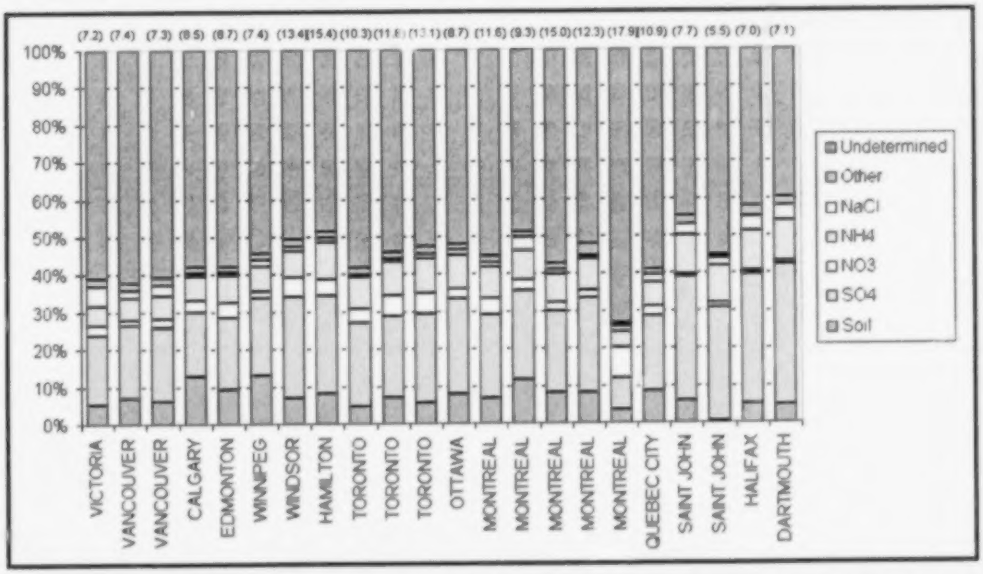

Figure 3.15 - The fractional chemical composition of $PM_{2.5}$ at various urban sites based on 1995-98 NAPS dichot data. (In parentheses are the mean mass concentrations in μg/m³. The "Undetermined" component is assumed to consist of black and organic carbon. The "Other" component consists of the major ions, metals and possibly water not allocated to the other components.)

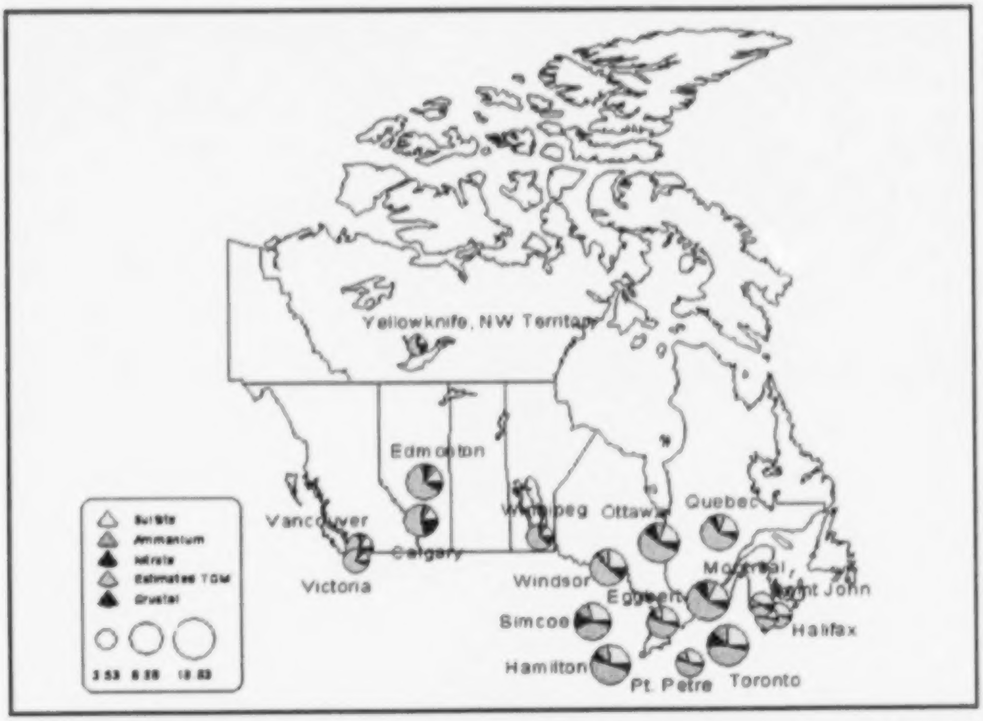
Yellowknife, NW Territory
Edmonton
Calgary
Vancouver
Victoria
Winnipeg
Ottawa
Quebec
Montreal
Saint John
Halifax
Windsor
Egbert
Simcoe
Hamilton
Pt. Petre
Toronto
Sulfate
Ammonium
Nitrate
Estimated TOM
Crustal

Figure 3.16 - $PM_{2.5}$ speciation data for NAPS network sites in Canada September 2001-August 2002. Size of pie graphs indicates average $PM_{2.5}$ concentration for the time period evaluated.

that episodic conditions at this rural site are driven by secondary NO_3^- formation in the winter season, and secondary $SO_4^=$ formation in the summer. In addition to the differences observed in $PM_{2.5}$ composition between seasons, it is suggested that there are major differences in PM composition between urban and rural sites. Samples of $PM_{2.5}$ from urban sites in Canada have higher average fractions of black and organic carbon and lower fractions of $SO_4^=$ and NO_3^- than rural sites. This is consistently attributed to the increased contribution of the mobile source sector (including on-road, off-road and diesel vehicles) in urban areas.

3.2.1.1 *Chemical Composition of the Organic Fraction of $PM_{2.5}$*

Of the organic mass that is chemically resolved in measurements, it is estimated that primary carbon is a larger component of the mass compared with the products of VOC oxidation. To date, it is possible to identify only 10 to 20 percent of the organic species composing the total organic carbon fraction of PM; however, monitoring technology for this fraction is evolving. At present, measurement information is insufficient for determining whether the unresolved portion of the organic mass originates as direct organic particle emissions, VOC emissions that condense directly to particles, or

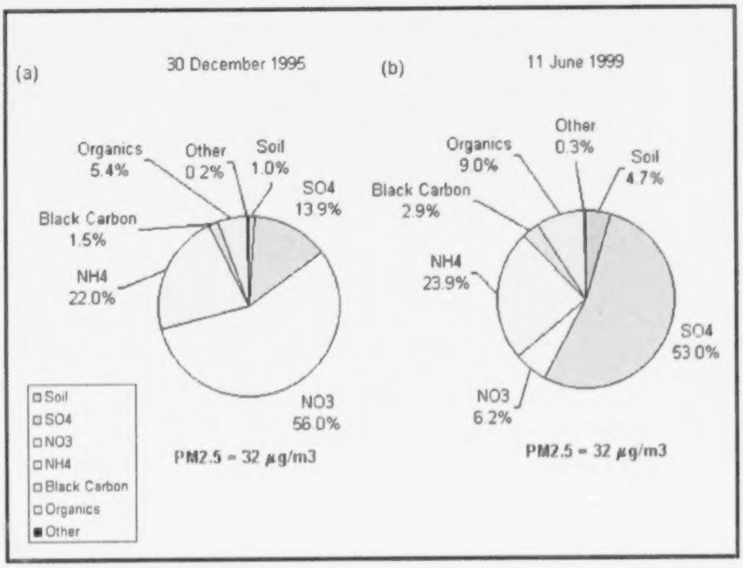

Figure 3.17 - The relative composition of $PM_{2.5}$ mass at Egbert (ON) during (a) a wintertime $PM_{2.5}$ episode December 30, 1995, and (b) a summertime episode June 11, 1999. (The data are from the GAViM (Guelph Aerosol and Visibility Monitoring) program (Njedley et al., 2003).)

the condensation of VOC oxidation products. Of the resolved portion of organic mass composing PM, researchers have identified organic acids, fatty acids, polycyclic aromatic hydrocarbons, petroleum biomarkers and straight-chain alkanes (Rogge et al., 1993; Schauer et al., 1996). In Canada, recent work has allowed the identification of each of these groups of compounds by various analytical techniques; however, the application of these techniques to ambient data is in the initial stages (Blanchard et al., 2002).

3.2.2 United States

Atmospheric $PM_{2.5}$ is composed of many different chemical components that vary by location, time of day, and time of year. Recent data from the rural IMPROVE network and from the urban speciation network provide indications of regional differences in composition for $PM_{2.5}$.

Figures 3.18 shows the composition of annual average $PM_{2.5}$ mass collected recently at several sites in nine different regions. Figure 3.18 identifies NH_4^+ as a separate component of $PM_{2.5}$ mass; however, it is associated with either $SO_4^=$ or NO_3^- (as $(NH_4)_2SO_4$ or NH_4NO_3) roughly in proportion to the amount of $SO_4^=$ and NO_3^- indicated.

In general, fine-fraction particles in the eastern U.S. regions are dominated by carbon compounds (TCM) and $(NH_4)_2SO_4$. In the western U.S. regions, fine-fraction particles have a greater mass of carbon compounds. With the exception of rural locations in the desert west region, crustal material is a very small portion of fine-fraction particles. The NH_4NO_3 component is more prevalent in urban aerosols than in rural aerosols, especially in the California region, but also in the Industrial Midwest and Northeast, and is an indication of population-driven NO_x sources, such as transportation activity and combustion sources. Similarly, the carbon component by estimated mass is larger in urban areas compared to surrounding rural areas and is an indication of local contributing sources.

Figures 3.19 and 3.20 illustrate how $SO_4^=$, NO_3^-, and TCM (black and organic carbon) along with other components, contribute to $PM_{2.5}$ concentrations across the United States. These maps represent the year with the most data where data analysis has been completed: September 2001-August 2002.

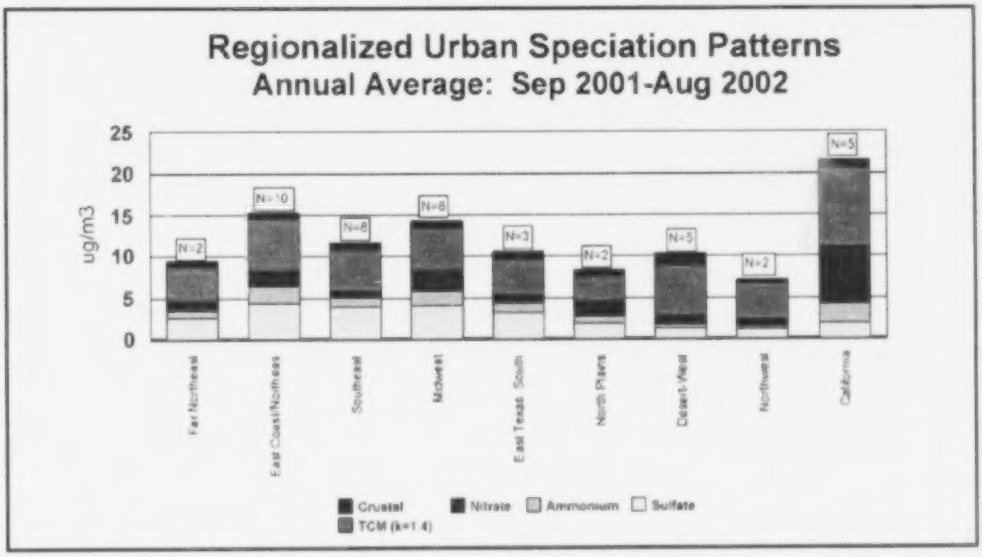

Figure 3.18 - Annual average composition of $PM_{2.5}$ in the United States by region (Urban data from the EPA Speciation Trends Network).

The U.S. EPA speciation data in Figure 3.19 illustrate that sites in urban areas generally have higher annual $PM_{2.5}$ concentrations than the rural stations shown in Figure 3.20. Urban sites in the East include a large percentage of TCM, $SO_4^=$, and associated NH_4^+, whereas, urban sites in the Midwest and far West include a large percentage of TCM and NO_3^-. These patterns are also evident at the Canadian locations (Figure 3.16). There are, however, several sites in southern California where the NO_3^- fraction is of equal or greater proportion than the carbon fraction.

The IMPROVE data in Figure 3.20 illustrate that $PM_{2.5}$ levels in the rural areas are highest in the eastern United States and southern California, as indicated by the larger circles. Sulphates and associated NH_4^+ dominate the east, with TCM as the next most prevalent component. Sulphate concentrations in the east largely result from SO_2 emissions from coal-fired power plants. In California and in the Midwest, TCM and NO_3^- make up most of the measured $PM_{2.5}$.

Sulphates play a major role in the East, Midwest, and South. Nitrates contribute to $PM_{2.5}$ mass most in the Midwest and Northern locations. Sites closest to the Canadian border (the North Plains and Northwest sub-regions) are seen to have relatively lower annual $PM_{2.5}$ mass and contain mostly carbon, $SO_4^=$, and NO_3^-, in that order. For the domain of sites investigated, it is also seen that the highest mass sites (for the year in question) are in the East Coast, Northeast, and Midwest.

Figure 3.21 shows seasonal variations for the same grouping of urban and rural sites. In urban areas, $SO_4^=$ and carbon dominate $PM_{2.5}$ mass in the summer season while NO_3^- and TCM dominate wintertime $PM_{2.5}$ mass. Fall and spring show transitional amounts of each of the species when compared to the summer and winter concentrations. There is more NO_3^- in the spring when compared to the fall and higher TCM in the fall compared to the spring.

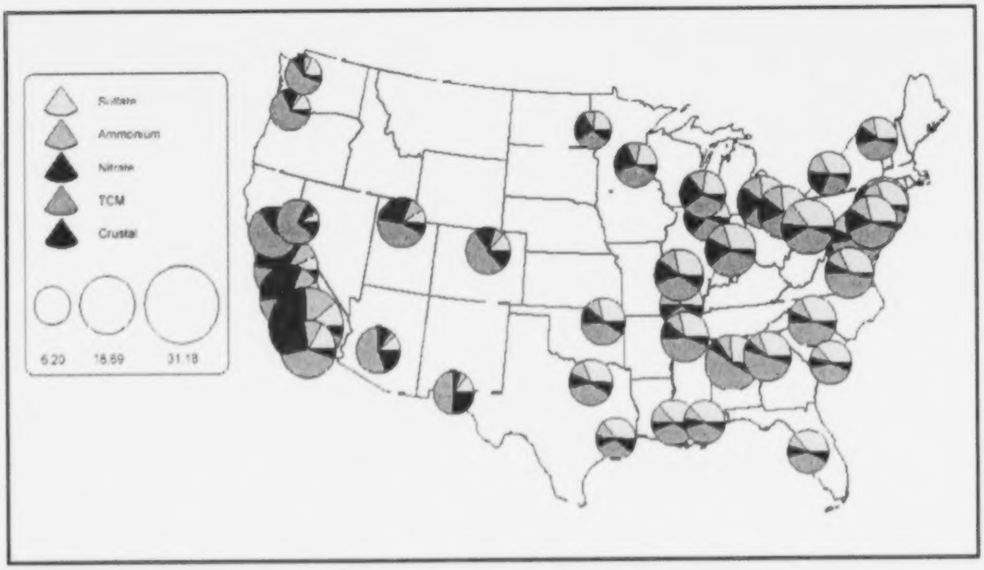
Sulfate
Ammonium
Nitrate
TCM
Crustal
6.20
18.69
31.18

Figure 3.19 - Summary of urban speciation data for $PM_{2.5}$ in the United States (EPA Speciation Network). Size of pie graphs indicates average $PM_{2.5}$ concentration for the time period evaluated.

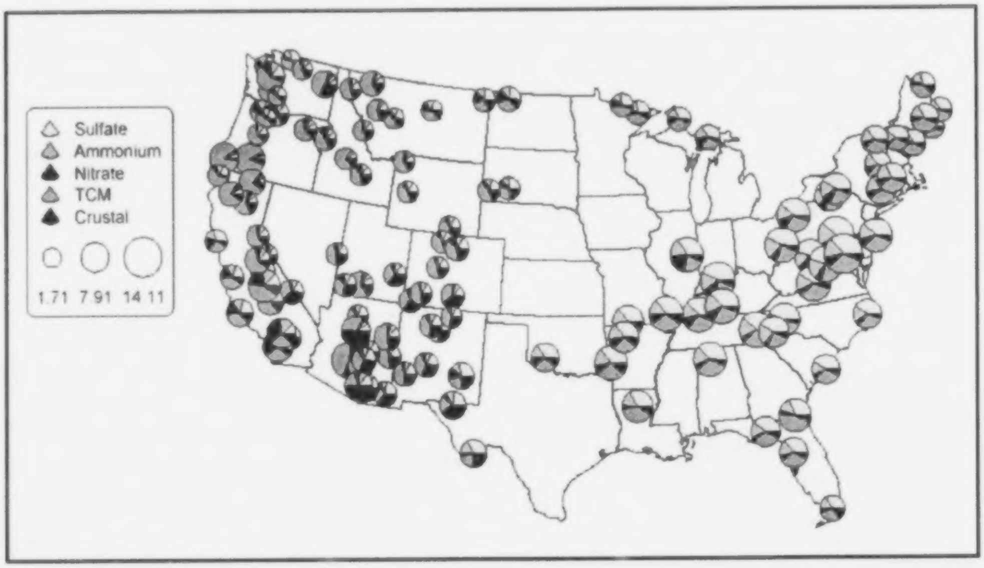
Sulfate
Ammonium
Nitrate
TCM
Crustal
1.71
7.91
14.11

Figure 3.20 - Summary of rural speciation data (IMPROVE network). Size of pie graphs indicates average $PM_{2.5}$ concentration for the time period evaluated.

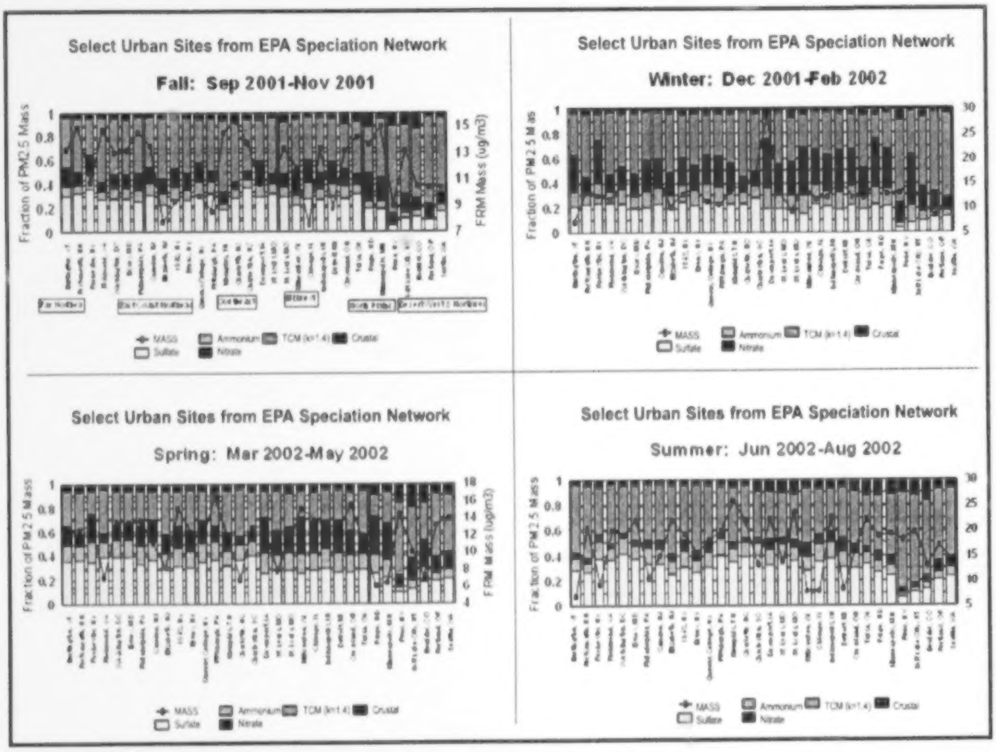

Figure 3.21 - Seasonal variation in PM species for selected urban areas in the United States

In the regions bordering Canada (Far Northeast, Northwest, and North Plains subregions), carbon and $SO_4^=$ are seen to be the dominant species in summer, fall, and spring $PM_{2.5}$ aerosols. Nitrates are a major species in the winter in the Northeast and TCM is a major species in the winter in the Northwest. FRM mass is seen to be highest in the winter and summer months.

3.3 LEVELS OF SULPHATE AND NITRATE DEPOSITION

Sulphate and nitrate are the products of SO_2 and NO_X oxidation respectively, reactions which may also involve cloud water. Water droplets turn into raindrops and precursors dissolved within these are removed from the atmosphere via precipitation. Falling rain droplets may pick up additional precursor gases as well as particle mass. Sulphate is a major component of fine particle mass in eastern North America and due to the relatively low deposition velocity; these particles can spread over large regions (Environment Canada, 2001). The prevalence of the $SO_4^=$ component of PM and the acidifying power of this compound demonstrates the linkage between PM and acid deposition.

3.3.1 Wet Sulphate Deposition and Critical Load Exceedances

Figure 3.22 illustrates the observed mean annual wet $SO_4^=$ deposition in eastern North America for 1996-2001. Levels range from less than 5 kg/ha/yr to greater than 25 kg/ha/yr. The highest levels of wet deposition are observed in the region of the

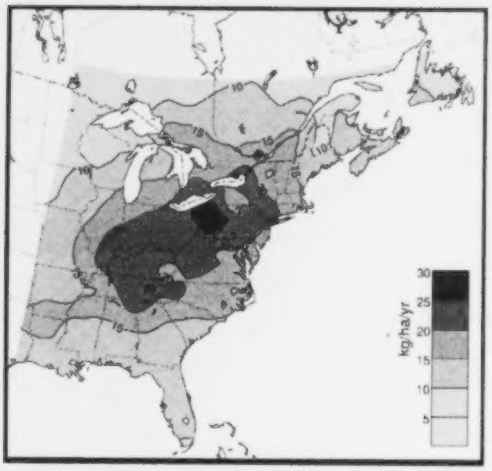

Figure 3.22 - Spatial distribution of wet $SO_4^=$ deposition (kg/ha/yr) in eastern North America, 1996-2001.

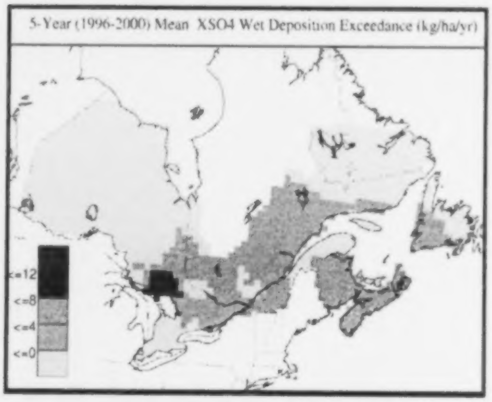
5-Year (1996-2000) Mean XSO4 Wet Deposition Exceedance (kg/ha/yr)
<=12
<=8
<=4
<=0

Figure 3.23 - Five-year (1996-2000) mean wet deposition exceedance of critical $SO_4^=$ loads (kg $SO_4^=$/ha/yr) for 95% lake protection level.

Ohio River Valley. When compared to the critical loads for wet $SO_4^=$ deposition in eastern Canada[1], large areas of eastern Canada are receiving wet $SO_4^=$ deposition in excess of critical loads (Figure 3.23).

There has been a decrease in observed lake acidity near Sudbury, Ontario as a result of substantial reductions in SO_2 emissions from local smelters and other sources outside the region. However, in other areas of Ontario, Quebec and Atlantic Canada, there has been a lack of change in acidity and acid neutralizing capacity. This is partly a result of the long-term depletion of base cations in watershed soils, which control lake chemistry as well as forest health. It is predicted that with current emission reduction commitments, an area of almost 800,000 km^2 in southeastern Canada will receive harmful levels of acid deposition in 2010.

Canada is currently using a geochemical model, Model of Acidification of Groundwater in Catchments (MAGIC), to analyze the current status of lakes, rivers and forest soils and to predict recovery timelines. The predicted response of lakes and rivers to a hypothetical 50-percent SO_2 reduction scenario, despite a quick pH recovery, is a base cation recovery lag time of 100 years (Clair et al., 2003). The recovery period is predicted to be much slower for forests.

3.3.2 Wet Nitrate Deposition

Nitrogen is a growth-limiting nutrient which is taken up and retained by vegetation. However, in many watersheds, prolonged NO_3^- deposition has resulted in soil acidification. It is possible that even with reduced $SO_4^=$ deposition received by ecosystems, the effects of continued NO_3^- acidification on forest and aquatic ecosystems will coun-

---

[1] Critical load values for wet $SO_4^=$ deposition to aquatic ecosystems in eastern Canada were estimated in 1990 (RMCC, 1990). Values were estimated using the average geochemical characteristics of tertiary watersheds and assigning a protection level for lakes of 95%. Areas with critical load values of less than 8 kg/ha/yr are considered to be very sensitive to acidification. It should be noted however, that the use of wet $SO_4^=$ deposition as the primary environmental criterion for ecosystem protection has two limitations. First, because the concurrent deposition of nitrate ions and base cations has not been included, such a criterion considers only residual $SO_4^=$ deposition rather than the more general issue of residual acidification. The second limitation concerns the use of wet deposition information only. In eastern Canada, depending on the distance downwind from source regions, up to an additional 40% of sulphur (and other chemical species) is dry deposited, contributing to acidification.

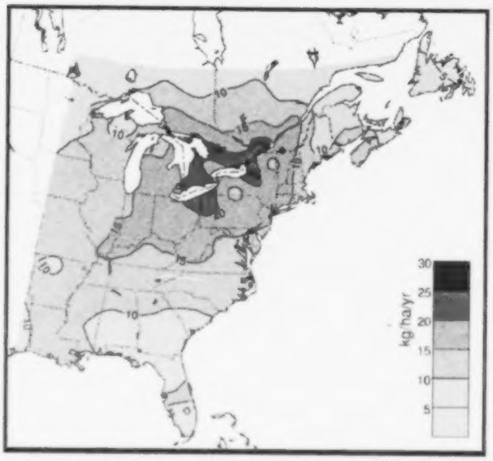

Figure 3.24 - Spatial distribution of wet NO_3^- deposition (kg/ha/yr) in eastern North America, 1996-2001.

teract the benefits gained from SO_2 emission reductions.

Figure 3.24 illustrates the observed mean annual wet NO_3^- deposition in eastern North America for 1996-2001. Levels range from less than 5 kg/ha/yr to greater than 25 kg/ha/yr. The highest levels of wet NO_3^- deposition are observed in the region of Lake Erie and eastern Lake Ontario.

3.4 KEY SCIENCE MESSAGES

- Current ambient levels of $PM_{2.5}$ in the border regions exceed both the Canadian and U.S. standards set for $PM_{2.5}$ in several regions of both countries (primarily urban locations). The eastern portion of the border domain (i.e., Northeastern United States, Industrial Midwest and the Windsor-Quebec City corridor) exhibits levels that exceed the 15 µg/m^3 annual standard in the United States and the 30 µg/m^3 98th percentile 3-year average Canadian standard for the time periods evaluated.
- There are sites with elevated $PM_{2.5}$ levels (with very few sites exceeding either standard for the time periods evaluated) in the Georgia Basin-Puget Sound airshed, but the problem is more confined, and the levels generally lower than in the Northeastern airshed.
- Urban concentrations of $PM_{2.5}$ are higher than rural sites in all regions of both Canada and the United States.
- Levels of $PM_{2.5}$ and PM precursors (SO_2, NO_x) have declined, particularly early on in the data record; however, since the mid-1990s, levels of $PM_{2.5}$ and PM precursors have generally remained unchanged.
- $PM_{2.5}$ in the border region at most sites examined consists of, in order of relative importance to annual $PM_{2.5}$ levels, organic and black carbon, $SO_4^=$, NO_3^-, NH_4^+, soil dust and trace elements. Secondary particulate (i.e., NH_4^+, NO_3^- and $SO_4^=$) is found to play a key role under episodic conditions in Ontario. In the border region, TCM and $SO_4^=$ are seen to be the dominant species in summer, fall, and spring $PM_{2.5}$ aerosols. Nitrates are a major species in the winter in the Northeast, and TCM is a major species in the winter in the Northwest.
- Ambient levels of PM precursors also contribute to the wet deposition of NO_3^- and $SO_4^=$, and resulting ecosystem acidification. The highest levels of deposition are located in the northeastern United States and eastern Canada, particularly in the border regions.

CHAPTER 4

EMISSIONS

4.1 DEVELOPMENT OF EMISSION INVENTORIES

4.1.1 Development of Canadian and U.S. Emission Inventories for REMSAD and AURAMS

National annual and seasonal emission inventories for Canada and the United States were developed for application with the Regional Modelling System for Aerosols and Deposition (REMSAD) and A Unified Regional Air Quality Modelling System (AURAMS). Applications of the two air-quality models were employed to examine the effects of U.S. and Canadian emission control strategies on ambient concentrations of $PM_{2.5}$ in North America in 2010 and 2020. The purpose of this section is to describe the assumptions used to develop the emission inventories and the emission files used in these model applications.

The emission inventories developed by Environment Canada and the U.S. EPA to support these analyses include the following:

- 1995/1996 Base Year;
- 2010 Base Case;
- 2010 Control Case;
- 2020 Base Case; and
- 2020 Control Case.

4.1.1.1 *Base Year Inventories*

The Canadian 1995 comprehensive Criteria Air Contaminants (CAC) emission inventory, version 2, and the U.S. 1996 National Emission Inventory (NEI) version 3.12 (EPA, 2001) were used for the model applications. These inventories include reported air pollutant emissions for oxides of nitrogen (NO_x), volatile organic compounds (VOC), carbon monoxide (CO), oxides of sulphur (SO_x), primary particulate matter with an aerodynamic diameter less than or equal to 10 micrometers and 2.5 micrometers (PM_{10} and $PM_{2.5}$) and ammonia (NH_3). The inventories include all stationary, mobile and other sources that emit criteria air pollutants. The specifics of the inventories are discussed below.

CANADA: The Canadian 1995 CAC inventory version 2 is produced via a collaborative effort between Environment Canada and the provincial and territorial governments. Due to confidentiality issues, Canadian point sources were processed by an outside consultant to maintain the confidentiality of the information. Temporal profiles for sources and sectors were made available for the inventory processing. Mobile emissions in the Canadian inventories were calculated using a hybrid MOBILE 5C model, incorporating many new MOBILE6 features for the on-road transportation sector for 1995 and future years. Emission information was then converted into a format compatible with the REMSAD model.

UNITED STATES: The NEI is a national database of air emission information with input from numerous state and local air agencies, tribes, and industry. The national inventories for this analysis were prepared for the 48 contiguous states at the county-level for on-highway mobile sources, electric generating units (EGUs), non-EGU point sources, stationary area sources, and non-road sources. The inventories do not include the states of Alaska and Hawaii. The inventories contain annual and typical summer season-day emissions for the pollutants.

4.1.1.2 *Base Case Inventories for 2010 and 2020*

CANADA: To project CAC emissions to 2010 and 2020, annual growth factors are applied to the 1995 emissions for each industrial sector at the provincial level. The growth factors are calculated from surrogate data or from indicators obtained from

Natural Resources Canada (NRCan) report "Canada's Emissions Outlook: An Update, December 1999". The national CAC forecast is the sum of the provincial and territorial forecasts.

Environment Canada "grew" the 1995 Canadian inventory to 2010 and 2020 using the Canadian CAC emission forecast scenario by province and sector. The changes from the base case to the future case scenario were then backed out of the resulting files. The base case 2010 and 2020 inventories incorporate all of the emission reduction measures that are already in place. These include: Tier 1 and NLEV vehicles, Tier 2, and heavy duty vehicle NMHC, NO_x, PM standards, and low sulphur on-road diesel and gasoline. Inputs from provincial and territorial governments and private industry were incorporated into the forecast.

UNITED STATES: The 2010 and 2020 projection year base case files were calculated using methods and models designed to support the U.S. EPA's Proposed Program for Low-Emission Nonroad Diesel Engines and Fuel (68 FR 28327) and the Clear Skies Initiative (EPA, 2003a). Included in the development of these estimates was an adjusted version of EPA's MOBILE 5B model, accounting for changes anticipated at the time of this analysis to be included in the first release of MOBILE 6, the March 2002 version of EPA's NONROAD model, and for stationary, point, and area sources, inventories (2020) and interpolations from projected inventories (2010) as designed to support the proposed nonroad rule (EPA, 2003b). The emission projection files were estimated using the 1996 base-year emission inventory by applying growth and control factors developed to simulate economic changes and control programs in place for each respective projection year and were designed to include the specific Clean Air Act Amendments emission reduction measures promulgated and proposed by the U.S. EPA at the time of the nonroad rule's publication in the Federal Register.

Projection-year unit-level output files from the EPA Modelling Applications 2003 version of the Integrated Planning Model (IPM) were generated by the U.S. EPA for the EGU sector base case for 2010 and 2020. Included in the base case runs were a court-remanded version of the Regional Transport NO_x SIP Call reductions and state-specific emission caps in Connecticut, Massachusetts, Missouri, New Hampshire, North Carolina, Texas, and Wisconsin. The IPM files include heat input, SO_2 emissions, NO_x emissions, and unit characteristics such as prime mover (boiler, gas turbine), primary fuel, boiler type, and firing type. In order to complete the file to include all criteria pollutants and data elements necessary to process the EGU sector through an emission model, the U.S. EPA added to the parsed IPM files emissions for VOC, CO, PM_{10}, $PM_{2.5}$, and NH_3 as well as physical characteristic data elements needed for modelling (e.g., county codes, coordinates, and stack parameters).

The base case assumptions between the U.S. and Canadian 2010 and 2020 non-road and non-EGU point source emissions differed slightly as a result of the timing of the generation of these files. The overall impact of these differences is believed to be insignificant and therefore did not warrant the rerun of the emission and air-quality models for this analysis.

4.1.1.3 *Control Case Inventories for 2010 and 2020*

Control cases for Canadian and U.S. emissions are based on proposed legislation or reduction initiatives that would further reduce emissions of contaminants that lead to ambient PM, acid deposition, and ground-level ozone.

CANADA: The control scenario for Canada includes further reductions in 2010 and 2020 emissions of SO_2 and NO_x as part of the Canada-Wide Standards for Particulate Matter and Ozone, and the Canada-Wide Acid Rain Strategy. The 2010 and 2020 emissions were produced by "growing" the 1995 base year inventory to the required years using Environment Canada's CAC forecast. Due to time considerations, the inventory was "grown" by province and sector. Due to a lack of information, the NH_3 portion of the inventory was held constant for the 1995, 2010 and 2020 data years (data on Canadian NH_3 trends for the 1995-2000 period are expected to be available in fall 2004).

UNITED STATES: The control scenario modelled for this analysis is based on the Clear Skies Initiative in the United States. The proposed Clear Skies legislation would create a mandatory program that would reduce power plant emissions of SO_2, NO_x, and mercury by setting a national cap on each pollutant. As in the base case, projection year unit-level output files from the EPA Modelling Applications 2003 version of IPM were generated by the U.S. EPA for the EGU sector control case for 2010 and 2020.

Clear Skies was proposed in response to a growing need for an emission reduction plan that will protect human health and the environment while providing regulatory certainty to the industry. Currently, the Clear Skies initiative has been modified and is now known as the Clean Air Interstate Rule. More information and a complete technical analysis of the 2003 proposed Clear Skies legislation are now available at http://www.epa.gov/clearskies/. Information on the Clean Air Interstate Rule can be found at http://www.epa.gov/air/interstateairquality/index.html.

4.1.2 Processing of Canadian and U.S. Emission Inventories for REMSAD and AURAMS

4.1.2.1 *Processing of Emission Inventories for* REMSAD

The emission files that were used in the REMSAD air-quality model runs were processed through the Sparse Matrix Operator Kernel Emissions (SMOKE) Modelling System for annual meteorological episodes on a 36-km square domain covering Canada and the United States. A description of SMOKE and the formats of its various required inputs can be found at http://www.emc.mcnc.org/products/smoke/.

Modifications were made to the emission-inventory input files processed with SMOKE in order to adjust the emission estimates to better match the regional modelling objectives and spatial scales and to provide a consistent basis between base and projection year modelling results for the development of relative reduction factors (RRF).

One modification to the emissions processed through SMOKE was the application of a crustal PM transport factor to some fugitive dust emissions. The purpose of this subgrid-scale adjustment factor was to account for the fugitive dust that is emitted into the atmosphere but is then removed near the source (i.e., not all suspendable particles are transported long distances: Watson and Chow, 2000; Countess et al., 2001). For the SMOKE input files, a factor of 25 percent (75 percent reduction) was applied to PM_{10} and $PM_{2.5}$ for the SCCs associated with fugitive dust activities in Canada and the United States. In addition, emissions from wind erosion of natural geogenic sources, on-site residential incineration, and forest wildfire emissions were excluded from the modelling files due to their episodic nature or unpredictability in future year emission estimates. This assumption is not unreasonable given that the focus of the future-year scenarios considered in this study are emission control strategies for two PM precursor gases, SO_2 and NO_x. Although prescribed fire activity was capped at base year levels in the U.S. inventory, this practice was not applied to Canadian emissions of the same source category.

A third modification relates to NH_3 emissions. The default seasonal temporal profile for NH_3 emissions from agricultural activities used by SMOKE is uniform or the same for each season, which is clearly unrealistic. This profile was replaced by one from EPA's Office of Research and Development based on the results of inverse modelling using observed NH_4^+ wet concentrations (Gilliland et al., 2003). U.S. NH_3 emissions from livestock activities were seasonally distributed using the new seasonal temporal profile, although this practice was not applied to Canadian emissions of the same source categories (EPA, 2001).

4.1.2.2 *Processing of Emission Inventories for* AURAMS

The Canadian AURAMS model data was processed in a different manner from REMSAD. Due to time and other constraints, the Canadian 1990 emission information that was contained in the model emission files was adjusted to reflect the 1995 Canadian and 1996 U.S. emission inventories by considering provincial and sectoral changes from 1990 to 1995. The result is that emission levels used correspond to 1995 and 1996 levels but the spatial distribution of emissions is based on the 1990 Canadian and U.S. emission inventories. Some of the limitations of this process are that:

- 1990 inventories were distributed more on a population basis than later inventories, which use more spatial gridding surrogates;
- The same scaling factors were applied to all provincial and state sources within sectors, which may have resulted in unrealistic emissions for some sources, given the larger number of point sources in later year inventories.

The AURAMS domain considered is shown in Chapter 5, Figure 5.15. The gas-phase chemistry mechanism considered is the ADOM-II mechanism. As well, six primary PM chemical components are considered: $SO_4^=$, NO_3^-, NH_4^+, BC, OC, and crustal material.

4.1.3 Development and Processing of Emissions used for CMAQ

The emission model selected to provide CMAQ with the required temporal, spatial, and speciation data was SMOKE, version 1.3. To the extent possible, the base year for emission data used in this study was 2000. When year 2000 data were unavailable, 1995 data were "grown" to the year 2000. U.S. data for 1996 were used alongside Canadian data for 1995. U.S. data for 2002 were used together with Canadian data for 2000, and where 2002 data were unavailable, 1999 data were used. Point, area, mobile (including marine), and biogenic emission datasets were prepared (RWDI, 2003a) at a resolution of 4-km. For the 12-km resolution simulations with CMAQ, the emission data were simply aggregated upward. Emission data were assembled for both the summer and winter periods. As with the REMSAD and AURAMS applications, wildfire emissions were not used due to their episodic nature.

It should be noted that there are differences between the lower Fraser Valley emission data used in the model and those in the final version of the GVRD year 2000 inventory. These small differences are the result of updated information and improved emission estimates that were not available at the time of preparation of the model input datasets. To gain insight into the impacts of transboundary transport of air pollutants, two emission scenarios were derived from the 2000 base case emissions. In the first, all U.S. anthropogenic sources were removed while in the second, all Canadian anthropogenic sources were removed (RWDI, 2003b). To gain insight into the impacts on ambient air quality of future emissions, forecasted emission inventories for the years 2010 and 2020 were prepared (RWDI, 2003c).

4.2 DESCRIPTION OF EMISSIONS IN THE UNITED STATES AND CANADA

4.2.1 Emissions Used in AURAMS and REMSAD

Table 4.1 lists the total emissions of $PM_{2.5}$, PM_{10}, PMc (coarse fraction PM) and their precursors for both Canada and the United States on an annual basis, used as input into the REMSAD model. Table 4.2 shows the same numbers for PM and PM precursors, used as input into the AURAMS model. These emissions are aggregated by state and province, and summed to give annual totals for each country. Between the base year of 1996 and the forecasted year 2010, SO_2, NO_x, and VOC emissions are all expected to decrease significantly in both countries, whereas NH_3 emissions are expected to increase slightly in the United States (Canadian NH_3 emissions were held constant). For the future-year scenarios, NO_x and SO_2 emissions in both countries are projected to decrease significantly, while CO, VOCs and NH_3 change only slightly between the base case and control scenarios.

Table 4.1 Country-total anthropogenic emissions for PM and PM precursors on the REMSAD domain for the 1996, 2010 base, 2010 control, 2020 base, and 2020 control inventory scenarios used as REMSAD input. Units are in kilotons per year (and NO_x as NO_2). Note: Canadian 1996 totals do not include point sources.

	Canada					United States				
Pollutant	**1996**	**2010b**	**2010c**	**2020b**	**2020c**	**1996**	**2010b**	**2010c**	**2020b**	**2020c**
CO	12,808	8,266	8,266	9,045	9,045	94,804	87,777	87,785	98,216	98,236
NO_x	3,023	2,262	2,184	2,183	1,994	24,653	17,733	15,968	14,578	12,313
VOC	2,928	2,391	2,370	2,542	2,507	18,245	13,803	13,802	13,899	13,898
NH_3	578	578	578	578	578	4,838	5,001	5,001	5,230	5,230
SO_2	2,563	2,017	1,858	1,843	1,692	18,423	15,306	11,735	14,678	10,074
PM_{10}	5,125	2,194	2,194	2,582	2,582	9,724	9,391	9,391	9,568	9,568
$PM_{2.5}$	1,021	660	660	729	729	3,678	3,358	3,358	3,378	3,378
PMC	4,104	1,534	1,534	1,853	1,853	6,046	6,033	6,033	6,190	6,189

Table 4.2 Country-total anthropogenic emissions for PM and PM precursors on the AURAMS domain for the 1996, 2010 base, 2010 control, 2020 base, and 2020 control inventory scenarios used as AURAMS input. Units are in kilotons per year (and NO_x as NO_2).

	Canada					United States				
Pollutant	**1996**	**2010b**	**2010c**	**2020b**	**2020c**	**1996**	**2010b**	**2010c**	**2020b**	**2020c**
CO	7,916	5,290	5,298	5,797	5,807	73,935	69,201	69,209	77,728	77,746
NO_x	1,461	1,105	1,047	1,009	937	20,116	14,277	12,796	11,726	9,776
VOC	1,440	1,236	1,181	1,343	1,271	14,565	11,110	11,109	11,218	11,217
NH_3	305	305	305	305	305	3,898	4,087	4,087	4,277	4,277
SO_2	1,702	1,520	1,335	1,373	1,165	16,715	13,943	10,424	13,227	8,720
PM_{10}	1,239	1,656	1,654	1,920	1,916	7,172	6,993	6,993	7,149	7,149
$PM_{2.5}$	320	403	401	447	443	2,740	2,494	2,494	2,511	2,511
PMC	919	1,253	1,253	1,473	1,473	4,432	4,499	4,499	4,638	4,638

Emission inputs to REMSAD and AURAMS for SO_2, NO_x, NH_3, $PM_{2.5}$, VOC, CO and PM_{10} for the 1996 base case and the 2010 and 2020 base and control cases are shown visually in Figures 4.1 through 4.7. The anticipated additional U.S. and Canadian control programs result in a significant reduction in SO_2 and NO_x emissions. Summer weekday SO_2 emission input to REMSAD for the 1996 base year is provided in Figure 4.1a. Summer weekday base-case SO_2 emission input to REMSAD for 2010 and 2020 is provided in Figures 4.1b and 4.2a, where summer refers to June, July, and August and summer weekday is an average of Mondays to Fridays throughout these three months. Summer seasonal SO_2 emissions are illustrated because emissions of SO_2 lead to the formation of particle $SO_4^=$ and summer concentrations of $SO_4^=$ exceed winter concentrations. Winter weekday NO_x emissions for the 1996 base year are illustrated in Figure 4.3a. Winter weekday base-case NO_x emission input to REMSAD for 2010 and 2020 are provided in Figures 4.3b and 4.4a. Winter NO_x emissions are shown as NO_x emissions lead to the formation of particle nitrate, and winter ambient concentrations of particle nitrate are higher than summer concentrations. Summer and winter NH_3 emissions for the 1996 base year are shown in Figures 4.5a and 4.5b. Summer base-case NH_3 emission inputs for 2010 and 2020 are provided in Figures 4.6a and 4.7a. Emissions of ammonia are significant due to the role of ammonia in the formation of ammonium sulphate and ammonium nitrate.

The reduction in summer weekday SO_2 emissions with the additional U.S. and Canadian controls for 2010 and 2020 are shown in Figures 4.1c and 4.2b. The reduction in winter weekday NO_x emissions with the additional U.S. and Canadian controls are shown in Figures 4.3c and 4.4b. Only reductions for these two PM precursors are shown because the additional control measures for 2020, discussed in Section 4.1.1.3, are concerned only with these two pollutants (plus mercury for the proposed Clear Skies legislation). Note that the reductions in both SO_2 and NO_x are concentrated in the eastern half of the domain, which suggests that the atmospheric response to these reductions will also be concentrated in this region. Winter base-case NH_3 emission inputs for 2010 and 2020 are provided in Figures 4.6b and 4.7b. The emissions of NH_3 in the winter season are significant because they are involved with the reaction of NO_x emissions to form particle ammonium nitrate. Winter NH_3 emission inputs are significantly less than summer NH_3 emission inputs, particularly in the U.S. portion of the domain.

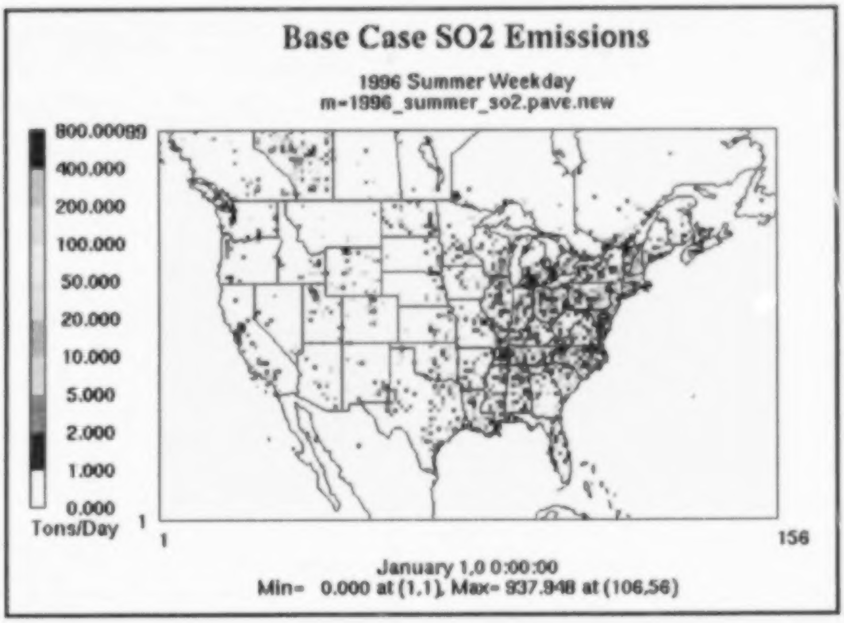
Base Case SO2 Emissions
1996 Summer Weekday
m-1996_summer_so2.pave.new
800.00089
400.000
200.000
100.000
50.000
20.000
10.000
5.000
2.000
1.000
0.000
Tons/Day
1
1
156
January 1,0 0:00:00
Min= 0.000 at (1,1), Max= 937.948 at (106,56)

Figure 4.1a - 1996 Summer weekday SO_2 emissions for Canada and the United States

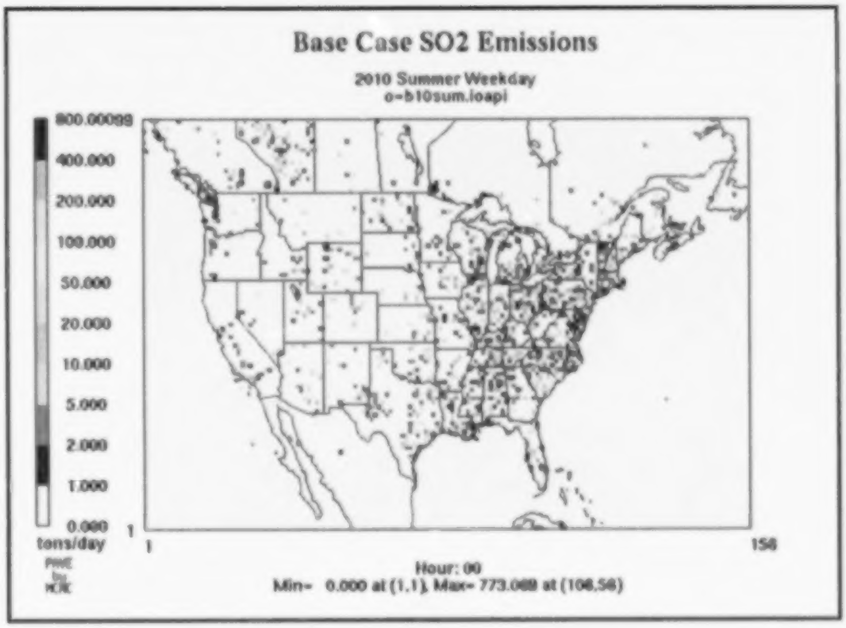
Base Case SO2 Emissions
2010 Summer Weekday
o-b10sum.ioapi
800.000 99
400.000
200.000
100.000
50.000
20.000
10.000
5.000
2.000
1.000
0.000
tons/day
1
1
156
PAVE by MCNC
Hour: 00
Min= 0.000 at (1,1), Max= 773.089 at (106,56)

Figure 4.1b - 2010 Summer weekday base case SO_2 emissions for Canada and the United States

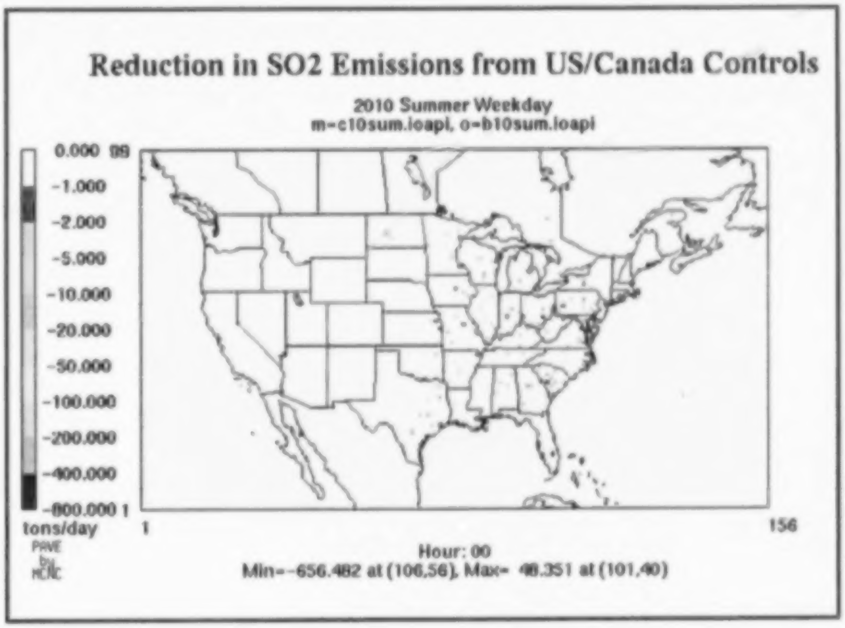
Reduction in SO2 Emissions from US/Canada Controls
2010 Summer Weekday
m-c10sum.ioapi, o-b10sum.ioapi
0.000 98
-1.000
-2.000
-5.000
-10.000
-20.000
-50.000
-100.000
-200.000
-400.000
-800.000 1
tons/day
1
156
PAVE by MCNC
Hour: 00
Min=-656.482 at (106,56), Max= 48.351 at (101,40)

Figure 4.1c - 2010 Summer weekday reductions in SO_2 emissions for Canada and the United States

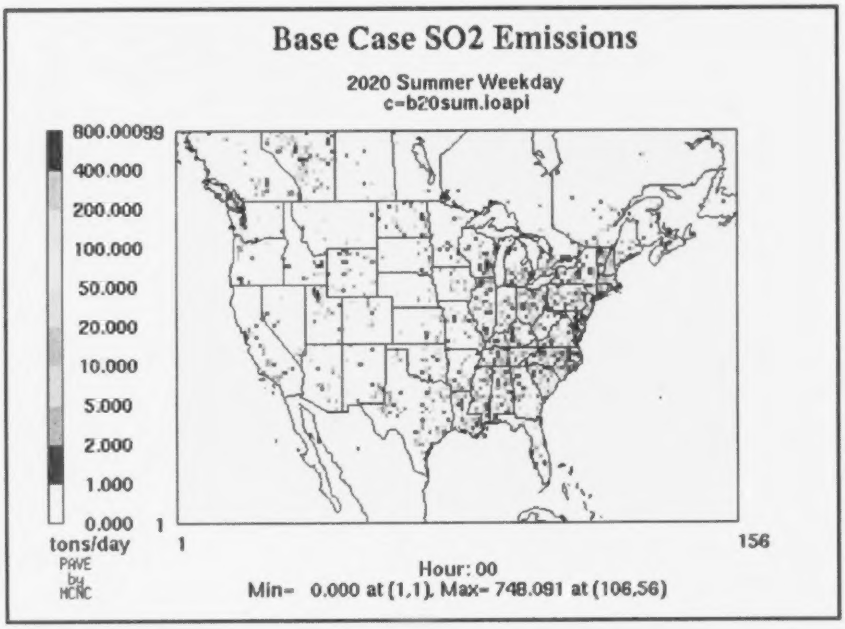
Base Case SO2 Emissions
2020 Summer Weekday
c=b20sum.ioapi
800.000
99
400.000
200.000
100.000
50.000
20.000
10.000
5.000
2.000
1.000
0.000
1
tons/day
PAVE
by
MCNC
1
156
Hour: 00
Min= 0.000 at (1,1), Max= 748.091 at (106,56)

Figure 4.2a - 2020 Summer weekday base case SO_2 emissions for Canada and the United States.

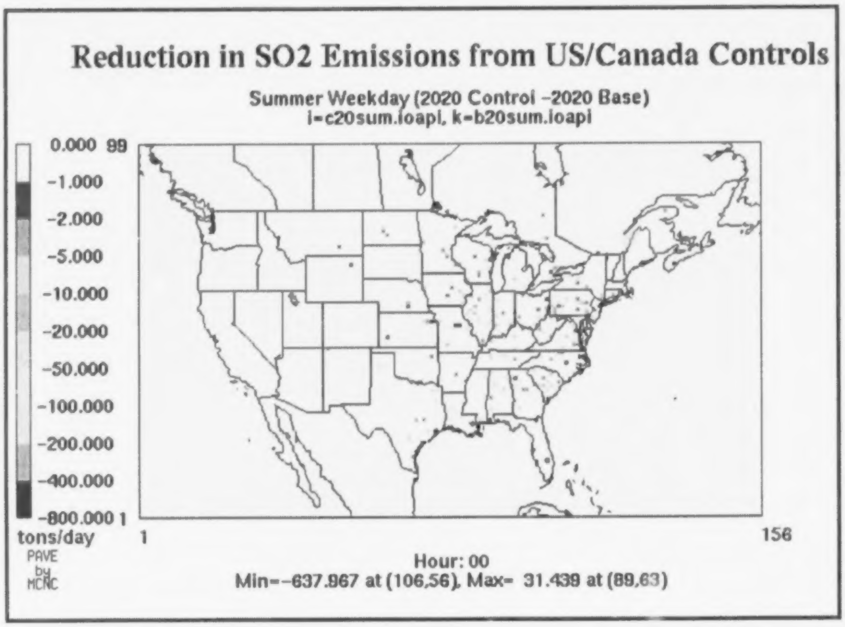
Reduction in SO2 Emissions from US/Canada Controls
Summer Weekday (2020 Control -2020 Base)
i=c20sum.ioapi, k=b20sum.ioapi
0.000
99
-1.000
-2.000
-5.000
-10.000
-20.000
-50.000
-100.000
-200.000
-400.000
-800.000
1
tons/day
PAVE
by
MCNC
1
156
Hour: 00
Min=-637.967 at (106,56), Max= 31.439 at (89,63)

Figure 4.2b - 2020 Summer weekday reductions in SO_2 emissions for Canada and the United States.

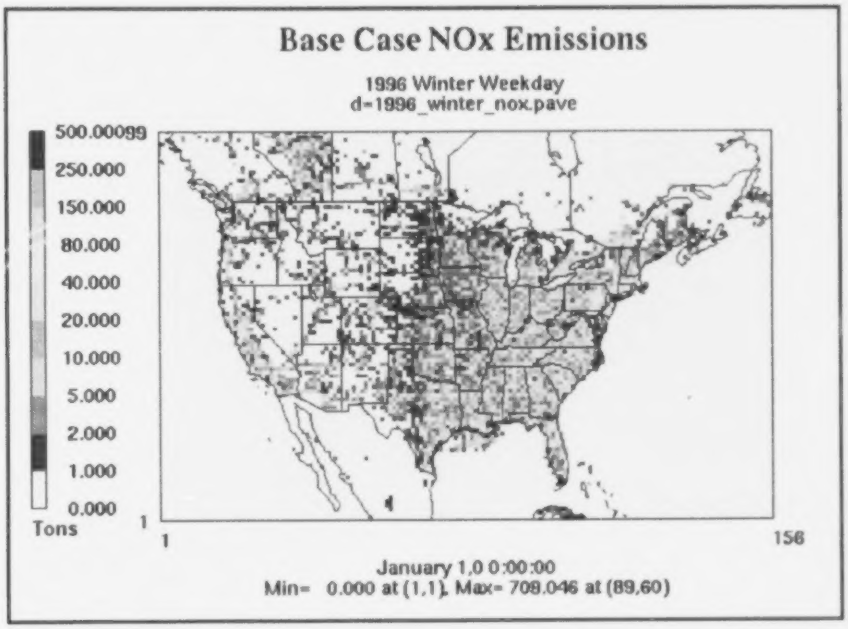
Base Case NOx Emissions
1996 Winter Weekday
d=1996_winter_nox.pave
500.00099
250.000
150.000
80.000
40.000
20.000
10.000
5.000
2.000
1.000
0.000
Tons
1
1
156
January 1,0 0:00:00
Min= 0.000 at (1,1), Max= 708.046 at (89,60)

Figure 4.3a - 1996 Winter weekday NO_x emissions for Canada and the United States

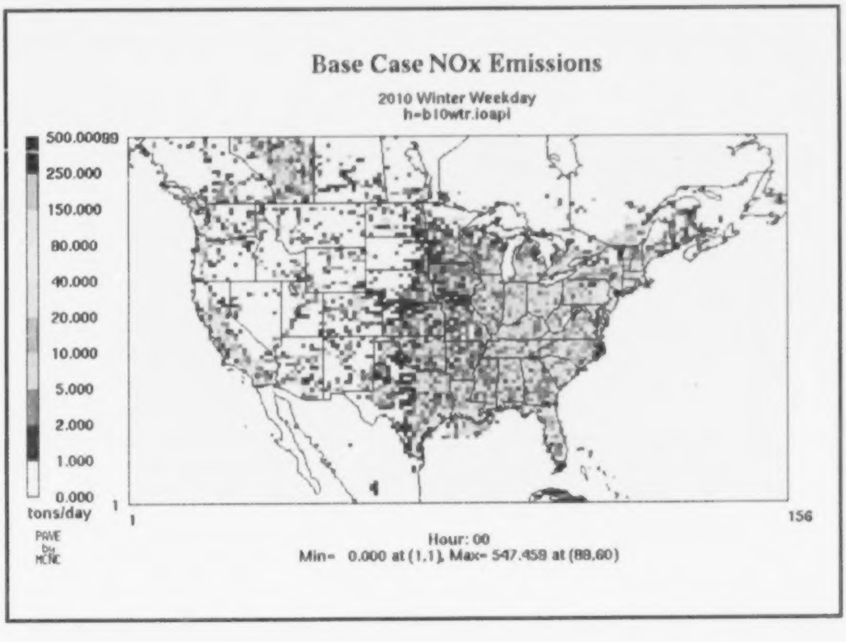
Base Case NOx Emissions
2010 Winter Weekday
h=b10wtr.ioapi
500.00099
250.000
150.000
80.000
40.000
20.000
10.000
5.000
2.000
1.000
0.000
tons/day
PAVE by MCNC
1
1
156
Hour: 00
Min= 0.000 at (1,1), Max= 547.459 at (88,60)

Figure 4.3b - 2010 Winter weekday base case NO_x emissions for Canada and the United States

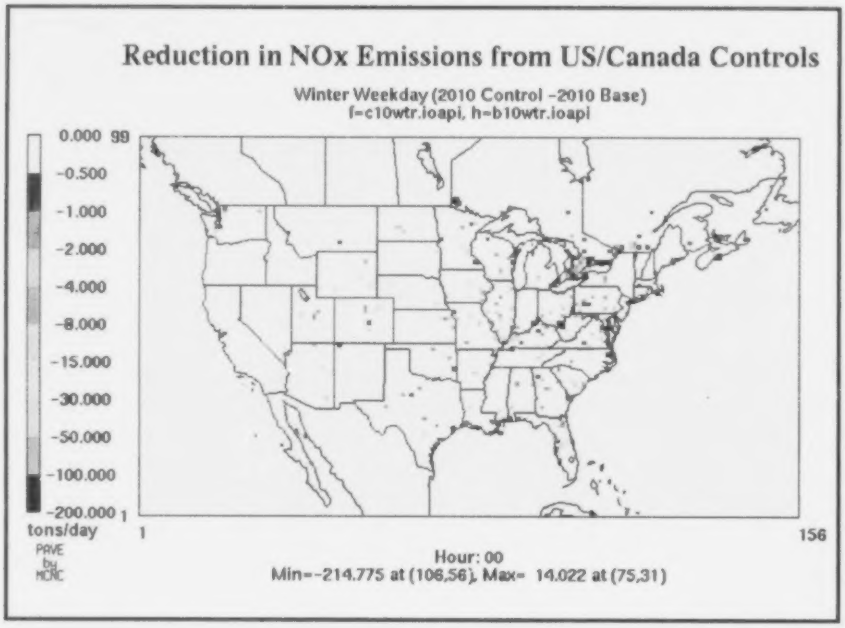
Reduction in NOx Emissions from US/Canada Controls
Winter Weekday (2010 Control -2010 Base)
f=c10wtr.ioapi, h=b10wtr.ioapi
0.000
-0.500
-1.000
-2.000
-4.000
-8.000
-15.000
-30.000
-50.000
-100.000
-200.000
tons/day
PAVE by MCNC
99
1
1
156
Hour: 00
Min=-214.775 at (106,56), Max= 14.022 at (75,31)

Figure 4.3c - 2010 Winter weekday reductions in NO_x emissions for Canada and the United States.

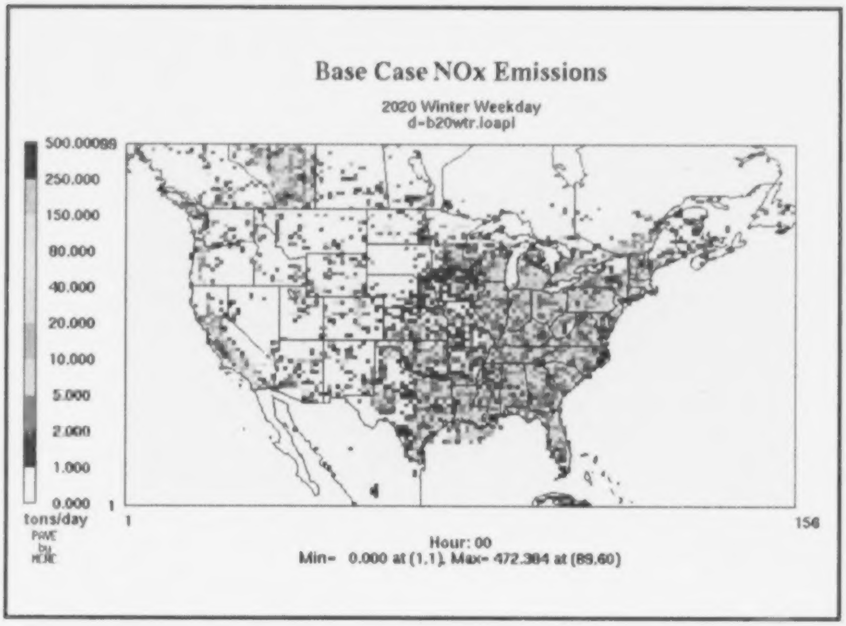
Base Case NOx Emissions
2020 Winter Weekday
d=b20wtr.ioapi
500.00099
250.000
150.000
80.000
40.000
20.000
10.000
5.000
2.000
1.000
0.000
tons/day
PAVE by MCNC
1
1
156
Hour: 00
Min= 0.000 at (1,1), Max= 472.384 at (89,60)

Figure 4.4a - 2020 Winter weekday base case NO_x emissions for Canada and the United States.

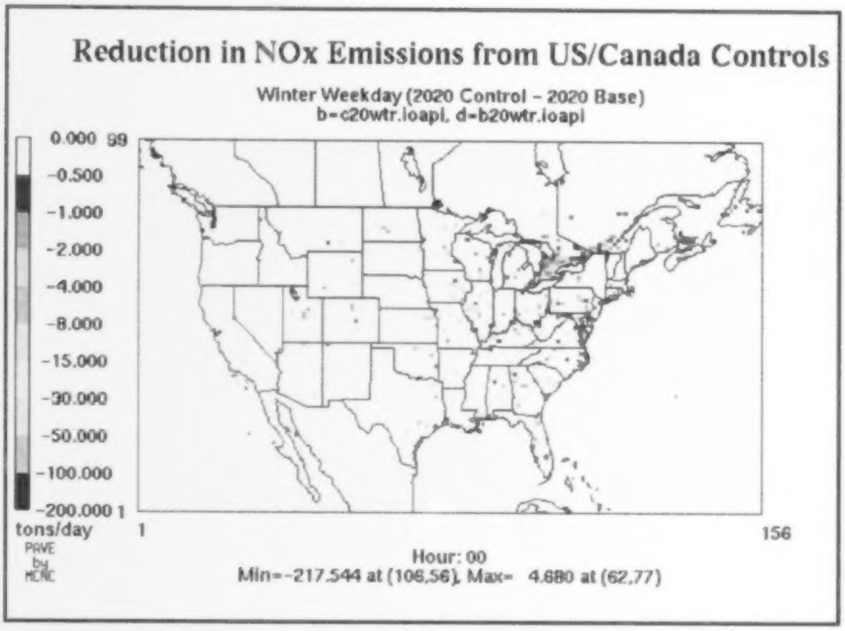
Reduction in NOx Emissions from US/Canada Controls
Winter Weekday (2020 Control - 2020 Base)
b=c20wtr.ioapi, d=b20wtr.ioapi
0.000 99
-0.500
-1.000
-2.000
-4.000
-8.000
-15.000
-30.000
-50.000
-100.000
-200.000 1
tons/day
PAVE by MCNC
1
156
Hour: 00
Min=-217.544 at (106,56), Max= 4.680 at (62,77)

Figure 4.4b - 2020 Winter weekday reductions in NO_x emissions for Canada and the United States

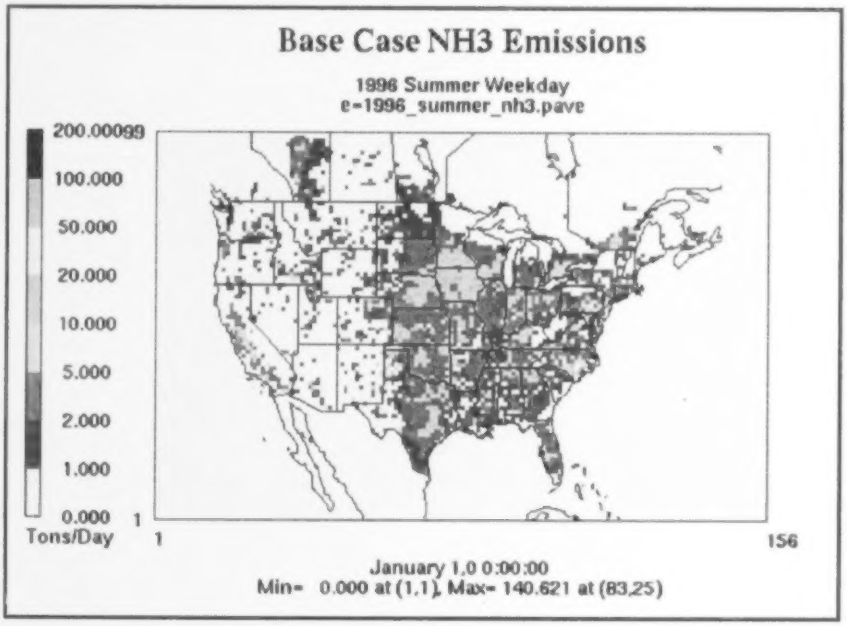
Base Case NH3 Emissions
1996 Summer Weekday
e=1996_summer_nh3.pave
200.00099
100.000
50.000
20.000
10.000
5.000
2.000
1.000
0.000 1
Tons/Day
1
156
January 1,0 0:00:00
Min= 0.000 at (1,1), Max= 140.621 at (83,25)

Figure 4.5a - 1996 Summer weekday NH_3 emissions for Canada and the United States.

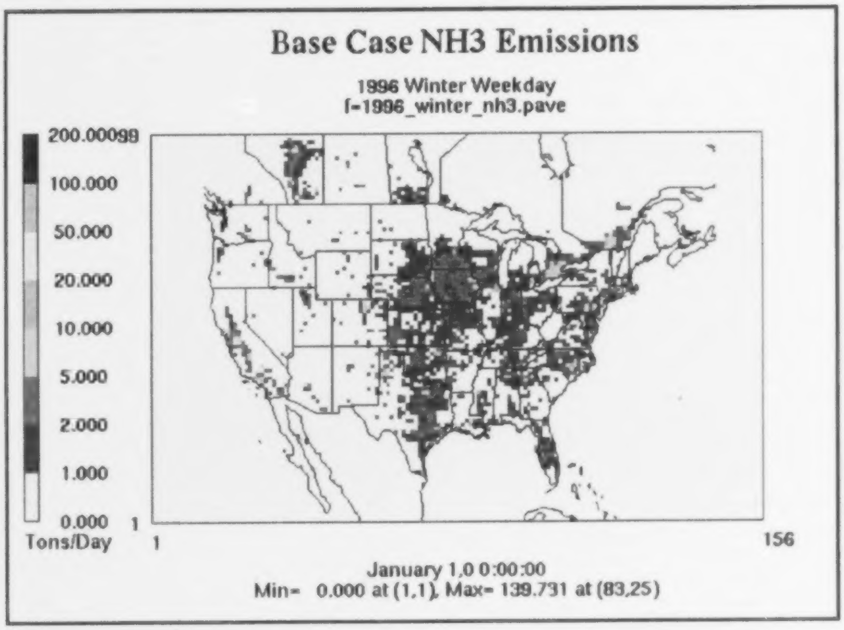
Base Case NH3 Emissions
1996 Winter Weekday
f=1996_winter_nh3.pave
200.00099
100.000
50.000
20.000
10.000
5.000
2.000
1.000
0.000
Tons/Day
1
1
156
January 1,0 0:00:00
Min= 0.000 at (1,1), Max= 139.731 at (83,25)

Figure 4.5b - 1996 Winter weekday NH_3 emissions for Canada and the United States.

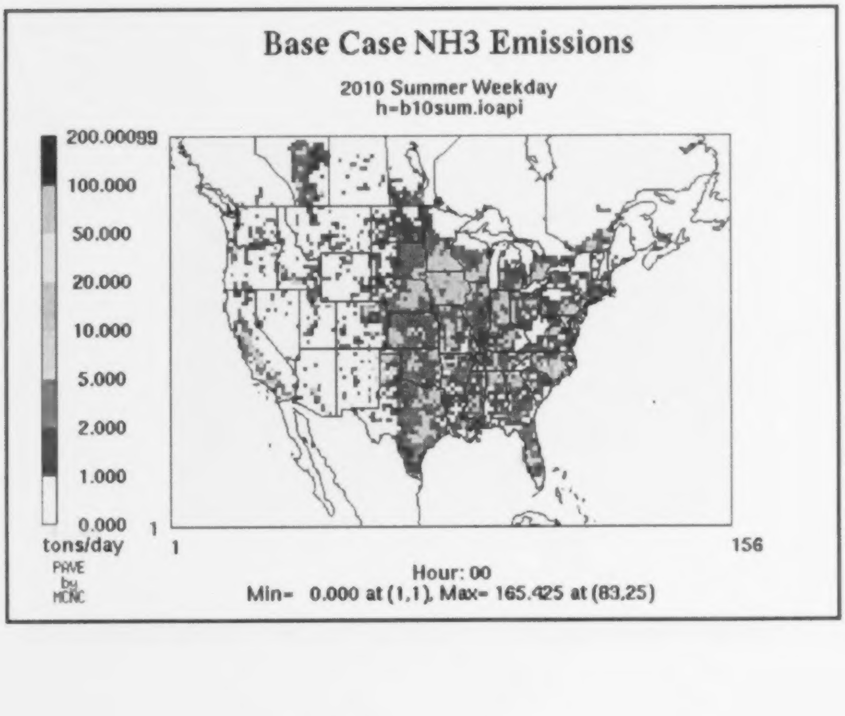
Base Case NH3 Emissions
2010 Summer Weekday
h=b10sum.ioapi
200.00099
100.000
50.000
20.000
10.000
5.000
2.000
1.000
0.000
tons/day
PAVE by MCNC
1
1
156
Hour: 00
Min= 0.000 at (1,1), Max= 165.425 at (83,25)

Figure 4.6a - 2010 Summer weekday base case NH_3 emissions for Canada and the United States.

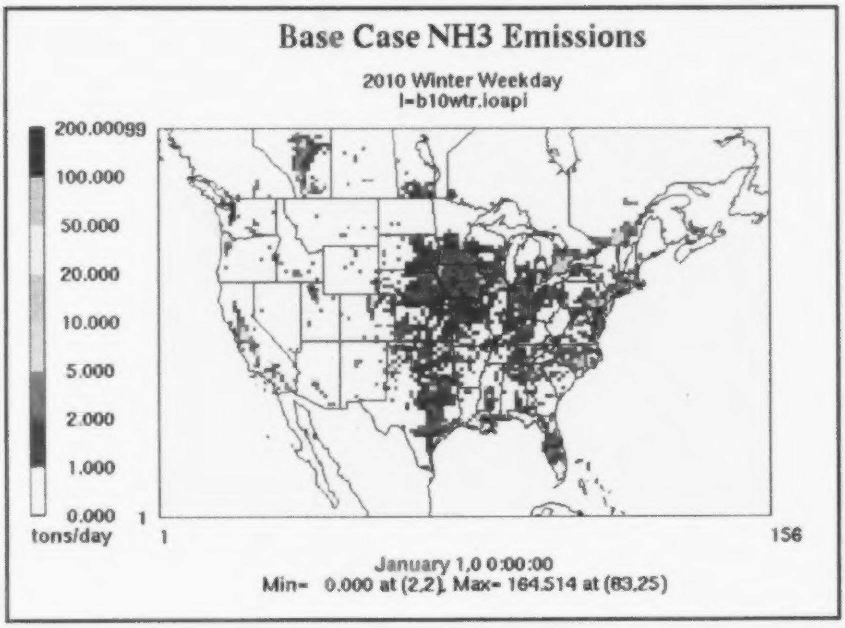
Base Case NH3 Emissions
2010 Winter Weekday
l=b10wtr.ioapi
200.00099
100.000
50.000
20.000
10.000
5.000
2.000
1.000
0.000
tons/day
1
1
156
January 1,0 0:00:00
Min= 0.000 at (2,2), Max= 164.514 at (83,25)

Figure 4.6b - 2010 Winter weekday base case NH_3 emissions for Canada and the United States.

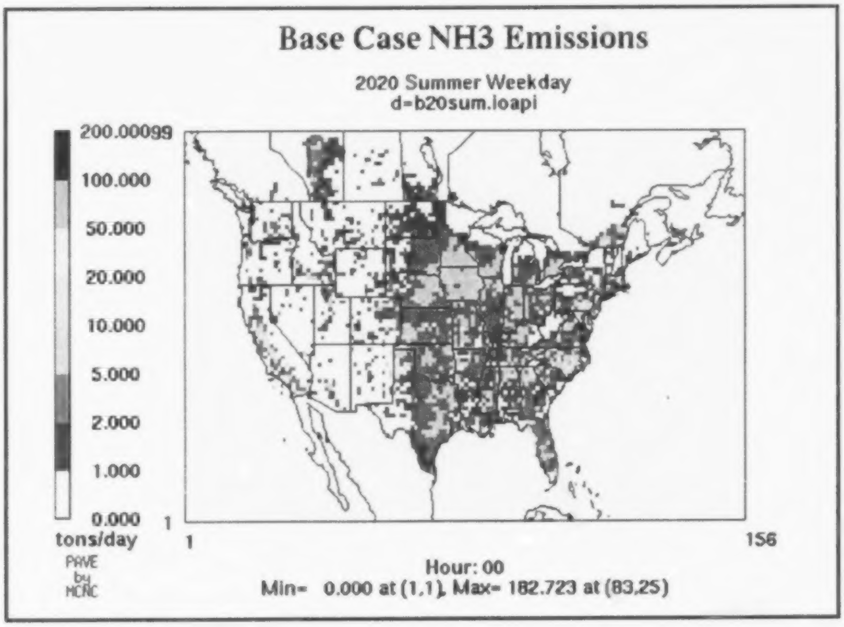
Base Case NH3 Emissions
2020 Summer Weekday
d=b20sum.ioapi
200.00099
100.000
50.000
20.000
10.000
5.000
2.000
1.000
0.000
tons/day
PAVE by MCNC
1
1
156
Hour: 00
Min= 0.000 at (1,1), Max= 182.723 at (83,25)

Figure 4.7a - 2020 Summer weekday base case NH_3 emissions for Canada and the United States

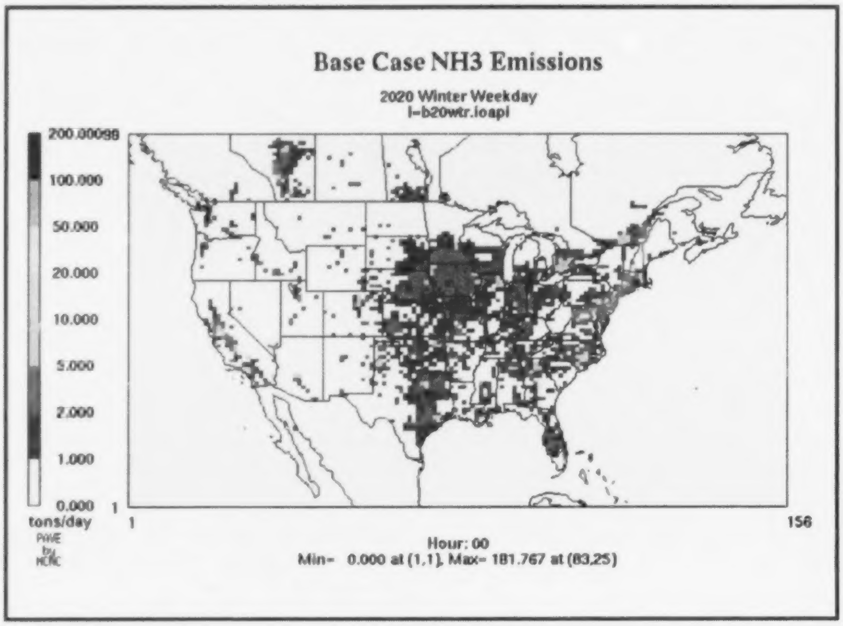
Base Case NH3 Emissions
2020 Winter Weekday
l-b20wtr.ioapi
200.00098
100.000
50.000
20.000
10.000
5.000
2.000
1.000
0.000
tons/day
PAVE by MCNC
1
1
156
Hour: 00
Min= 0.000 at (1,1), Max= 181.767 at (83,25)

Figure 4.7b - 2020 Winter weekday base case NH_3 emissions for Canada and the United States.

4.3 KEY SCIENCE MESSAGES

- Emission inventory information was combined for both Canada and the United States to provide input to two multi-pollutant models (AURAMS and REMSAD) for both base case and control scenarios for the years 2010 and 2020.
- Emissions of SO_2 and NO_x are projected to decrease while NH_3, VOCs and CO increase in the future-year base cases. SO_2 and NO_x emissions are projected to decrease further with the future-year control scenarios (2010 and 2020).
- Emissions of SO_2 and NO_x under all considered scenarios are concentrated in the Industrial Midwest, Northeastern United States and Southern Ontario, while emissions of NH_3 are typically concentrated further west in the central Midwest region.
- The emissions of SO_2, NO_x and NH_3, and their contributions to $PM_{2.5}$ levels vary seasonally. NH_3 emissions and biogenic NO_x (and VOC) emissions have the largest seasonal variations.

CHAPTER 5

AIR-QUALITY MODEL APPLICATIONS

Three emission-based PM air-quality models have been applied to address Objective 7 of this Assessment: *"To identify the impact of current and proposed emission reduction scenarios on fine PM levels in North America"*. The first air-quality model, REMSAD, was run for one year (1996) for a domain including the 48 contiguous U.S. states, southern Canada, and northern Mexico for the 1996 base case and four future-year emission control strategy scenarios (described in Chapter 4). REMSAD-predicted fields are presented for January and July 1996 as well as for the entire year to illustrate the impact of seasonality on $PM_{2.5}$ mass and chemical composition for the different scenarios. The second model, AURAMS, was run for the same five scenarios as REMSAD for one 2-week winter period and one 2-week summer period on a domain roughly corresponding to the eastern half of the REMSAD domain. As recommended in the NARSTO PM Assessment (Seigneur and Moran, 2003), the application of two different air-quality models to the same scenarios permits the similarity and consistency of the predictions of both models to be examined. The third model, CMAQ, was used on a smaller domain to investigate both (a) a base scenario and two future-year emission scenarios and (b) the role of transboundary transport in the western border region comprised of Washington state and southwestern British Columbia. A winter period and a summer period were considered using CMAQ.

As discussed in Chapter 4, the two pairs of future-year emission control strategy scenarios considered by REMSAD and AURAMS differed principally in the emissions of two PM gaseous precursors, SO_2 and NO_x. Emissions of VOCs, CO, NH_3, and primary PM changed by less than 1 percent between the 2010 and 2020 scenario pairs (see Tables 4.1 and 4.2). As a consequence, the analysis of the model results presented for REMSAD and AURAMS focus on changes in total $PM_{2.5}$ mass and on three inorganic PM components: SO_4, NO_3, and NH_4. Concentrations of other PM chemical components such as crustal material and black carbon should not differ for these scenarios, although secondary organic aerosol formation can be indirectly affected through the impact of NO_x emission changes on oxidant concentrations. For the CMAQ future-year emission scenarios, on the other hand, emissions of both primary PM and PM gaseous precursors were changed, so attention is focused on predicted changes in $PM_{2.5}$ total mass.

Results from REMSAD and AURAMS are presented first followed by results from CMAQ. REMSAD and AURAMS model predictions are compared with ambient measurements for the base case scenario in the Appendix in order to provide an indication of model skill and the uncertainty associated with predictions of different PM components. The model results in general are in agreement with the recent conclusions of Seigneur and Moran (2003), that state-of-the-science PM air quality models perform reasonably well in predicting the inorganic chemical components of $PM_{2.5}$, with greater certainty for $SO_4^=$ than for NH_4^+ (due to greater emissions uncertainties) and NO_3^- (due to complexities of gas-particle partitioning for this semi-volatile component).

5.1 RESULTS OF REMSAD CONTROL STRATEGY MODELLING

The Regional Modelling System for Aerosols and Deposition (REMSAD) Version 7.06 (ICF Kaiser, 2002) model was used as a tool for simulating base year and future air quality concentrations. Five one-year model runs were performed with REMSAD using 1996 meteorology. These runs were: (1) 1996 base case, (2) 2010 base case, (3) 2020 base case, (4) 2010 control case, and (5) 2020 control case. The 1996 base case results were used to evaluate the performance of REMSAD in predicting observed concentrations in 1996. The results of this model performance evaluation are provided in the Appendix. Existing controls (i.e. legislation/ agreements) in each country were included in the 2010 and 2020 base case runs while the 2010 and 2020 control runs contain additional anticipated controls for each country (as described in Chapter 4). The REMSAD model was used to estimate hourly air-quality concentrations and acid deposition for an entire year for each model run. This section reports results for the 2010 annual $PM_{2.5}$ concentration and the 2020 annual, January, and July $PM_{2.5}$, $SO_4^=$, NO_3^-, and NH_4^+ concentrations. The modelling domain used in REMSAD is shown in Figure 5.1.

5.1.1 REMSAD Results

Annual average ambient $PM_{2.5}$ concentrations for the 2010 base case are provided in Figure 5.2a while annual, January, and July average $PM_{2.5}$ concentrations for the 2020 base case are provided in Figures 5.3a, 5.4a, and 5.5a. Annual, January, and July average particle $SO_4^=$ concentrations for the 2020 base case are provided in Figures 5.6a, 5.7a, and 5.8a and annual, January, and July average particle NO_3^- concentrations for the 2020 base case are shown in Figures 5.9a, 5.10a, and 5.11a. Annual, January, and July average NH_4^+ concentrations for the 2020 base case are illustrated in Figures 5.12a, 5.13a, and 5.14a. Figure 5.2b shows annual average $PM_{2.5}$ air quality concentration reductions for 2010 that result from the implementation of controls in the United States and Canada. Annual, January, and July average $PM_{2.5}$ concentration reductions for the 2020 scenario are provided in Figures 5.3b, 5.4b, and 5.5b. Annual, January, and July average $SO_4^=$ concentration reductions that result from U.S. and Canadian controls in 2020 are shown in Figures 5.6b, 5.7b and 5.8b while Figures 5.9b, 5.10b, and 5.11b illustrate annual, January, and July average particle NO_3^- concentration reductions that result from U.S. and Canadian controls in 2020. Annual, January, and July average NH_4^+ concentration reductions that result from the 2020 controls are shown in Figures 5.12b, 5.13b and 5.14b. Many control measures already underway

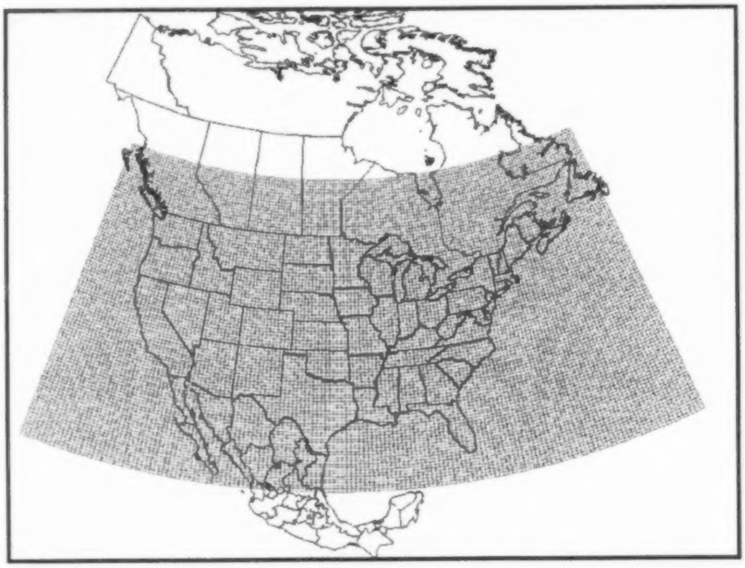

Figure 5.1 - REMSAD modelling domain (~36x36 km^2). Grid squares encompass 1/2 degree longitude, 1/3 degree latitude. E-W range: 54 degrees W - 132 degrees W; N-S range: 22 degrees N - 55 degrees N. Vertical extent: Ground to 16,200 meters (100mb) with 12 layers.

are incorporated into the 2010 and 2020 base case air quality results while the reductions predicted by the model result from additional U.S. and Canadian controls that are expected to be implemented.

In the 2010 and 2020 base cases, areas of the United States and Canada are above the U.S. annual air-quality standard of 15 µg/m^3. Some of the higher $PM_{2.5}$ concentrations in large Canadian cities result from a large quantity of unpaved road dust emissions being spatially allocated by population. This could be corrected by spatially allocating these emissions to actual unpaved roadways. U.S. and Canadian controls that are expected to be implemented result in a maximum annual $PM_{2.5}$ reduction of 1.8 µg/m^3 in 2010 and 2.3 µg/m^3 in 2020 with the maximum annual reductions predicted in Pennsylvania. Larger reductions in $PM_{2.5}$ concentrations occur however, over shorter averaging periods. The spatial pattern for the January average 2020 control case reduction of $PM_{2.5}$ mass is similar to the spatial pattern for the January particle NO_3^- reduction while the spatial pattern for the July average 2020 control case reduction of $PM_{2.5}$ is similar to the spatial pattern for the $SO_4^=$ reduction. The maximum January average $PM_{2.5}$ reduction in 2020 is 1.8 µg/m^3 and the maximum reduction in July average $PM_{2.5}$ mass is 3.3 µg/m^3. The 2010 and 2020 control cases will result in significantly more areas below the U.S. annual standard of 15 µg/m^3, but several areas in the eastern United States and Canada will remain above the U.S. standard.

The base case maximum annual $SO_4^=$ concentration in 2020 is predicted to be 4.9 µg/m^3. U.S. and Canadian controls that are expected to be implemented in 2020 result in annual reductions of $SO_4^=$ concentrations of up to 1.4 µg/m^3 with the maximum reductions predicted in Pennsylvania. $SO_4^=$ concentrations and predicted reductions in $SO_4^=$ with the additional U.S. and Canadian controls are much higher in July than in January. The maximum base case 2020 January average $SO_4^=$ air quality concentration is predicted to be 2.3 µg/m^3 while the maximum July average $SO_4^=$ concentration is predicted to be 7.0 µg/m^3. The 2020 control case results in a maximum reduction of January average $SO_4^=$ concentration of 0.6 µg/m^3 and a maximum reduction of July average $SO_4^=$ concentrations of 2.4 µg/m^3.

The maximum annual particle NO_3^- concentration in 2020 is predicted to be 4.2 µg/m^3. U.S. and Canadian controls that are expected to be implemented result in annual reductions of particle NO_3^- concentrations up to 0.6 µg/m^3 in 2020 with the maximum annual reduction located in Indiana. Particle NO_3^- concentrations and the corresponding reduction in particle NO_3^- with the additional U.S. and Canadian controls are much higher in January than July. The maximum base case 2020 January average particle NO_3^- concentration is predicted to be 5.9 µg/m^3 and the maximum July average particle NO_3^- concentration is predicted to be 2.4 µg/m^3. The 2020 control case results in a maximum reduction of January average particle NO_3^- concentrations of 1.1 µg/m^3 and a maximum reduction of July average particle NO_3^- concentrations of 0.4 µg/m^3.

The maximum annual NH_4^+ concentration is 2.8 µg/m^3 in 2020. U.S. and Canadian controls that are expected to be implemented result in predicted annual reductions of NH_4^+ concentrations of up to 0.6 µg/m^3 in 2020 with the maximum annual reductions predicted in Pennsylvania. The spatial pattern of NH_4^+ concentration reductions is similar to the spatial pattern of particle NO_3^- concentration reductions in January and close to the spatial pattern of sulphate concentration reductions in July. This is a result of the majority of NH_4^+ in winter being associated with NH_4NO_3 and the majority of NH_4^+ in the summer being associated with $(NH_4)_2SO_4$. Larger reductions in NH_3 with the additional U.S. and Canadian controls in 2020 will occur in the summer than in the winter. The 2020 control case results in a maximum January NH_4^+ concentration reduction of 0.4 µg/m^3 and a July maximum reduction of 0.8 µg/m^3. The REMSAD results are consistent with known atmospheric chemistry relationships between $SO_4^=$, NO_3^- and NH_4^+ in both the summer and the winter seasons.

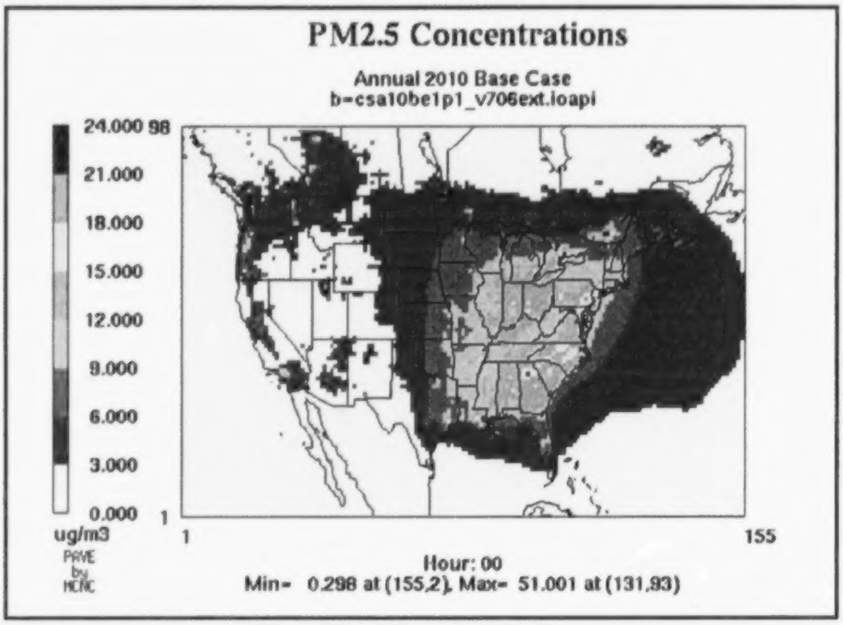
PM2.5 Concentrations
Annual 2010 Base Case
b=csa10be1p1_v706ext.ioapi
24.000 98
21.000
18.000
15.000
12.000
9.000
6.000
3.000
0.000
ug/m3
PAVE by MCNC
1
1
155
Hour: 00
Min= 0.298 at (155,2), Max= 51.001 at (131,93)

Figure 5.2a - Annual average $PM_{2.5}$ concentrations 2010 base case.

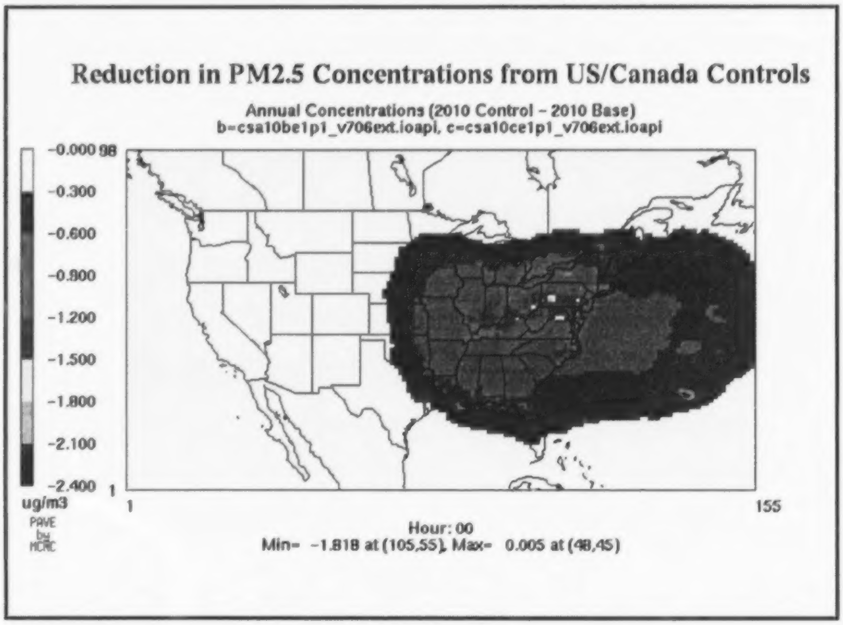
Reduction in PM2.5 Concentrations from US/Canada Controls
Annual Concentrations (2010 Control - 2010 Base)
b=csa10be1p1_v706ext.ioapi, c=csa10ce1p1_v706ext.ioapi
-0.000 98
-0.300
-0.600
-0.900
-1.200
-1.500
-1.800
-2.100
-2.400
ug/m3
PAVE by MCNC
1
1
155
Hour: 00
Min= -1.818 at (105,55), Max= 0.005 at (48,45)

Figure 5.2b - Reductions in annual $PM_{2.5}$ concentrations from controls in 2010

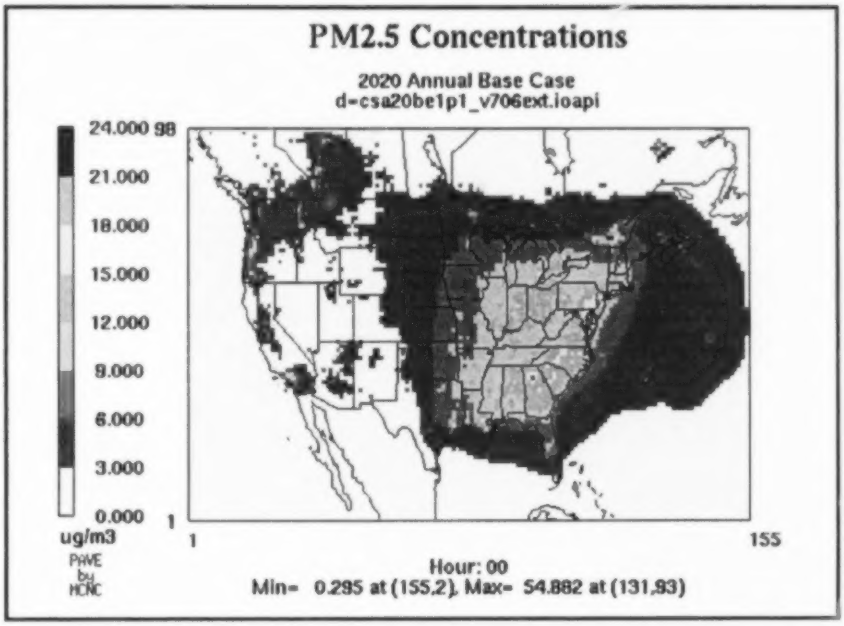
PM2.5 Concentrations
2020 Annual Base Case
d=csa20be1p1_v706ext.ioapi
24.000
21.000
18.000
15.000
12.000
9.000
6.000
3.000
0.000
ug/m3
98
1
1
155
PAVE by MCNC
Hour: 00
Min= 0.295 at (155,2), Max= 54.882 at (131,93)

Figure 5.3a - Annual average PM$_{2.5}$ concentrations 2020 base case.

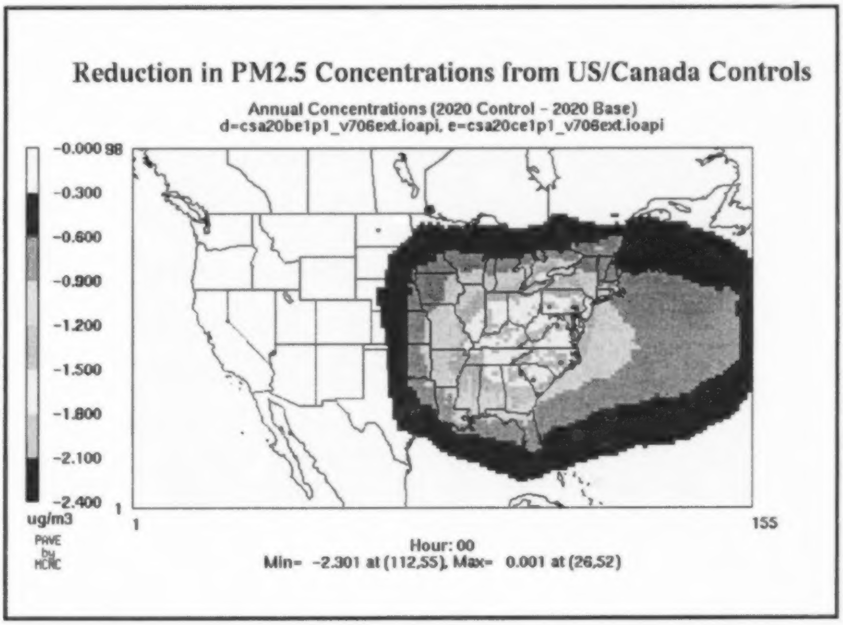
Reduction in PM2.5 Concentrations from US/Canada Controls
Annual Concentrations (2020 Control - 2020 Base)
d=csa20be1p1_v706ext.ioapi, e=csa20ce1p1_v706ext.ioapi
-0.000
-0.300
-0.600
-0.900
-1.200
-1.500
-1.800
-2.100
-2.400
ug/m3
98
1
1
155
PAVE by MCNC
Hour: 00
Min= -2.301 at (112,55), Max= 0.001 at (26,52)

Figure 5.3b - Reductions in annual PM$_{2.5}$ concentrations from controls in 2020

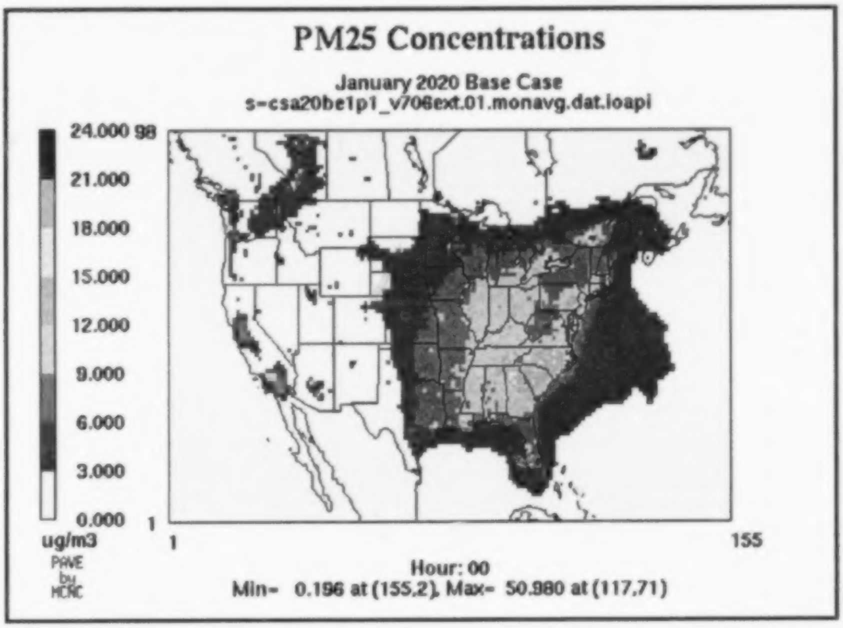
PM25 Concentrations
January 2020 Base Case
s=csa20be1p1_v706ext.01.monavg.dat.ioapi
24.000
21.000
18.000
15.000
12.000
9.000
6.000
3.000
0.000
ug/m3
98
1
1
155
PAVE by MCNC
Hour: 00
Min= 0.196 at (155,2), Max= 50.980 at (117,71)

Figure 5.4a - January average $PM_{2.5}$ concentrations 2020 base case.

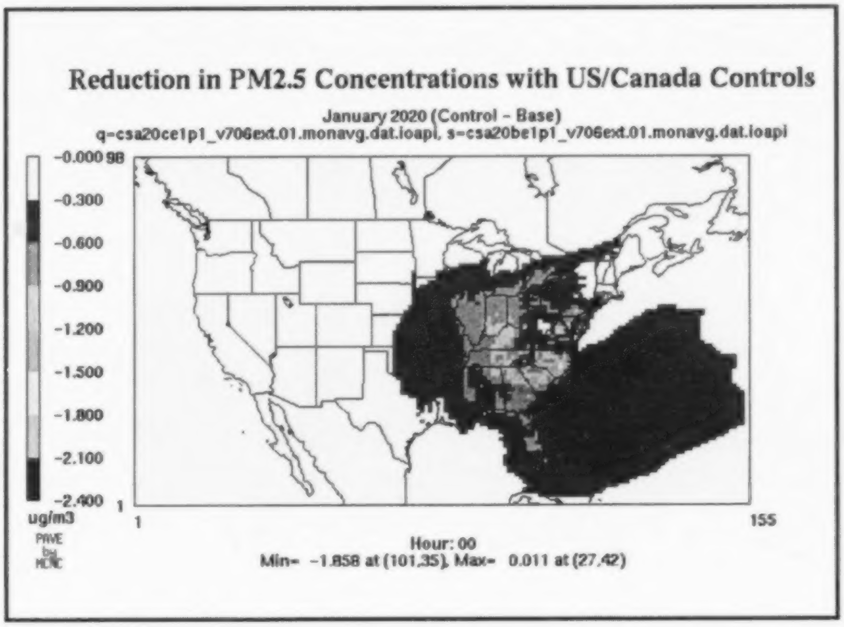
Reduction in PM2.5 Concentrations with US/Canada Controls
January 2020 (Control - Base)
q=csa20ce1p1_v706ext.01.monavg.dat.ioapi, s=csa20be1p1_v706ext.01.monavg.dat.ioapi
-0.000
-0.300
-0.600
-0.900
-1.200
-1.500
-1.800
-2.100
-2.400
ug/m3
98
1
1
155
PAVE by MCNC
Hour: 00
Min= -1.858 at (101,35), Max= 0.011 at (27,42)

Figure 5.4b - Reductions in January $PM_{2.5}$ concentrations from controls in 2020

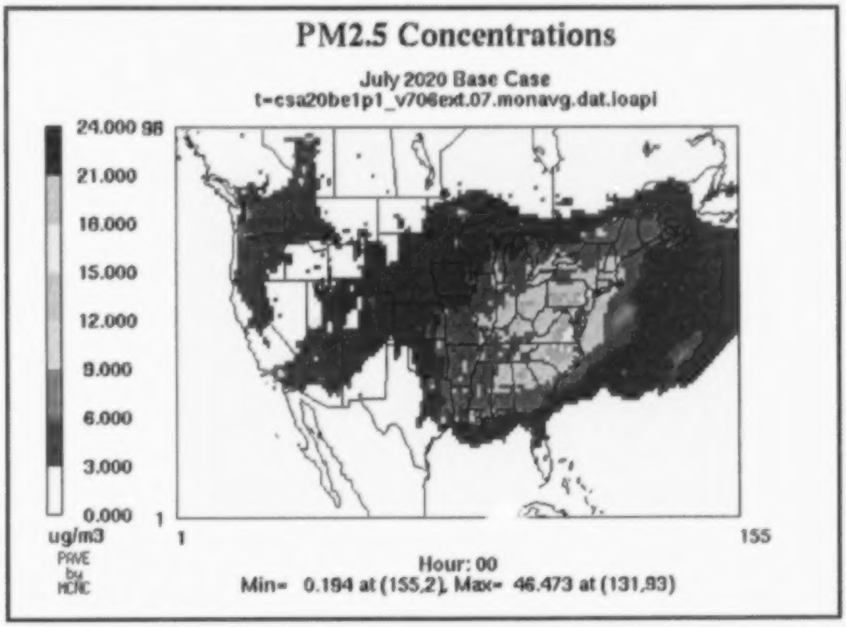
PM2.5 Concentrations
July 2020 Base Case
t=csa20be1p1_v706ext.07.monavg.dat.ioapi
24.000
21.000
18.000
15.000
12.000
9.000
6.000
3.000
0.000
ug/m3
PAVE by MCNC
96
1
1
155
Hour: 00
Min= 0.194 at (155,2), Max= 46.473 at (131,93)

Figure 5.5a - July average $PM_{2.5}$ concentrations 2020 base case.

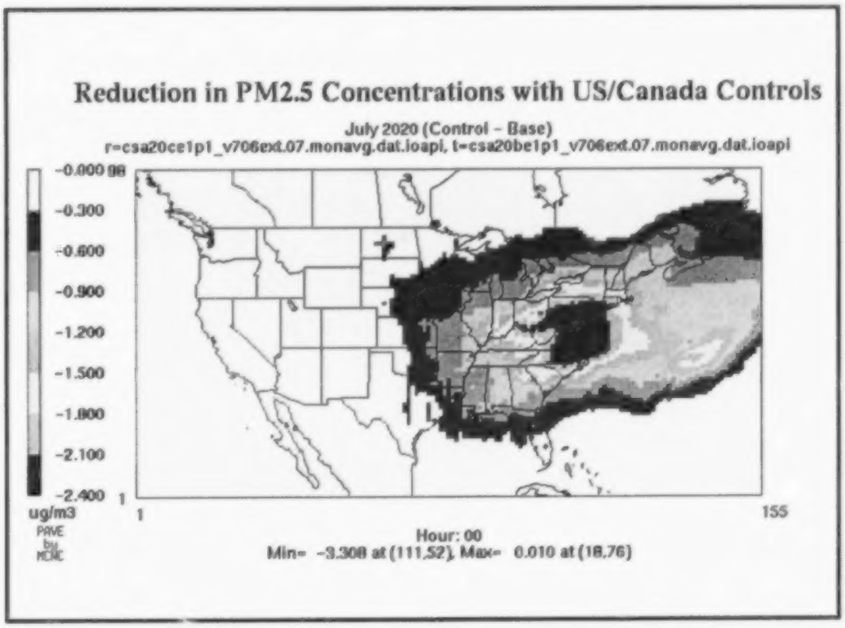
Reduction in PM2.5 Concentrations with US/Canada Controls
July 2020 (Control - Base)
r=csa20ce1p1_v706ext.07.monavg.dat.ioapi, t=csa20be1p1_v706ext.07.monavg.dat.ioapi
-0.000
-0.300
-0.600
-0.900
-1.200
-1.500
-1.800
-2.100
-2.400
ug/m3
PAVE by MCNC
98
1
1
155
Hour: 00
Min= -3.308 at (111,52), Max= 0.010 at (18,76)

Figure 5.5b - Reductions in July $PM_{2.5}$ concentrations from controls in 2020.

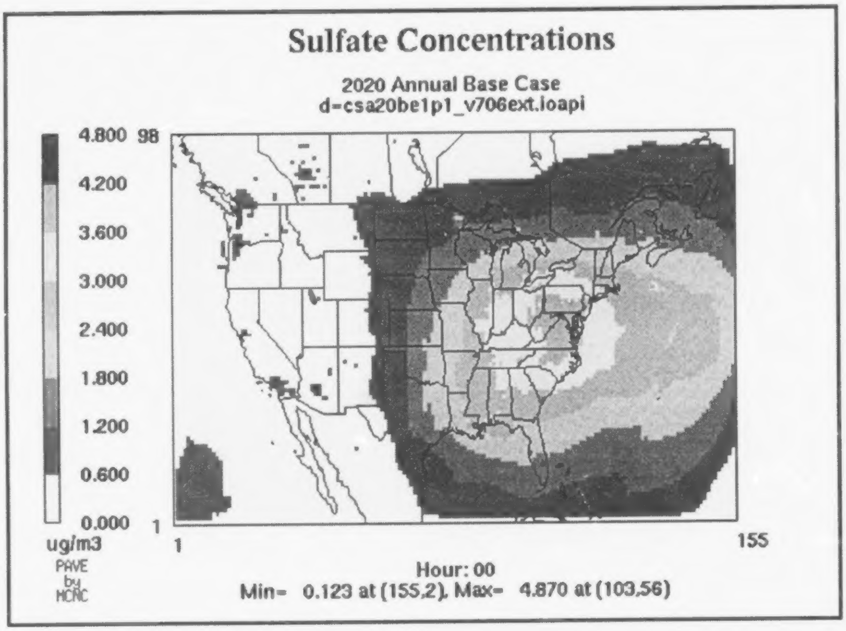
Sulfate Concentrations
2020 Annual Base Case
d=csa20be1p1_v706ext.ioapi
4.800
4.200
3.600
3.000
2.400
1.800
1.200
0.600
0.000
ug/m3
98
1
1
155
PAVE by MCNC
Hour: 00
Min= 0.123 at (155,2), Max= 4.870 at (103,56)

Figure 5.6a - Annual average $SO_4^=$ concentrations 2020 base case.

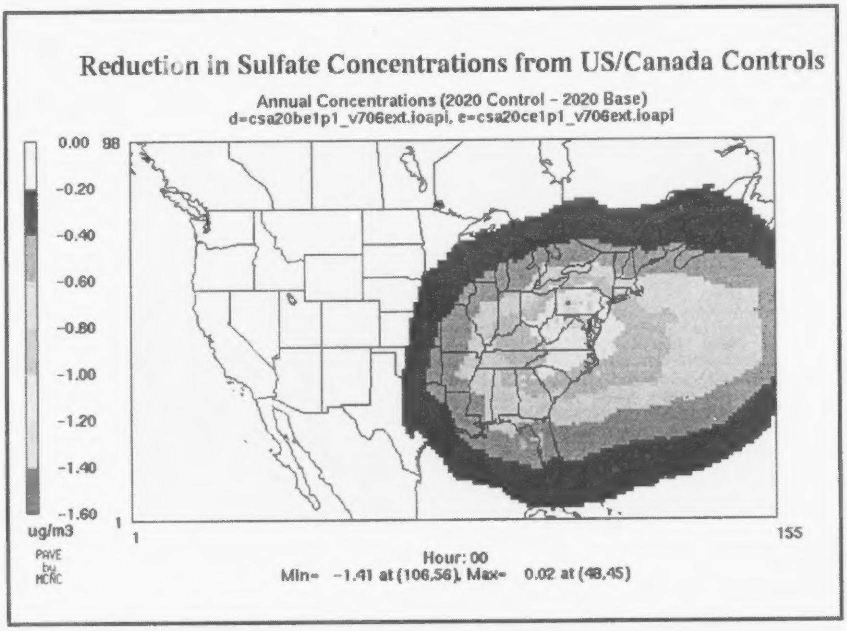
Reduction in Sulfate Concentrations from US/Canada Controls
Annual Concentrations (2020 Control - 2020 Base)
d=csa20be1p1_v706ext.ioapi, e=csa20ce1p1_v706ext.ioapi
0.00
-0.20
-0.40
-0.60
-0.80
-1.00
-1.20
-1.40
-1.60
ug/m3
98
1
1
155
PAVE by MCNC
Hour: 00
Min= -1.41 at (106,56), Max= 0.02 at (48,45)

Figure 5.6b - Reductions in annual $SO_4^=$ concentrations from controls in 2020

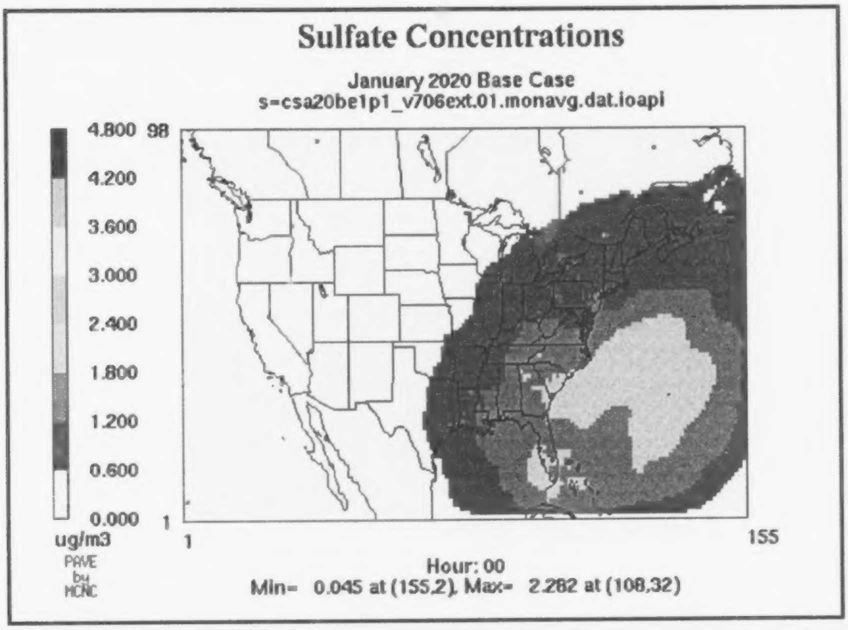
Sulfate Concentrations
January 2020 Base Case
s=csa20be1p1_v706ext.01.monavg.dat.ioapi
4.800
4.200
3.600
3.000
2.400
1.800
1.200
0.600
0.000
ug/m3
98
1
1
155
PAVE by MCNC
Hour: 00
Min= 0.045 at (155,2), Max= 2.282 at (108,32)

Figure 5.7a - January average $SO_4^=$ concentrations 2020 base case.

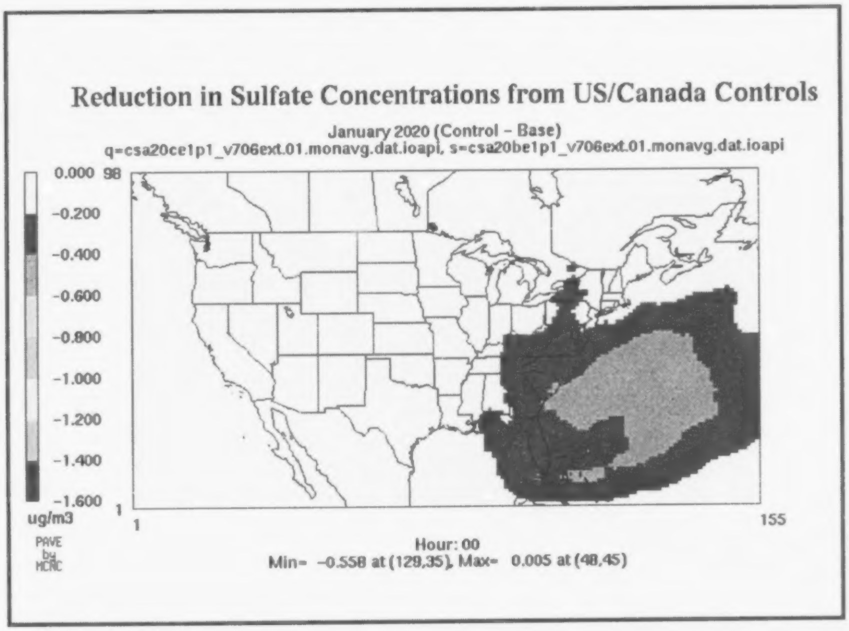
Reduction in Sulfate Concentrations from US/Canada Controls
January 2020 (Control - Base)
q=csa20ce1p1_v706ext.01.monavg.dat.ioapi, s=csa20be1p1_v706ext.01.monavg.dat.ioapi
0.000
-0.200
-0.400
-0.600
-0.800
-1.000
-1.200
-1.400
-1.600
ug/m3
98
1
1
155
PAVE by MCNC
Hour: 00
Min= -0.558 at (129,35), Max= 0.005 at (48,45)

Figure 5.7b - Reductions in January $SO_4^=$ concentrations from controls in 2020.

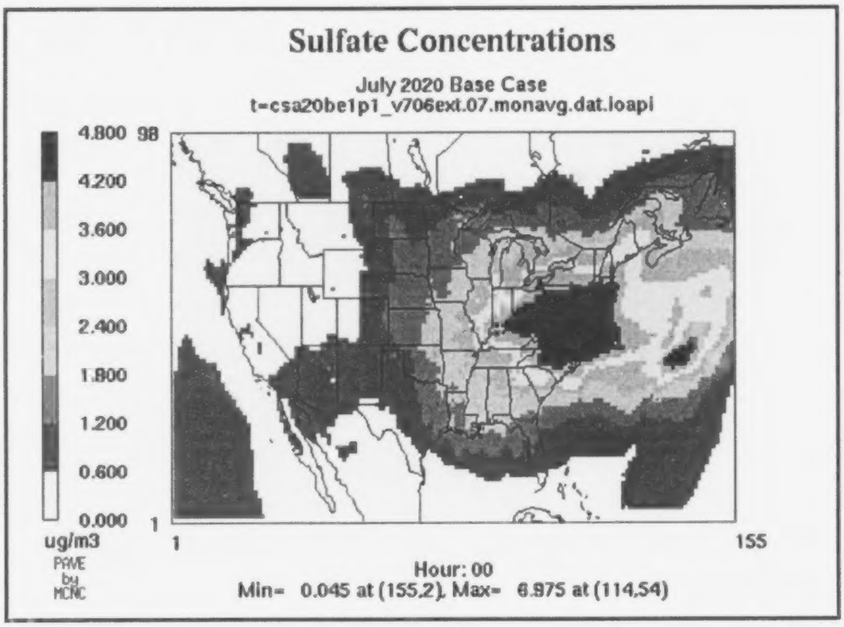
Sulfate Concentrations
July 2020 Base Case
t=csa20be1p1_v706ext.07.monavg.dat.ioapi
4.800
4.200
3.600
3.000
2.400
1.800
1.200
0.600
0.000
ug/m3
PAVE by MCNC
98
1
1
155
Hour: 00
Min= 0.045 at (155,2), Max= 6.975 at (114,54)

Figure 5.8a - July average $SO_4^=$ concentrations 2020 base case.

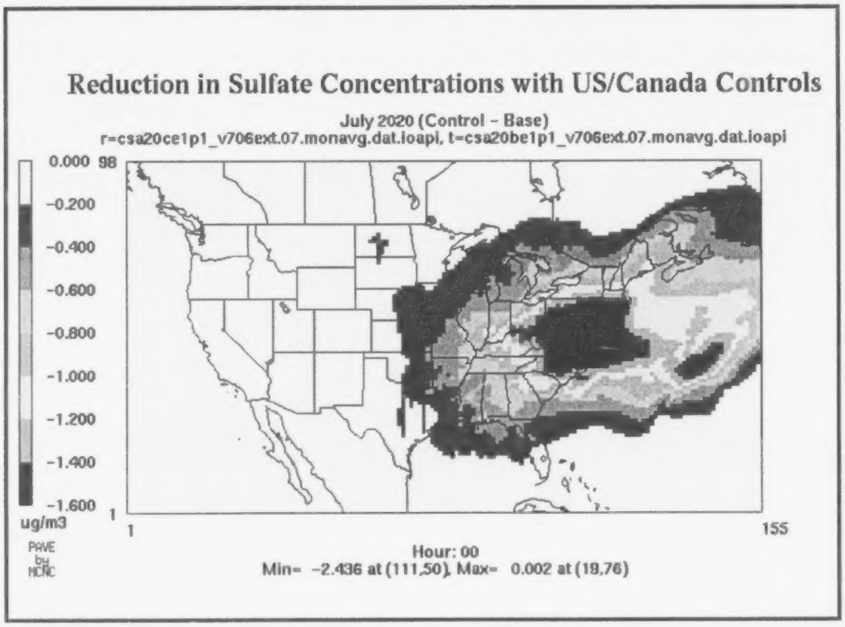
Reduction in Sulfate Concentrations with US/Canada Controls
July 2020 (Control - Base)
r=csa20ce1p1_v706ext.07.monavg.dat.ioapi, t=csa20be1p1_v706ext.07.monavg.dat.ioapi
0.000
-0.200
-0.400
-0.600
-0.800
-1.000
-1.200
-1.400
-1.600
ug/m3
PAVE by MCNC
98
1
1
155
Hour: 00
Min= -2.436 at (111,50), Max= 0.002 at (19,76)

Figure 5.8b - Reductions in July $SO_4^=$ concentrations from controls in 2020.

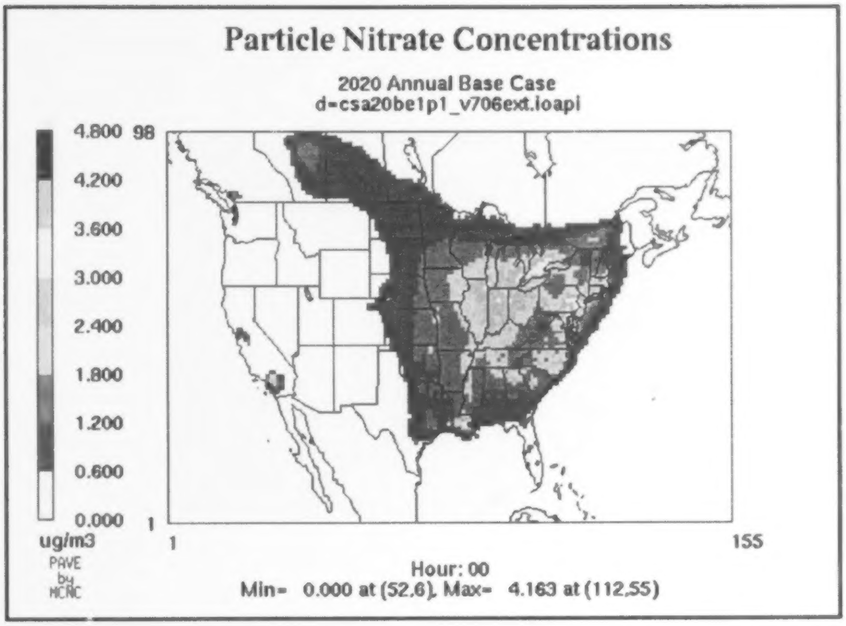
Particle Nitrate Concentrations
2020 Annual Base Case
d=csa20be1p1_v706ext.ioapi
4.800
4.200
3.600
3.000
2.400
1.800
1.200
0.600
0.000
ug/m3
98
1
1
155
PAVE by MCNC
Hour: 00
Min= 0.000 at (52,6), Max= 4.163 at (112,55)

Figure 5.9a - Annual average NO_3^- concentrations 2020 base case.

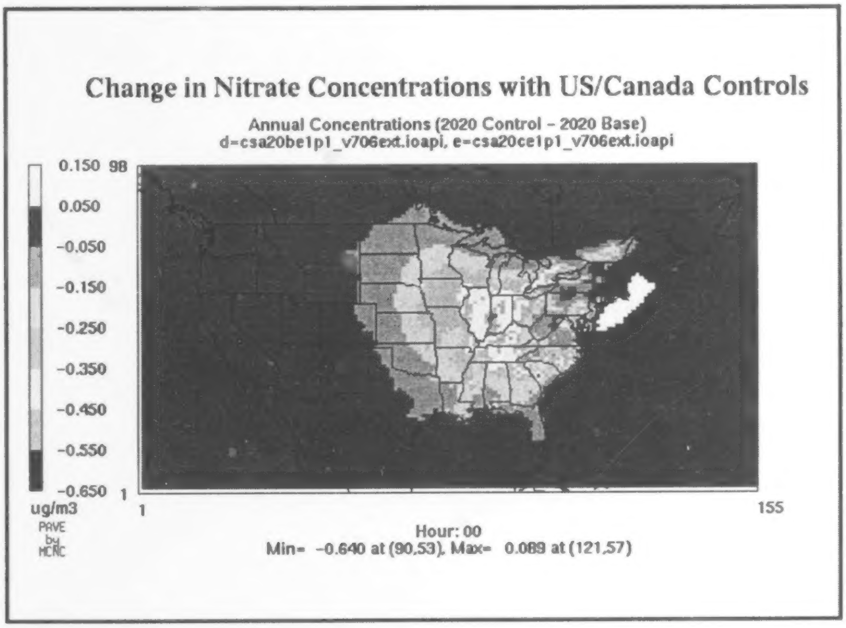
Change in Nitrate Concentrations with US/Canada Controls
Annual Concentrations (2020 Control - 2020 Base)
d=csa20be1p1_v706ext.ioapi, e=csa20ce1p1_v706ext.ioapi
0.150
0.050
-0.050
-0.150
-0.250
-0.350
-0.450
-0.550
-0.650
ug/m3
98
1
1
155
PAVE by MCNC
Hour: 00
Min= -0.640 at (90,53), Max= 0.089 at (121,57)

Figure 5.9b - Reductions in annual NO_3^- concentrations from controls in 2020.

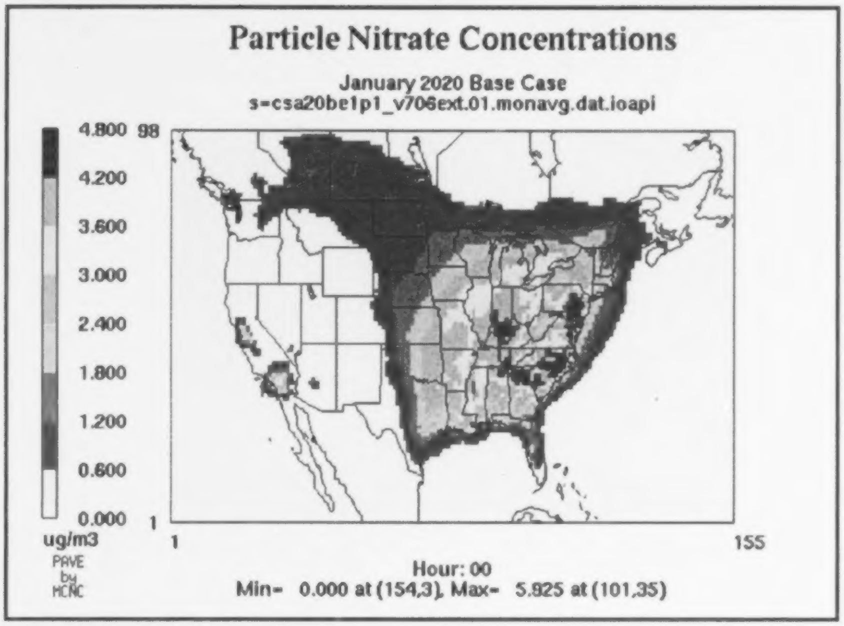
Particle Nitrate Concentrations
January 2020 Base Case
s=csa20be1p1_v706ext.01.monavg.dat.ioapi
4.800
4.200
3.600
3.000
2.400
1.800
1.200
0.600
0.000
ug/m3
PAVE
by
MCNC
98
1
1
155
Hour: 00
Min= 0.000 at (154,3), Max= 5.925 at (101,35)

Figure 5.10a - January average NO$_3^-$ concentrations 2020 base case.

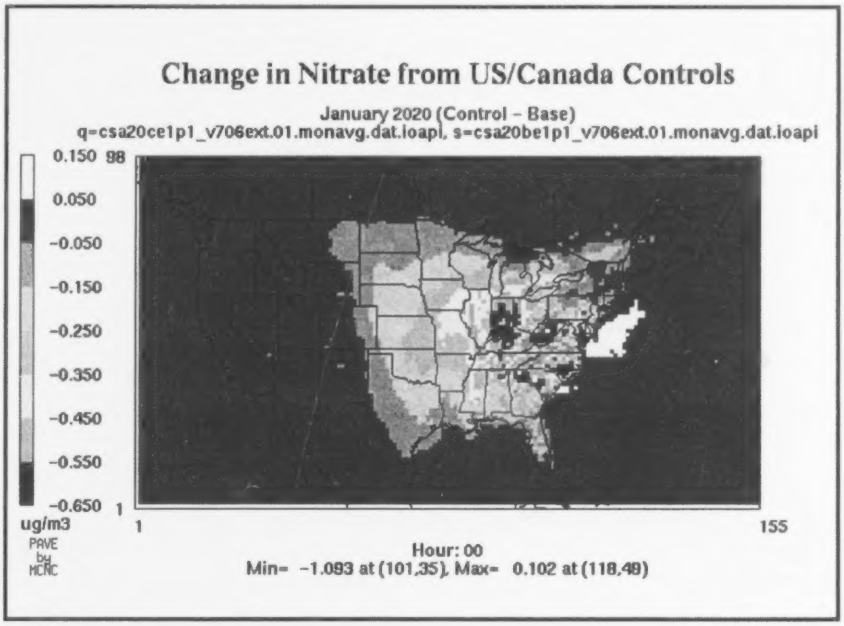
Change in Nitrate from US/Canada Controls
January 2020 (Control – Base)
q=csa20ce1p1_v706ext.01.monavg.dat.ioapi, s=csa20be1p1_v706ext.01.monavg.dat.ioapi
0.150
0.050
-0.050
-0.150
-0.250
-0.350
-0.450
-0.550
-0.650
ug/m3
PAVE
by
MCNC
98
1
1
155
Hour: 00
Min= -1.083 at (101,35), Max= 0.102 at (118,49)

Figure 5.10b - Reductions in January NO$_3^-$ concentrations from controls in 2020.

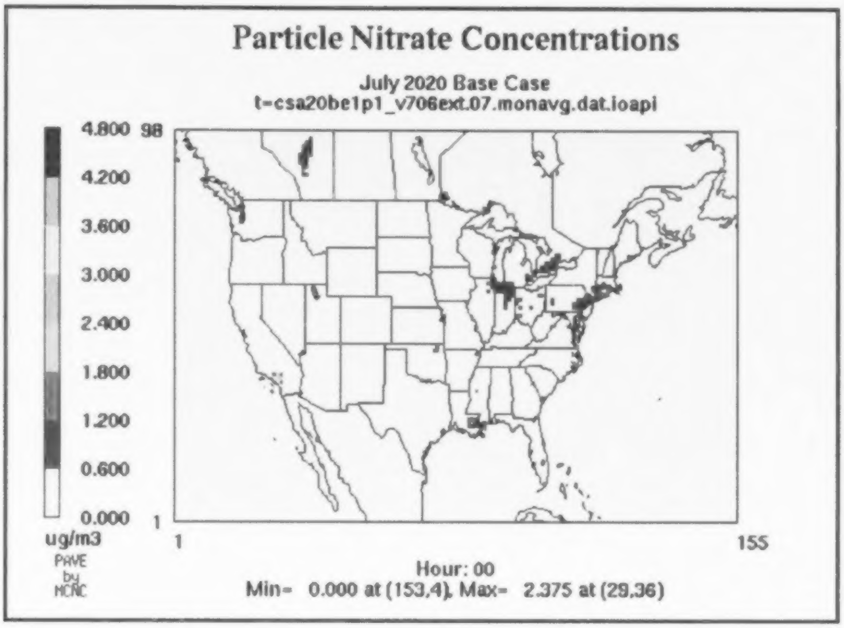

Particle Nitrate Concentrations

July 2020 Base Case
t=csa20be1p1_v706ext.07.monavg.dat.ioapi
4.800
4.200
3.600
3.000
2.400
1.800
1.200
0.600
0.000
ug/m3
PAVE by MCNC
98
1
1
155
Hour: 00
Min= 0.000 at (153,4), Max= 2.375 at (29,36)

Figure 5.11a - July average NO_3^- concentrations 2020 base case

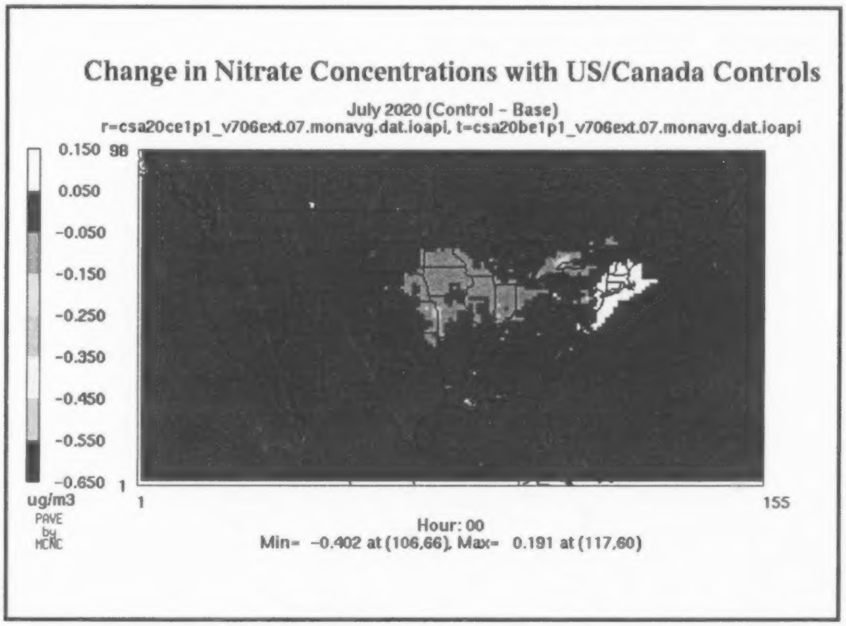

Change in Nitrate Concentrations with US/Canada Controls

July 2020 (Control - Base)
r=csa20ce1p1_v706ext.07.monavg.dat.ioapi, t=csa20be1p1_v706ext.07.monavg.dat.ioapi
0.150
0.050
-0.050
-0.150
-0.250
-0.350
-0.450
-0.550
-0.650
ug/m3
PAVE by MCNC
98
1
1
155
Hour: 00
Min= -0.402 at (106,66), Max= 0.191 at (117,60)

Figure 5.11b - Reductions in July NO_3^- concentrations from controls in 2020.

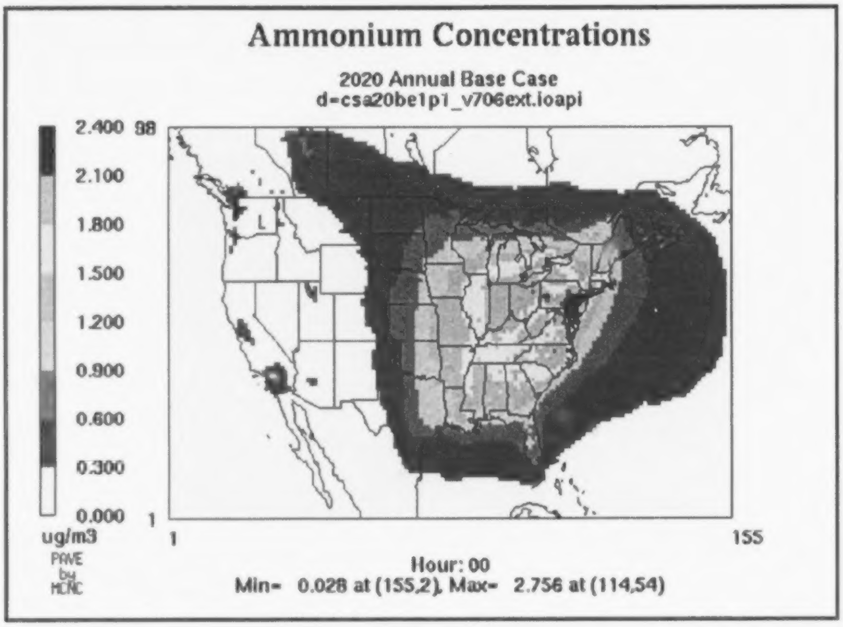

Ammonium Concentrations

2020 Annual Base Case
d=csa20be1p1_v706ext.ioapi

2.400
2.100
1.800
1.500
1.200
0.900
0.600
0.300
0.000
ug/m3
PAVE
by
MCNC
98
1
1
155
Hour: 00
Min= 0.028 at (155,2), Max= 2.756 at (114,54)

Figure 5.12a - Annual average NH_4^+ concentrations 2020 base case.

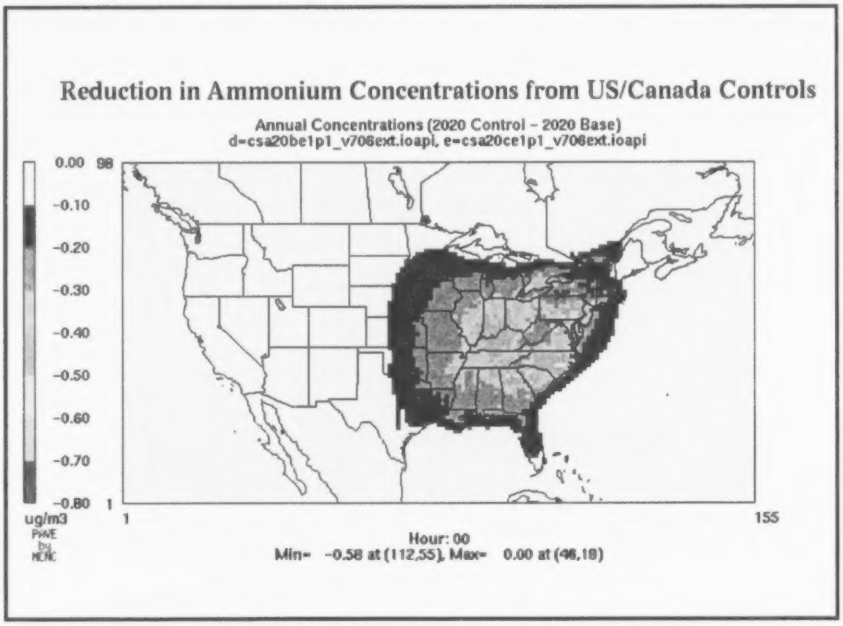

Reduction in Ammonium Concentrations from US/Canada Controls

Annual Concentrations (2020 Control - 2020 Base)
d=csa20be1p1_v706ext.ioapi, e=csa20ce1p1_v706ext.ioapi

0.00
-0.10
-0.20
-0.30
-0.40
-0.50
-0.60
-0.70
-0.80
ug/m3
PAVE
by
MCNC
98
1
1
155
Hour: 00
Min= -0.58 at (112,55), Max= 0.00 at (46,18)

Figure 5.12b - Reductions in annual NH_4^+ concentrations from controls in 2020.

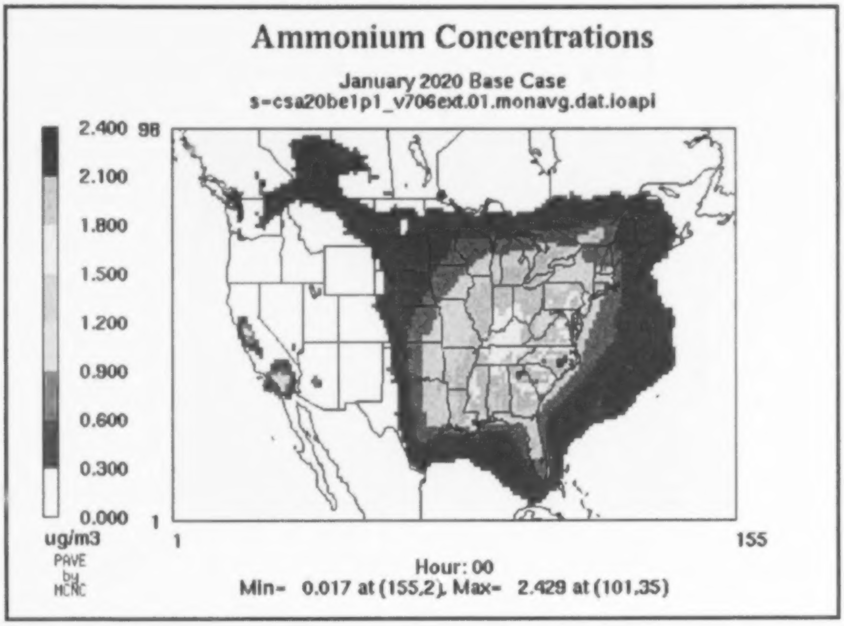
Ammonium Concentrations
January 2020 Base Case
s=csa20be1p1_v706ext.01.monavg.dat.ioapi
2.400
2.100
1.800
1.500
1.200
0.900
0.600
0.300
0.000
ug/m3
PAVE by MCNC
98
1
1
155
Hour: 00
Min= 0.017 at (155,2), Max= 2.429 at (101,35)

Figure 5.13a - January average NH_4^+ concentrations 2020 base case.

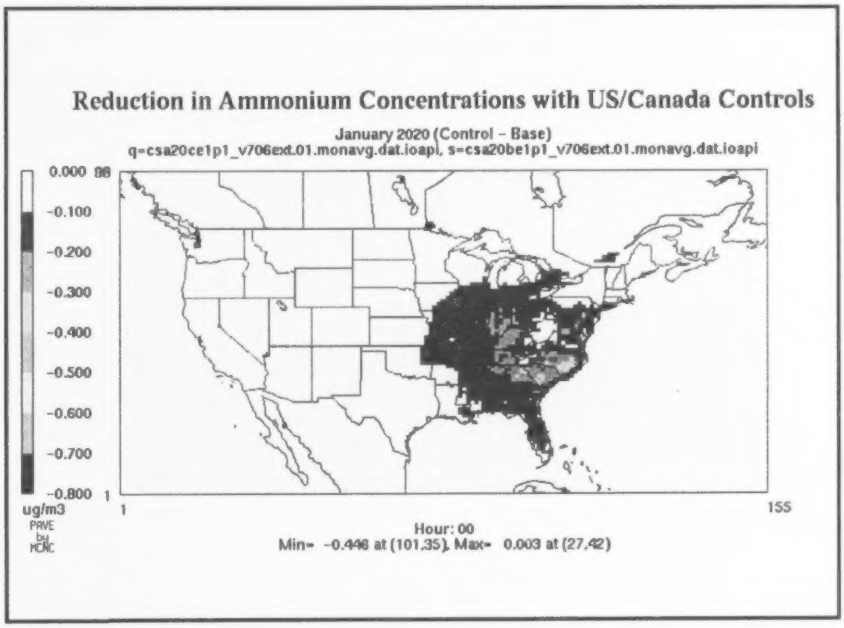
Reduction in Ammonium Concentrations with US/Canada Controls
January 2020 (Control - Base)
q=csa20ce1p1_v706ext.01.monavg.dat.ioapi, s=csa20be1p1_v706ext.01.monavg.dat.ioapi
0.000
-0.100
-0.200
-0.300
-0.400
-0.500
-0.600
-0.700
-0.800
ug/m3
PAVE by MCNC
98
1
1
155
Hour: 00
Min= -0.446 at (101,35), Max= 0.003 at (27,42)

Figure 5.13b - Reductions in January NH_4^+ concentrations from controls in 2020.

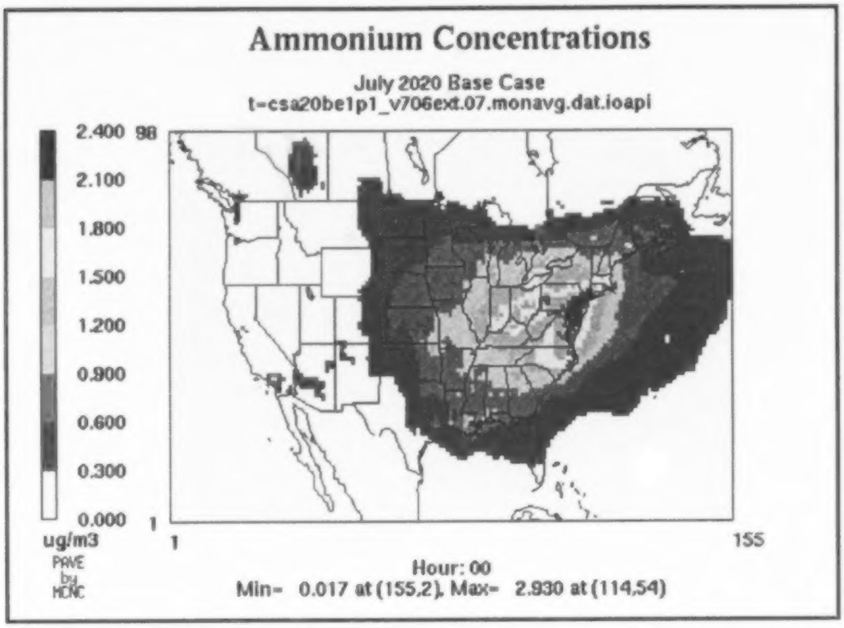
Ammonium Concentrations
July 2020 Base Case
t=csa20be1p1_v706ext.07.monavg.dat.ioapi
2.400
2.100
1.800
1.500
1.200
0.900
0.600
0.300
0.000
ug/m3
98
1
1
155
PAVE by MCNC
Hour: 00
Min= 0.017 at (155,2), Max= 2.930 at (114,54)

Figure 5.14a - July average NH_4^+ concentrations 2020 base case.

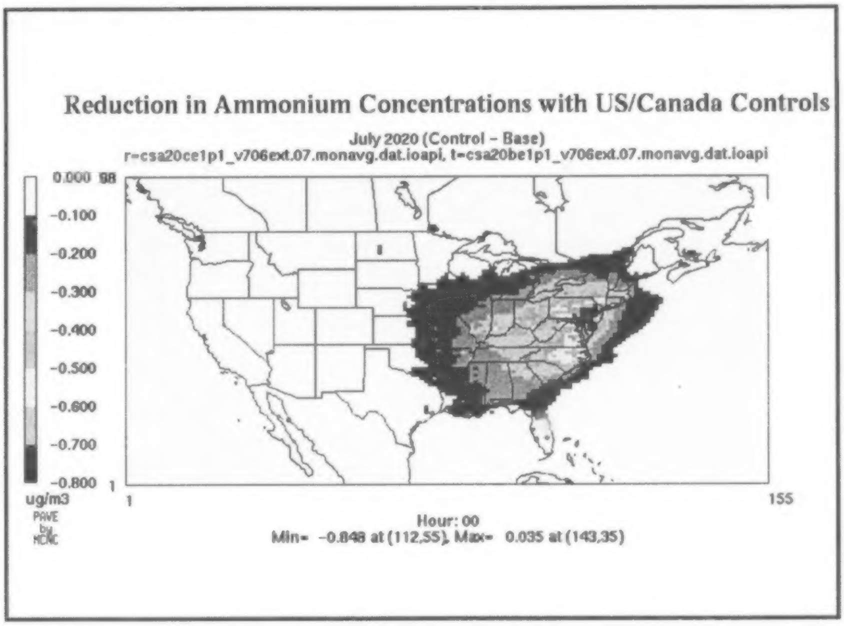
Reduction in Ammonium Concentrations with US/Canada Controls
July 2020 (Control - Base)
r=csa20ce1p1_v706ext.07.monavg.dat.ioapi, t=csa20be1p1_v706ext.07.monavg.dat.ioapi
0.000
-0.100
-0.200
-0.300
-0.400
-0.500
-0.600
-0.700
-0.800
ug/m3
98
1
1
155
PAVE by MCNC
Hour: 00
Min= -0.848 at (112,55), Max= 0.035 at (143,35)

Figure 5.14b - Reductions in July NH_4^+ concentrations from controls in 2020.

5.1.2 Conclusions

$PM_{2.5}$ concentrations are composed of $SO_4^=$, NO_3^-, NH_4^+, OC and BC, soil, and other components. The U.S. and Canadian controls that are expected to be implemented will reduce $PM_{2.5}$ concentrations in both countries in 2010 and 2020 although the reduction is predicted to be larger in 2020 than 2010. The reductions in $PM_{2.5}$ concentrations are larger in the eastern portion of the modelling domain than the western portion of the modelling domain. Implementation of controls results in SO_2 and NO_x emissions reductions, with these emissions reductions leading to corresponding reductions in particle $SO_4^=$ and NO_3^- concentrations in both the United States and Canada. Sulphate concentrations are highest and are reduced more significantly in the summer months while particle NO_3^- concentrations are highest and reduced more significantly during the winter months. Although NH_3 emissions are not currently addressed in the strategies that are expected to be implemented by 2020, NH_4^+ concentrations are predicted to be reduced in both countries. Ammonia emissions participate in reactions with gaseous SO_2 and NO_x, resulting in the formation of $(NH_4)_2SO_4$ and NH_4NO_3 particles. When SO_2 and NO_x are reduced, there are fewer SO_2 and NO_x emissions available for NH_3 emissions to react with to form NH_4^+. Thus, reducing both SO_2 and NO_x emissions leads to a concurrent reduction in particle NH_4^+ concentrations in addition to ambient $SO_4^=$ and NO_3^- concentrations. The reduction in NH_4^+ in the winter months is dominated by NH_4^+ associated with NH_4NO_3 and the reduction in NH_4^+ in the summer months is dominated by NH_4^+ associated with $(NH_4)_2SO_4$. Since the future controls that are expected to be implemented only reduce SO_2 and NO_x emissions, these controls will not reduce the OC and BC, soil, and other components of $PM_{2.5}$. It is predicted that implementation of the U.S. and Canadian controls will greatly reduce the areas in both countries exceeding the U.S. annual standard of 15 $\mu g/m^3$.

5.2 RESULTS OF AURAMS CONTROL STRATEGY MODELLING

AURAMS (A Unified Regional Air-quality Modelling System) is a new size- and composition-resolved, episodic, regional PM modelling system developed by the Meteorological Service of Canada. AURAMS (version 0.30a) was run for two 2-week periods for the same five emission scenarios as REMSAD in order to provide an independent evaluation of the relative impact of these scenarios. Both a winter period and a summer period were simulated to allow consideration of the seasonal impact of the emission reductions. The winter simulations span the period from the 1st to the 15th of February 1998; this period was chosen in part because of the occurrence of a wintertime regional PM episode during the second week (Vet et al., 2001). The summer simulation spans the period from the 1st to the 18th of July 1995; this period includes a regional ozone episode (July 12-15) that was also associated with high levels of PM in both Canada and the United States. As well, this episode occurred during the summer 1995 NARSTO Northeast ozone field campaign so enhanced measurement data are available for the period (e.g., Ryan et al., 1998).

While AURAMS is a more complex model than REMSAD in a number of important respects, including its representations of gas-phase chemistry (ADOM-II mechanism vs. micro-CB-IV mechanism), heterogeneous chemistry (HETV vs. MARS-A), and $PM_{2.5}$ size distribution (8 size sections vs. one size section), it is also much more demanding computationally. For this report, AURAMS was run for four weeks and five scenarios whereas REMSAD was run for a one-year period for the same five scenarios. Given these differences in model sophistication and run length, it is of interest to see how similar (qualitatively) the REMSAD and AURAMS results and conclusions are for the same scenarios.

5.2.1 Model Setup, Emission Files, and Post-Processing

The horizontal modelling domain for all of the AURAMS air-quality simulations is presented in Figure 5.15. The horizontal domain is 85 by 105 grid points with 42 km grid spacing. In the vertical, the model is set up with 29 levels up to about 22 km above ground. Nineteen of the levels are below 5 km. The model uses a 15-minute timestep.

Two sets of meteorological fields were prepared to drive the AURAMS simulations, one set of fields for the summer simulations and one for the winter simulations. The Global Environmental Multiscale (GEM) model (Côté et al., 1993; 1998a, b), version 3.0.3 with version 3.8 of the physics package, was used in the Canadian Meteorological Centre's variable-grid regional configuration to provide the meteorological fields. The regional GEM grid includes a uniform mesh with 24-km horizontal grid spacing over North America and 28 vertical levels up to 10 hPa (about 30 km). Horizontal interpolation of the meteorological fields was required to go from the 24-km GEM grid to the 42-km AURAMS grid as was vertical interpolation to go from GEM's η vertical coordinate to AURAMS's modified Gal-Chen vertical coordinate. GEM employed a 7.5-minute timestep, so that AURAMS was presented with meteorological fields from every second GEM timestep.

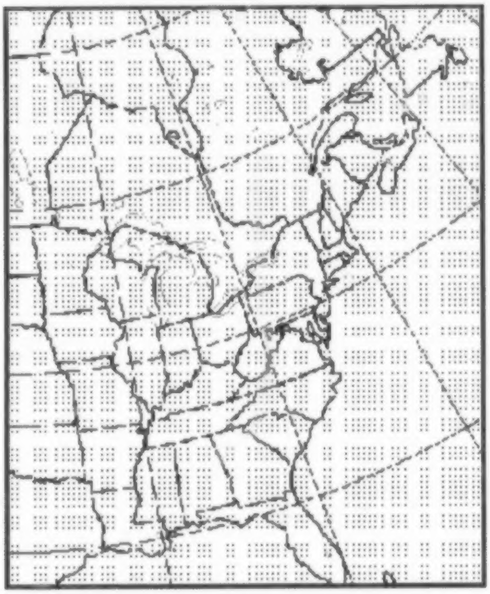

Figure 5.15 - AURAMS domain for all simulations (85x105 grid points, Δx=42 km). For each simulation period, one "present-day" AURAMS base simulation was run along with four future-year emission reduction scenario simulations. In all, ten AURAMS simulations were available to be compared either to observations or to each other. All of the future-year scenario runs were identical in all respects to their present-day base simulation except for the anthropogenic emission files that were provided to the model.

For each simulation period, one "present-day" AURAMS base simulation was run along with four future-year emission reduction scenario simulations. In all, ten AURAMS simulations were available to be compared either to observations or to each other. All of the future-year scenario runs were identical in all respects to their present-day base simulation except for the anthropogenic emission files that were provided to the model.

As discussed in Chapter 4, ten different sets of anthropogenic emissions files were constructed, five for the winter period and five for the summer period. For the two present-day base case simulations, 1990 and 1995 Canadian and 1990 and 1996 U.S. emission-inventory data were used to produce the emissions files. For the future-year emission reduction scenarios, four sets of emissions files were prepared for year 2010 and four for year 2020. For each of these future years, there were two "Approved" (or "base") emissions cases – one each for winter and summer – and two "Proposed" (or "control") cases. The "Approved" emission scenarios contain only the effects of legislation that has already passed in both the United States and Canada. The "Proposed" cases add the effects of a few major pieces of legislation still being debated in either the United States or Canada (see Chapter 4).

A summary description of the ten cases is presented in Table 5.1 while Table 5.2 provides a summary of the relative differences in anthropogenic primary $PM_{2.5}$ and gaseous precursor emissions between three scenario pairs (cf. Table 4.2). Note from Table 5.2 that the change in emissions

Table 5.1 Characteristics of ten AURAMS simulations.

Description	Episode	Emission Year	Reductions Included
1995 summer base case	1-18 July 1995	1995 Can. / 1996 U.S.	None
2010 summer base case	1-18 July 1995	2010	Approved
2020 summer base case	1-18 July 1995	2020	Approved
2010 summer control case	1-18 July 1995	2010	Proposed
2020 summer control case	1-18 July 1995	2020	Proposed
1995 winter base case	1-15 February 1998	1995 Can. / 1996 U.S.	None
2010 winter base case	1-15 February 1998	2010	Approved
2020 winter base case	1-15 February 1998	2020	Approved
2010 winter control case	1-15 February 1998	2010	Proposed
2020 winter control case	1-15 February 1998	2020	Proposed

Table 5.2 Percent differences between scenario emissions of primary $PM_{2.5}$ and PM precursors on the AURAMS domain for three pairs of scenarios (based on Table 4.2). A positive value indicates an increase in emissions in going from the first scenario to the second scenario of the pair.

Emitted Pollutant	2010B Vs. 2020B			2010B Vs. 2010C			2020B Vs. 2020C		
	Can.	U.S.	Dom.	Can.	U.S.	Dom.	Can.	U.S.	Dom.
$PM_{2.5}$	10.9	0.1	2.1	-0.6	0.0	-0.1	-0.9	0.0	-0.1
SO_2	-9.7	-5.1	-5.6	-12.2	-25.2	-23.9	-15.1	-34.1	-32.3
NO_x	-8.7	-17.9	-17.2	-5.3	-10.4	-10.0	-7.2	-16.6	-15.9
VOC	8.7	1.0	1.7	-4.5	0.0	-0.5	-5.4	0.0	-0.6
NH_3	0.0	4.7	4.3	0.0	0.0	0.0	0.0	0.0	0.0

between the 2010 base and 2020 base cases is qualitatively different from the change in emissions between the 2010 base and 2010 control and the 2020 base and 2020 control scenario pairs. More species have emission changes and in both directions in this first pair of cases than in the other two pairs of cases. For biogenic emissions, winter and summer emissions files were produced based on each of the two sets of meteorology. The same wintertime biogenic emission files were used for all five winter simulations and the same summertime biogenic emission files were used for all five summer simulations.

Only the last part of each simulation was used to evaluate model performance and/or summarize results (see the Appendix for a performance evaluation of AURAMS for the two present-day base simulations). This allows enough time for AURAMS to spin-up in the first week of each simulation. A two-day spin-up period is usually thought to be sufficient for ozone chemistry, but previous experiments with AURAMS have shown that four to five days may be needed to reach steady state for particulate matter. Results from the emission-reduction scenarios were averaged for the last nine days of the winter period (Feb. 7-15, 1998) and for the last 11 days of the summer period (July 8-18, 1995).

5.2.2 Evaluation of Emission Reduction Impacts

5.2.2.1 *Winter Period*

Figures 5.16 to 5.19 summarize the AURAMS model results for the winter scenario simulations. The four panels in Figures 5.16 and 5.18 show the predicted ground-level $PM_{2.5}$ mass and $PM_{2.5}$ $SO_4^=$, NH_4^+, and NO_3^- concentration fields averaged over the last nine days of the simulations (Feb. 7-15, 1998) for the 2010 and 2020 base cases, respectively.

The same colour scheme used for the REMSAD PM concentration plots in Section 5.1 has also been used for the AURAMS PM concentration plots, but note that the contour intervals selected for the AURAMS plots are *larger* than those for the REMSAD plots. This choice is a consequence of the shorter averaging time used for the episodic AURAMS results (9 days vs. 91 days or 365 days), which results in greater variability since the 9-day period includes a $PM_{2.5}$ episode and hence larger maximum values. "Hotter" colours indicate higher concentrations.

It is evident from inspection of Figures 5.16 and 5.18 that NH_4NO_3 is predicted to be the dominant inorganic compound in $PM_{2.5}$ during this period as the NH_4^+ and $PM_{2.5}$ mass fields have similar distributions to the nitrate field. Sulphate is present in the 3-5 µg/m³ range in the Ohio Valley and U.S. Southeast and is still the dominant inorganic compound in the Southeast (e.g., Georgia, Florida, Alabama). Note that the elevated $PM_{2.5}$ levels predicted by AURAMS over the Atlantic Ocean are not due to anthropogenic emissions but rather are the result of sea-salt emissions from the ocean in the presence of strong winter winds. Note that as the predicted sea-salt emissions are determined only by meteorology, they will be the same for all of the winter simulations and hence will cancel out in any difference calculations.

Table 5.2 shows that on a model-domain basis, VOC, NH_3, and primary $PM_{2.5}$ emissions are modestly larger for the 2020 base case than for the 2010 base case (2 percent, 4 percent, and 2 percent, respectively) whereas SO_2 and NO_x emissions are smaller by 6 percent and 17 percent, respectively. This would suggest *a priori* that $PM_{2.5}$ $SO_4^=$ concentrations should be smaller for the 2020 base case than for the 2010 base case while $PM_{2.5}$ total mass, $PM_{2.5}$ NO_3^-, and $PM_{2.5}$ NH_4^+ concentrations might either increase or decrease. Comparing Figures 5.16 and 5.18, we see that maximum $PM_{2.5}$ mass increases slightly, maximum $PM_{2.5}$ NO_3^- decreases slightly, and maximum $PM_{2.5}$ NH_4^+ increases slightly for the 2020 base case relative to the 2010 base case. However, maximum $PM_{2.5}$ $SO_4^=$ also increases even though SO_2 emissions have decreased. Based on additional analysis, a likely explanation for the predicted wintertime increase in $SO_4^=$ concentration, despite the decrease in SO_2 emissions, is an increase in oxidant concentrations (OH and O_3) and hence in gas-phase and aqueous-phase SO_2-to-$SO_4^=$ conversion due to the concomitant decreases in NO_x emissions. This explanation is consistent with the predicted ground-level NO_2 and O_3 fields south of the Great Lakes for these two cases (not shown), for which the 2020 base NO_2 field is a few ppb higher than the 2020 control NO_2 field and the 2020 base O_3 field is a few ppb lower than the 2020 control O_3 field, suggesting reduced NO_2 titration of O_3 in the 2020 control case. Other studies have also suggested the possibility of such nonlinear responses in $SO_4^=$ concentrations for multiple emission reduction scenarios (e.g., Stein and Lamb, 2002).

The four panels in Figures 5.17 and 5.19 show the predicted ground-level $PM_{2.5}$ mass and $PM_{2.5}$ $SO_4^=$, NH_4^+, and NO_3^- *difference* fields averaged over the last nine days of the winter simulations (Feb. 7-15, 1998) for the 2010 control case minus the 2010 base case and for the 2020 control case minus the 2020 base case, respectively. Again, the same colour scheme used for the REMSAD PM concentration difference plots in Section 5.1 has also been used for the AURAMS PM concentration difference plots, but the contour intervals that have been selected for the AURAMS plots are again larger than those for the REMSAD plots. The contour intervals are also slightly shifted. For the $PM_{2.5}$ mass and $PM_{2.5}$ v and NH_4^+ difference fields, the colour "gray" corresponds to positive differences, bluish colours indicate smaller negative differences, and the hotter colours indicate larger negative differences. Note that a negative difference indicates a reduction in going from the base case to the control case (i.e., the predicted control field is smaller in magnitude than the predicted base field). The $PM_{2.5}$ NO_3^- difference field required special treatment because increases and decreases of comparable magnitude are predicted to occur for this field. Accordingly, the zero difference value maps to the light blue colour in the middle of the colour bar.

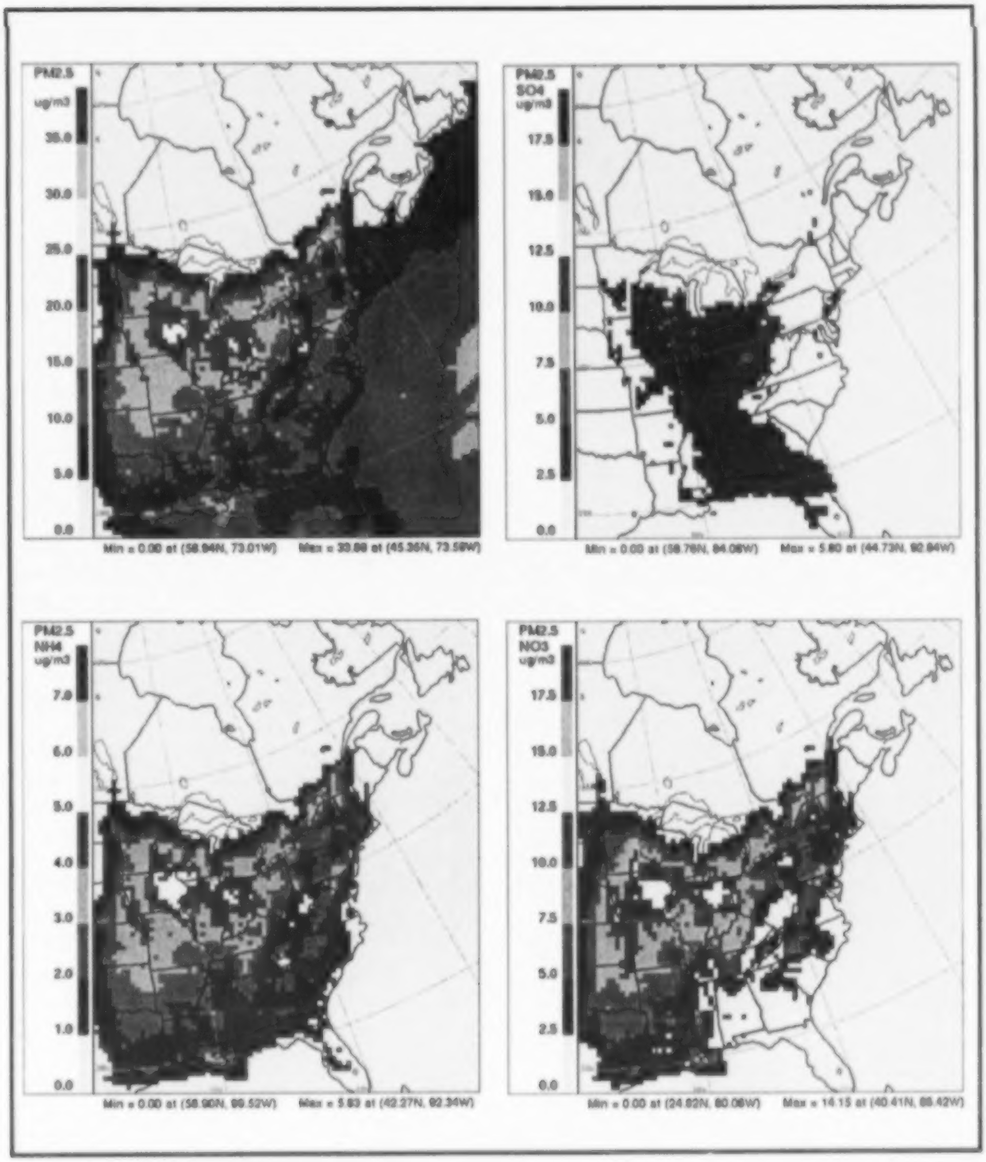
PM2.5
ug/m3
35.0
30.0
25.0
20.0
15.0
10.0
5.0
0.0
Min = 0.00 at (58.94N, 73.01W)
Max = 30.88 at (45.36N, 73.58W)
PM2.5
SO4
ug/m3
17.5
15.0
12.5
10.0
7.5
5.0
2.5
0.0
Min = 0.00 at (58.76N, 84.08W)
Max = 5.80 at (44.73N, 92.84W)
PM2.5
NH4
ug/m3
7.0
6.0
5.0
4.0
3.0
2.0
1.0
0.0
Min = 0.00 at (58.90N, 99.52W)
Max = 5.83 at (42.27N, 92.34W)
PM2.5
NO3
ug/m3
17.5
15.0
12.5
10.0
7.5
5.0
2.5
0.0
Min = 0.00 at (24.82N, 80.08W)
Max = 14.15 at (40.41N, 88.42W)

Figure 5.16 - Nine-day-average $PM_{2.5}$ mass concentration field and $PM_{2.5}$ inorganic chemical component concentration fields predicted by AURAMS for the Feb. 7-15, 1998 winter period for the "2010 base" case emissions. (a) top left panel - $PM_{2.5}$ mass; (b) top right panel - $PM_{2.5}$ $SO_4^{=}$ mass; (c) lower left panel - $PM_{2.5}$ NH_4^+ mass; (d) lower right panel - $PM_{2.5}$ NO_3^- mass. All fields are at 15 m height in units of μg/m³.

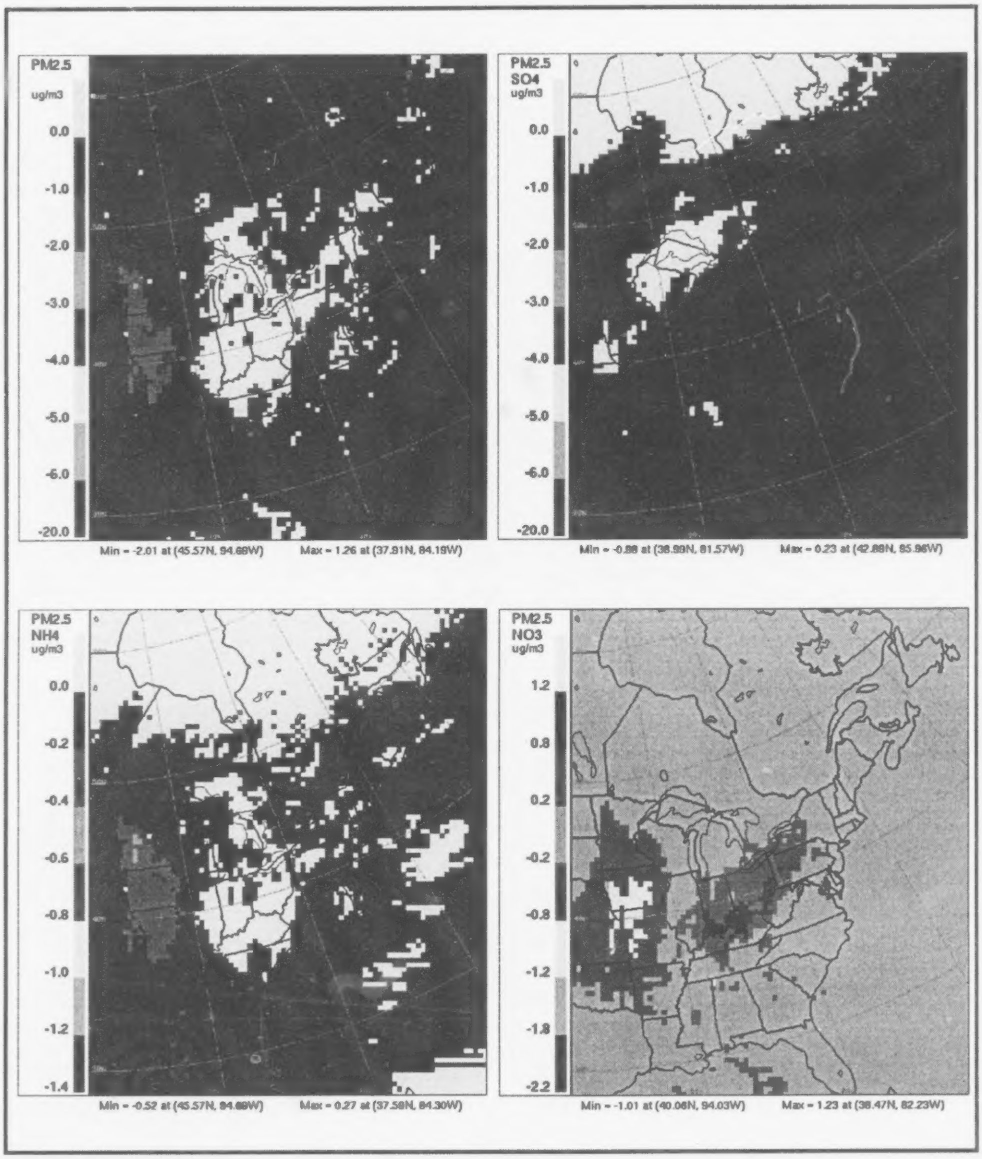
PM2.5
ug/m3
0.0
-1.0
-2.0
-3.0
-4.0
-5.0
-6.0
-20.0
Min = -2.01 at (45.57N, 94.68W)
Max = 1.26 at (37.91N, 84.19W)
PM2.5
SO4
ug/m3
0.0
-1.0
-2.0
-3.0
-4.0
-5.0
-6.0
-20.0
Min = -0.88 at (38.99N, 81.57W)
Max = 0.23 at (42.88N, 85.86W)
PM2.5
NH4
ug/m3
0.0
-0.2
-0.4
-0.6
-0.8
-1.0
-1.2
-1.4
Min = -0.52 at (45.57N, 94.68W)
Max = 0.27 at (37.58N, 84.30W)
PM2.5
NO3
ug/m3
1.2
0.8
0.2
-0.2
-0.8
-1.2
-1.8
-2.2
Min = -1.01 at (40.06N, 94.03W)
Max = 1.23 at (38.47N, 82.23W)

Figure 5.17 - Nine-day-average $PM_{2.5}$ mass concentration difference field and $PM_{2.5}$ inorganic chemical component concentration difference fields predicted by AURAMS for the Feb. 7-15, 1998 winter period for the "2010 control" case minus the "2010 base" case: (a) top left panel - $PM_{2.5}$ mass; (b) top right panel - $PM_{2.5}$ $SO_4^=$ mass; (c) lower left panel - $PM_{2.5}$ NH_4^+ mass; (d) lower right panel - $PM_{2.5}$ NO_3^- mass. All fields are at 15 m height in units of µg/m³. Negative values denote a reduction for the "2010 control" case relative to the "2010 base" case.

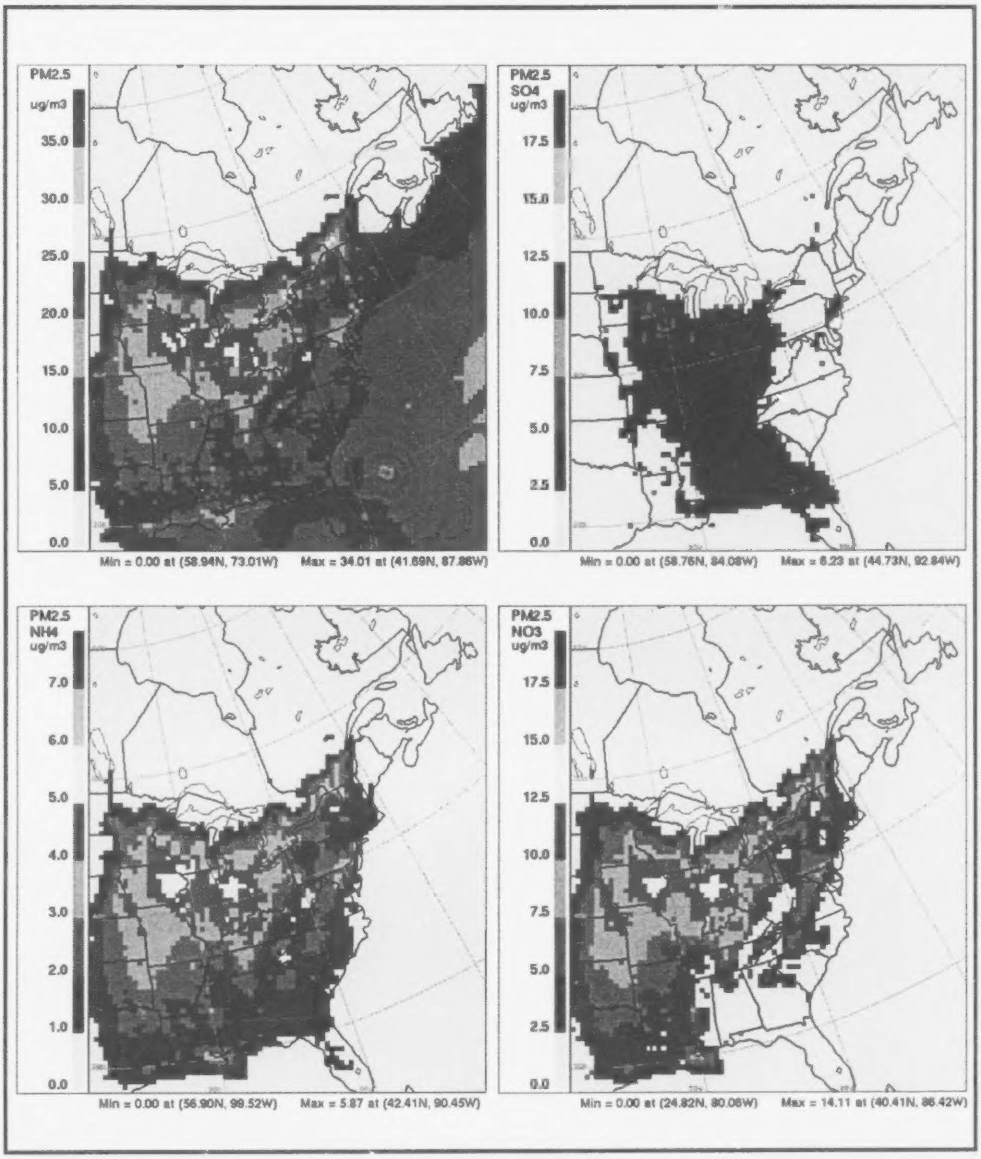
PM2.5
ug/m3
35.0
30.0
25.0
20.0
15.0
10.0
5.0
0.0
Min = 0.00 at (58.94N, 73.01W)
Max = 34.01 at (41.69N, 87.86W)
PM2.5
SO4
ug/m3
17.5
15.0
12.5
10.0
7.5
5.0
2.5
0.0
Min = 0.00 at (58.76N, 84.08W)
Max = 6.23 at (44.73N, 92.84W)
PM2.5
NH4
ug/m3
7.0
6.0
5.0
4.0
3.0
2.0
1.0
0.0
Min = 0.00 at (56.90N, 99.52W)
Max = 5.87 at (42.41N, 90.45W)
PM2.5
NO3
ug/m3
17.5
15.0
12.5
10.0
7.5
5.0
2.5
0.0
Min = 0.00 at (24.82N, 80.06W)
Max = 14.11 at (40.41N, 86.42W)

Figure 5.18 - Same as Figure 5.16 but for the "2020 base" case emissions.

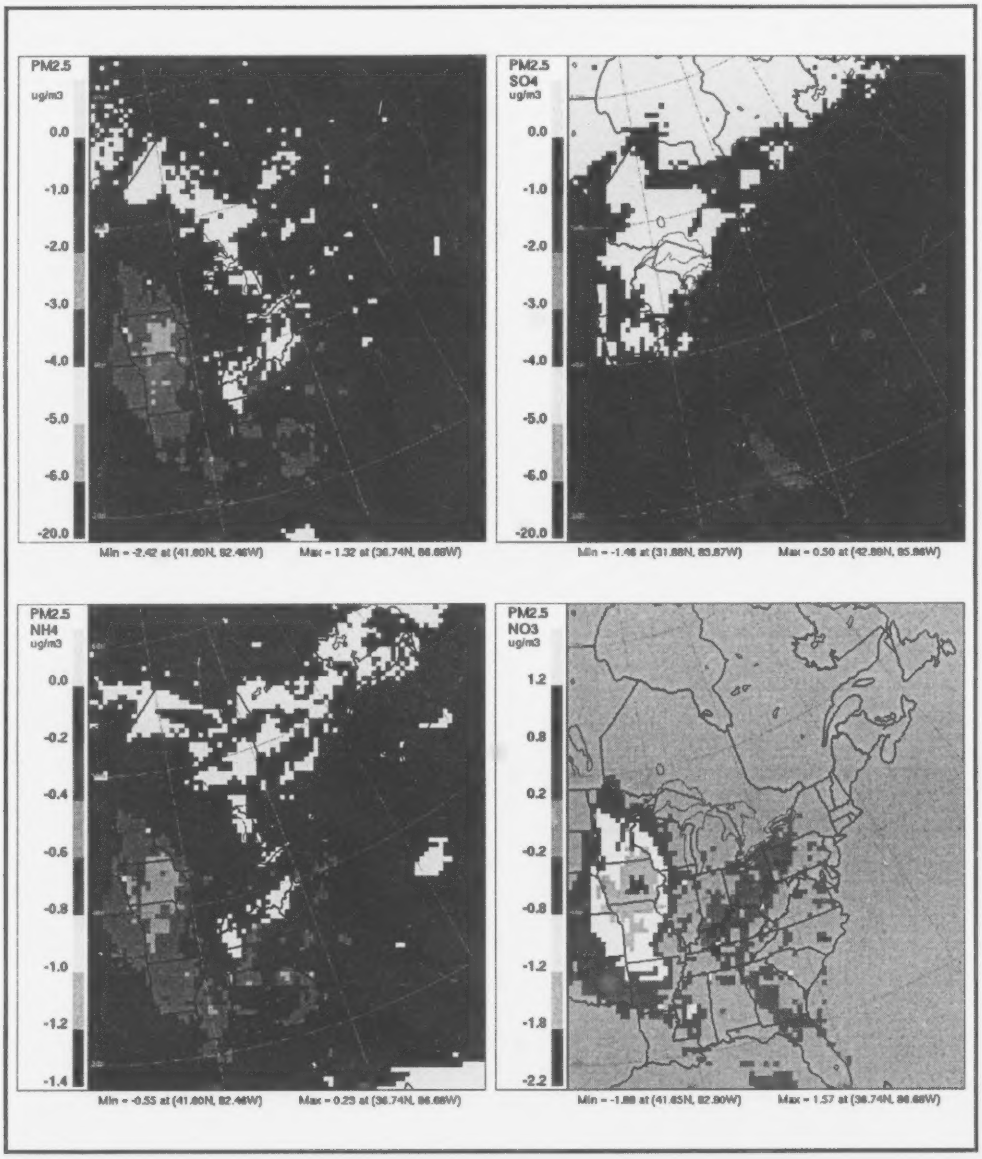
PM2.5
ug/m3
0.0
-1.0
-2.0
-3.0
-4.0
-5.0
-6.0
-20.0
Min = -2.42 at (41.60N, 82.46W)
Max = 1.32 at (36.74N, 86.68W)
PM2.5
SO4
ug/m3
0.0
-1.0
-2.0
-3.0
-4.0
-5.0
-6.0
-20.0
Min = -1.46 at (31.88N, 83.87W)
Max = 0.50 at (42.88N, 85.86W)
PM2.5
NH4
ug/m3
0.0
-0.2
-0.4
-0.6
-0.8
-1.0
-1.2
-1.4
Min = -0.55 at (41.60N, 82.46W)
Max = 0.23 at (36.74N, 86.68W)
PM2.5
NO3
ug/m3
1.2
0.8
0.2
-0.2
-0.8
-1.2
-1.8
-2.2
Min = -1.88 at (41.65N, 82.80W)
Max = 1.57 at (36.74N, 86.66W)

Figure 5.19 - Same as Figure 5.17 but for the "2020 control" case minus the "2020 base"

Comparison of the 2010 and 2020 winter control case simulations with the corresponding base case simulations (Figures 5.17 and 5.19) indicates that the additional SO_2 and NO_x emissions reductions proposed beyond current (i.e., "Approved") legislation result in a small net reduction in $PM_{2.5}$ mass in the lower atmosphere in the winter in much of the AURAMS domain, although small $PM_{2.5}$ mass increases up to 1 $\mu g/m^3$ are predicted in the Ohio Valley. The explanation for such a nonlinear response when emissions of both SO_2 and NO_x have decreased significantly (by 24 percent and 10 percent and by 32 percent and 16 percent, respectively, on a domain basis) and emissions of other species are effectively unchanged (see Table 5.2) can be seen from the behaviour of the three $PM_{2.5}$ inorganic ions.

Whereas $PM_{2.5}$ $SO_4^=$ and NH_4^+ experience reductions in most of the domain, $PM_{2.5}$ NO_3^- behaves quite differently. The region east of the Mississippi River, where $SO_4^=$ levels are high and NH_4^+ values are low (e.g., Figure 5.16 b-c), is known to be NH_3-limited. Large reductions in SO_2 emissions in this region will result in reduced $SO_4^=$ levels and may permit "NO_3^- substitution", a phenomenon where reductions in $SO_4^=$ concentration may free up NH_3 gas which can then react with HNO_3 vapour to form NH_4NO_3 (e.g., West et al., 1999). When this occurs, the net result is a smaller corresponding decrease or even an increase in $PM_{2.5}$ levels. West of the Mississippi River, on the other hand, $SO_4^=$ levels are lower, NH_4NO_3 occurs more commonly, and decreases in NO_x emissions result in predicted decreases in particle NO_3^- levels. The decreases are larger for the 2020 control-base scenario pair, consistent with the larger NO_x reductions for this scenario.

5.2.2.2 *Summer Period*

Figures 5.20 to 5.23 summarize the AURAMS $PM_{2.5}$ predictions for the summer episode simulations. Figures 5.20 and 5.22 are summer-period counterparts to Figures 5.16 and 5.18 for the winter period; the four panels in Figures 5.20 and 5.22 show the predicted ground-level $PM_{2.5}$ mass and $PM_{2.5}$ $SO_4^=$, NH_4^+, and NO_3^- concentration fields averaged over the last 11 days of the simulations (July 8-18, 1995) for the 2010 and 2020 base cases, respectively. The colour scheme and contour intervals are the same for these two figures and are also identical to those used in the two winter-period figures, allowing easy comparison of seasonal variations.

The relative contributions of particle $SO_4^=$ and NO_3^- are reversed for the summer period vis-à-vis the winter period. It is clear from Figures 5.20 and 5.22 that $SO_4^=$ is predicted to be the dominant constituent of $PM_{2.5}$ during the summer over eastern North America, with $SO_4^=$ contributing over half of $PM_{2.5}$ mass east of the Mississippi. (Note that the $SO_4^=$ contours are exactly half the magnitude of the $PM_{2.5}$ contours.) Particle NO_3^- on the other hand, is predicted to be a minor component restricted to a few areas with high NH_3 emissions and lower $SO_4^=$ levels. Note that the $PM_{2.5}$ levels predicted by AURAMS over the western Atlantic Ocean are due to both transport of continental pollutants and sea-salt emissions from the ocean surface. The contribution of sea-salt emissions is also evident in northern Canada in Hudson Bay and James Bay, where $PM_{2.5}$ levels were predicted to be much lower in this same area in the winter time due to the presence of sea-ice cover (cf., Figures 5.16 and 5.18).

As noted in Section 5.2.2.1, Table 5.2 shows that domain-total emissions of VOC, NH_3, and primary $PM_{2.5}$ are larger for the 2020 base case than for the 2010 base case whereas SO_2 and NO_x emissions are smaller. This suggests *a priori* that $PM_{2.5}$ $SO_4^=$ concentrations should be smaller for the 2020 base case relative to the 2010 base case while $PM_{2.5}$ total mass, $PM_{2.5}$ NO_3^-, and $PM_{2.5}$ NH_4^+ concentrations might either increase or decrease. Comparing Figures 5.20 and 5.22, we see that maximum $PM_{2.5}$ $SO_4^=$ does decrease for the 2020 base case (by 3 $\mu g/m^3$), maximum $PM_{2.5}$ NH_4^+ decreases slightly (by 0.1 $\mu g/m^3$), maximum $PM_{2.5}$ NO_3^- also decreases (by 1 $\mu g/m^3$), but maximum $PM_{2.5}$ mass increases slightly (by 0.06 $\mu g/m^3$). The probable explanation for the predicted increase in summer maximum $PM_{2.5}$ mass, despite the decrease in $SO_4^=$, NO_3^-, and NH_4^+ concentrations, is a larger increase in local primary $PM_{2.5}$ emissions (see Table 5.2).

The four panels in Figures 5.21 and 5.23 show the predicted ground-level $PM_{2.5}$ mass and $PM_{2.5}$ $SO_4^=$, NH_4^+, and NO_3^- *difference* fields averaged over the last 11 days of the summer simulations (July 8-18, 1995) for the 2010 control case minus the 2010 base case and for the 2020 control case minus the 2020 base case, respectively. Again, the colour scheme and contour intervals for these two figures are identical to those used in the two winter-period difference-field figures (Figures 5.17 and 5.19), allowing easy comparison of seasonal variations.

Comparison of the 2010 and 2020 summer control case simulations with the corresponding base case simulations (Figures 5.17 and 5.19) indicates that the additional SO_2 and NO_x emissions reductions proposed beyond current (i.e., "Approved") legislation result in reductions in $PM_{2.5}$ mass of up to over 6 $\mu g/m^3$ across most of the AURAMS domain. These reductions are driven by reductions in $PM_{2.5}$ $SO_4^=$ mass and related but much smaller reductions in $PM_{2.5}$ NH_4^+ mass.

Interestingly, as in the winter period, a small increase in $PM_{2.5}$ NO_3^- concentration (in the 0.2-1.0 $\mu g/m^3$ range) is predicted to occur in the U.S. Northeast and the Atlantic and Gulf of Mexico states in spite of the overall decreases in NO_x emissions for these two scenario pairs (10% and 16%, respectively). Again, as in the winter case, the probable explanation for this is NO_3^- substitution. This explanation is supported by the differences between Figures 5.21b and 5.23b and Figures 5.21d and 5.23d in the southeastern U.S. Comparing Figures 5.21b and 5.23b, the predicted reduction in $SO_4^=$ levels over Alabama and eastern Tennessee is noticeably larger for the 2020 scenario pair than for the 2010 scenario pair. This difference is consistent with the geographic variations in the imposed SO_2 emission reductions. If the SO_2 emission reductions for the 2010 control-base scenario pair and 2020 control-base scenario pair are tabulated on a regional basis, the decreases in SO_2 emissions for the 2010 and 2020 scenario pairs are 33 percent and 35 percent, respectively, for the states near the Great Lakes (MI, OH, KY, IN, IL, WI), 35 percent and 43 percent for the northeastern U.S. states, but 12 percent and 35 percent for the southeastern states (NC, SC, GA, FL, AL, MS, TN). The relatively larger decrease in $SO_4^=$ concentrations in the Southeast is then accompanied by a relatively larger increase in $PM_{2.5}$ NO_3^- concentration in the Southeast as compared to the U.S. Northeast or Great Lakes regions.

5.2.3 Comparison with REMSAD Results

It is not appropriate to compare results from the two sets of episodic AURAMS simulations directly with the REMSAD 1996 annual results presented in Section 5.1 due to issues of representativeness. However, the monthly REMSAD results for January and July 1996 that are also presented in Section 5.1 provide more suitable reference points and permit a qualitative comparison between the two models' predictions of seasonal differences in atmospheric response to the same emission reductions. [A direct comparison is still not appropriate since the simulation periods and hence the meteorological conditions are different.] This comparison can in turn provide additional weight of evidence to support the reasonableness of both models' predictions (when two such independent models agree at least qualitatively with each other) or else raise questions when the predictions disagree both quantitatively and qualitatively (e.g., Seigneur and Moran, 2003).

For the 2020 base case in mid-winter, AURAMS and REMSAD both predict NH_4NO_3 to be the dominant inorganic compound over eastern North America (compare Figure 5.18 and Figures 5.4a, 5.7a, and 5.10a). Like AURAMS, REMSAD also predicts a west-to-east decrease in $PM_{2.5}$ NO_3^- differences across the U.S. Midwest and Ohio Valley for January 1996 (see Figures 5.10b and 5.19d) and the occurrence of some particle NO_3^- increases (i.e., disbenefits) for NO_x emission reductions.

For the 2020 base case in the summer, AURAMS and REMSAD both predict $PM_{2.5}$ $SO_4^=$ to be the dominant inorganic species by mass (compare Figure 5.22 and Figures 5.5a, 5.8a, and 5.11a). The AURAMS and REMSAD $PM_{2.5}$ NO_3^-fields in the summer have quite similar spatial patterns, characterized by scattered pockets of elevated NO_3^- along the southern shore of Lake Michigan, the northern shore of Lake Erie, and in the Mississippi

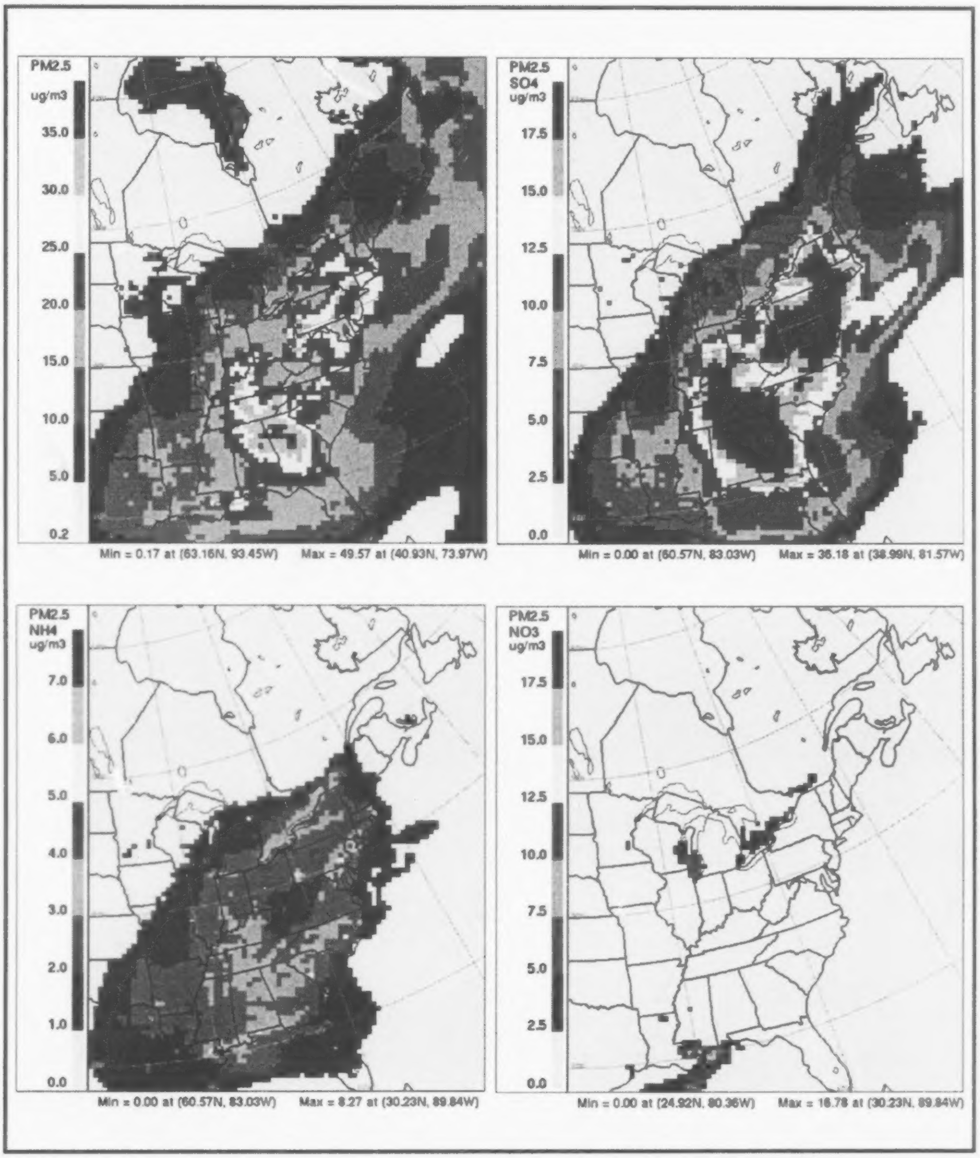
PM2.5
ug/m3
35.0
30.0
25.0
20.0
15.0
10.0
5.0
0.2
Min = 0.17 at (63.16N, 93.45W)
Max = 49.57 at (40.93N, 73.97W)
PM2.5
SO4
ug/m3
17.5
15.0
12.5
10.0
7.5
5.0
2.5
0.0
Min = 0.00 at (60.57N, 83.03W)
Max = 36.18 at (38.99N, 81.57W)
PM2.5
NH4
ug/m3
7.0
6.0
5.0
4.0
3.0
2.0
1.0
0.0
Min = 0.00 at (60.57N, 83.03W)
Max = 8.27 at (30.23N, 89.84W)
PM2.5
NO3
ug/m3
17.5
15.0
12.5
10.0
7.5
5.0
2.5
0.0
Min = 0.00 at (24.92N, 80.36W)
Max = 16.78 at (30.23N, 89.84W)

Figure 5.20 - : Eleven-day-average $PM_{2.5}$ mass concentration field and $PM_{2.5}$ inorganic chemical component concentration fields predicted by AURAMS for the July 8-18, 1995 summer period for the "2010 base" case emissions: (a) top left panel - $PM_{2.5}$ mass; (a) top right panel - $PM_{2.5}$ $SO_4^=$ mass; (c) lower left panel - $PM_{2.5}$ NH_4^+ mass; (d) lower right panel - $PM_{2.5}$ NO_3^- mass. All fields are at 15 m height in units of µg/m³.

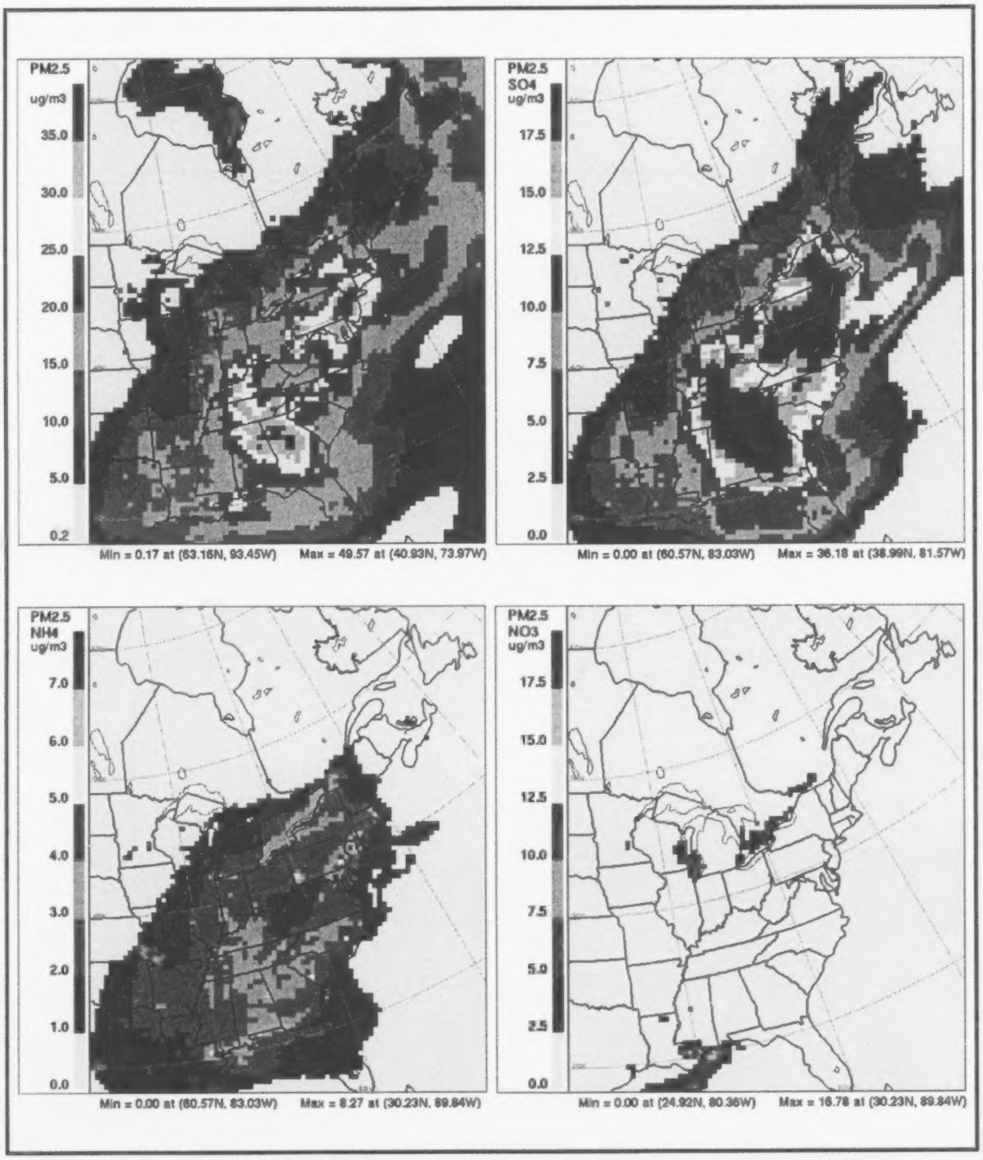
PM2.5
ug/m3
35.0
30.0
25.0
20.0
15.0
10.0
5.0
0.2
Min = 0.17 at (63.16N, 93.45W)
Max = 49.57 at (40.93N, 73.97W)
PM2.5
SO4
ug/m3
17.5
15.0
12.5
10.0
7.5
5.0
2.5
0.0
Min = 0.00 at (60.57N, 83.03W)
Max = 36.18 at (38.99N, 81.57W)
PM2.5
NH4
ug/m3
7.0
6.0
5.0
4.0
3.0
2.0
1.0
0.0
Min = 0.00 at (60.57N, 83.03W)
Max = 8.27 at (30.23N, 89.84W)
PM2.5
NO3
ug/m3
17.5
15.0
12.5
10.0
7.5
5.0
2.5
0.0
Min = 0.00 at (24.92N, 80.36W)
Max = 16.78 at (30.23N, 89.84W)

Figure 5.21 - : Eleven-day-average $PM_{2.5}$ mass concentration difference field and $PM_{2.5}$ inorganic chemical component concentration difference fields predicted by AURAMS for the July 8-18, 1995 summer period for the "2010 control" case minus the "2010 base" case: (a) top left panel - $PM_{2.5}$ mass; (b) top right panel - $PM_{2.5}$ $SO_4^=$ mass; (c) lower left panel - $PM_{2.5}$ NH_4^+ mass; (d) lower right panel - $PM_{2.5}$ NO_3^- mass. All fields are at 15 m height in units of μg/m³. Negative values denote a reduction for the "2010 control" case relative to the "2010 base" case.

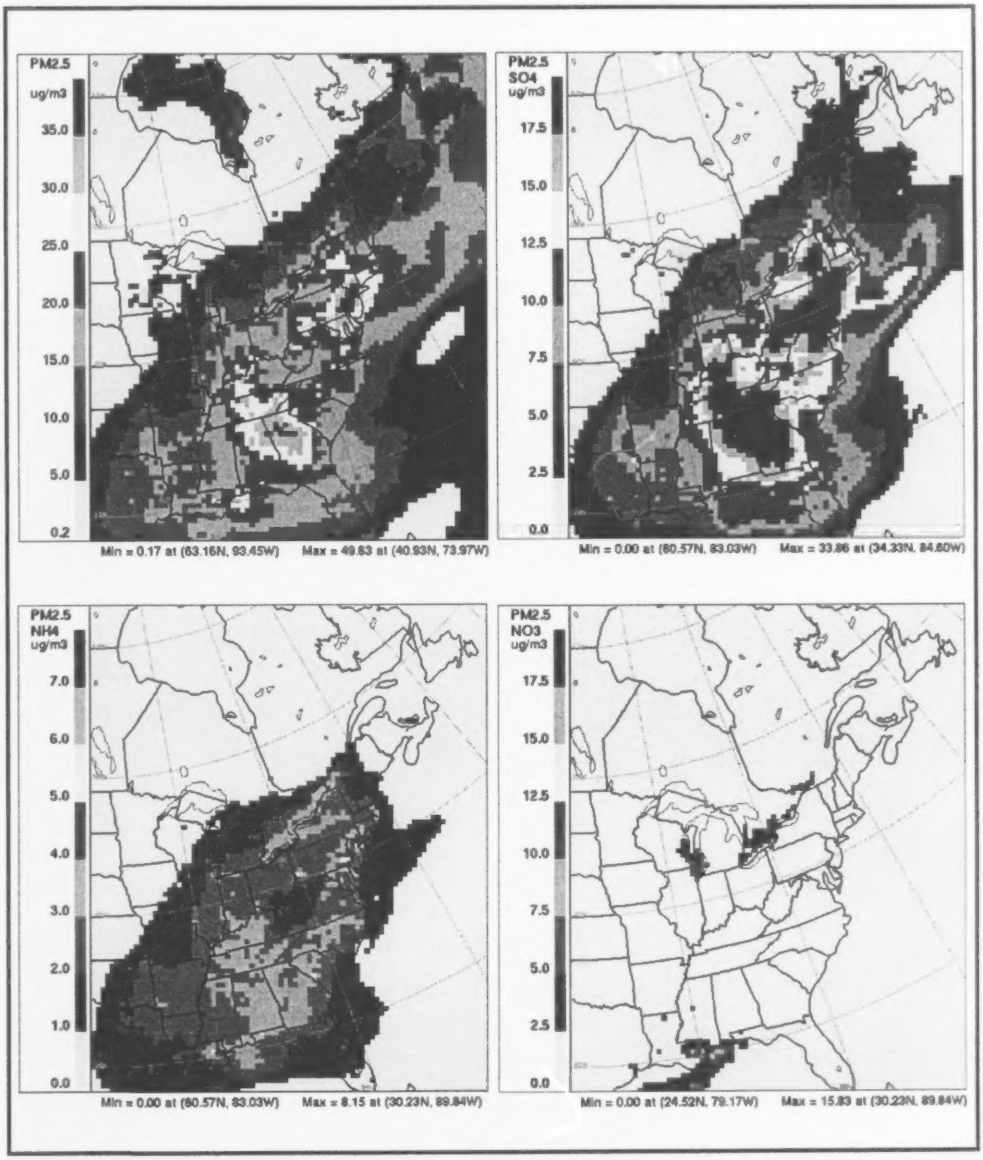
PM2.5
ug/m3
35.0
30.0
25.0
20.0
15.0
10.0
5.0
0.2
Min = 0.17 at (63.16N, 93.45W)
Max = 49.63 at (40.93N, 73.97W)
PM2.5
SO4
ug/m3
17.5
15.0
12.5
10.0
7.5
5.0
2.5
0.0
Min = 0.00 at (60.57N, 83.03W)
Max = 33.86 at (34.33N, 84.60W)
PM2.5
NH4
ug/m3
7.0
6.0
5.0
4.0
3.0
2.0
1.0
0.0
Min = 0.00 at (60.57N, 83.03W)
Max = 8.15 at (30.23N, 89.84W)
PM2.5
NO3
ug/m3
17.5
15.0
12.5
10.0
7.5
5.0
2.5
0.0
Min = 0.00 at (24.52N, 79.17W)
Max = 15.83 at (30.23N, 89.84W)

Figure 5.22 - Same as Figure 5.20 but for the "2020 base" case emissions.

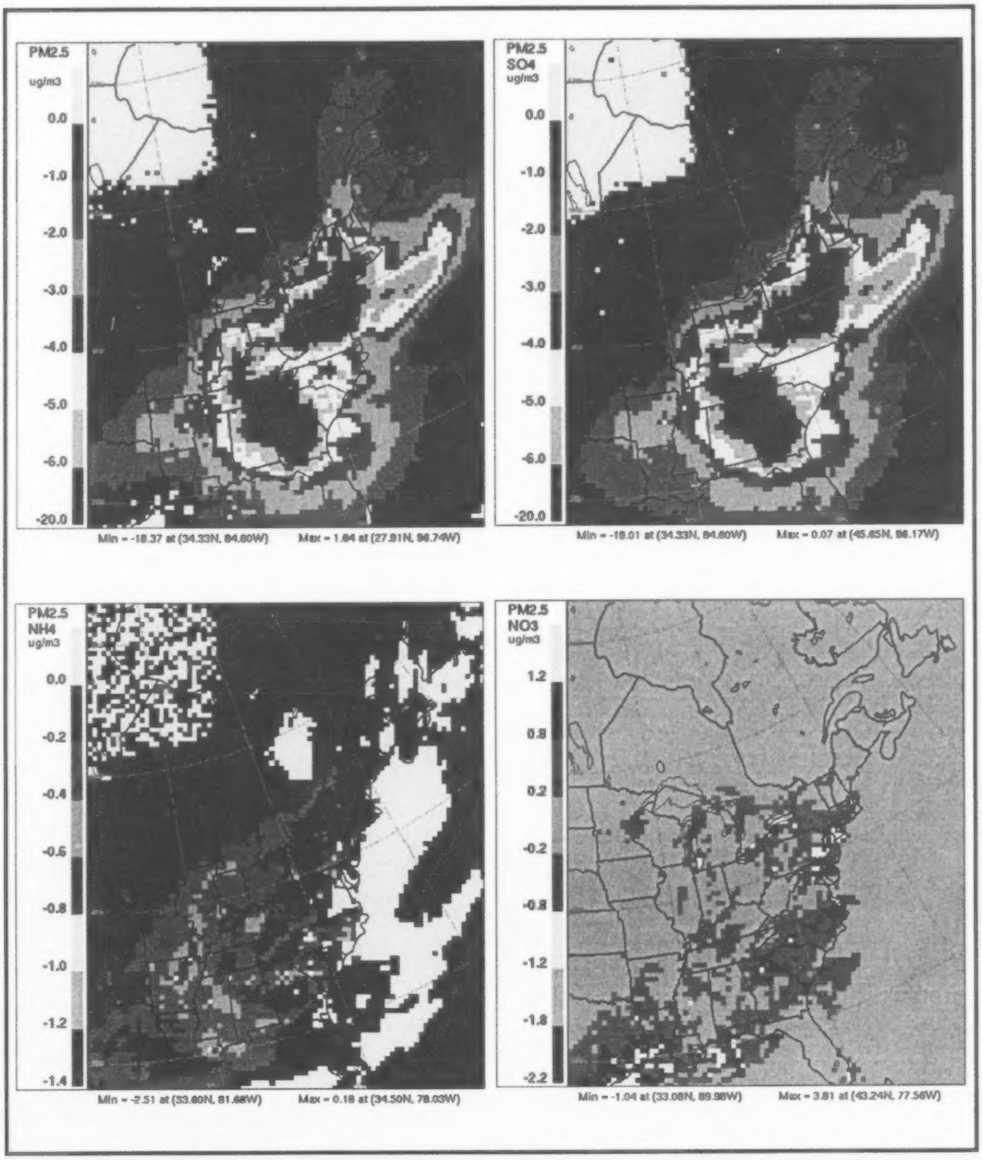
PM2.5
ug/m3
0.0
-1.0
-2.0
-3.0
-4.0
-5.0
-6.0
-20.0
Min = -18.37 at (34.33N, 84.60W)
Max = 1.84 at (27.91N, 96.74W)
PM2.5
SO4
ug/m3
0.0
-1.0
-2.0
-3.0
-4.0
-5.0
-6.0
-20.0
Min = -18.01 at (34.33N, 84.60W)
Max = 0.07 at (45.65N, 96.17W)
PM2.5
NH4
ug/m3
0.0
-0.2
-0.4
-0.6
-0.8
-1.0
-1.2
-1.4
Min = -2.51 at (33.60N, 81.68W)
Max = 0.18 at (34.50N, 78.03W)
PM2.5
NO3
ug/m3
1.2
0.8
0.2
-0.2
-0.8
-1.2
-1.8
-2.2
Min = -1.04 at (33.08N, 89.98W)
Max = 3.81 at (43.24N, 77.56W)

Figure 5.23 - Same as Figure 5.21 but for the "2020 control" case minus the "2020 base" case.

delta (Figures 5.11a and 5.22d). The spatial patterns of the REMSAD 2020 control–base scenario pair differences for July 1996 are also qualitatively similar to the AURAMS difference fields for $PM_{2.5}$ and $PM_{2.5}$ $SO_4^=$ (Figure 5.5b vs. Figure 5.23a and Figure 5.8b vs. Figure 5.23b, respectively), but less so for $PM_{2.5}$ NH_4^+ (Figure 5.14b vs. Figure 5.23c) and not at all for $PM_{2.5}$ NO_3^- (Figure 5.11b vs. Figure 5.23d). The agreement for $SO_4^=$ changes and disagreement for NO_3^- changes between the two models is consistent with current assessments of PM model performance that uncertainties are larger for NO_3^- prediction than for $SO_4^=$ prediction (e.g., see Appendix).

Both AURAMS and REMSAD predict the maximum wintertime reductions in $PM_{2.5}$ to be smaller than, and to occur to the west of, the maximum summertime reductions (Figure 5.19a vs. Figure 5.23a; Figure 5.4b vs. Figure 5.5b), although AURAMS does not support the REMSAD predictions of large wintertime reductions of $PM_{2.5}$ in the Carolinas. Finally, despite the mix of emission increases and decreases between the 2010 base and 2020 base cases (Table 5.2), both AURAMS and REMSAD predict the $PM_{2.5}$ mass to be larger (on an annual basis) for the 2020 base case than for the 2010 base case (Figures 5.2a and 5.3a and Figures 5.20 and 5.22).

5.2.4 Summary and Conclusions

The AURAMS scenario simulations indicate that proposed additional SO_2 and NO_x emission reductions should provide additional reductions in ambient $PM_{2.5}$ levels in eastern North America. These reductions, however, are related most strongly to reductions in $PM_{2.5}$ $SO_4^=$ mass. Since this species has a well known seasonal cycle, with maximum values occurring in the summer and minimum values occurring in the winter, it is likely that the magnitude of the resulting $PM_{2.5}$ mass reductions will also vary by season. The AURAMS simulations support this expectation. The AURAMS simulations also predict that the largest $PM_{2.5}$ reductions may occur west of the Mississippi in the winter but east of the Mississippi in the summer.

The results are more complicated for SO_x emission reductions that are not accompanied by adequate NO_x emission reductions, since AURAMS predicts that these will be associated with decreases in $PM_{2.5}$ NO_3^- mass in some parts of eastern North America but with *increases* in other areas due to the phenomenon of nitrate substitution. Nitrate substitution is in turn determined by existing ambient ammonia and sulphate levels and by the magnitude of $SO_4^=$ reductions. The predicted occurrence of NO_3^- substitution suggests that there may be value in investigating potential benefits due to ammonia emission reductions in conjunction with SO_2 and NO_x emission reductions (for the 2010 and 2020 control-base scenario pairs considered here, NH_3 emissions were held constant). On the other hand, NO_x emission reductions will produce co-benefits in terms of reduced summertime ozone levels and reduced TNO_3 (i.e., the sum of HNO_3 and p-NO_3^-) deposition to land surfaces and to water bodies.

Comparisons of the AURAMS winter and summer predictions with REMSAD winter and summer predictions showed good qualitative agreement or consistency for all four PM fields and for both seasons in terms of the atmospheric response to the same emission reductions. That is, the two models predicted the same directional changes for all species for both seasons and also the same relative rankings of the changes between species and between seasons (e.g., changes in $PM_{2.5}$ NH_4^+ mass are larger in the summer than the winter; changes in $PM_{2.5}$ NH_4^+ mass are larger than changes in $PM_{2.5}$ NO_3^- mass in the summer, etc). And despite their very different treatments of chemistry, both models predicted the occurrence of $PM_{2.5}$ NO_3^- increases in both the winter and summer seasons. On the other hand, the changes predicted by AURAMS were always larger in magnitude than those predicted by REMSAD (consistent with the shorter episodes and averaging periods considered in the AURAMS modelling) and the predicted spatial distributions were sometimes quite different (e.g., summertime 2020 control-base $PM_{2.5}$ NO_3^- differences).

5.3 RESULTS OF CMAQ MODELLING IN THE GEORGIA BASIN – PUGET SOUND REGION

The Community Multiscale Air Quality (EPA, 1999; MCNC, 2001) modelling system was applied over the Pacific Northwest to gain insight into the significance of the transboundary transport of air pollutants across the international border separating British Columbia and Washington State, and to determine the impacts of forecast changes in pollutant emissions expected by 2010 and 2020 on ambient air quality in 2000.

The version of CMAQ used for this work is the June 2001 version that was parallelised (RWDI, 2003a) for a PC/Linux cluster running Redhat Linux v7.3. The photochemical mechanism used was the 'radm2_ae2_aq' mechanism. This mechanism was selected in order to be compatible with CMAQ modelling being performed by others over the Pacific Northwest. The CMAQ modelling domain used encompasses the Pacific Northwest stretching from central Oregon to central British Columbia and from western Idaho to the Pacific Ocean, or in other words an 800 km wide domain straddling 500 km each side of the Canada/US border with a domain resolution of 12 km. Nested within this domain is a 4-km fine resolution subdomain centred over the Georgia Basin and Puget Sound. Resolutions of this magnitude are required in order to try to account for the complex terrain and marine environments of the Pacific Northwest. See Figure 5.24 for geographical references and domain extents.

In this case, the CMAQ chemistry transport model is driven using the MC2 (Mesoscale Compressible Community) meteorological model. MC2 is based on the Euler equations and is a fully compressible non-hydrostatic model using generalised terrain-following coordinates. Complete descriptions of MC2 are available in Laprise (1997). The MC2 meteorology is at a resolution of 3.3 km using version 4.9.1 of the MC2 dynamics

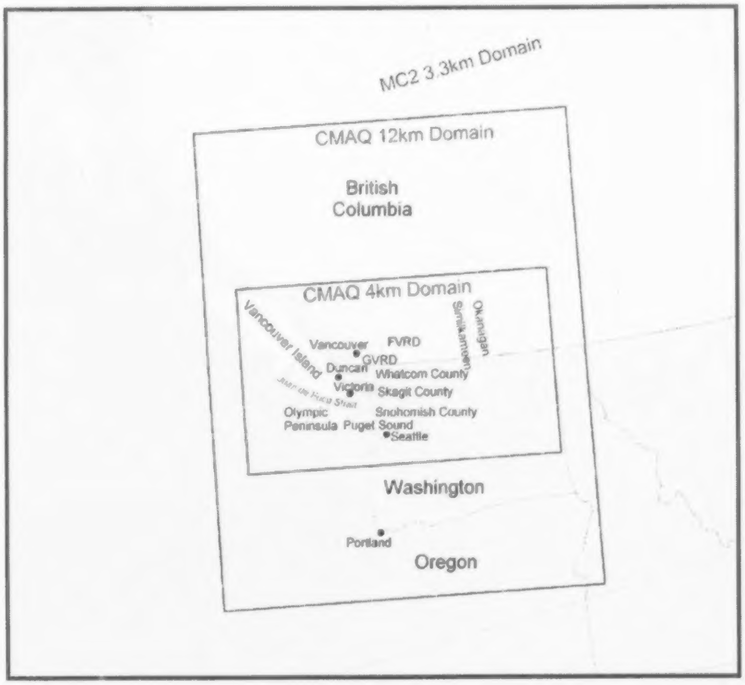
MC2 3.3km Domain
CMAQ 12km Domain
British Columbia
CMAQ 4km Domain
Vancouver Island
Vancouver
FVRD
GVRD
Duncan
Whatcom County
Victoria
Skagit County
Juan de Fuca Strait
Olympic Peninsula
Snohomish County
Puget Sound
Seattle
Similkameen
Okanagan
Washington
Portland
Oregon

Figure 5.24 - Geographical references and domain extents for the CMAQ model. The Strait of Georgia, not indicated in the figure, lies between southern Vancouver Island and mainland British Columbia. The lower Fraser Valley, also not indicated, stretches from Vancouver to the Fraser Valley Regional District.

and version 3.7 of the RPN/CMC physics package. This meteorology was then interpolated and reprojected onto the CMAQ grid and remapped for ingest by meteorology/chemistry interface processor (MCIP) of CMAQ and for ingest by the SMOKE emissions model.

The CMAQ simulations were performed using meteorology for a typical summer period and for a typical winter period. The summer period selected was August 09-20, 2001. This period embraced a dry blocking weather pattern of two regimes: a stagnant phase, and a well-mixed phase. This period coincided with the Pacific 2001 Field Study (Li, 2001) from which there was a rich meteorological and chemical dataset. The winter period selected was December 01-13, 2002. This period comprised a short stagnant phase, followed by a weak blocking pattern, and ended with a transient, well-mixed phase. For both summer and winter periods, 2000 emissions inventory data were used. There were no known significant anthropogenic emission differences between 2000, 2001, and 2002.

The Pacific 2001 field study dataset was used to evaluate CMAQ performance over the Georgia Basin-Puget Sound region. In spite of the complex terrain and marine environment challenges of the Pacific Northwest, it was felt that the CMAQ performance was consistent with that found by others in Canada and the United States. Overall, the model performed well for predicting $PM_{2.5}$ at both the 12-km resolution and 4-km resolution domains. It should be noted that the CMAQ "I+J" particle mass was used as if it were $PM_{2.5}$, even though the difference can be substantial both conceptually and quantitatively. Subsequent references will not make this distinction.

Overall, the diurnal patterns and magnitude of the modelled daily average $PM_{2.5}$ levels were quite good. In general, the 4-km $PM_{2.5}$ results were better than those for the 12-km domain, particularly at night. This is believed to be the results of local emission sources and the more heterogeneous nature of $PM_{2.5}$ as a regional pollutant compared to ozone. Secondary particulate matter can form very rapidly or slowly depending on the environmental conditions and emission source characteristics.

5.3.1 Qualitative Analysis of Simulations for the 2000 Base Case

5.3.1.1 *Summer* $PM_{2.5}$

In the 12-km grid domain, $PM_{2.5}$ starts to build up in the vicinity of the major primary sources (urban/industrial/marine areas) after about 24 hours of model 'spin-up'. The combination of sea breeze and an onshore westerly flow pushes the $PM_{2.5}$ concentrations inland, toward the east away from the urban and marine areas during the daytime. And, mountain flows from the northeast along the Fraser Valley push the pollutants back toward the west during the night. This day-night pattern in $PM_{2.5}$ levels persists until the onset of the well-mixed phase. In the 4-km simulations, results are similar but show somewhat improved resolution of local hotspots near the sources of primary $PM_{2.5}$ emissions (Figure 5.25).

5.3.1.2 *Winter* $PM_{2.5}$

During the model 'spin-up' and stagnant meteorological periods (December 01-07), $PM_{2.5}$ levels build up around and slightly downwind (east) of the urbanized areas of the Greater Vancouver Regional District (GVRD), Seattle, and Portland. During the weak blocking period (December 07-10), offshore flows and land breeze effects push the urban plumes toward the west and over the Pacific

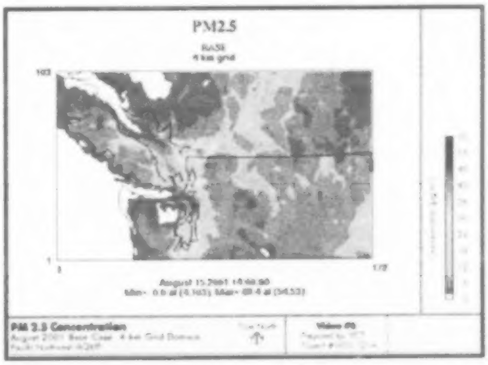

Figure 5.25 - $PM_{2.5}$ concentrations for the August, 2001 summer base case, predicted over the CMAQ domain on a 4x4 km^2 grid.

Ocean. It is notable that during December 07-09, high-concentrations of $PM_{2.5}$, which originally formed in the Seattle area and over the GVRD, moved north and westward toward Vancouver Island. This polluted air mass then spreads to the northwest along the Strait of Georgia, westward along the Juan de Fuca Strait, and over the southern coast of Vancouver Island. The result was relatively high $PM_{2.5}$ levels over southern Vancouver Island (e.g., Victoria, Duncan), the Strait of Georgia, and the coastal area of the GVRD. In contrast to the local-scale impacts, these impacts are more transboundary in nature. December 10-13 is marked by a well-mixed phase with much stronger southerly and southwest wind flows that effectively purge the polluted air mass, resulting in significantly lower $PM_{2.5}$ levels throughout the 12-km domain.

5.3.2 Significance of Transboundary Transport

The approach used to look at the significance of transboundary transport was to compare the ambient air concentrations of $PM_{2.5}$ in the base case scenarios (all emissions left on) with those that resulted when either all of the Canadian anthropogenic emissions ("NOCAN" scenario) or all of the American anthropogenic emissions were turned off ("NOUS" scenario). The comparisons were carried out for the same typical summer and winter periods identified for the base case. The relationship between emissions and ambient air quality is not linear although the simulations provide a reasonable indication of the relative impacts associated with transboundary pollutant transport.

5.3.2.1 *Qualitative Analysis of the No-U.S. Anthropogenic Emissions Scenario*

Summer $PM_{2.5}$: Biogenic and soil emissions of VOCs, NO_x and NH_3 in the United States continue to contribute to the formation of $PM_{2.5}$ over the U.S. portion of the domain. Due to onshore westerly flows, the $PM_{2.5}$ plumes form over the GVRD/FVRD (Fraser Valley Regional District) and the Strait of Georgia (from marine emissions), then move eastward along the Canada/U.S. border. Peak NOUS $PM_{2.5}$ levels in the GVRD from August 11-16 are lower (about 36 µg/m^3) than what is seen when the U.S. emissions are left on (about 50 µg/m^3), which suggest that, under these meteorological conditions, U.S. emissions contribute to precursor concentrations and resulting Canadian ambient $PM_{2.5}$ levels. However, this impact of transboundary pollutant transport is relatively short-ranged.

On several occasions, $PM_{2.5}$ levels build up over Juan de Fuca Strait and around the southern tip of Vancouver Island before travelling southward over the northern tip of the Olympic Peninsula and Puget Sound. Marine emission sources and emissions from Victoria are thought to play the major role in this phenomenon. Emissions from the GVRD can also be seen to drift southward and impact northern Whatcom County.

Winter $PM_{2.5}$: The model results for the NOUS scenario show low $PM_{2.5}$ levels in the United States compared to the base case, except for on December 02-03 when easterly winds change to northerly winds for a period of time. During this period, the $PM_{2.5}$ plume moves from GVRD/FVRD and Strait of Georgia to the northern tip of the Olympic Peninsula and to Seattle. Other minor intrusions into the United States occur all along the valleys that line the Canada/U.S. border during these periods. In contrast, the NOUS $PM_{2.5}$ levels over Vancouver Island are lower than the base case, indicating that elevated $PM_{2.5}$ levels from the United States typically travelled northward over Vancouver Island. On the other days during this episode, there is little or no cross-boundary impact from Canada to the United States due to the predominantly easterly to southerly wind flows.

5.3.2.2 *Qualitative Analysis of the No-Canadian Anthropogenic Emissions Scenario*

Summer $PM_{2.5}$: Due to the onshore westerly flow, the urban $PM_{2.5}$ plumes over and downwind of Seattle and Portland move generally eastward, parallel to the Canada/U.S. border, resulting in relatively little transboundary transport into the

GVRD/FVRD and the southern portion of the Strait of Georgia for a number of hours during the simulation. However, at other times (such as during the late afternoon of the last four to five days of the episode) $PM_{2.5}$ levels in north-central Washington in the NOCAN simulation are much lower than the base case results (about 15 to 20 µg/m^3 lower). This suggests that a normally polluted air mass from the Canadian side of the border, likely associated with marine emissions, moves southward into the United States.

Winter $PM_{2.5}$: The NOCAN simulation results point to some unique transboundary phenomena. From December 01-05, easterly flows dominate the entire domain and the $PM_{2.5}$ plumes formed over the Seattle and Portland regions move offshore to the west, over the Pacific Ocean. There are no significant transboundary impacts from the United States on Canada, except for the lower tip of Vancouver Island (e.g. Victoria) and the GVRD area.

However during December 06-10, the wind flow patterns veer to the southeast, causing the $PM_{2.5}$ plume from the Seattle region to move northwestward across the straits of Georgia and Juan de Fuca and over the southern coast of Vancouver Island. Compared to the base case results, the $PM_{2.5}$ concentrations from NOCAN simulations in these areas are quite high with peaks of around 24 µg/m^3 (i.e., about 50 to 60 percent of base case levels can be attributed to transport from the United States). There is relatively little evidence of transboundary transport elsewhere in the model domain.

5.3.2.3 *Summary and Conclusions*

The NOUS and NOCAN simulations indicate that, for the specific meteorological and synoptic patterns evaluated, local/urban-scale air quality impacts from transboundary transport occur along the border (within ±50 km) with some frequency. However, the incidence of long-range/regional transport (over 100 km) is low. The long-range transport results may be different for other study periods with different meteorology. The winter simulations are indicative of a bigger long-range transport issue. For example, during December 06-10, with a southeast wind pattern, plumes travel from the Seattle area to Vancouver Island. Due to the combination of geography, nature of emissions, and regional wind flow patterns, there is little longer range transboundary transport evident elsewhere in the model domain.

Based on these model results, there appear to be different regimes of transboundary pollutant transport that depend on the specific meteorological conditions and geography of the region. Long-range transport does occur, but less often than the more local-scale transboundary transport. Local transboundary transport occurs all along the British Columbia/Washington border, particularly in the vicinity of the GVRD and southern Vancouver Island.

5.3.3 Impacts of Forecast Emissions for 2010 and 2020

The approach used to determine the impacts of forecast changes in pollutant emissions on ambient air quality was to substitute the 2000 anthropogenic emissions with those forecasted for 2010 and 2020 and then compare changes in simulated air quality.

Overall, carbon monoxide (CO), VOC, and NO_x emissions increase in Washington State but generally decrease in British Columbia for both the 2010 and 2020 scenario years. The overall decrease in NO_x emissions projected throughout British Columbia results from decreased emissions from mobile sources. Emissions of PM_{10} are projected to increase generally in both Washington State and British Columbia by 2010 and 2020 however, in the FVRD a decrease is projected. Emissions of $PM_{2.5}$ are projected to increase in Washington State by the same percentage as the PM_{10} emissions, but are expected to remain relatively unchanged in British Columbia. Impacts associated with these and other regional variations in emissions trends can be seen in the CMAQ model results.

5.3.3.1 *Qualitative Analysis of Simulations for the 2010 Forecast*

Summer $PM_{2.5}$: Overall, the 2010 $PM_{2.5}$ pattern is similar to 2000, with maximum $PM_{2.5}$ levels occurring in urban areas during the early morning when meteorological conditions are least favourable for dispersion. In the GVRD, peak 1-hour $PM_{2.5}$ concentrations increase by up to 20 µg/m^3 compared to 2000, predominantly due the projected increase in primary $PM_{2.5}$ emissions in that area possibly along with increased NO_x and SO_x from marine vessel emissions leading to increased secondary formation of PM or with decreased NO_x from on-road vehicles.. Conversely, peak $PM_{2.5}$ concentrations in the FVRD decrease by up to 20 µg/m^3 due to the projected decrease in primary $PM_{2.5}$ emissions at that location. This occurs even though agricultural emissions, and subsequent secondary PM formation, are increased. Near Seattle and Portland, peak $PM_{2.5}$ concentrations increase slightly (by 1 or 2 µg/m^3) which is consistent with the modest projected increase in primary $PM_{2.5}$ emissions between the base case and 2010 scenarios. Elsewhere in the model domain, peak $PM_{2.5}$ concentrations exhibit relatively little change.

Winter $PM_{2.5}$: Generally, the $PM_{2.5}$ pattern in the 2010 simulations is similar to 2000. The 2010 results show a modest increase in $PM_{2.5}$ levels in the large urban areas (generally less than about 10 µg/m^3) and a small increase downwind of the urban areas. For December 01-05, easterly flows dominate the entire domain and $PM_{2.5}$ plumes that form over the urban centres of Vancouver, Seattle, and Portland move offshore to the west and northwest. From December 06-10, the wind regime is dominated by southeast flow, causing $PM_{2.5}$ from the Seattle and Puget Sound regions to move northwest across the Strait of Georgia, the Strait of Juan de Fuca, and southern Vancouver Island. Increased $PM_{2.5}$ concentrations in these areas are predominantly due to the projected increase in primary $PM_{2.5}$ emissions in the urban areas, particularly the GVRD. The GVRD levels are potentially further enhanced due to secondary PM formation from increased marine vessel emissions of NO_x and SO_x or from decreased NO_x emissions from on-road vehicles. In the FVRD, the decrease in $PM_{2.5}$ levels that is predicted to occur (up to about 15 µg/m^3) is consistent with the projected reduction in primary PM emissions in that area. Elsewhere in the domain, predicted changes in $PM_{2.5}$ concentrations are small.

5.3.3.2 *Qualitative Analysis of Simulations for the 2020 Forecast*

Summer and Winter $PM_{2.5}$: The overall summer $PM_{2.5}$ pattern in the 2020 simulations is similar to 2010. In the GVRD, the increase in $PM_{2.5}$ concentrations relative to the base case is more pronounced (up to 30 µg/m^3 higher) than in 2010. The overall winter $PM_{2.5}$ pattern in 2020 is similar to 2010 but again the changes in emissions relative to the base case are more pronounced.

5.3.3.3 *Summary and Conclusions*

The fairly drastic differences in emission growth or decline by geographic region greatly affect the model results. This is particularly evident in the lower Fraser Valley, where projected emission trends in the GVRD are different from those in the FVRD. Peak $PM_{2.5}$ levels are projected to increase modestly in urban areas and increase slightly downwind of urban areas throughout the domain during both the summer and winter simulations. This result is consistent with a projected increase in primary $PM_{2.5}$ emissions in urban areas. The larger increase in the GVRD urban location may be due to either the additional secondary PM formation from increased NO_x/SO_x emissions from marine vessels or to decreased NO_x emissions from on-road vehicles. $PM_{2.5}$ levels are predicted to decrease significantly in the FVRD, as a result of a projected large decrease in primary $PM_{2.5}$ emissions in that region.

5.4 CO-BENEFITS OF EMISSION REDUCTIONS

Reductions in emissions of $PM_{2.5}$ precursors have an impact on other air-quality issues such as ground-level ozone, acid deposition and visibility. Model applications for ground-level ozone and acid deposition endpoints have been completed by the U.S. and Canadian models for the same time periods as discussed in sections 5.1 and 5.2. The output from these simulations is not dis-

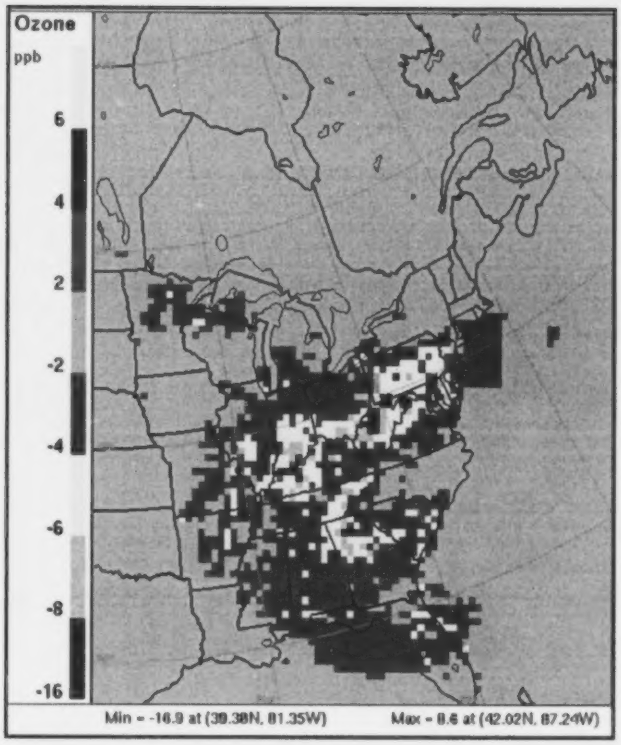
Ozone
ppb
6
4
2
-2
-4
-6
-8
-16
Min = -16.9 at (39.38N, 81.35W)
Max = 8.6 at (42.02N, 87.24W)

Figure 5.26 - Peak ozone concentration difference field at 15 m height for the July 12-15, 1995 summer period for the "2020 control" case minus the "2020 base" case. The two peak ozone concentration fields were constructed by averaging over the afternoon period (15 - 21 UTC) for 4 days (July 12th to 15th) corresponding to a regional ozone episode.

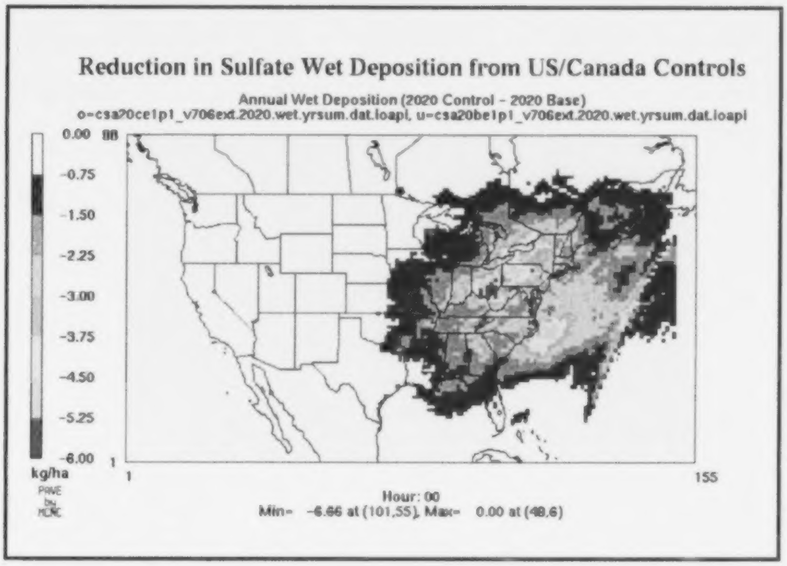
Reduction in Sulfate Wet Deposition from US/Canada Controls
Annual Wet Deposition (2020 Control - 2020 Base)
o=csa20ce1p1_v706ext.2020.wet.yrsum.dat.loapi, u=csa20be1p1_v706ext.2020.wet.yrsum.dat.loapi
0.00
-0.75
-1.50
-2.25
-3.00
-3.75
-4.50
-5.25
-6.00
kg/ha
PAVE
by
MCNC
88
1
1
155
Hour: 00
Min= -6.66 at (101,55), Max= 0.00 at (48,6)

Figure 5.27 - Annual reduction in $SO_4^=$ wet deposition from additional U.S. and Canadian controls (2020 control vs. base)

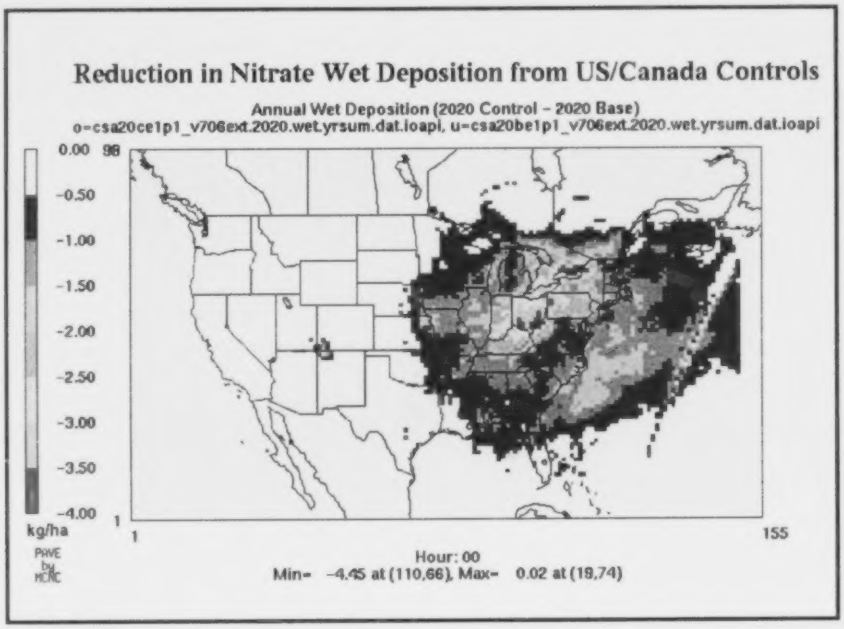
Reduction in Nitrate Wet Deposition from US/Canada Controls
Annual Wet Deposition (2020 Control - 2020 Base)
o=csa20ce1p1_v706ext.2020.wet.yrsum.dat.ioapi, u=csa20be1p1_v706ext.2020.wet.yrsum.dat.ioapi
0.00
-0.50
-1.00
-1.50
-2.00
-2.50
-3.00
-3.50
-4.00
kg/ha
98
1
1
155
PAVE by MCNC
Hour: 00
Min= -4.45 at (110,66), Max= 0.02 at (19,74)

Figure 5.28 - Annual reduction in NO_3^- wet deposition from additional U.S. and Canadian controls (2020 control vs. base).

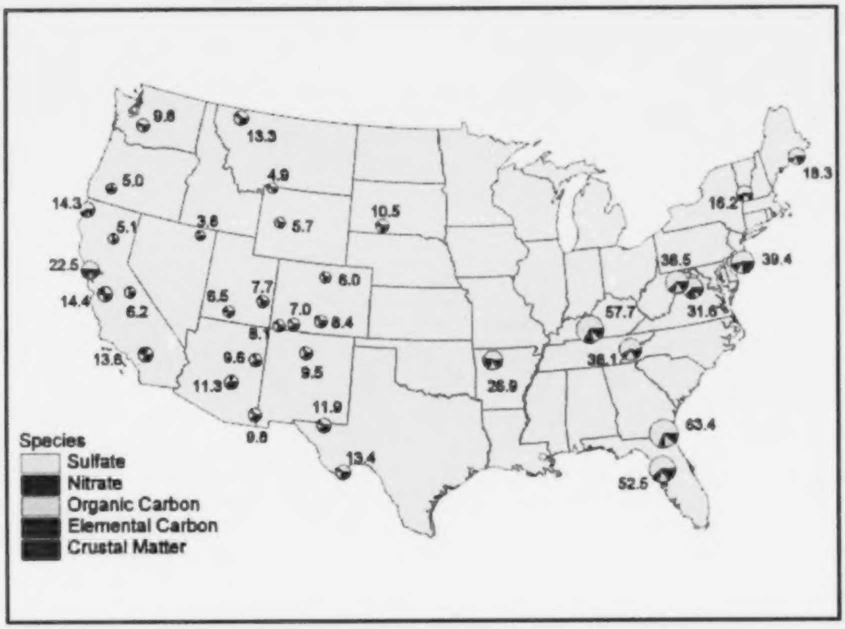
9.8
13.3
18.3
5.0
4.9
14.3
5.1
3.8
5.7
10.5
16.2
22.5
38.5
39.4
14.4
6.2
6.5
7.7
6.0
7.0
8.4
57.7
31.6
8.1
13.6
9.6
9.5
36.1
11.3
26.9
11.9
63.4
9.8
13.4
52.5
Species
Sulfate
Nitrate
Organic Carbon
Elemental Carbon
Crustal Matter

Figure 5.29 - Aerosol light extinction (in Mm^{-1}) for the haziest 20 percent days and contribution by individual particulate matter constituents, based on 1997-1999 IMPROVE data (USEPA, 1999).

cussed in great detail in this report, but the linkages between emissions reductions and the resulting co-benefits for other air quality issues are key considerations in the determination of appropriate domestic and international policies.

Figure 5.26 shows reductions in peak ozone levels of up to 5–10 ppb predicted by AURAMS to result from NO_x emission reductions between the 2020 control scenario and the 2020 base scenario.

In addition to reducing ozone and $PM_{2.5}$ $SO_4^{=}$ concentrations and, in much of eastern North America, $PM_{2.5}$ NO_3^- and NH_4^+ concentrations, the implementation of additional U.S. and Canadian controls will result in significant reductions in $SO_4^{=}$ wet deposition and TNO_3 wet deposition in 2010 and 2020. The annual reduction in 2020 $SO_4^{=}$ and TNO_3 wet deposition predicted by REMSAD to occur with the implementation of additional U.S. and Canadian controls are provided in Figures 5.27 and 5.28, respectively. The reductions in wet deposition are larger in the eastern portion of the modelling domain than the western portion of the modelling domain. These controls result in annual reductions of $SO_4^{=}$ wet depositions that are up to 6.7 kg/ha in 2020. These controls also result in annual reductions of NO_3^- wet deposition that are up to 4.5 kg/ha in 2020. The largest reductions in $SO_4^{=}$ and TNO_3 wet deposition are located in Ohio, Pennsylvania, western New York State, and southern Ontario.

Figure 5.29 illustrates aerosol light extinction for the 20 percent haziest days in the United States. Sulphate is the most significant contributor to reduced visibility, due to the particle's ability to scatter light. A reduction in sulphur compounds will result in improved visibility, particularly for the northeast, where visibility reduction at rural sites is the most significant.

5.5 KEY SCIENCE MESSAGES

- Comparisons of the AURAMS and REMSAD predictions showed good qualitative agreement and consistency for all four PM fields and both winter and summer in terms of the atmospheric response to emission reductions, with the exception of predicted responses in summertime $PM_{2.5}$ NO_3^- concentrations.
- Proposed additional SO_2 and NO_x emission reductions should provide additional reductions in ambient $PM_{2.5}$ levels in eastern North America. The observed $PM_{2.5}$ reductions may vary by season.
- SO_x reductions that are not accompanied by adequate NO_x reductions may result in NO_3^- increases in some areas. Reductions in NO_x emissions will correspond to decreases in $PM_{2.5}$ NO_3^- mass in some parts of eastern North America but increases in other areas due to NO_3^- substitution (i.e., for $SO_4^{=}$ reductions in NH_3-limited locations, the replacement of $SO_4^{=}$ by NO_3^- in the particle phase). There is significance placed on the role of NH_3 in this relationship, suggesting there may be value in investigating possible benefits due to NH_3 emission reductions in conjunction with SO_2 and NO_x emission reductions.
- In the Georgia Basin - Puget Sound region, episodic impacts from transboundary transport occur along the border (within ± 50 km) with some frequency; however, the incidence of long-range/regional transport (over 100 km) was low. Peak $PM_{2.5}$ levels are projected to increase modestly in urban areas as well as downwind of urban areas during both summer and winter simulations.
- Co-benefits of emission reductions scenarios include reduced ground-level ozone levels, reductions in NO_3^- and $SO_4^{=}$ wet deposition, and improved visibility.
- Additional model runs should be carried out to confirm and extend the model results presented in this chapter, such as annual runs of AURAMS and CMAQ and additional annual runs of REMSAD for a different meteorological year.

CHAPTER 6

RELATIONSHIPS BETWEEN SOURCES AND AMBIENT LEVELS OF PM

6.1 ATTRIBUTING SOURCES TO AMBIENT LEVELS OF PM$_{2.5}$

The complicated physical and chemical nature of transport and transformation of PM precursors requires advanced analytical techniques to characterize PM levels. Direct observation of PM events using satellite sensors can provide a qualitative perspective. However, the process of attributing sources to ambient levels of PM - that is, quantifying the relationship between sources and measured ambient PM levels - is difficult. To facilitate the determination of this relationship, three different techniques have been employed: observational receptor-oriented analyses, positive matrix factorization (PMF) and principal component analysis. All of these techniques use differences in chemical composition, particle size, meteorology, and spatial and temporal patterns, to identify emission sources that influence particle composition and particle mass. The following sections discuss applications of these techniques in Canada and the United States.

6.1.1 Observational Receptor-Oriented Analyses

Many semi-quantitative methods can be used to attribute sources to ambient levels of PM. These observational receptor-oriented analyses include time series analysis, spatial patterns, and concentration directionality.

6.1.1.1 *Quantifying the Transboundary Transport of PM$_{2.5}$ using a Geographic Information System*

Speciated IMPROVE measurements for 17 Class I sites in the eastern United States were examined in an analysis (Kenski, 2003) at the Lake Michigan Air Directors Consortium. Three-day back trajectories for these sites were calculated using HYSPLIT for the 5-year period from 1997 through 2001 (start time of noon, start height of 200 m). Using ArcView 3.2, hourly endpoints from the back trajectories were plotted. Each endpoint (1 per hour, 72 per trajectory) is associated with concentrations corresponding to the IMPROVE sample for the trajectory start date. These concentrations are averaged by state and province, as shown in Figure 6.1.

The data presented in Figure 6.1 indicate which states are associated with high concentration air masses arriving at Class I areas, but do not take into account the frequency with which air masses traverse a particular area or state. States that are closer to Class I sites will tend to contribute more PM$_{2.5}$ to those sites, because the air masses spend more time over those nearby states and emissions from nearby sources have less time to disperse and deposit than emissions from sources further away. These areas of more frequent transport can be associated with PM$_{2.5}$ concentrations that are high, low, or moderate. By combining this frequency information with the concentration information, this study derives an average contribution to PM$_{2.5}$ mass from each state/province to the Class I areas.

For example, the percent contribution from any state A to any Class I area can be estimated from the set of trajectories originating at that Class I site as:

$$\frac{Avg.Concn._{StateA}\ No.endpts_{StateA}}{\sum_{AllStates}(Concn * Endpts)} * 100$$

Table 6.1 gives the average concentration and percent PM$_{2.5}$ mass contributed by selected states and provinces to a sample of the Class I areas examined (mass contributions greater than 5 percent are highlighted).

These results can be thought of as an indicator combining the upwind status of a state/province, the geographic size of the state/province, and the magnitude of source emissions within the state/province. A state or province that is close to, and frequently upwind of, multiple Class I areas will generally contribute more mass than states or provinces that are seldom upwind, unless the concentration difference is marked. For example, Minnesota contributes a large percentage of mass to Boundary Waters (35.2 percent) although the average concentration associated with air masses in Minnesota is less than 6 µg/m³. Similarly, the Canadian provinces make significant contributions to the border-area Class I sites; Ontario provides about 16 percent of the annual $PM_{2.5}$ mass at Boundary Waters and Quebec provides about 18 percent to Acadia. Ohio and Pennsylvania are associated with high-concentration air masses at the three Class I sites shown, but only make significant (>5 percent) contributions to annual $PM_{2.5}$ mass at the nearby Dolly Sods Wilderness site.

In an exactly analogous manner, the contribution of each state and province to the joint set of 17 Class I areas was derived (not shown). The results indicate that some states associated with high-concentration air masses nevertheless contribute only a small amount of mass to the collective group of Class I sites; conversely, states (or provinces) with low average concentrations can be major mass contributors.

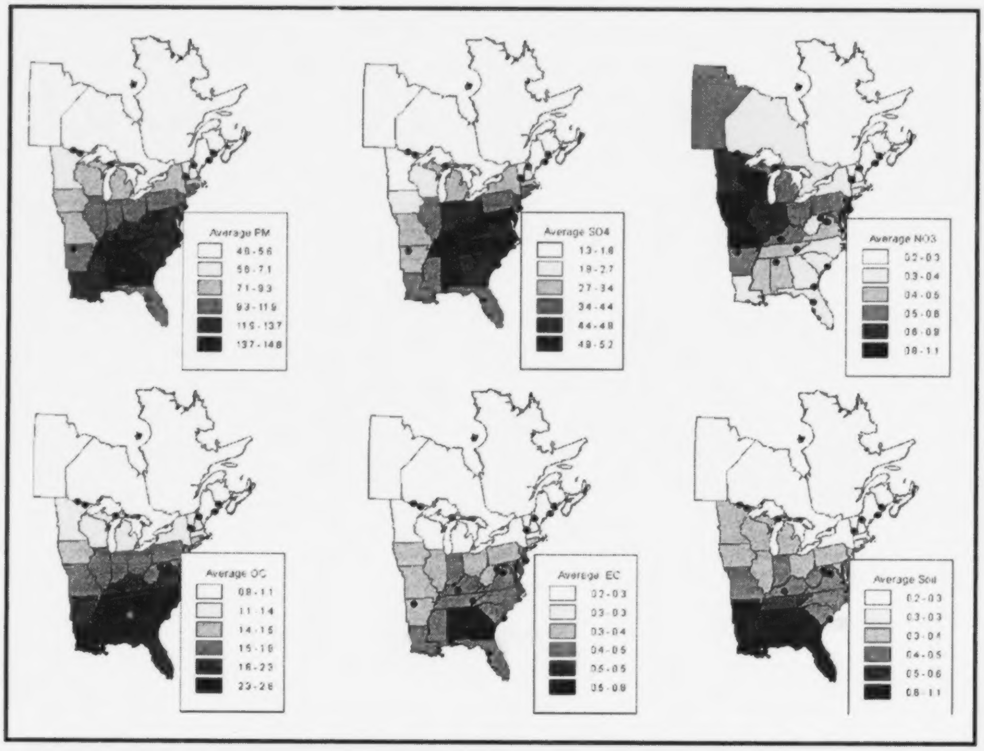
Average PM
48-56
56-71
71-93
93-119
119-137
137-148
Average SO4
13-18
18-27
27-34
34-44
44-48
48-52
Average NO3
02-03
03-04
04-05
05-08
08-09
08-11
Average OC
08-11
11-14
14-15
15-18
18-23
23-28
Average EC
02-03
03-03
03-04
04-05
05-05
05-08
Average Soil
02-03
03-03
03-04
04-05
05-06
08-11

Figure 6.1 - Average concentrations of $PM_{2.5}$ and components (µg/m³) by state and province (IMPROVE sites shown as blue dots). Each trajectory endpoint is associated with concentrations corresponding to the IMPROVE sample for the trajectory start date.

Table 6.1 Average concentration and percent mass selected state contributions to Class I areas (mass contributions >5 percent are highlighted).

State/Province	Acadia		Boundary Waters		Dolly Sods	
	Conc.	%Mass	Conc.	%Mass	Conc.	%Mass
Illinois	10.8	0.4	9.5	1.7	8.7	1.6
Indiana	17.1	0.9	12.5	0.6	11.0	3.2
Iowa	7.6	0.2	8.1	5.0	8.5	0.9
Kentucky	11.8	0.5			14.0	8.6
Maine	5.6	12.6			8.6	0.1
Michigan	7.6	1.7	6.2	1.7	10.1	2.6
Minnesota	7.1	0.6	5.7	35.2	8.6	1.0
New Hampshire	8.6	2.0				
New Jersey	18.9	1.0			8.4	0.1
New York	8.2	4.4			9.1	0.8
North Carolina	13.9	0.3	10.0	0.1	12.0	3.1
Ohio	10.6	1.2	12.8	0.2	11.5	8.8
Pennsylvania	13.2	3.0			10.9	5.1
Tennessee	9.9	0.2			13.4	4.9
Vermont	8.3	1.8				
Virginia	14.2	0.9			11.8	7.6
West Virginia	18.4	0.5	10.0	0.1	14.0	26.4
Wisconsin	6.2	0.6	7.1	7.6	9.0	1.3
Provinces						
Ontario	6.0	7.7	3.5	16.4	9.2	4.8
Quebec	4.9	17.8	2.4	0.2	6.6	0.7

6.1.1.2 *Sources of $PM_{2.5}$ to Urban Areas in the United States*

Rao et al. (2003) investigated the local and regional source contributions of $PM_{2.5}$ to urban areas at 13 urban locations in the United States. The 'urban excess' for the 13 cities is presented in Figure 6.2. Evaluating the differences between urban and rural sites is a first indicator of local versus regional transport, as determined by 'excess' of the components at urban sites in comparison to rural sites. This analysis was accomplished by matching urban sites to nearby rural sites and comparing the appropriate concentrations of chemical constituents and mass. Although there is uncertainty in the measured mass and in measurement protocols, it is clear that carbonaceous mass is prevalent everywhere (average of 5.1 μg/m^3) and is the major component of urban excess at all of the sites studied. At the western sites, the Total Carbon Material (TCM) urban excess ranges from 4.5 to 10.5 μg/m^3, whereas at the eastern sites, TCM urban excess ranges from 2 to 5.4 μg/m^3. Similarly, nitrates are prevalent n the estimates for the north and west (2 to 6 μg/m^3). Consistent with other studies that find most $SO_4^=$ is associated with regional sources of SO_2; the urban excess of this chemical component is invariably small in the eastern United States. These results indicate the regional nature of $SO_4^=$ contribution to total $PM_{2.5}$ mass and by implication the role of the transport of $SO_4^=$ associated $PM_{2.5}$.

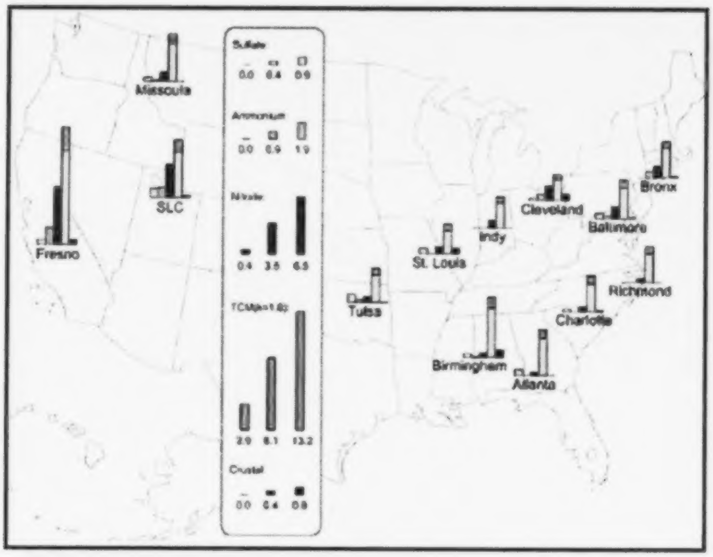

Figure 6.2 - Urban Excess Analysis for $SO_4^=$, NH_4^+, NO_3^-, TCM and crustal material for 13 urban areas in the United States

(Note: k=1.8 in order to convert carbonaceous mass into TCM).

6.1.1.3 *Sources of* $PM_{2.5}$ *to Eastern North America*

An ensemble-trajectory analysis technique known as Quantitative Transport Bias Analysis (QTBA; Keeler and Samson, 1989) was applied to determine which geographic areas systematically contributed to above- and below-average fine particle mass ($PM_{2.5}$) over eastern North America (Brook et al., 2004). Six-hour average measurements from 12 rural or suburban locations in eastern North America, collected using the TEOM measurement method, were individually associated with corresponding 3-day back-trajectories for the warm seasons (May through September) of 2000 and 2001. Much of the populated area of northeastern Canada and the United States was implicated in the build-up of $PM_{2.5}$ to "above average" concentrations (Figure 6.3). Average concentrations were determined by calculating the mean concentration at each of the sites during the warm seasons of 2000 and 2001. The finer structure of the QTBA pattern indicated that transport from the Ohio River Valley was most often associated with the highest $PM_{2.5}$ concentrations, particularly the eastern portion of this area. In addition, air masses traversing a relatively large area from southeast Ohio to the western part of Virginia and the western Kentucky to central Tennessee area tend to result in relatively high $PM_{2.5}$ concentrations over northeastern North America. These observation-based findings are consistent with the spatial distribution of the major SO_2 and NO_x point sources (Figure 4.1a and Figure 4.3a).

6.1.1.4 *Back-trajectory Analysis of* $PM_{2.5}$ *Transport to Eastern Canada*

Using hourly TEOM $PM_{2.5}$ observations from May-September of the years 1998-2000, Brook et al. (2002) have quantified the impact of various transport directions on $PM_{2.5}$ concentrations in eastern Canada using back-trajectory analysis. Comparisons of $PM_{2.5}$ levels at different sites reveal that on average, the local contribution to total $PM_{2.5}$ in the Greater Toronto Area is approximately 30 to 35 percent. This implies that the regional or long-range contribution comprises the remaining 65 to 70 percent. Furthermore, at sites in eastern Canada, average $PM_{2.5}$ concentrations were 2 to 4 times greater under south/southwesterly flow than under northerly flow conditions during May through September of 1998 and 1999 (see

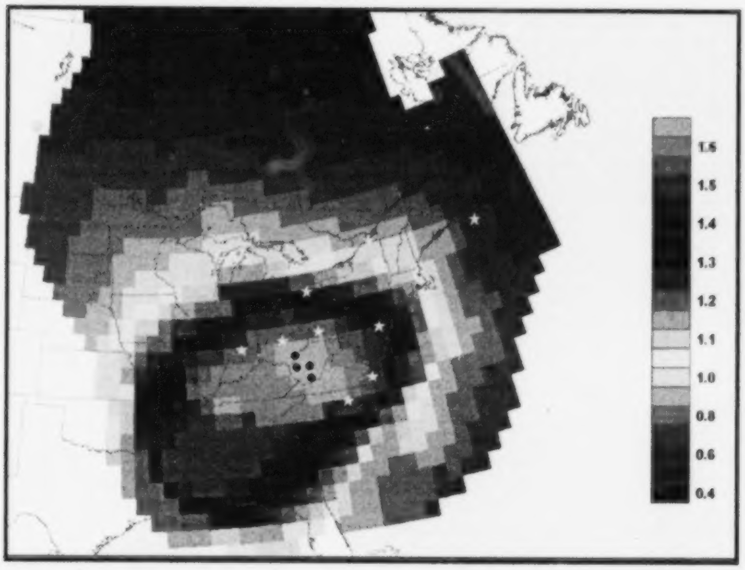

Figure 6.3 - Combined QTBA plot derived using 2000 and 2001 TEOM $PM_{2.5}$ measurements for the warm months (May-September). The locations of the 10 measurement sites (receptors) are shown by stars and the locations of the maximum QTBA values are indicated by the black circles. QTBA values greater than 1.0 indicate a high likelihood of air masses passing over that area bringing above-average warm-season $PM_{2.5}$ to the receptor.

Figure 2.2). This observation suggests that the majority of $PM_{2.5}$ at these locations is arriving from the transport of $PM_{2.5}$ and $PM_{2.5}$ precursors from sources south of this region.

6.1.1.5 *Sources of PM to Glacier National Park, Montana*

Trajectory Clustering/Time Series Analysis was applied to Glacier National Park in Montana (Sirois and Vet, pers.comm.). This preliminary analysis identifies the potential influence of western Canadian and U.S. sources to visibility impairment at Glacier National Park. Qualitatively, SO_2 sources in Alberta, Saskatchewan, Montana and North Dakota contribute to $SO_4^=$-induced low visibility events at Glacier National Park. High concentrations of NO_3^- observed at the Park were associated with westerly air flow from the Vancouver/Seattle area. Total OC and total BC, the major contributors to visibility impairment at the Park, were associated with air flows from the Vancouver/Seattle, Oregon, and Northern California areas.

6.1.1.6 *Sources of PM and Acid Rain Precursors to Southwestern Ontario: Study 1*

Trajectory Clustering/Time Series Analysis was applied to observed concentrations of particle $SO_4^=$ and NO_3^- in air, and to pH, $SO_4^=$ and NO_3^- in precipitation at the Longwoods measurement site of the Canadian Air and Precipitation Monitoring Network (CAPMoN) in southwestern Ontario to determine source-receptor relationships (Vet and Sirois, pers.comm.). The technique combined 3-day back-trajectories with daily PM and ion measurements. The technique involved categorizing the air mass trajectories into two geographical sectors (Figure 6.4) and sorting the data at the Longwoods site according to the sector that each trajectory fell within. The criteria for categorizing the trajectories were as follows: 1) if at least 70 percent of the points along the trajectory path fell within a sector, the trajectory was categorized as originating from this sector; and 2) if less than 70 percent of the points along a trajectory fell within a sector, the trajectory was categorized as "not attributable" (N/A). Figures 6.5 and 6.6 illustrate the long-term trends and median concentrations of particle $SO_4^=$

and NO_3^- in air and pH, $SO_4^=$ and NO_3^- in precipitation associated with trajectories from the Canadian and U.S. sectors.

Air: Results of this study for airborne SO_2 indicate that concentrations in air masses originating in Canada decreased markedly throughout the period 1983-2001 while concentrations from U.S. air masses gradually increased during the same time period (Figure 6.5a, Note: logarithmic scale). During this period, the median concentration of SO_2 in air masses from the United States was approximately 2.8 times greater than concentrations in air masses from Canada (Figure 6.5b). The amount of particle $SO_4^=$ in air masses from Canada declined slightly while concentrations in air masses from the U.S. remained relatively constant over the 19-year time period (Figure 6.5c). Median concentrations of $SO_4^=$ in U.S. air masses were also 2.8 times greater than concentrations in air masses from Canada (Figure 6.5d). Concentrations of total NO_3^- (i.e., TNO_3^- = the sum of particle NO_3^- and gaseous HNO_3) in air masses from Canada declined slightly between 1983-2001 while concentrations in air masses from the United States increased from 1983 to 1992 and remained relatively constant from 1992 to 2001 (Figure 6.5e). Overall, the median concentration of TNO_3^- in air masses from the United States was three times higher than concentrations in air masses from Canada (Figure 6.5f).

Precipitation: Results indicate that the pH of precipitation associated with trajectories from Canada increased during the 1980s, declined from the late 1980s to mid-1990s and increased again from the mid-1990s to 2001 (Figure 6.6a). The pH of precipitation from U.S. air masses increased slightly and gradually from 1983 to 2001 (Figure 6.6a). The median pH of precipitation from air masses from the United States is significantly lower than the pH of precipitation from air masses that originate from the Canadian sector (Figure 6.6b). The amount of $SO_4^=$ in precipitation associated with trajectories from Canada declined during the early 1980s to 1990, increased during the 1990s and then declined more rapidly from 1997 to 2001 (Figure 6.6c). Sulphate levels in precipitation associated with U.S. trajectories exhibited a more gradual decline throughout the measurement period (Figure 6.6c). The median concentration of $SO_4^=$ in precipitation associated with the United States was approximately twice that of trajectories originating from Canada (Figure 6.6d). The amount of NO_3^- in precipitation associated with trajectories from Canada also declined during the early 1980s to 1990 but leveled off between the 1990s and 2001 (Figure 6.6e). Nitrate levels in precipitation associated with trajectories from the United States remained relatively constant from the early 1980s to 1999 and a slight decline from 1999 to 2001 (Figure 6.6e). The median concentration of NO_3^- in precipitation associated with trajectories from the United States was approximately twice that of trajectories originating from Canada (Figure 6.6f).

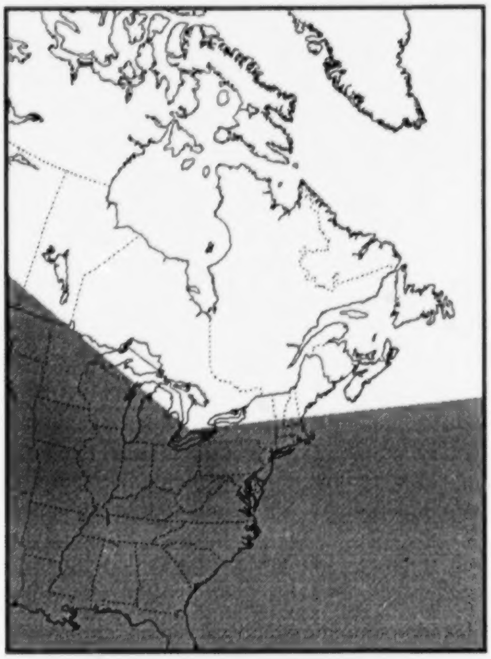

Figure 6.4 - Sectors used to categorize 3-day back-trajectories of air masses at Longwoods, Ontario. Light shading represents the Canadian sector. Dark shading represents the U.S. sector.

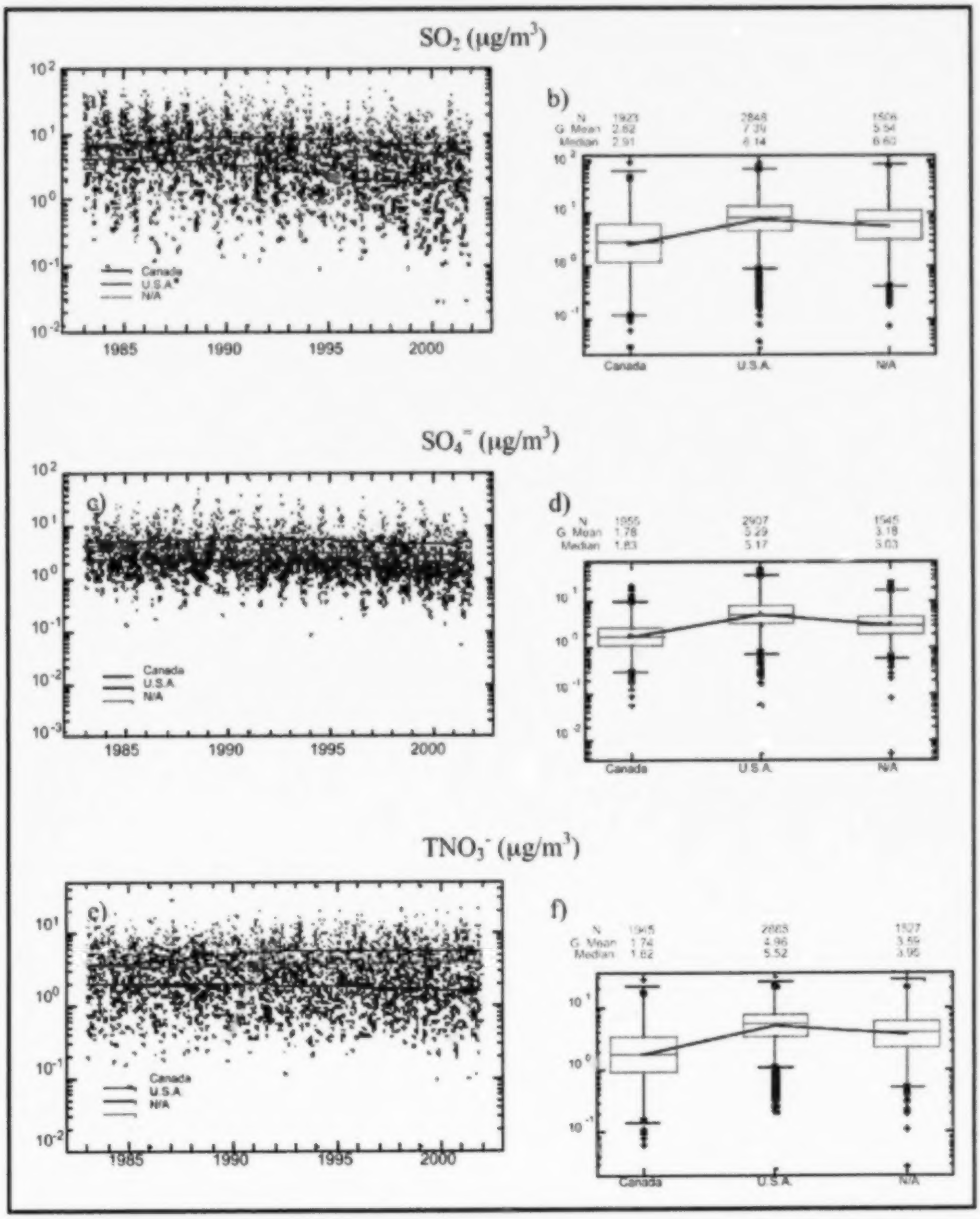

Figure 6.5 - Long-term trends and median concentrations of SO_2 (a and b, respectively), particle $SO_4^=$ (c and d, respectively) and particle NO_3^- (e and f, respectively) in air at Longwoods, Ontario associated with three-day back trajectories from Canada, the United States and "Not Attributable" (N/A) to either sector. The trend line in the box plots connects the geometric means, the line dividing the boxes represents the median, the upper and lower sides of the boxes represent the 75th and 25th percentile of the data, respectively and the upper and lower bars on the box plots represent the 75th percentile plus 1.5 times the inter-quartile range and the 25th percentile minus 1.5 times the inter-quartile range, respectively.

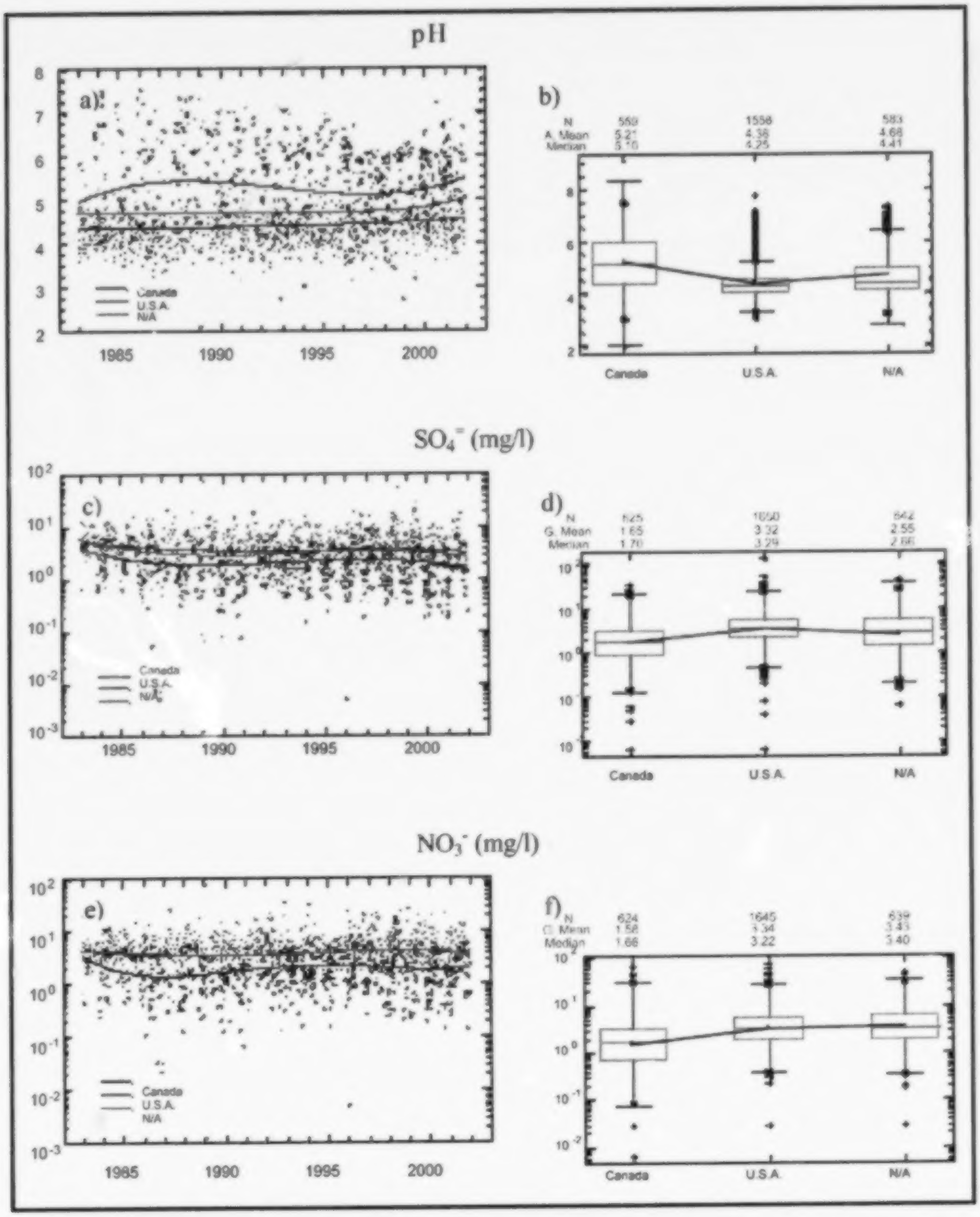

Figure 6.6 - Long-term trends and median concentrations of pH (a and b, respectively), $SO_4^=$ (c and d, respectively) and NO_3^- (e and f, respectively) in precipitation at Longwoods, Ontario associated with 72-hour back trajectories from Canada, the United States and "Not Attributable" (N/A) to either sector. The trend line in the box plots connects the geometric means, the line dividing the boxes represents the median, the upper and lower sides of the boxes represent the 75th and 25th percentile of the data, respectively and the upper and lower bars on the box plots represent the 75th percentile plus 1.5 times the inter-quartile range and the 25th percentile minus 1.5 times the inter-quartile range, respectively.

6.1.1.7 *Sources of PM and Acid Rain Precursors to Southwestern Ontario: Study 2*

An analysis was also performed to assess the impact of Canadian versus U.S. emission sources on air quality at Longwoods, Ontario (Vet et al., pers. comm.). The results, illustrated in Figure 6.7, were generated by combining daily ambient air concentrations at the Longwoods site with air mass trajectories for the individual measurement days. The method, developed by Seibert et al. (1994), calculates for each grid square, the geometric mean concentration of the chemical in air measured at the Longwoods site for the particular subset of trajectories that passed through that grid square. Thus, the red squares on the figure identify those emission areas associated with the highest concentrations at Longwoods and the blue areas identify those areas associated with the lowest concentrations. Figure 6.7 illustrates that the highest SO_2, $SO_4^=$ and TNO_3^- concentrations measured at this site are associated with air transported from areas in the Midwest and northeastern United States. These geographic regions are also associated with high SO_2 and NO_x emissions. In contrast, the lowest concentrations occur when air is transported from areas in Canada to the north and east of the site. A similar analysis for precipitation chemistry (not shown) indicates a more complex pattern of emission sources affecting the precipitation at Longwoods. High acidity at the site is primarily associated with air transported from the Ohio Valley. High concentrations of $SO_4^=$ and NO_3^- are associated with air transported from the central and eastern United States, northern Alberta and the central United States and northern Alberta and Saskatchewan, respectively.

6.1.1.8 *Sources of $PM_{2.5}$ to Southern Quebec*

Source-receptor relationships describing $PM_{2.5}$ levels at a site in southern Quebec during July, 2001, were determined using the START (Suivi du Transport Atmospherique Regional et Transfrontalier) model (Dion, 2003). START uses emission information and back-trajectories from the Canadian Meteorological Centre to estimate the origin of $PM_{2.5}$ and its precursors within 72 hours for each back-trajectory. Application of the model indicates that as ambient levels of $PM_{2.5}$ at the receptor site increase, the origin of pollutants shifts from Quebec to Ontario to the United States. As levels of $PM_{2.5}$ decrease, the origin of pollutants shifts back to primarily Quebec.

The model was also used to estimate the percentage of $PM_{2.5}$ at St. Anicet in southern Quebec originating from the United States, Ontario, Quebec and other areas during the summer (May to September) and winter (November to March) seasons of 1999 and 2000 (Table 6.2). Results indicated that the United States was a significant source of $PM_{2.5}$ at St. Anicet contributing slightly greater than 50 percent of $PM_{2.5}$ mass. Canadian sources contributed the remaining $PM_{2.5}$, with Ontario contributing approximately a quarter, followed by Quebec, with approximately 17 percent. Using this technique, the origin of $PM_{2.5}$ did not appear to vary substantially between the winter and summer season.

Table 6.2 Proportions (percent) of $PM_{2.5}$ mass with respect to 3-day back-trajectories at 950hPa (1999-2002).

Season/ Region	U.S.	Ontario	Quebec	Other	#traj
Summer	55	26	17	3	2410
Winter	57	24	17	3	2400

6.1.1.9 *Sources of $PM_{2.5}$ to Nova Scotia and New Brunswick*

$PM_{2.5}$ data were used in conjunction with trajectory analyses to determine atmospheric transport patterns at Kejimkujk National Park, NS and St. Andrews, NB (Waugh et al., 2002). This analysis used five-day back-trajectories, four times per day between 1999 and 2001. Trajectories calculated for this project were produced from the Canadian Meteorological Centre Trajectory Model.

A non-parametric statistical analysis program (SL-PSCF) was used to isolate the top ("polluted") and bottom ("unpolluted") quartile events for $PM_{2.5}$. An event was defined as a 6-hour period during which there was at least one hourly observation in the top or bottom 25th percentile. The

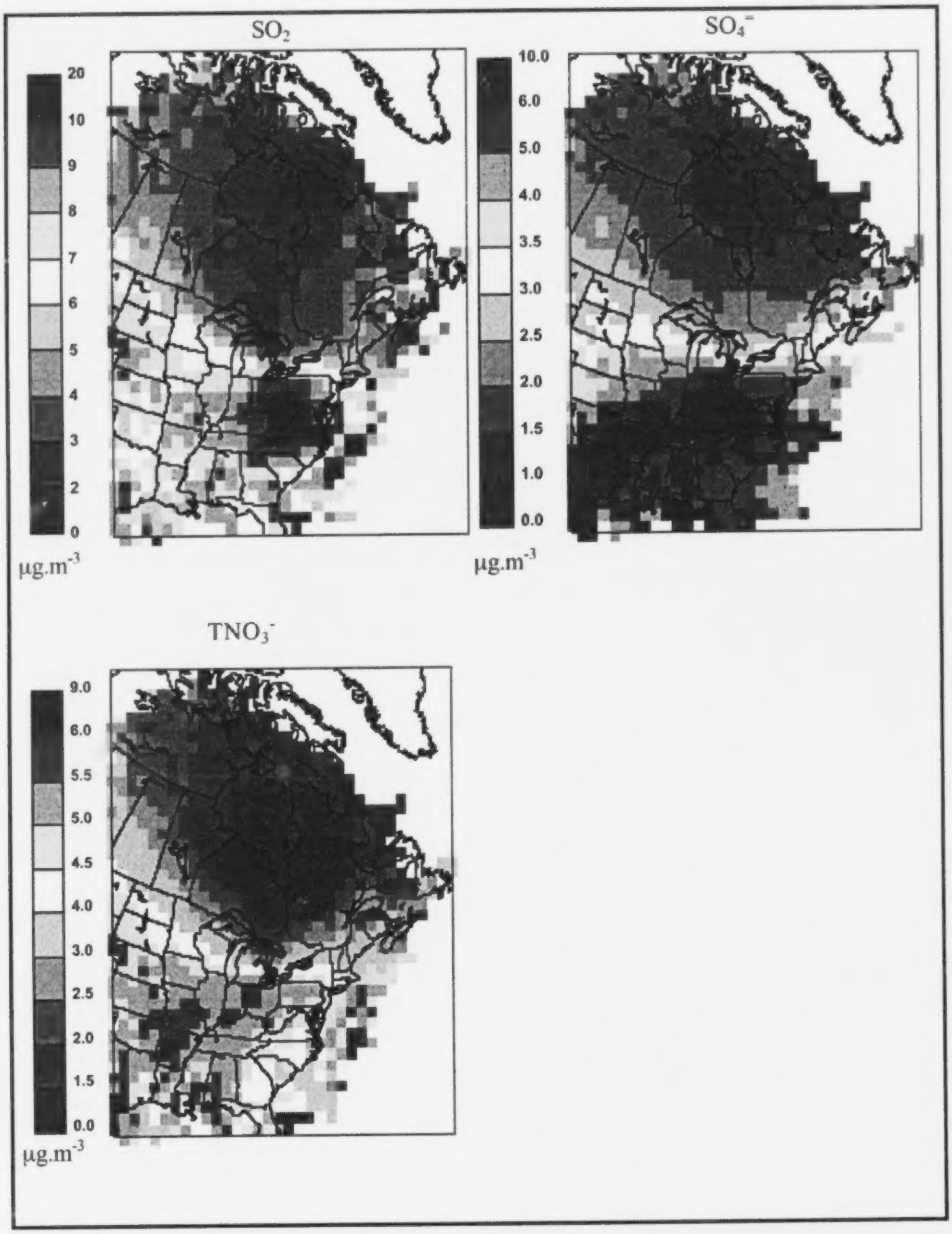
SO₂
20
10
9
8
7
6
5
4
3
2
0
µg.m⁻³
SO₄⁼
10.0
6.0
5.0
4.0
3.5
3.0
2.5
2.0
1.5
1.0
0.0
µg.m⁻³
TNO₃⁻
9.0
6.0
5.5
5.0
4.5
4.0
3.0
2.5
2.0
1.5
0.0
µg.m⁻³

Figure 6.7 - The geometric mean concentration of SO$_2$, SO$_4^=$ and TNO$_3^-$ measured in air at Longwoods, ON (1983-2000) for the particular subset of air mass trajectories that passed through that grid square.

resulting dates and times of these events were selected and attributed to appropriate trajectories. This resulted in a subset of trajectories related to both polluted (top 25th percentile) and unpolluted (bottom 25th percentile) events.

The influence of the continental emission source regions to the top 25th percentile PM$_{2.5}$ concentrations at Kejimkujik (first panel on the right) is shown by the darker black-red sections in Figure 6.8. Results from the event climatology for PM$_{2.5}$ (Figure 6.8) also show the significance of this region to the top 25th percentile concentrations at St. Andrews. The investigation of the top 25th percentiles of the pollutants confirms the significant impact of the emission areas of the eastern United States, southern Ontario and southern Prairies on elevated concentrations at these two sites in Nova Scotia and New Brunswick.

6.1.2 Positive Matrix Factorization

The application of Positive Matrix Factorization (PMF) to air quality studies has become an increasingly popular tool for elucidating source apportionment (Yakovleva and Hopke, 1999; Paterson et al., 1999; Prendes et al., 1999). Given the appropriate PM$_{2.5}$ dataset, one of the main challenges in the application of PMF is to determine the number of source types contributing at a given location. Identifying or "naming" the sources contributing to the observed source types also presents a challenge, and in both cases some subjectivity is involved. The ideal solution is to utilize multiple approaches (i.e., independent receptor model types) and to look for consensus.

6.1.2.1 *Sources of PM to Toronto, Ontario and Vancouver, British Columbia*

To better understand the processes influencing PM$_{2.5}$ concentration, and to determine its sources and to learn more about its health effects, the chemical composition of Toronto and Vancouver PM$_{2.5}$ was measured daily from January to December 2001 and February 2000 to February 2001, respectively (Lee et al., 2003). Source apportionment was undertaken using PMF. The PMF analysis identified eight and six sources contribut-

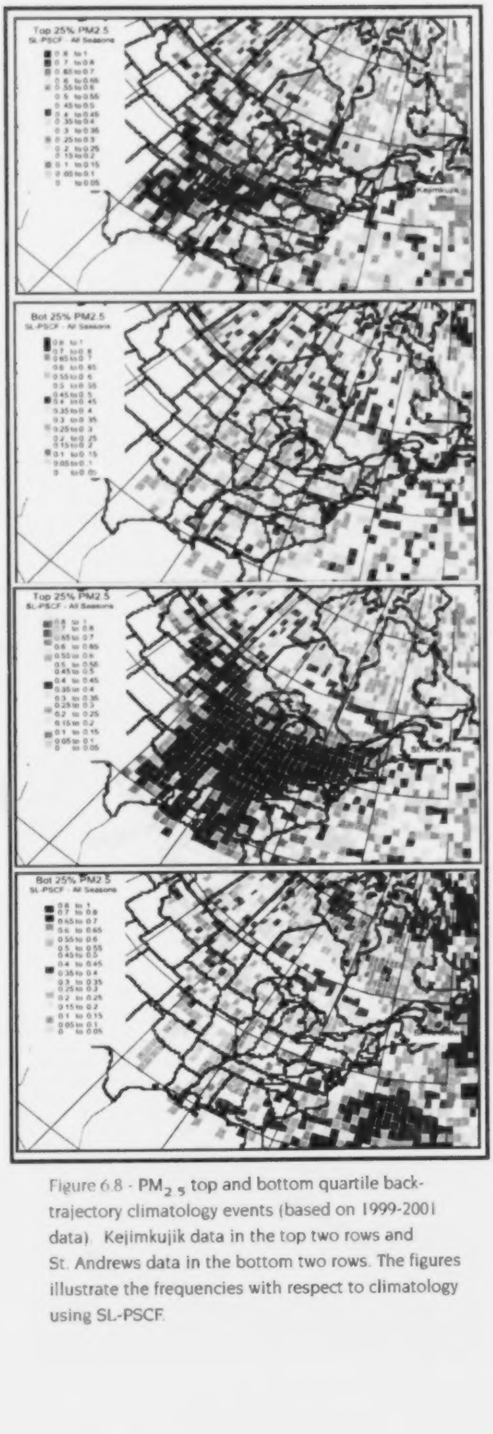

Figure 6.8 - PM$_{2.5}$ top and bottom quartile back-trajectory climatology events (based on 1999-2001 data). Kejimkujik data in the top two rows and St. Andrews data in the bottom two rows. The figures illustrate the frequencies with respect to climatology using SL-PSCF.

ing to PM$_{2.5}$ in Toronto and Vancouver respectively (Figure 6.9). In Toronto, the main components of PM$_{2.5}$ identified were coal combustion (30 percent) related to regional transport, secondary NO$_3^-$ (34 percent) related to both local and upwind sources of NO$_x$ and NH$_3$, secondary organic aerosols and biomass burning (9 percent) and motor vehicle traffic (9 percent). Coal combustion was related to regional transport (both from Canada and the United States) as there are no significant emission sources of coal combustion in the immediate area. As a result, the signal detected using the PMF analysis is related to transport into the area from non-local sources. The other detectable components were road salt (winter), road dust/soil (yearly), smelters or related industry, and oil combustion. In Vancouver, the three major components were secondary NH$_4$NO$_3$ (49 percent), secondary organic acid with SO$_4^=$ (23 percent), and motor vehicles (20 percent). The minor components were road dust/soil, sea salt and oil combustion. The average PM$_{2.5}$ mass in Vancouver was observed to be approximately 44 percent lower than PM$_{2.5}$ levels in Toronto. The total influence of localized vehicle-related sources was estimated to be 36 percent and 51 percent in Toronto and Vancouver respectively.

6.1.2.2 *Comparability of Receptor Model Results on PM$_{2.5}$ Sources in Toronto*

The raw data from Lee et al. were subsequently conveyed to a team of U.S. analysts at the Vermont Department of Environmental Conservation, where they were analyzed using a second receptor model, UNMIX. The independent PMF and UNMIX results were then compared, refined and revised with local surface meteorological data and ensemble backward trajectory techniques then applied to help evaluate and interpret the results. Annual average PM$_{2.5}$ mass contributions from the resulting PMF and UNMIX sources are displayed in Figure 6.10.

The average annual PM$_{2.5}$ mass concentration during this period was 14 µg/m^3 (just below the level of the U.S. standard), with maximum 24-hour concentrations (98th percentile) of 35 µg/m^3 (just above the Canadian standard). Both models reproduced the measured annual and daily PM$_{2.5}$ mass measurements in terms of the identified contributors, which included smelters (5 percent),

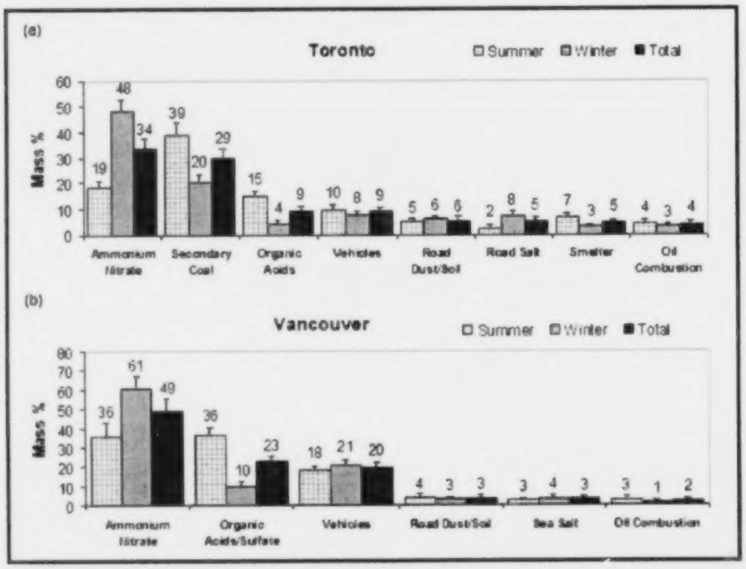

Figure 6.9 - Percent contribution, by component, to PM$_{2.5}$ mass observed in a) Toronto and b) Vancouver as determined using PMF-MLR.

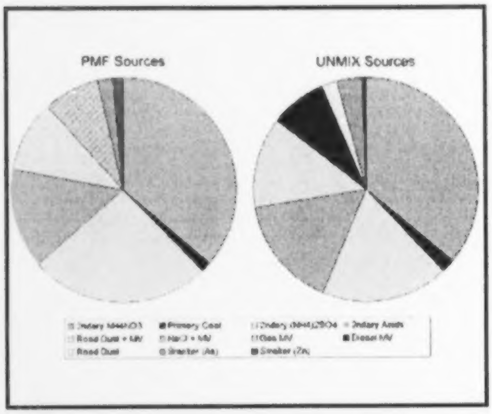

Figure 6.10 - Annual average modelled $PM_{2.5}$ contributions in Toronto, (February 2000 – February 2001) using UNMIX (a) and PMF (b) receptor modelling techniques

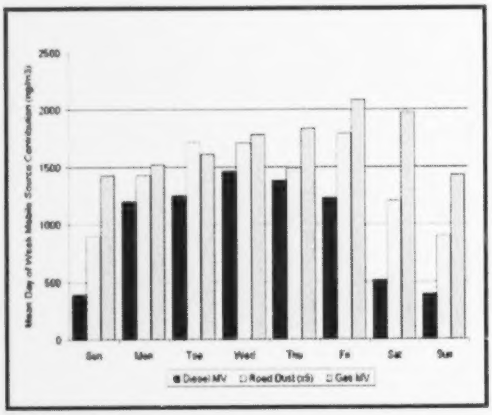

Figure 6.11 - Average day of week variations in UNMIX motor vehicle sources.

motor vehicles (20 percent), NH_4NO_3 (36 percent) and coal combustion (36 percent).

Figures 6.11 and 6.12 display the temporal characteristics of several components, which provide insight into source characteristics. Figure 6.11 displays the average day-of-week contributions for the three identified UNMIX "motor vehicle-related" sources. All three of these sources decline substantially on weekends, with the relative reduction on Sundays being greatest from

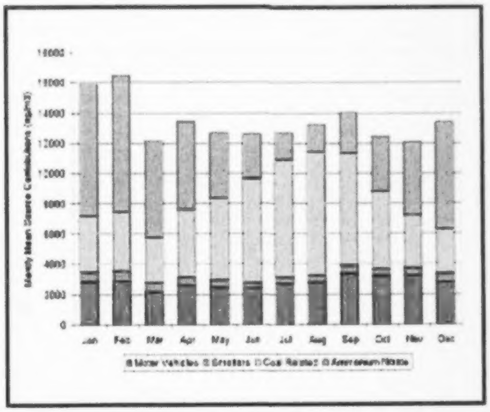

Figure 6.12 - Seasonal variations in Toronto PMF & UNMIX source contributions.

diesel vehicles, least from gasoline vehicles, and intermediate for road dust.

Figure 6.12 shows the seasonal patterns in four major categories, shown for averaged PMF and UNMIX results. The total influence from motor vehicles and smelter sources is relatively constant over the year, while the NH_4NO_3 and coal-related components show strong winter and summer peaks respectively.

An evaluation of the receptor model daily source contributions as a function of local surface meteorology is illustrated for the UNMIX "motor vehicle-related" and "coal-related" sources in Figure 6.13. The influence of the mobile source does not vary greatly with wind direction, but is consistently higher for directions as wind speed decreases (blue-shaded sectors), indicative of a predominantly local origin. The coal-related sources show a different pattern, all increasing substantially with surface winds from the south (southeast through southwest), and consistently higher from this direction as wind speed increases (red-shaded sectors), indicative of more distant source influences.

Figure 6.14 (left panel) shows similar back trajectory-based "incremental probability fields" for

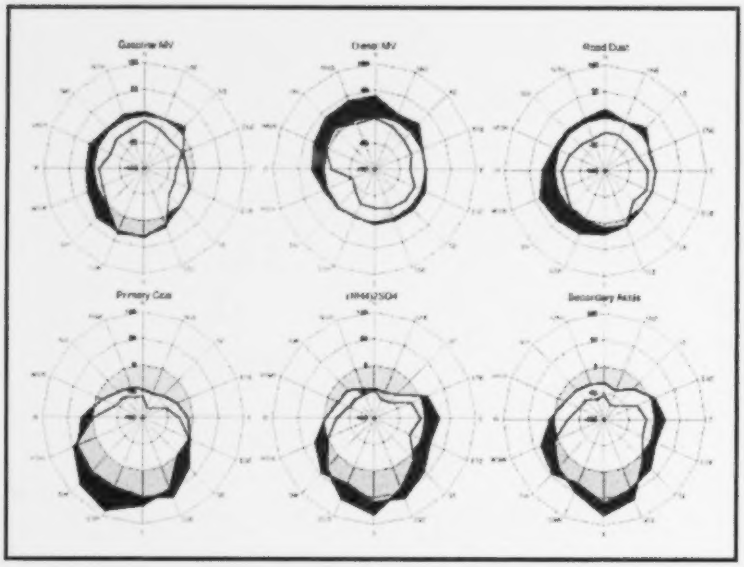

Figure 6.13 - UNMIX motor vehicle and coal-related sources vs. local surface wind speed and direction. Blue shading emphasizes directions from which source influence is greatest at low wind speeds. Pink shading emphasizes directions where source influence increases at all wind speeds. Red shading emphasizes directions from which source influence increases at high wind speeds.

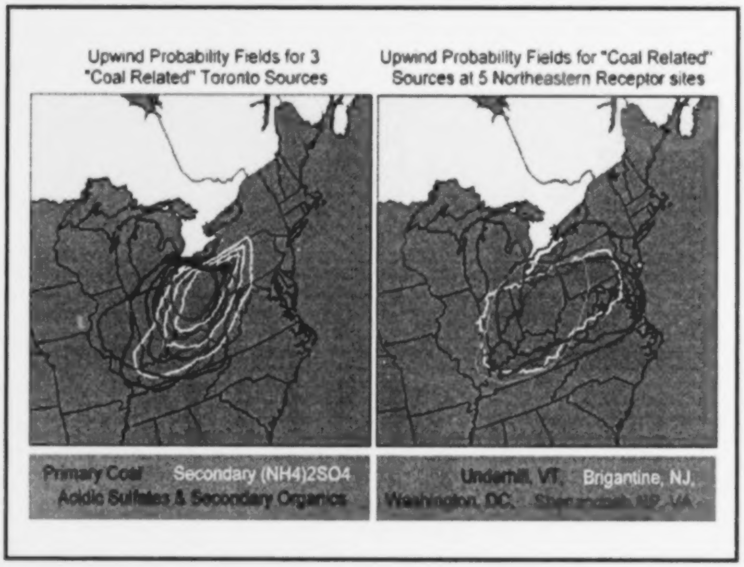
Upwind Probability Fields for 3 "Coal Related" Toronto Sources
Upwind Probability Fields for "Coal Related" Sources at 5 Northeastern Receptor sites
Primary Coal
Secondary (NH4)2SO4
Acidic Sulfates & Secondary Organics
Underhill, VT.
Brigantine, NJ.
Washington, DC.
Shenandoah NP, VA

Figure 6.14 - Incremental probability fields for coal-related sources at Toronto and other eastern sites.

coal-related sources to Toronto $PM_{2.5}$. This coal-related source can be split into three separate components based on the PMF and UNMIX analyses: primary coal (emitted from the source in particle phase), secondary $(NH_4)_2SO_4$ and acidic sulphates/secondary organics. While there is not a perfect correspondence in their upwind probability fields, the most probable upwind locations for all three sources are similar and converge on a U.S. region of high-density emissions from coal-fired utilities. In the right hand panel of Figure 6.14, the probability fields for the three Toronto "coal-related" sources are combined and compared (at similar incremental probability contours of 0.002) with

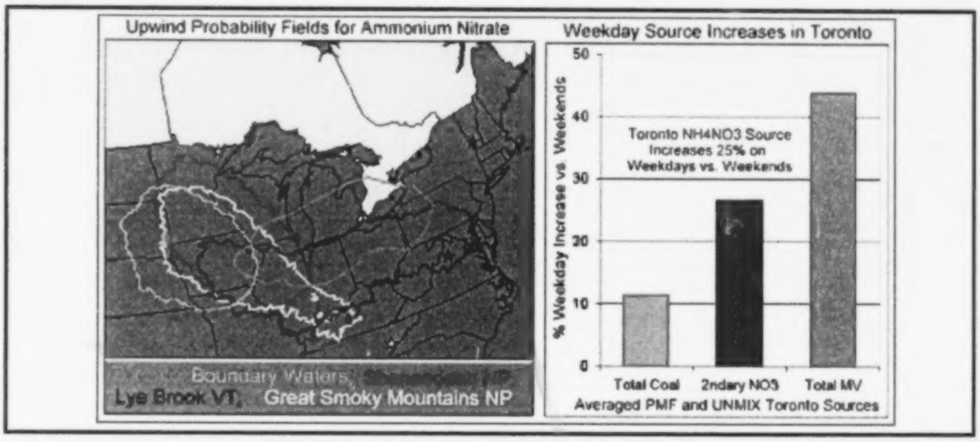

Figure 6.15 - Incremental probability fields and day-of-week patterns in Toronto NH_4NO_3 "sources."

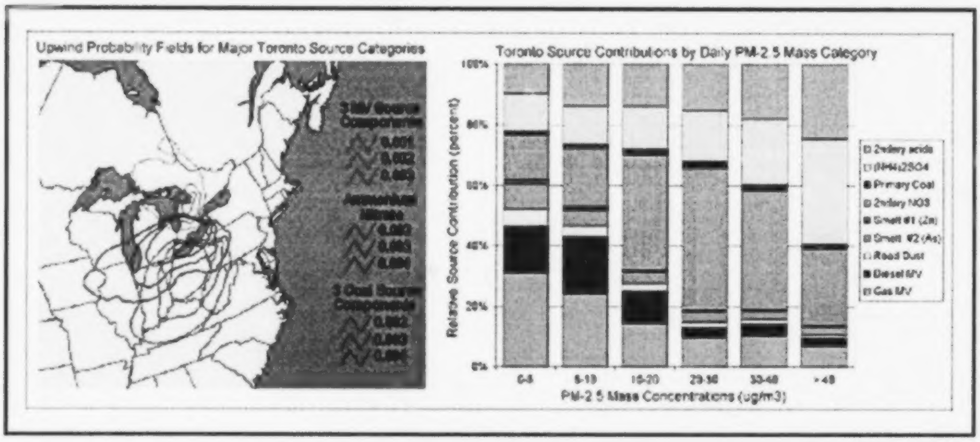

Figure 6.16 - Summary of major Toronto source regions and influences on daily $PM_{2.5}$ mass concentrations.

similar results from other recent studies which have applied a similar combination of PMF and or UNMIX receptor models and ensemble back trajectory techniques. The consistency and convergence of results from these different model applications adds confidence to the Toronto results, and suggests a common "universal donor" source region influencing multiple receptor locations in the Northeast transboundary region.

Certain features of the modelled NH_4NO_3 component also suggest a complex "causality".

The left side of Figure 6.15 compares the incremental probability field for the Toronto NH_4NO_3 sources with those from other recent receptor modelling studies at (rural) eastern U.S. sites. There is a moderately strong degree of convergence in the most common upwind areas for high NO_3^- from these widely separated receptor sites, which suggests a critical influence from agricultural (fertilizer and livestock) NH_3 emissions in the north-central U.S. "corn belt." However, as indicated on the right side of Figure 6.15, there is a moderately strong weekday increase in the influence of nitrate in Toronto, suggesting that local, as well as more distant sources of NO_x and/or NH_3 are also important contributors. The implied "co-causality" here raises additional questions for control strategy development. If aerosol NH_4NO_3 is limited by the availability of NH_3, would reductions in SO_2 lead to reductions in aerosol $SO_4^=$ but increases in aerosol NO_3^-? If NH_3 emissions were reduced, would we expect to see decreases in aerosol NO_3^-, but increases in $SO_4^=$ acidity and secondary organic aerosol formation?

Figure 6.16 summarizes the trajectory-based upwind probability fields for the three major modelled categories in Toronto, and also shows the relative contributions from the UNMIX components on days with different total fine mass concentrations.

Local motor vehicle sources (and small nearby smelter or industrial sources) have a relatively constant influence, and are most evident on the cleanest days (which also tend to occur with northerly wind flows). Secondary NH_4NO_3, formed when temperature conditions are favourable, from precursor emissions of both local and more distant (Canadian and U.S.) emission sources, is the largest contributor to annual average fine mass and on days of moderate to high $PM_{2.5}$ concentrations. The coal-related source influences have a substantial transboundary contribution from U.S. sources, and are especially important contributors on the days of highest $PM_{2.5}$ concentration.

6.1.2.3 PMF *and Back Trajectory Analysis at Eight U.S. Cities*

Under contract, the U.S. EPA prepared a study of eight cities using source apportionment and trajectory analyses. The source apportionment analysis at each of the eight cities provides evidence of the types and locations of sources that are most likely to be major contributors to $PM_{2.5}$ mass at each city. The source apportionment and back trajectory studies used speciated $PM_{2.5}$ data from eight EPA Trend Sites located in Birmingham, Alabama; Bronx, New York; Charlotte, North Carolina; Houston, Texas; Indianapolis, Indiana; Milwaukee, Wisconsin; St. Louis, Missouri; and Washington, D.C. These sites are in urban areas, and are expected to be affected by both local and distant sources of PM. The results of both the source apportionment and back trajectory analyses are consistent with this expectation.

The preliminary source identifications were based first on the chemical composition of the $PM_{2.5}$ profiles. These were then balanced against the relative contribution of the source to the various species and time series output. Second, local monitoring personnel were contacted to discuss potential sources of PM measured at the receptor. Third, back trajectories were used to identify source locations for sources that are 3 to 72 hours upwind. Pollution roses were used to identify source directions from local winds. Attempts were made to verify that local point sources exist approximately in the directions indicated.

For each site, the $PM_{2.5}$ was apportioned into six to eight components. There were several commonly identified contributors, including secondary $SO_4^=$ (Figure 6.17), fireworks, industrial activities, forest fires, diesel, and crustal matter. The $PM_{2.5}$ apportioned to forest fires at the Washington, D.C site was clearly linked to the July 2002 forest fires in eastern Canada (see Section 6.1.3.1).

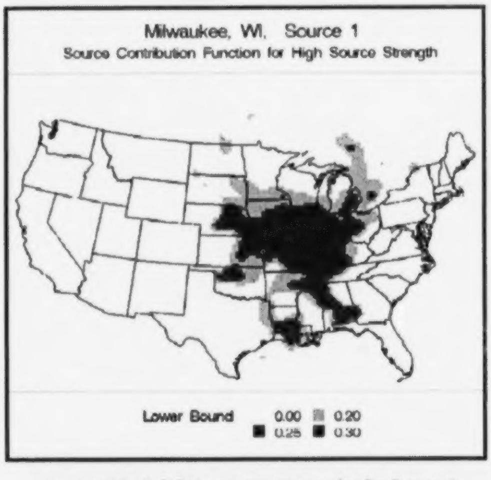

Figure 6.17 - Sulphate source region plot for Source 1, $(NH_4)_2SO_4$, at Milwaukee, WI.

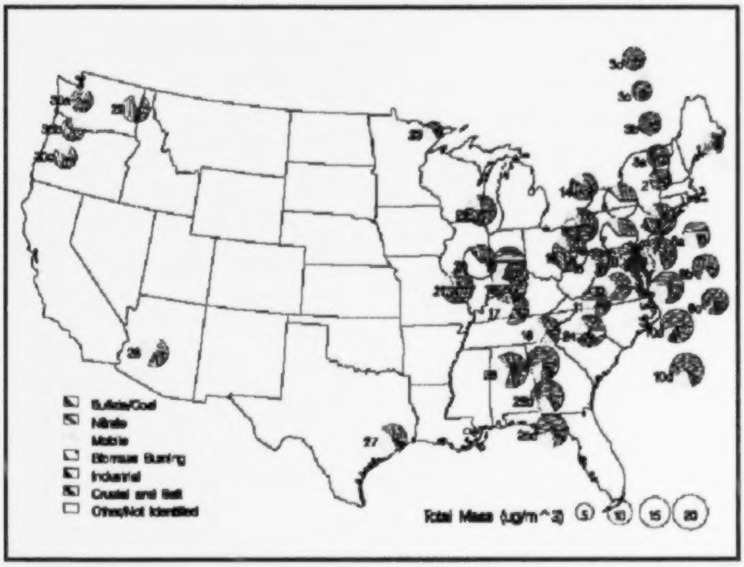

Figure 6.18 - Pie charts of the source apportionment results for various locations in the United States. (Some charts moved for clarity)

Back-trajectory analyses and wind/pollution roses yield source location information for the apportioned $PM_{2.5}$ contributors. Nitrate sources are associated with the Midwest farming regions while the back-trajectory analyses for the oil-based $SO_4^=$ component indicated large southern source regions. The analysis for the $SO_4^=$ component is complicated by the fact that some of the sources seem to be related to high-pressure systems (as evidenced by the clockwise swirl of many of the back trajectories for the high source days).

Sulphate, from either coal-or oil-based sources, accounts for about one-third of $PM_{2.5}$ mass. The next largest portion is either from NO_3^- components or mobile sources with all three of these categories showing long-range transport components. The smaller source contributions are more site-specific, except for crustal dust. As many as eight source categories, including marine influences, metal production, general industrial, and fuel oil, are within the range of resolvability with approximately one year of speciation data at current levels of technology. Linking wind trajectories with the source apportionment results allows one to develop source regions (i.e., geographic regions with a high probability of being the origin of the mass associated with a source profile). These source regions provide evidence that at least some of the particles associated with the source profiles are likely transported over long distances. For example, the highest probability source region for the coal combustion source profile for Birmingham includes parts of the following states: Missouri, Illinois, Indiana, Ohio, Kentucky, Virginia, North Carolina, South Carolina, Alabama, and Mississippi.

6.1.2.4 *Compilation of $PM_{2.5}$ Source Apportionment Studies from the United States*

The U.S. EPA summarized the findings of 27 source apportionment studies covering over 30 locations. The literature compilation found that contributions from secondary $SO_4^=$ and coal combustion sources were the largest or one of the largest sources of $PM_{2.5}$ in nearly every study, often contributing more than 50 percent of $PM_{2.5}$ to the receptor. Furthermore, these trajectory analyses often pointed to source regions containing coal-fired power plants. In addition, if the study time frame was sufficiently long, secondary $SO_4^=$ and coal combustion had different winter and summer profiles which were attributed to extremes of atmospheric chemistry between source regions and receptors. Studies looking at longer time periods observed reductions in contributions for some sources (power plants, smelters), attributed to reductions in emissions, fuel switching (from oil to natural gas), and changes in meteorological conditions (warm winters in late 1990s). For the western locations, mobile sources and vegetative burning tend to have larger contributions to total PM. Figure 6.18 shows pie charts of the various apportionment results for areas across the United States.

In general, the results from many of the studies were similar. A few receptors were studied repeatedly, such as Underhill, Vermont, and Brigantine, New Jersey. The contributors identified are grouped into seven categories: $SO_4^=$/coal, mobile, NO_3^-, biomass burning, industrial, crustal and salt, and other/not identified. Note that in Figure 6.18 the results from neighboring sites are generally quite similar.

6.1.2.5 *Source Locations and Time Series Analyses in U.S. Cities*

A number of studies have assessed sources of observed $PM_{2.5}$ in U.S. cities. In these studies, PMF and UNMIX were either used individually or in tandem to apportion sources to observed $PM_{2.5}$ levels. All back trajectory analyses for sites in the eastern United States associate the $SO_4^=$ component of PM with the Ohio River Valley area. Several studies noted transport across the Canadian border, specifically $SO_4^=$ from the midwestern United States into Canada, and smelter emissions from Canada into the northeastern United States. There are plans to use the back-trajectory data to quantify the transport; however, these studies are not yet complete. All of the studies looked at long-term averages and most looked at seasonal (3-month) averages. There was very little analysis of daily or weekly events, with a few exceptions. (For the most part, the studies considered are motivated by long-term concerns, such as trends in regional haze.) Lee et al. (2003 a) followed up on a crustal source by identifying several days that were possibly influenced by Saharan dust. Coutant et al. (2002) mention the influence of fireworks in Houston, Texas. Long (2002) studied a particular event (2002 Winter Olympics) and documented changes in the source proportions (mobile sources were higher) and temporal changes (mobile

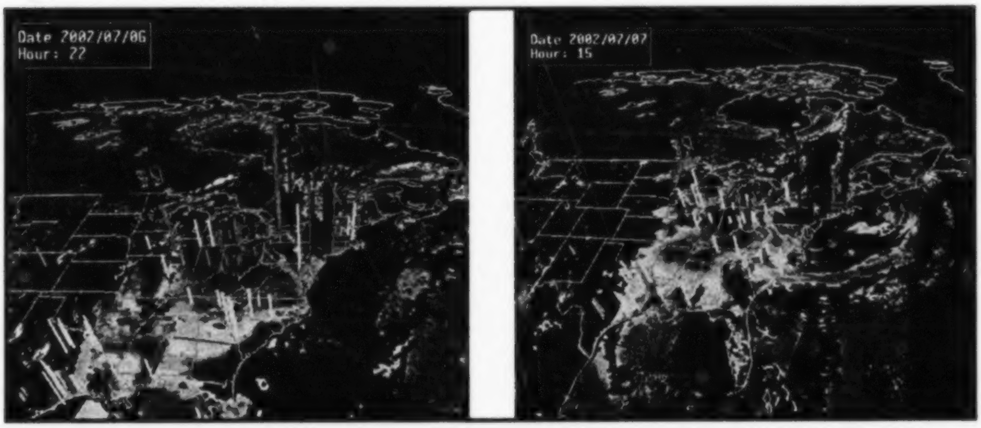

Figure 6.19 - The composites of MODIS-derived aerosol optical depth (color) and cloud optical depth (black-white) superimposed over continuous $PM_{2.5}$ monitors (bars) for July 6th and 7th, 2002. The hourly $PM_{2.5}$ mass concentration is indicated by the height of the bar, while the color of the bar represents the 24-hour running average mass concentration color coded to the US EPA Air Quality Index. The yellow to red colors of aerosol optical depth show elevated aerosol concentrations and have been found to correlate strongly with $PM_{2.5}$ levels. Note the elevated PM associated with both measures of aerosol in Canada and the northeast United States.

sources were evenly distributed instead of exhibiting a diurnal pattern). In several cases where datasets covering very long time periods were evaluated, reductions in emissions were observed from power plants (Poirot et al., 2001), fuel oil (Lee et al., 2003a), and smelters (Battye, 2002). These were attributed to increased emission controls, fuel switching (e.g., from oil to natural gas), and meteorological conditions (e.g., warmer winters in the late 1990s).

6.1.3 Satellite Observations

6.1.3.1 *Impact of PM from Forest Fires to Eastern North America*

Direct observation of PM aerosol events using satellite sensors can provide a qualitative perspective of sources and receptors of PM and PM precursors. The boreal forest wildfires in southern Quebec during the summer of 2002 produced large amounts of aerosol loading within the lower troposphere. Meteorological conditions provided the mechanism for southerly transport of particulate, increasing ground level $PM_{2.5}$ concentrations in large portions of the eastern United States. Daily aerosol optical depth values from the MODIS terra satellite captured the transport of this smoke across Canada and into the Northeastern United States. Figure 6.19 shows the transport of the smoke plume through eastern Canada on July 6th, 2002, and the subsequent transport of PM across much of the northeastern United States on July 7th, 2002.

6.2 KEY SCIENCE MESSAGES

- $PM_{2.5}$ is transported across the border region between Canada and the United States, leading to elevated concentrations of PM in both countries. Most of the analyses point to SO_2 and NO_x emissions as being primarily regional contributors to PM, while organic/black carbon and other PM constituents tend to be more local in nature.
- Carbonaceous mass is prevalent everywhere, and is the major component of urban excess at sites in the northeastern United States. Consistent with other studies, most sulphates are associated with regional sources of SO_2; the urban excess of the $SO_4^=$ component is small.
- Contributors to $PM_{2.5}$ in both Vancouver and Toronto include secondary nitrate, regional transport of coal combustion products, diesel motor vehicles, secondary organic acids and road dust. Both the NH_4NO_3 and coal combustion components show seasonal variability. Emissions from primary and secondary coal and secondary organic acids are transported greater distances in comparison to diesel vehicles and road dust.
- Local motor vehicle sources (and small nearby smelter or industrial sources) have a relatively constant influence on $PM_{2.5}$ concentrations in Toronto, and are most evident on the cleanest days (which also tend to occur with northerly wind flows). Coal-related sources have a substantial transboundary contribution from the United States, and are especially important on days of high $PM_{2.5}$ concentration.
- Natural sources of PM (i.e., forest fires) can also influence ambient air quality. Satellite observations confirm the impact of Canadian forest fire events on U.S. aerosol optical depth.

CHAPTER 7

CONCLUSIONS

As a cumulative result of three bi-national workshops, and of discussions therein, seven key objectives were identified for this Transboundary Particulate Matter Science Assessment. These objectives have been addressed using a combination of ambient observations, data analysis, and application of modelling tools in both Canada and the United States. In each step of the Assessment, key science messages were captured to synthesize the current state of knowledge on the transboundary transport of $PM_{2.5}$, in keeping with the information needs of the bi-national policy community. The conclusions of this Assessment focus the key science messages on the seven objectives, and thus provide scientific support for further regulatory and technical programs.

OBJECTIVE 1:

Is there a fine PM problem in the border regions?

- Current ambient levels of $PM_{2.5}$ in the border regions exceed the standards set for $PM_{2.5}$ in several regions of both Canada and the United States. The eastern portion of the border domain (i.e., northeastern United States, Industrial Midwest, and the Windsor-Quebec City corridor) exhibits levels that exceed the 15 $\mu g/m^3$ annual standard in the United States and the 30 $\mu g/m^3$ 98th percentile three-year average Canadian standard for the time periods evaluated.
- There are sites with elevated $PM_{2.5}$ levels (with very few sites exceeding either standard for the time periods evaluated) in the Georgia Basin - Puget Sound airshed, but the problem is more confined, and the levels generally lower than in the northeastern airshed.
- $PM_{2.5}$ is transported across the border region between Canada and the United States, leading to elevated concentrations of $PM_{2.5}$ in both countries. Most of the analyses point to SO_2 as a primarily regional contributor and NO_x as both a local and regional contributor to $PM_{2.5}$, while organic/black carbon and other PM constituents tend to be more local in nature. Carbonaceous mass is prevalent everywhere, but is the major component of urban excess at sites in the northeastern United States.
- Comparisons of $PM_{2.5}$ levels at different sites reveal that on average, the local contribution to total $PM_{2.5}$ in Toronto, Canada is approximately 30 to 35 percent. At sites in eastern Canada (e.g., Chapter 2, Figure 2.2), average $PM_{2.5}$ concentrations were 2 to 4 times greater under south/southwesterly flow compared to northerly flow conditions. This observation suggests that the majority of $PM_{2.5}$ at these locations is arriving from sources south of this region.
- Canadian provinces have been found to contribute approximately 13 percent of $PM_{2.5}$ measured at 17 Class I sites in the United States, while the transport of $PM_{2.5}$ and PM precursors across the border region leads to 'above average' $PM_{2.5}$ concentrations in eastern Canada.

OBJECTIVE 2:

What is the extent of the problem (if standards are exceeded, by how much, where and when are they exceeded)?

- Current ambient levels of $PM_{2.5}$ in the border regions exceed the standards set for $PM_{2.5}$ in several regions of both Canada and the United

States. Annual levels of $PM_{2.5}$ are as high as 18 μg/m^3 in the northeastern United States for the period 2000-2003.

- A large portion of sites in the eastern portion of the border domain (i.e. northeastern United States, Industrial Midwest and the Windsor-Quebec City corridor) exhibit levels that also exceed the 30 μg/m^3 98th percentile three-year average (of 24-hour values) Canadian standard for the years 2000-2002. The 98th percentile values are as high as 65 μg/m^3 in some areas of the northeastern United States.
- No sites in western Canada exhibit levels that exceed the U.S. or Canadian standards (with the exception of one point-source-influenced site in British Columbia) for the data included in this Assessment.
- $PM_{2.5}$ concentrations are highest (on average) in the winter (Dec, Jan, Feb) and summer (June, July, Aug).

OBJECTIVE 3:

Does the PM issue vary geographically?

- Elevated concentrations of $PM_{2.5}$ are found more often in the following regions: northeastern United States, Industrial Midwest, southwestern Ontario and the northwestern United States.
- Areas in the midwestern United States and Canada do not exhibit elevated average $PM_{2.5}$ concentrations in comparison, but still record high $PM_{2.5}$ concentrations during episodic conditions.
- Urban concentrations of $PM_{2.5}$ are higher than rural concentrations in all regions of both Canada and the United States; however, rural sites can exhibit very high $PM_{2.5}$ levels during large-scale PM episodes.

OBJECTIVE 4:

What PM precursors are of most concern regionally and sub-regionally?

- The highest particle $SO_4^=$ and NO_3^- concentrations are found in areas with high SO_2 and NO_x emissions. These areas include the northeastern United States and southwestern Ontario.
- Levels of $PM_{2.5}$ and PM precursors (SO_2, NO_x) have declined, particularly early on in the data record however, since the mid-1990s, levels of PM and PM precursors have generally remained flat.
- $PM_{2.5}$ in the border region consists of, in order of relative importance to annual $PM_{2.5}$ levels, organic/black carbon, $SO_4^=$, NH_4^+, NO_3^-, soil dust and trace elements. Secondary particulate (i.e., NH_4^+, NO_3^- and $SO_4^=$) is found to play a key role under episodic conditions in Ontario. In the border region, organic and black carbon and $SO_4^=$ are seen to be the dominant species in summer, fall, and spring $PM_{2.5}$ aerosols. Nitrates are a major species in the winter in the northeast and carbon is a major species in the winter in the northwest.
- Carbonaceous mass is prevalent everywhere, and is the major component of urban excess at sites in the northeastern United States. Consistent with other studies, most sulphates are associated with regional sources of SO_2; the urban excess of the $SO_4^=$ component is small.
- Ambient levels of PM precursors also contribute to the wet deposition of NO_3^- and $SO_4^=$, and resulting ecosystem acidification. The highest levels of deposition are located in the northeastern United States and eastern Canada, particularly in the border regions.
- In the western regions, fine particles have a greater percentage of mass as carbon compounds relative to the east, where secondary components are more prevalent.

OBJECTIVE 5:

What are the sources (or source regions) of PM and PM precursors in the context of geographic regions (i.e., west, central, east)?

- Components and contributing sources to $PM_{2.5}$ identified in both Vancouver and

Toronto include secondary NO_3^-, regional transport of coal combustion products, diesel motor vehicles, secondary organic acids and road dust. Both the NH_4NO_3 and coal combustion contributors show seasonal variability. Primary and secondary coal and secondary organic acids are considered to be more regional in nature in comparison to diesel vehicles and road dust, which can be considered to be more local sources.

- Local motor vehicle sources (and small nearby smelter or industrial sources) have a relatively constant influence on $PM_{2.5}$ concentrations in Toronto, and are most evident on the cleanest days (which also tend to occur with northerly wind flows). Coal-related sources have a substantial transboundary contribution from the United States, and are particularly important on days of high $PM_{2.5}$ concentration.
- Analysis of upwind probability fields for coal related sources and NH_4NO_3 in Toronto indicates a region of high density emissions from coal fired utilities in the northeastern United States is influencing $PM_{2.5}$ concentrations. A similar analysis for NH_4NO_3 indicates a more widespread source region, in the northeastern United States as well as the north-central United States, a region of high agricultural NH_3 emissions.
- Natural sources of PM (i.e., forest fires and biogenic sources) can also influence ambient air quality. Satellite observations confirm the impact of Canadian forest fire events on U.S. aerosol optical depth.
- Emissions from the northeastern United States and southern Canada have an impact on $PM_{2.5}$ levels in many areas of the two countries, including as far east as Nova Scotia and New Brunswick, particularly influencing the top 25th percentile of $PM_{2.5}$ concentrations in these regions.
- Visibility is impaired at Glacier National Park, Montana, as a result of particle NO_3^-, $SO_4^=$ and organic carbon from source regions in both Canada and the United States.
- Transport of $SO_4^=$ from the midwestern United States to Canada was observed in several studies. As well, smelter emissions from Canada were observed to contribute to PM levels in the United States in several studies.
- Source-receptor analyses indicate that there are several areas which contribute to elevated PM levels in eastern North America. These areas include, but are not limited to, the following:
  - Air masses originating from a relatively large area from southeast Ohio to the western part of Virginia and western Kentucky to central Tennessee tended to result in relatively high $PM_{2.5}$ concentrations over northeastern North America.
  - The Windsor-Quebec City Corridor
  - The U.S. Midwest and Boston to Washington corridor
  - The Ohio River Valley
  - Northern Alberta and Saskatchewan and the central United States (Montana, North Dakota)
  - Vancouver/Seattle, Oregon and northern California
- The Georgia Basin - Puget Sound airshed is relatively small; hence, sources and receptors of PM and PM precursors, responsible for the majority of transboundary transport, are found throughout the region.
- The precise contribution of U.S. versus Canadian sources to air-quality levels (specifically PM) in the two respective countries is not addressed in detail in this Assessment. More specific model applications and source-receptor analyses are recommended.

OBJECTIVE 6:

How are PM precursor emissions spatially distributed, and what are the transport characteristics of these emissions?

- Emissions of SO_2 and NO_x are projected to decrease while emissions of NH_3, VOCs and CO are projected to increase between the base case and control scenarios.

- Emissions of SO_2 and NO_x under all considered scenarios are concentrated in the Industrial Midwest, northeastern United States and southern Ontario, while emissions of NH_3 are concentrated further west in the central Midwest region.
- The emissions of SO_2, NO_x and NH_3, and their contributions to $PM_{2.5}$ levels vary seasonally.
- Transport of PM and PM precursors from the Ohio River Valley has been observed to be associated with the highest $PM_{2.5}$ concentrations observed in the heavily populated areas in eastern Canada and the northeastern United States. These observation-based findings are consistent with the spatial distribution of the main SO_2 emissions sources and the major NO_x point sources.
- Trajectory analyses (Ch. 6) indicate that there is significant transport of PM and PM-precursors across the Canada-U.S. border.

OBJECTIVE 7:

What are the impacts of current and proposed emission reductions scenarios on fine PM levels in North America?

- U.S. and Canadian controls that are expected to be implemented result in maximum annual reductions of $PM_{2.5}$ of 1.8 $\mu g/m^3$ in 2010 and 2.3 $\mu g/m^3$ in 2020. The reductions vary temporally and spatially, with larger reductions in the eastern portion of the REMSAD modelling domain.
- Proposed additional SO_2 and NO_x emission reductions should provide additional reductions in ambient $PM_{2.5}$ levels in eastern North America. The observed $PM_{2.5}$ reductions may vary by season and depend strongly on reductions in $PM_{2.5}$ $SO_4^=$ mass.
- Simultaneous reductions in both SO_2 and NO_x may also provide concurrent reductions in NH_4^+, due to the reduction of gaseous SO_2 and NO_x available to react with gaseous NH_3.
- Reductions in NO_x emissions will correspond to decreases in $PM_{2.5}$ NO_3^- mass in some parts of eastern North America but increases in other areas due to NO_3^- substitution. There is significance placed on the role of NH_3 in this relationship, suggesting there may be value in investigating possible benefits due to NH_3 emission reductions in conjunction with SO_2 and NO_x emission reductions.
- Comparisons of the AURAMS and REMSAD predictions showed good qualitative agreement and consistency for all four PM fields and both seasons in terms of the atmospheric response to emission reductions.
- In the Georgia Basin - Puget Sound region, impacts from transboundary transport occur along the border (within ± 50 km) with some frequency; however, the incidence of long-range/regional transport (over 100 km) was low. Peak $PM_{2.5}$ levels are projected to increase modestly in urban areas as well as downwind of urban areas during both summer and winter simulations.
- Co-benefits of emission reduction scenarios include reduced ground-level ozone levels, reductions in NO_3^- and $SO_4^=$ deposition, and improved visibility.

REFERENCES

AETG. 1997. Towards a National Acid Rain Strategy. Report by Acidifying Emissions Task Group for the Canadian National Air Issues Coordinating Committee. October, 98 pp. [Available from http://www.ec.gc.ca/acidrain/towards_e.html].

Battye, W. 2002. Compendium of existing back-trajectory analyses relating to U.S.-Canada transboundary impacts of fine particulate and regional haze. Draft Report for the USEPA. Contract No. 68-D-98-006.

Blanchard, P., Brook, J.R., and Brazal, P. 2002. Chemical characterization of the organic fraction of atmospheric aerosol at two sites in Ontario, Canada. Journal of Geophysical Research. 107(21).

Brook, J.R., Dann, T.F., and Burnett, R.T. 1997. The relationship among TSP, PM_{10}, $PM_{2.5}$ and inorganic constituents of atmospheric particulate matter at multiple Canadian locations. Journal of the Air and Waste Management Association. 47: 2-19.

Brook J.R., and Dann, T.F. 1999. Contribution of nitrate and carbonaceous species to $PM_{2.5}$ observed in Canadian cities. Journal of the Air and Waste Management Association. 49: 193-199.

Brook, J.R., Dann, T.F., and Bonvalot, Y. 1999. Observations and interpretations from the Canadian fine particle monitoring program. Journal of the Air and Waste Management Association. 49: PM35-44.

Brook, J.R., Lillyman, C.D., Shepherd, M.F., and Mamedov, A. 2002. Regional transport and urban contributions to fine particulate concentrations in Southeastern Canada. Journal of the Air and Waste Management Association. 52: 855-866.

Brook, J.R., Johnson, D., and Mamedov. A. 2004. Determination of the source areas contributing to regionally high warm season $PM_{2.5}$ in eastern North America. Journal of the Air and Waste Management Association. In press.

Butler T.J., Likens, G.E., Vermeylen, F., and Stunder, B. 2003. The relation between NO_x emissions and precipitation NO_3^- in the eastern USA. Atmospheric Environment. 37: 2093-2104.

Butler T.J., Likens, G., and Stunder, B. 2001. Regional-scale impacts of Phase I of the Clean Air Act Amendments in the USA: the relation between emissions and concentrations, both wet and dry. Atmospheric Environment. 35: 1015-1028.

Byun, D.W., and Dennis, R. 1995. Design artifacts in Eulerian air quality models: evaluation of the effects of layer thickness and vertical profile corrections on surface ozone concentrations. Atmospheric Environment. 29: 105-126.

Cheng, L., Sandhu, H.S., Angle, R.P., McDonald, K.M., and Myrick, R.H. 2000. Rural particulate matter in Alberta, Canada. Atmospheric Environment. 34: 3365-3372.

Clair, T.A., Dennis, I., and Cosby, B. 2003. Probable changes in lake chemistry in Canada's Atlantic Provinces under proposed North American emission reductions. Hydrology and Earth System Sciences. 7(4): 574-582.

Côté, J., Roch, M., Staniforth, A., and Fillion, L. 1993. A variable-resolution semi-Lagrangian finite-element global model of the shallow-water equations. Monthly Weather Review. 121: 231-243.

Côté, J., Gravel, S., Méthot, A., Patoine, A., Roch, M., and Staniforth, A. 1998a. The operational CMC-MRB global environmental multiscale (GEM) model. Part I: Design considerations and formulation. Monthly Weather Review. 126: 1373-1395.

Côté, J., Desmarais, J.G., Gravel, S., Méthot, A., Patoine, A., Roch, M., and Staniforth, A. 1998b. The operational CMC-MRB global environmental multiscale (GEM) model. Part II: Results. Monthly Weather Review. 126: 1397-1418.

Countess, R.J., Barnard, W.R., Claiborn, C.S., Gillette, D.A., Latimer, D.A., Pace, T.G., and Watson, J.G. 2001. Methodology for estimating fugitive windblown and mechanically re-suspended road dust emissions applicable for regional scale air quality modelling. Report No. 30203-9, Western Regional Air Partnership, Denver, CO, 113 pp. [Available from: www.wrapair.org/forums/dejf/documents/FugitiveDustFinal.pdf].

Coutant, B., Kelly, T., Ma, J., Scott, B., Wood, B., and Main, H. 2002. Source apportionment analysis of air quality monitoring data: Phase 1 Final Report. Prepared for the Mid-Atlantic-Northeast Visibility Union and Midwest Regional Planning Organization by Battelle Memorial Institute and Sonoma Technology Inc.

Dion, J. 2003. START - A Regional and transboundary atmospheric transport analysis tool. User's Manual. Version 2003.05.22 for START 1 (version 1.0.1.0) and companion software. Environment Canada.

Dutkiewicz, V.A., Mita, D., and Liaquat, H. 2000. The relationship between regional SO_2 emissions and downwind aerosol sulphate concentrations in the northeastern U.S. Atmospheric Environment. 34: 1821-1832.

Environment Canada. 1997. The 1997 Canadian Acid Rain Assessment. Volume 2: Atmospheric science assessment report. Meteorological Service of

Canada. Environment Canada, Downsview, Ontario, 296 pp.

Environment Canada. 2001. Precursor contributions to ambient fine particulate matter in Canada. Meteorological Service of Canada, Environment Canada, Downsview, Ontario, 237 pp.

Environment Canada. 2002. 2001 Annual progress report on the Canada-Wide Acid Rain Strategy for Post-2000. Environment Canada, Hull, Quebec, 16 pp. [Available from: http://www.ccme.ca/assets/pdf/acid_rain_e.pdf]

EPA (U.S. Environmental Protection Agency). 1996. Review of the national ambient air quality standard for particulate matter: Policy assessment of scientific and technical information. EPA-452\R-96-013. Washington, D.C.: U.S. Environmental Protection Agency, Office of Air Quality Planning and Standards.

EPA. Office of Research and Development, 1999. Science Algorithms of the EPA Models-3 Community Multiscale Air Quality (CMAQ) Modelling System, EPA/600/R-99/030, edited by D. W. Byun and J. K. S. Ching.

EPA. 1999. Procedures document for the National Emission Inventory, Criteria Air Pollutants 1985-1999. EPA-454/R-01-006.

EPA. 2001. Inverse modelling to estimate seasonal ammonia emissions. Poster presentation: International Emission Inventory Conference, "One Atmosphere, One Inventory, Many Challenges." Denver, CO, April 30, 2001.

EPA. 2003a. The Clear Skies Act. Technical Support Package. [Available from: http://www.epa.gov/clearskies/technical.html, July 2003]

EPA. 2003b. Procedures for developing base year and future year mass emission inventories for the non-road diesel engine rulemaking. EPA-454/R-03-009, April 2003.

Gong S.L., Zhang, X.Y., Zhao, T.L., McKendry, I.G., Jaffe, D.A. and Lu, N.M. 2002: Characterization of soil dust distribution in China and its transport during ACE-Asia 2: model simulation and validation. Journal of Geophysical Research (submitted).

Gong, S.L., Barrie, L.A., Blanchet, J.-P., von Salzen, K., Lohmann, U., Lesins, G., Spacek, L., Zhang, L.M., Girard, E., Lin, H., Leaitch, R., Leighton, H., Chylek, P., and Huang, P. 2003a. Canadian Aerosol Module: A size segregated simulation of atmospheric aerosol processes for climate and air quality models: Part 1. Module development. Journal of Geophysical Research, 108(D1), 4007, doi:10.1029/2001JD002002, 16 pp.

Gong, W., Dastoor, A.P., Bouchet, V.B., Gong, S., Makar, P.A., Moran, M.D., and Pabla, B. 2003b. Cloud processing of gases and aerosols in a regional air quality model (AURAMS) and its evaluation against precipitation-chemistry data. Proceedings of the 5th AMS Conference on Atmospheric Chemistry, 2.3 (CD-ROM), Feb. 9-13th, 2003. Long Beach, California, American Meteorological Society, Boston.

Gilliland A.B., Dennis, R.L., Roselle, S.J., and Pierce, T.E. 2003. Seasonal NH_3 emission estimates for the eastern United States. Journal of Geophysical Research, 108, doi:10.1029/2002JD003063.

Grell, G., Dudhia, J., and Stauffer, D. 1994. A Description of the Fifth-Generation Penn State/NCAR Mesoscale Model (MM5), NCAR/TN-398+STR., 138 pp, National Center for Atmospheric Research, Boulder CO.

Griffin, R., Cocker III, D., Flanagan, R., and Seinfeld, J. 1999. Organic aerosol formation from the oxidation of biogenic hydrocarbons. Journal of Geophysical Research. 104: 3555-35667.

GVRD. 2002. 2000 Emission inventory for the Lower Fraser Valley airshed. [Available from: http://www.gvrd.bc.ca/services/air/emissions/reports/LFV2000EI.pdf.]

ICF Kaiser, 2002. User's guide to the Regional Modelling System for Aerosols and Deposition (REMSAD) Version 7. San Rafael, CA.

Kang, D., Eder, B.K., and Schere, K.L. 2003. The evaluation of regional scale air quality models. Proceedings of the 26th NATO-CCMS International Technical Meeting, Istanbul, May, 2003.

Keeler, G.J., and Samson, P.J. 1989. Spatial representativeness of trace element ratios. Environmental Science and Technology. 23: 1358-1364.

Kenski, D.M. Quantifying transboundary transport of $PM_{2.5}$: A GIS analysis. Proceedings of the 97th AWMA Annual Conference, Indianapolis, IN, June, 2004.

Kim, Y., Seinfeld, J., and Saxena, P. 1993. Atmospheric gas-aerosol equilibrium I. thermodynamic model. Aerosol Science and Technology, 19, 157-181.

Kit, A., Lock, S., Madland, C., Vaino, M., and Vaters, M. 2000. Air chemistry background analysis at Royal Roads University September 2000, Final Report, Royal Roads University, 81pp.

Laprise, R., Caya, D., Bergeron, G., and Giguere, M. 1997. The Formulation of the Andre Robert MC2 (Mesoscale Compressible Community) Model. numerical methods in atmospheric and oceanic modelling, C. Lin, R. Laprise, and H. Ritchie, Eds. Canadian Meteorological and Oceanographic Society, 195-220.

Lee, J.H., Yoshida, Y., Turpin, B.J., Hopke, P.K., Poirot, R.L., Lioy, P.J., and Oxley, J.C. 2002. Identification of sources contributing to mid-Atlantic regional aerosol. Journal of the Air and Waste Management Association. 52(10): 1186-1205.

Lee, P.K.H., Brook, J.R., Dabek-Zlotorzynska, E., and Mabury, S.A. 2003. Identification of the major sources contributing to $PM_{2.5}$ observed in Toronto. Environmental Science and Technology. 37(21): 4831-4840.

Li, S.-M. 2001. Project Plan for the Pacific 2001 Field Study, http://www.pnl.gov/pnw2001/canadian.pdf.

Li, S.-M., Anlauf, K.G., Wiebe, H.A., Bottenheim, J.W., and Puckett, K.J. 1994. Evaluation of a comprehensive Eulerian air quality model with multiple chemical species measurements using principal component analysis. Atmospheric Environment. 28: 3449-3461.

Likens G.E., Butler, T.J., and Buso, D.C. 2001. Long- and short-term changes in sulphate deposition: effects of the 1990 Clean Air Act Amendments. Biogeochemistry. 52:1-11.

Long, R.W. 2002. Measurement of $PM_{2.5}$, including semi-volatile components, in the EPA EMPACT and STAR programs: Results from the Salt Lake City, Bountiful and Lindon, Utah studies and implications for public awareness, health effects and control strategies. [dissertation]. Provo (Utah): Brigham Young University.

Lowenthal, D.H., Wittorff, D., and Gertler, A.W. 1994. CMB Source Apportionment During REVEAL (Regional Visibility Experiment in the Lower Fraser Valley), report Air Resources Branch, Ministry of Environment, Lands and Parks, ENV 484410/10/94, 50pp.

Lurmann, F.W., Lloyd, A.C., and Atkinson, R. 1986. A chemical mechanism for use in long-range transport/acid deposition computer modelling. Journal of Geophysical Research. 91: 10905-10936.

Lynch, J.A., Bowersox, V.C., and Grimm, J.W. 2000. Changes in sulphate deposition in eastern USA following implementation of Phase I of Title IV of the Clean Air Act Amendments of 1990. Atmospheric Environment. 34: 1665-1680.

Makar, P.A., Moran, M.D., Scholtz, M.T., and Taylor, A. 2003a. Speciation of volatile organic compound emissions for regional air quality modelling of particulate matter and ozone. Journal of Geophysical Research, 108 (D2): 4041, doi:10.1029/2001JD000797, 51 pp.

Makar, P.A., Bouchet, V.S., and Nenes, A. 2003b. Inorganic chemistry calculations using HETV - a vectorized solver for the SO_4^{2-}- NO_3^--NH_4^+ system based on the ISORROPIA algorithms. Atmospheric Environment. 37: 2279-2294.

McKendry, I.G., Hacker, J.P., Stull, R., Sakiyama, S., Mignacca, D., and Reid, K. 2001. Long-range transport of Asian dust to the Lower Fraser Valley, British Columbia, Canada. Journal of Geophysical Research. 106(18): 361-370.

MCNC, Environmental Programs. 2001. Community Multiscale Air Quality (CMAQ) modelling protocol for the "WRAP Regional Modelling Centre – Short-term Modelling Analysis" Project, Research Triangle Park, NC.

MCNC. 2000. Sparse Matrix Operator Kernel Emissions (SMOKE) Modelling System. [Available from: http://www.emc.mcnc.org/products/smoke/].

Mebust, M.R., B.K. Eder, F.S. Binkowski, and S.J. Roselle. 2003. Model-3 Community Multiscale Air quality (CMAQ) model aerosol component. 2. Model evaluation. Journal of Geophysical Research. 108(D6): 4184, doi:10.1029/2001JD001410.

Moran, M.D. 1997. Evaluation of the impact of North American SO_2 emission control legislation on the attainment of SO_4 critical loads in eastern Canada. Paper 97-TA28.01, Proceedings of the 90th AWMA Annual Meeting, June 8-13, Toronto, Canada, Air & Waste Management Association, Pittsburgh.

MSC. 1997. Canadian 1996 NO_x/VOC Science Assessment. Modelling of ground-level ozone in the Windsor Quebec city corridor and in the southern Atlantic Region.

National Research Council. 1993. Protecting visibility in national parks and wilderness areas: committee on haze in National Parks and wilderness areas, National Academy Press, Washington, D.C.

Natural Resources Canada. 1999. Canada's Emissions Outlook: An Update, December 1999. Natural Resources Canada, Ottawa.

Nenes, A., Pilinis, C., and Pandis, S.N. 1998. ISORROPIA: A new thermodynamic equilibrium model for multiphase multicomponent marine aerosols. Aquatic Geochemistry. 4: 123-152.

Nejedly Z., Campbell, J.L., Brook, J.R., Vet, R., and Eldred, R., 2003. Evaluation of elemental and black carbon measurements from the GAViM and IMPROVE Networks. Aerosol Science and Technology. 37(1).

Odum, J.R., Hoffman, T., Bowman, F., Collins, D., Flagan, R.C., and Seinfeld, J.H. 1996. Gas/particle partitioning and secondary aerosol formation. Environmental Science & Technology. 30: 2580-2585.

Odum, J., T. Jungkamp, R Griffin, H. Forstner, R. Flagan, and J. Seinfeld, 1997. Aromatics, reformulated gasoline, and atmospheric organic aerosol formulation. Environmental Science & Technology. 31: 1890-1897.

Paterson, K.G., Sagady, J.L., Hooper, D.L., Bertman, S.B., Carroll, M.A., and Shepson, P.B. 1999. Analysis of air quality data using Positive Matrix Factorization. Environmental Science and Technology. 33(4): 635-641.

Poirot, R.L., Wishinski, P.R., Hopke, P.K., and Polissar, A.V. 2001. Comparative application of multiple receptor methods to identify aerosol sources in Northern Vermont. Environmental Science and Technology. 35(33): 4622-4636.

Prendes, P., Andrade, J.M., Lopez-Mahia, P., and Prada, D. 1999. Source apportionment of inorganic ions in airborne urban particles from Coruna City (N.W. of Spain) using positive matrix factorization. Talanta. 49: 164-178.

Pryor, S.C., and Barthelmie, R. J. 1999. REVEAL II Characterizing fine aerosols in the Fraser Valley. Report to the Fraser Valley Regional District.

Rao, V., Neil, F., Rush, A., and Dimmick, F. 2003. Chemical speciation of $PM_{2.5}$ in urban and rural areas. National Air Quality and Emissions Trends Report, 2003 Special Studies Edition.

Rebust M.R., Eder, B.K., Binkowski, F.S., and Roselle, S.J. 2003. Model-3 Community Multiscale Air quality (CMAQ) model aerosol component. 2. Model evaluation, Journal of Geophysical Research, 108, D6, 4184-4202.

RMCC. 1990. The 1990 Canadian long-range transport of air pollutants and acid deposition assessment report: Part 4 – aquatic effects. Federal/Provincial Research and Monitoring Coordinating Committee, Ottawa, Ontario, 151pp.

Rogge, W.F., Mazurek, M.A., Hildemann, L.M., Cass, G.R., and Simoneit, B.R.T. 1993. Quantification of urban organic aerosols at a molecular level: identification, abundance, and seasonal variation. Atmospheric Environment. 27A(8): 1309-1330.

RWDI. 2003a. Pacific Northwest International Air Quality Modelling Project, Phase 1 Report, Environment Canada – Pacific & Yukon Region, prepared by RWDI West Inc., August 28, 2003.

RWDI. 2003b. Pacific Northwest International Air Quality Modelling Project, Phase 2a Report, Environment Canada – Pacific & Yukon Region, prepared by RWDI West Inc., August 28, 2003.

RWDI. 2003c. Pacific Northwest International Air Quality Modelling Project, Phase 2b Report, Environment Canada – Pacific & Yukon Region, prepared by RWDI West Inc., August 28, 2003.

Ryan, W.F., Doddridge, B.G., Dickerson, R.R., Morales, R.M., Hallock, K.A., Roberts, P.T., Blumenthal, D.L., Anderson, J.A., and Civerolo, K.L. 1998. Pollutant transport during a regional O_3 episode in the mid-Atlantic states. Journal of the Air & Waste Management Association. 48: 786-797.

Sandberg, D.V., Ottmar, R.D., Peterson, J.L., and Core, J. 2002. Wildland fire in ecosystems: effects of fire on air. General Technical Report RMRS-GTR-42-vol. 5. Ogden, UT: U.S. Department of Agriculture, Forest Service, Rocky Mountain Research Station. 79 pp.

Saxena, P., Hudischewskyj, A., Seigneur, C., and Seinfeld, J. 1986. A comparative study of equilibrium approaches to the chemical characteristics of secondary aerosols. Atmospheric Environment. 20:1471-1483.

Schauer, J.J., Rogge, W.F., Hildemann, L, M., Mazurek, M.A., Cass, G.R., Simoneit, B.R.T. 1996. Source apportionment of airborne particulate matter using organic compounds as tracers. Atmospheric Environment. 30(22): 3837-3855.

Seibert, P., Kromp-Kold, H., Baltensperger, U., Jost, D.T., Schwikowski, M., Kasper, A., and Puxbaum, H. 1994. Trajectory analysis of aerosol measurements at high alpine sites. In: Proceedings of EUROTRAC Symposium '94. Ed. P.M. Borrell, P. Borrell, T. Cvitas and W. Seiler. Academic Publishing bv, The Hague, Garish-Partenkirchen, Germany. pp. 689-693.

Seigneur, C., and Moran, M.D. 2003. Using models to estimate particle concentration. Chapter 8 in Particulate Matter Science for Policy Makers. A NARSTO Assessment, P. McMurry, M. Shepherd, and J. Vickery, Editors, February, 42 pp.

Shannon, J. 1999. Regional trends in wet deposition of sulphate in the United States and SO_2 emissions from 1980 through 1995. Atmospheric Environment. 33: 807-816.

Sirois, A., and Vet, R. Pers.comm. An exploratory evaluation of potential Canadian emission contributions to reduced visibility and particulate matter concentrations at Glacier National Park, Montana.

Snyder B., Brook J.R., and Strawbridge, K. 2002. Pollutant build-up over the Strait of Georgia and the role of mesoscale flow patterns (A71A – 0089). American Geophysical Union Annual Meeting, December 2002, San Francisco, USA.

Stein, A.F., and Lamb, D. 2002. Chemical indicators of sulphate sensitivity to nitrogen oxides and volatile organic compounds. Journal of Geophysical Research.107: doi:10.1029/2001JD001088.

Stoddard, J.L., Kahl, J.S., Deviney, F.A., DeWalle, D.R., Driscoll, C.T., Herlihy, A.T., Kellogg, J.H., Murdoch, P.S., Webb, J.R., and Webster, K.E. 2003. Response of surface water chemistry to the Clean Air Act Amendments of 1990. EPA/620/R-03/001, U.S. Environmental Protection Agency, Washington, D.C.

Tonnesen, G., Wang, Z., Omary, M., Chien, C-J., and Wang, B. 2002. Summary of CMAQ results for 1996 BASE Year regional haze modelling. WESTAR Annual Technical Meeting, Riverside, CA, Feb. 12, 2002.

USEPA. 1999. National air quality and emissions trends report. [Available from: http://www.epa.gov/air/aqtrnd99/toc.html]

Vet, R.J., Brook, J.R., Dann, T.F., and Dion, J. 2001. The nature of $PM_{2.5}$ mass, composition and precursors in Canada. In: Precursor Contributions to Ambient Fine Particulate Matter in Canada, MSC Report, Catalogue No. En56-167/2001E, May, Meteorological Service of Canada, Environment Canada, Downsview, Ontario, pp85-142.

Waugh, D., Tordon, R., Ketch, L., Beauchamp, S. 2002. Multi-pollutant trajectory analysis: Kejimkujik National Park, Nova Scotia, St. Andrews, New Brunswick. Internal Report from the Atmospheric Sciences Division, Meteorological Service of Canada. Dartmouth, Nova Scotia.

Watson, J.G., and Chow, J.C. 2000. Reconciling urban fugitive dust emissions inventory and ambient source contribution estimates: summary of current knowledge and needed research. Report No. 6110.4F prepared for the USEPA by Desert Research Institute, Reno, NV, May, 240 pp. [Available from: http://www.wrapair.org/forums/dejf/documents/fugitive1.pdf.]

West, J.J., Ansari, A.S., and Pandis, S.N. 1999. Marginal $PM_{2.5}$: Nonlinear aerosol mass response to sulphate reductions in the eastern United States. Journal of the Air & Waste Management Association. 49: 1415-1424.

Whitten, G.Z. 1999. Computer efficient photochemistry for simultaneous modelling of smog and secondary particulate precursors. Systems Application International, San Rafael, CA.

Working Group on Air Quality Objectives and Guidelines (WGAQOG), National Ambient Objectives for Particulate Matter: Science Assessment Document, Cat. No. H46-2/98-220-1E, Environment Canada and Health Canada, 1999.

Wotawa, G., and Trainer, M. 2000. The influence of Canadian forest fires on pollutant concentrations in the United States. Science. 288:324-328.

Yakovleva, E., Hopke, P.K., and Wallace, L. 1999. Receptor modelling assessment of particle total exposure assessment methodology data. Environmental Science and Technology 33(20): 3645-3652.

Zhang, L., Gong, S.-L., Padro, J., and Barrie, L. 2001. A size-segregated particle dry deposition scheme for an atmospheric aerosol module. Atmospheric Environment. 35: 549-560.

Zhang, L., Moran, M.D., Makar, P.A., Brook, J.R., and Gong, S. 2002. Modelling gaseous dry deposition in AURAMS — A Unified Regional Air-quality Modelling System. Atmosperic Environment. 36: 537-560.

APPENDIX

REMSAD AND AURAMS MODEL PERFORMANCE

A1.0 REMSAD MODEL PERFORMANCE

Scatter plots displaying REMSAD model performance for the 1996 base case are shown on the following pages. The REMSAD base case was run using 1996 meteorology and emissions. The $PM_{2.5}$ and $PM_{2.5}$ components ($SO_4^=$, NO_3^-, NH_4^+, OC, BC, and soil) predicted by REMSAD were then compared to available ambient monitoring data for 1996. The scatter plots contain model-predicted concentrations at the grid cell where an air-quality monitor is located versus the observed monitoring site concentrations for the averaging period of interest. The following scatter plots are generally for seasonal averaging periods. In addition, $PM_{2.5}$ scatter plots are provided for an annual averaging period to coincide with the U.S. air-quality standard for $PM_{2.5}$. Scatter plots for the United States are provided primarily for the Interagency Monitoring of Protected Visual Environments (IMPROVE) network, which contained measurements of $PM_{2.5}$, $SO_4^=$, particle NO_3^-, OC, BC, and soil. Also, scatter plots for $SO_4^=$ and total NO_3^- from the Clean Air Status and Trends Network (CASTNET) are provided for the United States. Scatter plots are provided for the Canadian National Air Pollution Surveillance (NAPS) monitoring network for $PM_{2.5}$, $SO_4^=$, NO_3^-, and NH_4^+. In addition, scatter plots are provided from the Canadian Air and Precipitation Monitoring Network (CAPMoN) for $SO_4^=$, NO_3^-, and NH_4^+. Note that NAPS is represented by NAP in the scatter plot headings and CAPMoN is represented by CAPM in the scatter plot headings.

The annual $PM_{2.5}$ concentrations predicted by REMSAD are generally within 30% of observed values at the eastern IMPROVE monitoring sites without much bias toward over or under-prediction. At the western IMPROVE monitoring sites, there is a bias toward model under-prediction of annual $PM_{2.5}$ concentrations. The majority of model-predicted seasonal averages at the eastern IMPROVE sites are generally within 30% of the observed seasonal averages. The western IMPROVE sites show a seasonal bias towards model under-prediction in all seasons with the strongest under-prediction bias in the summer. The annual $PM_{2.5}$ concentrations predicted by REMSAD at the NAPS sites show a bias toward over-prediction at both the eastern and western monitors with the over-predictions generally significantly less than 100%. The REMSAD-predicted seasonal $PM_{2.5}$ concentrations at the NAPS sites also show a bias towards over-prediction. The summer season has the least bias toward over-prediction at the eastern NAPS sites where model predicted $PM_{2.5}$ concentrations are generally within 30% of the observed $PM_{2.5}$ concentrations.

The seasonal $SO_4^=$ concentrations at the eastern IMPROVE sites are generally within 30% of the observed seasonal concentrations for all seasons. The western IMPROVE monitors generally show the model-predicted seasonal $SO_4^=$ concentrations to be biased toward under-prediction. The seasonal $SO_4^=$ scatter plots for the CASTNET dry deposition monitoring network show model-predicted seasonal $SO_4^=$ concentrations to generally be within 30% of observed $SO_4^=$ concentrations at the eastern monitors. In the winter, when there are substantially fewer monitors and observed $SO_4^=$ concentrations are much lower than the other seasons, there is a somewhat larger percentage bias toward under-prediction at the eastern CASTNET monitors. The western CASTNET dry deposition scatter plots show a bias toward $SO_4^=$ concentration under-prediction for all seasons. The seasonal REMSAD model predicted $SO_4^=$ concentrations are generally within 30% of the monitored $SO_4^=$ concentrations for the eastern NAPS Canadian monitoring sites. The largest percent bias toward under-prediction for the eastern NAPS sites is in the winter when observed $SO_4^=$ concentrations are lowest. The model predicted $SO_4^=$ concentrations at all the western NAPS sites are biased toward under-prediction. Seasonal model predicted $SO_4^=$ concentrations at the eastern CAPMoN sites are generally within 30% of observed monitored concentrations. As has been seen at the other $SO_4^=$ monitoring networks, the greatest bias toward under-prediction at the eastern CAPMoN monitors is in the winter when $SO_4^=$ concentrations are lowest. The model-predicted $SO_4^=$ concentrations at the western CAPMoN sites show a bias toward under-prediction.

Seasonal model-predicted particle NO_3^- concentrations at the eastern IMPROVE sites are biased high for every season with the least bias occurring in the summer. Seasonal model-predicted particle NO_3^- concentrations at the western IMPROVE monitors are generally unbiased, except in the summer where they are biased low. Seasonal model-predicted particle NO_3^- concentrations at the eastern and western NAPS sites are biased high with the least bias at the western sites in the winter. The REMSAD model-predicted particle NO_3^- concentrations at the CAPMoN sites do not show the strong over-prediction of particle NO_3^- shown at the other monitoring networks. The majority of model-predicted particle NO_3^- concentrations at the eastern CAPMoN sites are within 30% of the observed values in each season except the summer where there is a significant under-prediction of observed NO_3^- concentrations. Seasonal NO_3^- concentrations are generally under-predicted by the model at the western CAPMoN sites. The CASTNET DRY scatter plot is for total NO_3^-, which consists of particle NO_3^- plus NO_3^- from gaseous HNO_3. The IMPROVE, NAPS, and CAPMoN scatter plots are for only particle NO_3^-. The majority of the seasonal total NO_3^- concentrations predicted by REMSAD at the eastern CASTNET sites are within a factor of two of the observed concentrations with the largest over-prediction bias in the fall. The model-predicted seasonal total NO_3^- concentrations show a bias toward under-prediction at the western CASTNET sites.

REMSAD tends to over-predict NH_4^+ concentrations at the at the eastern NAPS sites for all seasons except the summer. In the summer, the predicted NH_4^+ concentrations are generally within 30% of observed NH_4^+ concentrations at the eastern NAPS sites. There is a tendency for the model to over-predict NH_4^+ concentrations at the western NAPS sites for all seasons except winter. The majority of seasonal NH_4^+ concentrations predicted by the model at the eastern and western CAPMoN sites are within 30% of observed NH_4^+ concentrations.

The majority of the model-predicted seasonal OC concentrations at the eastern IMPROVE monitoring sites are within 30% of observed seasonal OC concentrations with the summer displaying a somewhat larger over-prediction bias. There does not appear to be a substantial bias toward under- or over-prediction of the model-predicted seasonal organic concentrations at the western IMPROVE sites. However, at any single western IMPROVE monitoring site, the model can over or under-predict the seasonal organic carbon concentration by a factor of two or more.

The scatter plots of model-predicted BC concentrations at the eastern IMPROVE sites show little bias toward over- or under-prediction. The majority of the eastern IMPROVE sites show seasonal model-predicted BC within 30% of observed seasonal BC concentrations. At the western IMPROVE monitor sites, the seasonal scatter plots do not show a distinctive bias toward under- or over-prediction.

The model significantly over-predicts the soil concentrations at the eastern IMPROVE monitoring sites for all seasons. At the western IMPROVE monitoring sites, the model is bias toward over-predicting the soil concentrations for winter and fall and under-predicting the soil concentrations for summer and spring.

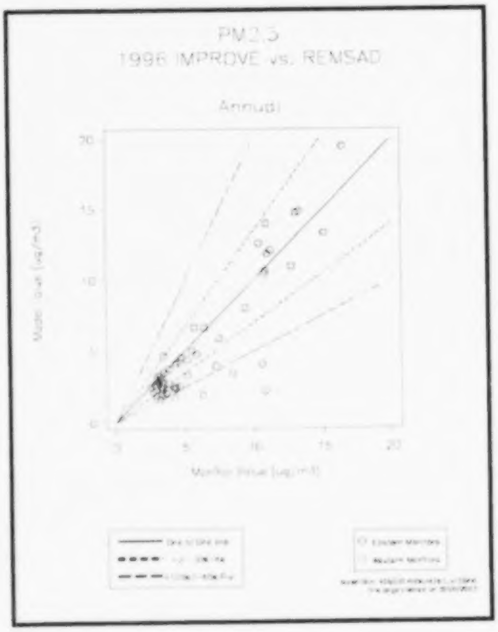
PM2.5
1996 IMPROVE vs. REMSAD
Annual
Model Value (ug/m3)
Monitor Value (ug/m3)
0
5
10
15
20
One to One line
+/- 50% line
+100%/-50% line
Eastern Monitors
Western Monitors

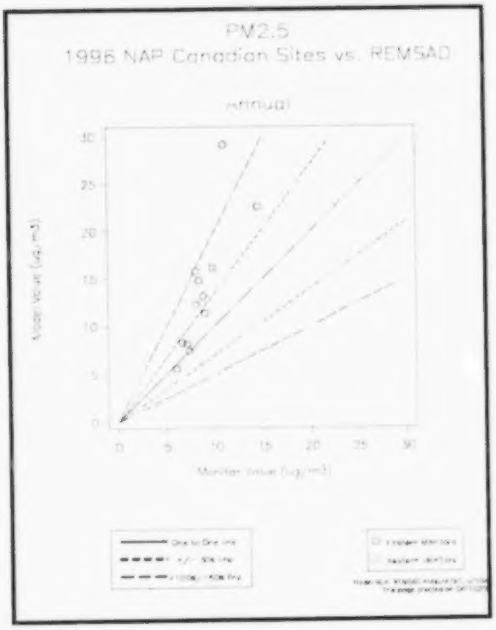
PM2.5
1996 NAP Canadian Sites vs. REMSAD
Annual
Model Value (ug/m3)
Monitor Value (ug/m3)
0
5
10
15
20
25
30
One to One line
+/- 50% line
+100%/-50% line
Eastern Monitors
Western Monitors

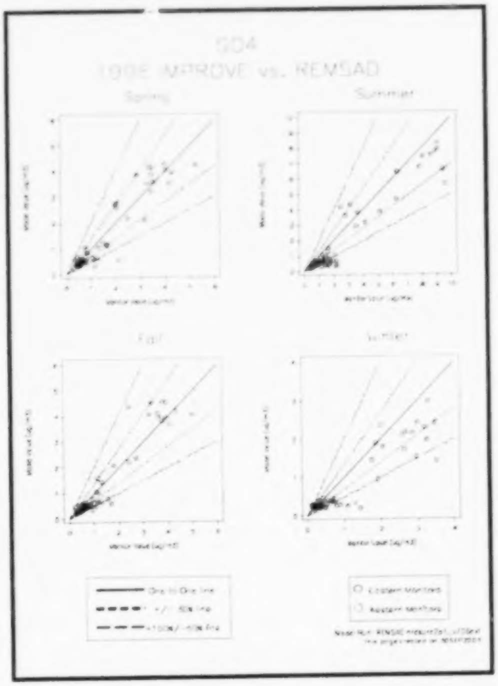
SO4
1996 IMPROVE vs. REMSAD
Spring
Summer
Fall
Winter
Model Value (ug/m3)
Monitor Value (ug/m3)
One to One line
+/- 50% line
+100%/-50% line
Eastern Monitors
Western Monitors

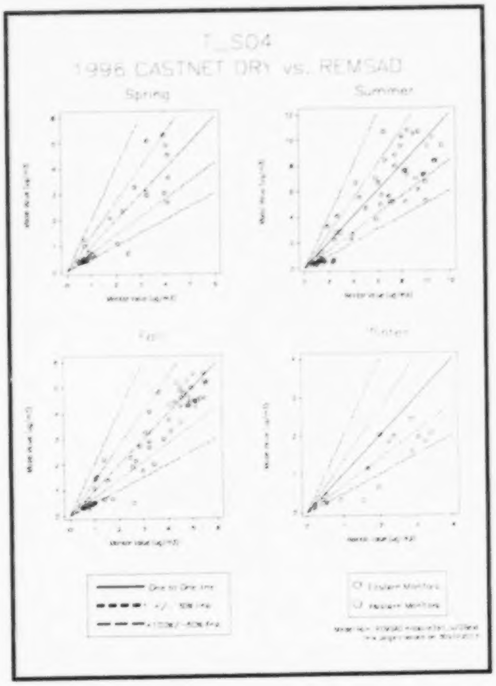
T_SO4
1996 CASTNET DRY vs. REMSAD
Spring
Summer
Fall
Winter
Model Value (ug/m3)
Monitor Value (ug/m3)
One to One line
+/- 50% line
+100%/-50% line
Eastern Monitors
Western Monitors

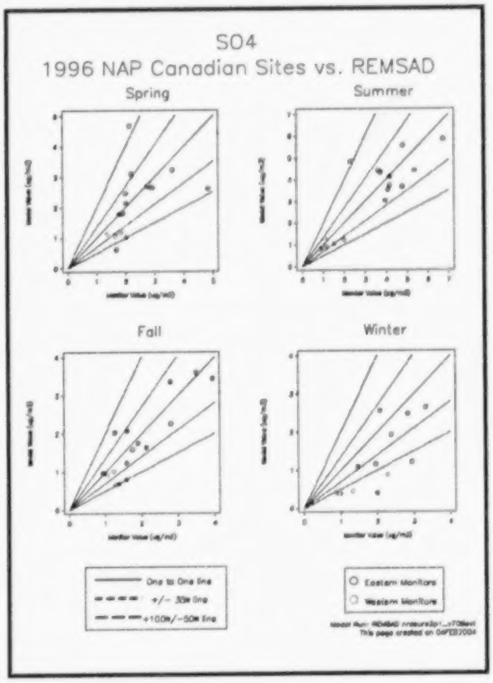
SO4
1996 NAP Canadian Sites vs. REMSAD

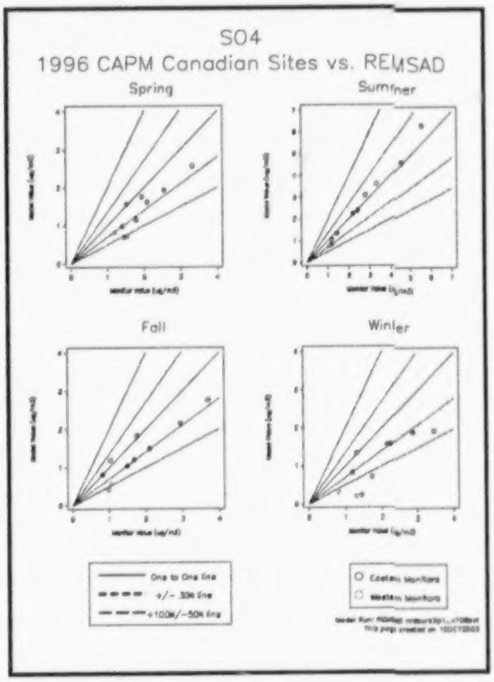
SO4
1996 CAPM Canadian Sites vs. REMSAD

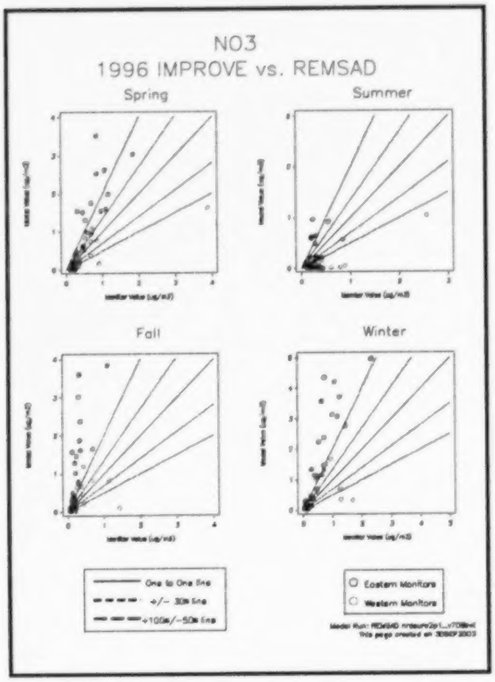
NO3
1996 IMPROVE vs. REMSAD

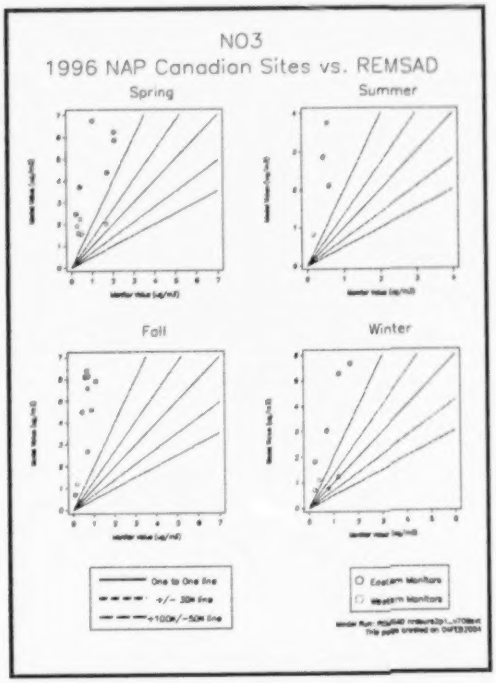
NO3
1996 NAP Canadian Sites vs. REMSAD

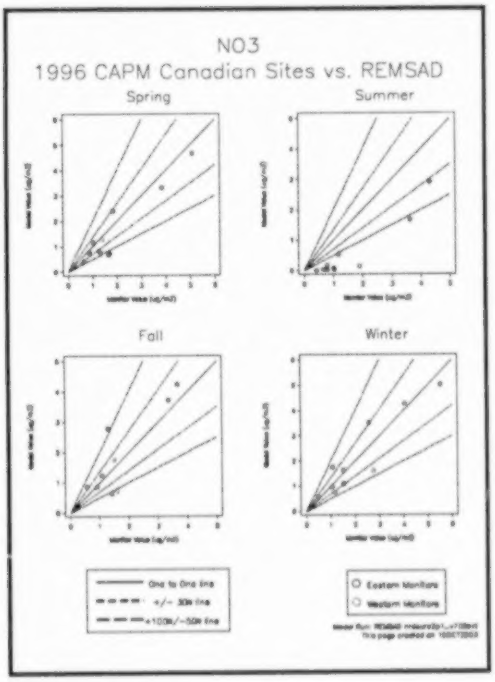
NO3
1996 CAPM Canadian Sites vs. REMSAD

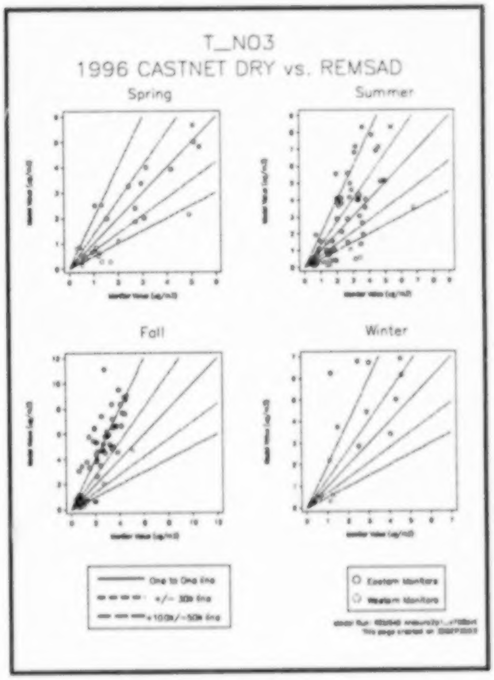
T_NO3
1996 CASTNET DRY vs. REMSAD

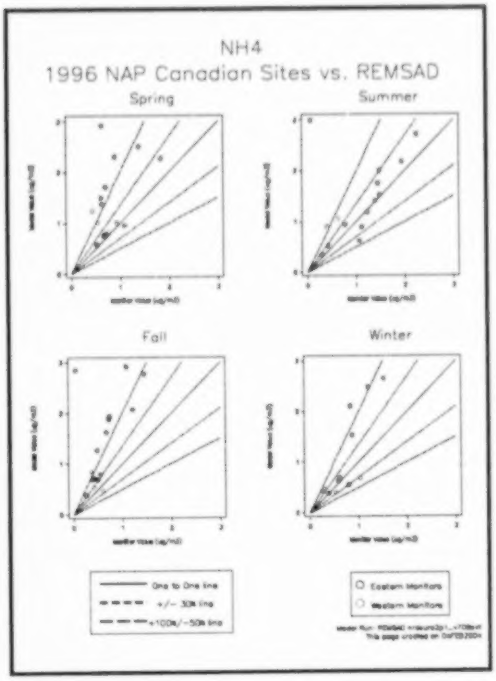
NH4
1996 NAP Canadian Sites vs. REMSAD

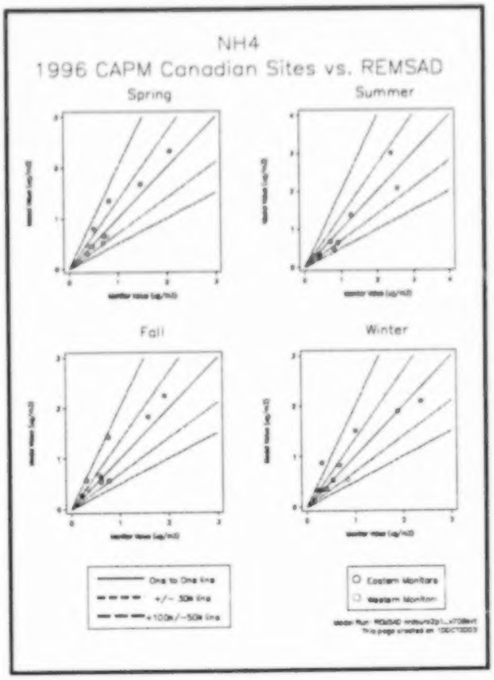
NH4
1996 CAPM Canadian Sites vs. REMSAD

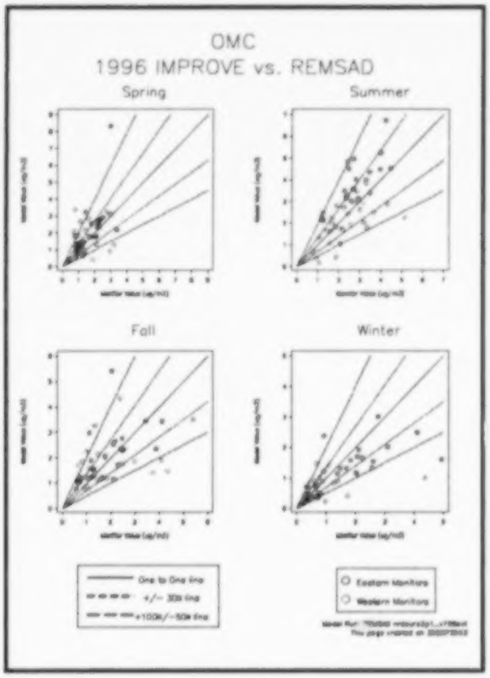

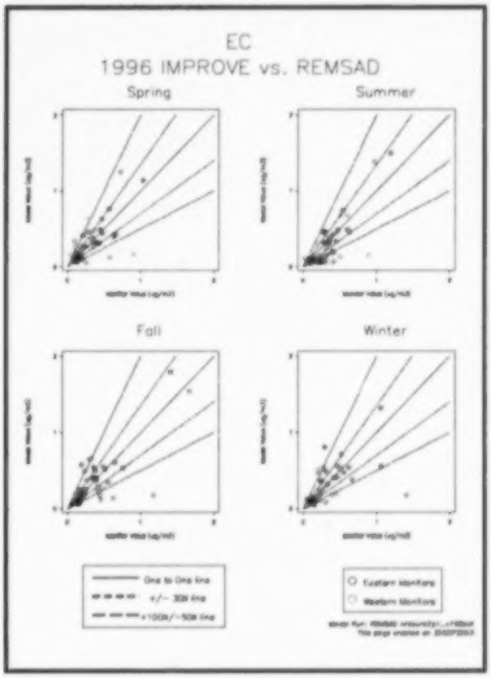

A2.0 AURAMS EVALUATION FOR TWO BASE CASES

A2.1 Data Availability

Model evaluation for both of the AURAMS base cases (1-15 February 1998; 1-18 July 1995) was complicated by the relatively small number of $PM_{2.5}$ measurements available. While a significant number of ozone measurement stations were in operation for these two periods, the opposite was true for the $PM_{2.5}$ species. This problem was compounded by the fact that some PM networks sample less frequently than daily. As an example, prior to 2000 the IMPROVE network only made measurements on Wednesdays and Saturdays. Such non-daily sampling complicates evaluation of multi-day model simulations, since the most intense days of a pollution episode could occur on a day with significantly fewer stations reporting. For example, Figure A.1 compares the $PM_{2.5}$ measurements from 24-hour filters that are available for Saturday, July 1st and Sunday, July 2nd, 1995; the stations available on each day are colour-coded according to the measured concentration of $PM_{2.5}$. The figure shows that U.S. $PM_{2.5}$ measurements are available for July 1st but not for July 2nd.

There were also more $PM_{2.5}$ measurements available for the winter 1998 period than for the summer 1995 period, including more hourly measurements. As a consequence, the $PM_{2.5}$ performance evaluation for the summer will be somewhat more qualitative as compared to the winter evaluation. Table A.1 summarizes the Canadian and U.S. measurement networks used to evaluate both episodes (see also Chapter 3) for $PM_{2.5}$ mass, $PM_{2.5}$ inorganic chemical components, and ozone. Note the heterogeneity of the different measurement sets. Note too that the hourly $PM_{2.5}$ measurements avoid the problem of intermittent non-daily sampling as they are obtained from continuous instruments (TEOMs).

AURAMS performance is considered here for both ozone and $PM_{2.5}$ so as to take advantage of the better spatial and temporal coverage of the ozone monitoring networks. Given that the future-year emission reductions discussed in Chapter 4 will impact both ground-level ozone and particulate matter, and given that secondary $PM_{2.5}$ production and gas-phase photochemistry are closely linked, it is natural to consider both pollutants together.

A2.2 Model Evaluation for Winter 1998

Figure A.2 shows observed and modelled time series of $PM_{2.5}$ mass from February 7th until February 14th, 1998 at three locations in south-eastern Canada: Kitchener, Ontario (2a);

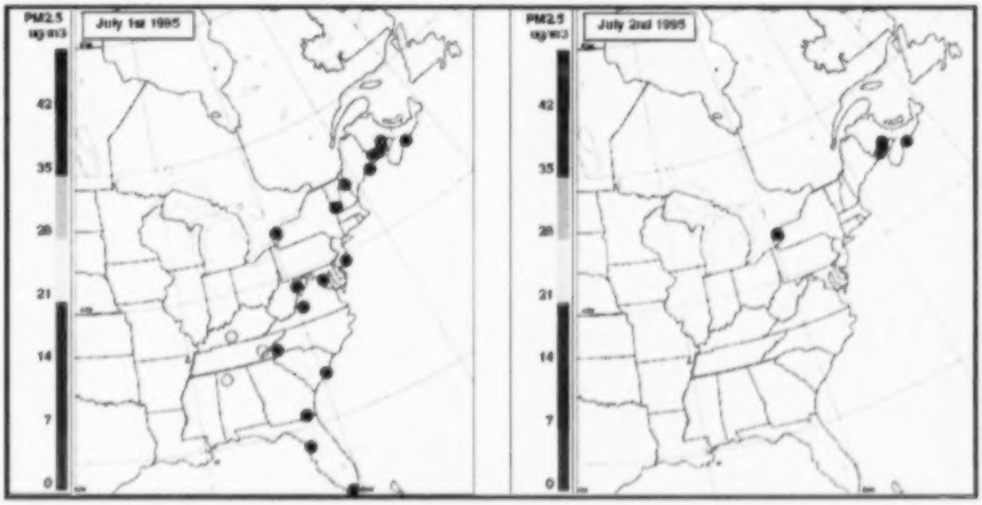

Figure A-1 · Maps of stations reporting 24-hour total $PM_{2.5}$ concentrations for two consecutive July 1995 days. 21 stations reported on July 1st compared to only 9 stations reporting on July 2nd.

Table A.1 Data networks available for model evaluation for two AURAMS simulation periods.

				Species Measured (size cut in μm)							
Network	# Stations	Type	Frequency	$SO_4^=$	NO_3^-	NH_4^+	EC	OC	PM_{10}	$PM_{2.5}$	O_3
CAPMoN	9*, 7**	24-hr filters	Daily	n.d.	n.d.	n.d.					
CAAMP*	5	24-hr filters	Daily	2.1*	2.1*	2.1*			10*	2.5*	
GAViM	2	24-hr filters	2 / 7 days	2.6	2.6	2.6				2.5	
IMPROVE	18	24-hr filters	2 / 7 days	2.6	2.6	2.6	2.6	2.6	10	2.5	
NAPS	56*,93**	24-hr filters	1 / 6 days	2.6 10	2.6 10	2.6 10				2.5	
	104**	TEOM	Hourly						10**	2.5**	
	104**	UV absorption	Hourly								n.a.
AIRS	520**	TEOM	Hourly						10**	2.5**	
	386*, 520**	UV absorption	Hourly								n.a.

*available for summer case only, **available for winter case only
n.a. = non available, n.d. = non determined

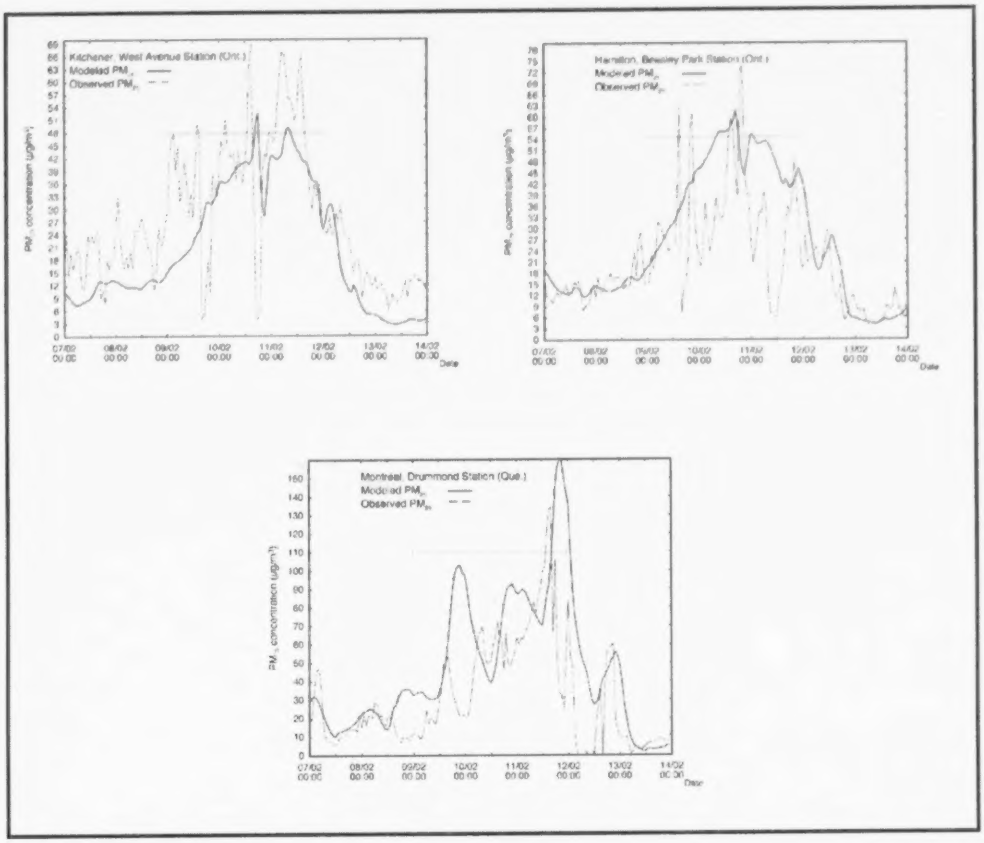

Figure A-2 - Time series of modelled and observed $PM_{2.5}$ from February 7th to 14th 1998 for (a) Kitchener, Ontario., (b) Hamilton, Ontario, and (c) Montreal, Quebec. Solid line: AURAMS simulation (µg/m³); Dashed line: Observations (µg/m³).

Hamilton, Ontario (2b): and Montreal, Quebec (2c). This period is of interest because of the strong $PM_{2.5}$ episode that occurred in eastern Canada, beginning on February 9th in Kitchener and Hamilton and on February 10th in Montreal. Hourly $PM_{2.5}$ concentrations as high as 70 µg/m³ were measured at the two Ontario stations while the peak observed $PM_{2.5}$ concentration for Montreal was over 130 µg/m³. AURAMS is able to predict the observed day-to-day variation in particle mass over this one-week period, giving a good representation of the mid-week increase in particle mass. The modelled time traces are much smoother than the continuous measurement record, which can be attributed, at least in part, to the spatial resolution of AURAMS of 42 km. At this resolution, AURAMS can only capture some of the features that are measured at a particular point, due to fine-scale variations in meteorology and emissions (i.e., point vs. grid-volume incommensurability). Note too that the TEOM measurements are likely to be biased low, especially at night, due to the impact of the heated inlet on semi-volatile PM components entering the instrument from wintertime ambient conditions.

Figure A.3 shows the corresponding ozone time series plot for Hamilton, Ontario. The $PM_{2.5}$ episode was reflected in the ozone concentration time series by very low ozone levels, possibly as a result of enhanced NO_2 titration associated with

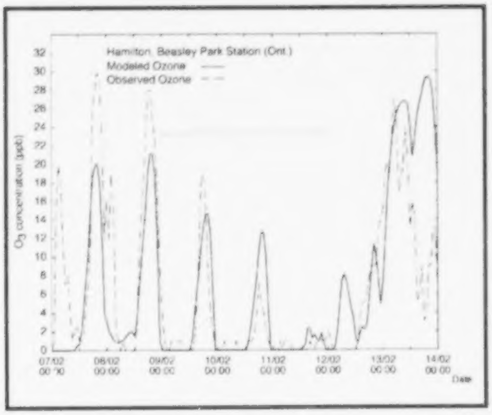

Figure A.3 - Time series of modelled and observed ozone (ppb) for Hamilton, Ontario from February 7th to 14th 1998. Solid line: AURAMS simulation; dashed line: observations.

stagnant conditions. AURAMS again tracked the changes in ozone concentration very well.

Model-vs-measurement scatter plots of hourly ozone and hourly $PM_{2.5}$ concentrations are shown in Figure A.4 for this same one-week period. On the left, the ozone scatter plot shows a bias towards under-prediction of hourly ozone concentrations (slope of 0.63,) and an R^2 value of 0.48. The $PM_{2.5}$ scatter plot also shows an overall bias to under-prediction (slope of 0.65), but some of the smallest value can be grossly over-predicted, driving the offset of the regression line to a value of 10.5 $\mu g/m^3$ (see Table A.2). For $PM_{2.5}$ the R^2 value is 0.26. Note that hourly $PM_{2.5}$ concentrations as high as 160 $\mu g/m^3$ were both observed and modelled for this period. A summary of the performance statistics corresponding to Figure A.4 is given in Table A.2.

Figures A.5 and A.6 present scatter plots comparing observed and predicted daily mass concentrations for $PM_{2.5}$ and its three inorganic chemical components for two sets of $PM_{2.5}$ samples: the IMPROVE and GAViM $PM_{2.5}$ measurements were reported for ambient conditions (Figure A.5) whereas the NAPS $PM_{2.5}$ measurements were reported at STP (Figure A.6). AURAMS PM predictions are for ambient conditions, but an STP conversion was done in the preparation of Figure A.6 to allow a direct comparison with the NAPS data. Note that particle NH_4^+ was not measured by the IMPROVE network for that time period but was measured by the GAViM network. These plots are characterized by relatively few measurements (see Table A.3) and large scatter, particularly for the three chemical components, but such scatter is characteristic of comparisons of air-quality model predictions made for such short averaging periods. Aside from one or two outliers, agreement is better than an order-of-magnitude, and there seems to be a tendency to under-predict SO_4 and over-predict NO_3. Predictions of total $PM_{2.5}$ mass do not display much bias. Note too that the time averaging associated with daily measurements rather than hourly measurements does reduce scatter (e.g., Figure A.4b vs. Figure A.6a). The performance statistics corresponding to Figures A.5 and A.6 are provided in Tables A.3 and A.4. Interestingly, a relatively high R^2 and a low RMSE are obtained for the NO_3^- PM component when comparing with IMPROVE and GAViM measurements, whereas the situation is reversed when comparing with the NAPS observations. The number of speciated NAPS data for that period is very limited, however, which limits the meaningfulness of the statistics.

Table A.2 Performance statistics for hourly ozone and $PM_{2.5}$ mass at all stations over the domain from February 7th to 14th 1998. (where n: number of observed values; R2: correlation coefficient; RMSE: root mean square error; NME: normalized mean error; MB: mean bias; NMB: normalized mean bias (Kang et al., 2003))

Species	n	R^2	σ_{mod}*	σ_{obs}**	$\sigma_{mod\text{-}obs}$***	RMSE	NME	MB	NMB	curve fitting equation
Hourly O_3	34060	0.48	170	206	129	12.0	42.7	-5.2	-24.2	mod = 0.63 obs + 2.80
Hourly $PM_{2.5}$	2739	0.26	582	360	232	22.0	61.4	2.8	13.1	mod = 0.65 obs + 10.50

Legend: *variance of model data, **variance of observation data, ***covariance

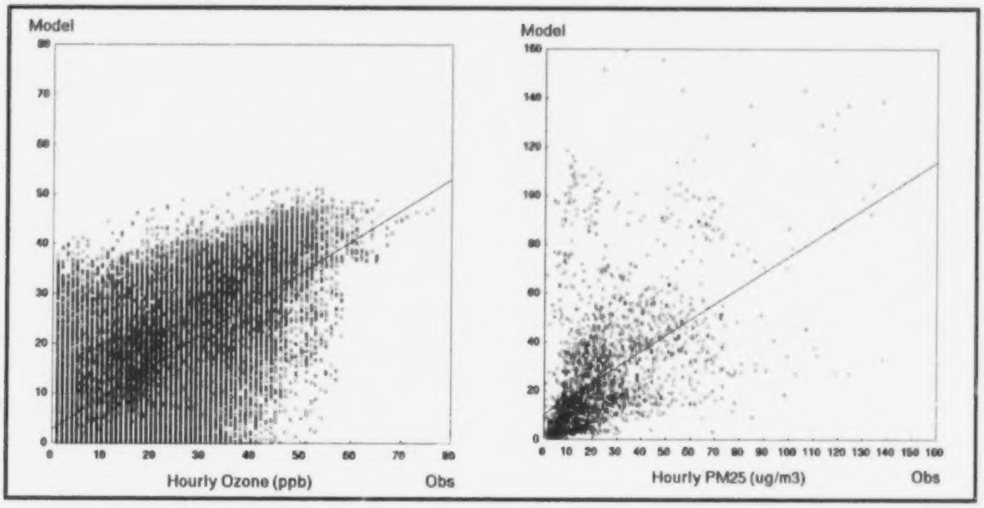

Figure A-4 - Scatter plots for hourly ozone (left panel) and hourly $PM_{2.5}$ (right panel) at all stations over the domain for all hours from February 7th to 14th 1998. Gray lines are 10:7, 1:1, 7:10 and 2:1, 1:1, 1:2 model-to-observation ratio lines in left and right panels, respectively.

Table A.3 Performance statistics for $PM_{2.5}$ mass, $PM_{2.5}$ SO_4, $PM_{2.5}$ NH_4, and $PM_{2.5}$ NO_3 concentrations at all available IMPROVE and GAViM stations over the AURAMS domain for all days from February 7th 00Z to 14th 00Z 1998. (see Table A.2 for definitions)

Species	n	R^2	σ_{mod}*	σ_{obs}**	$\sigma_{mod\text{-}obs}$***	RMSE	NME	MB	NMB	curve fitting equation
$PM_{2.5}$ mass	31	0.23	297	19	36	15.9	67.1	3.2	29.0	mod = 1.87 obs - 6.37
$PM_{2.5}$ SO_4	30	0.02	1.8	3.4	0.3	2.4	59.4	-1.1	-37.1	mod = 0.09 obs + 1.66
$PM_{2.5}$ NH_4	8	0.36	22	0.4	1.9	5.2	276.1	2.8	260.4	mod = 4.28 obs - 0.73
$PM_{2.5}$ NO_3	30	0.42	67	1.5	6.5	8.2	294.2	3.4	271.4	mod = 4.33 obs - 0.78

Legend: *variance of model data. **variance of observation data. ***covariance

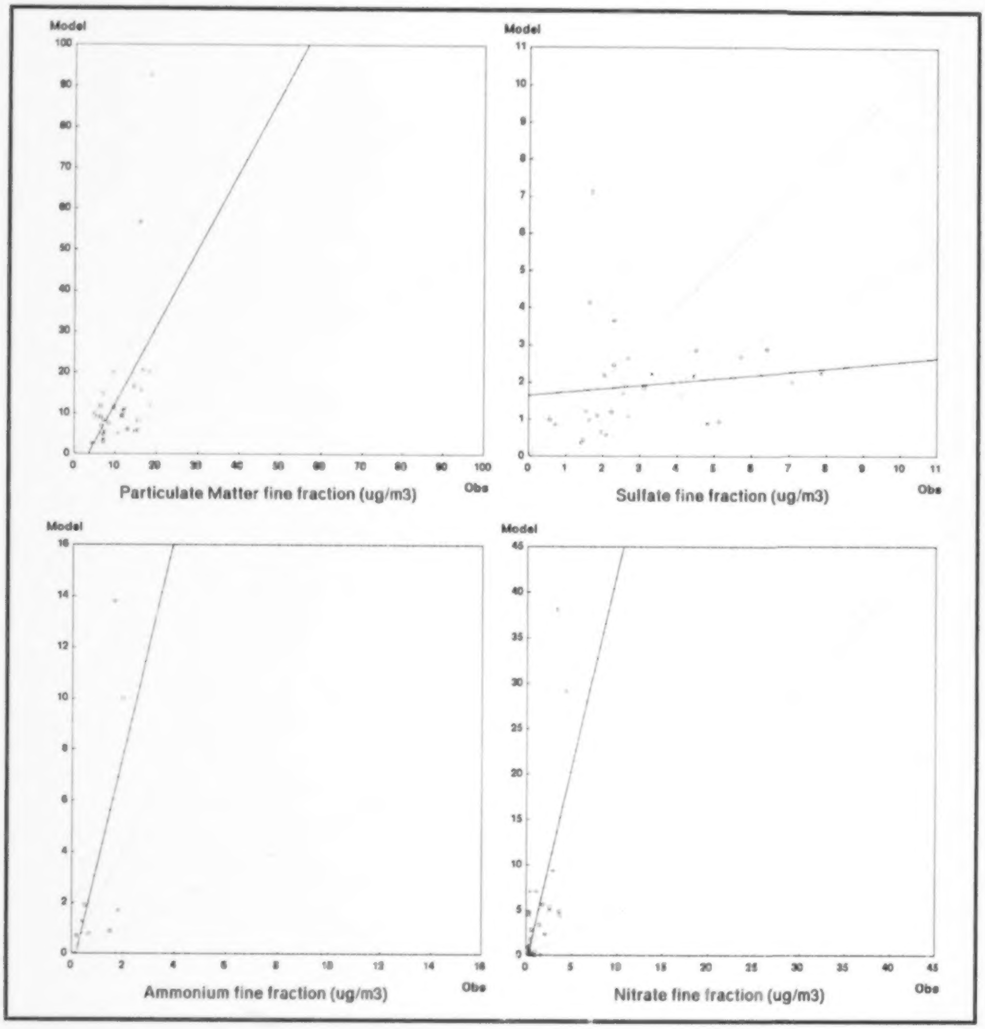

Figure A.5 Scatter plots of daily (a) $PM_{2.5}$ mass, (b) $PM_{2.5}$ $SO_4^=$, (c) $PM_{2.5}$ NH_4^+, and (d) $PM_{2.5}$ NO_3^- concentrations at all available IMPROVE and GAViM stations over the AURAMS domain for all days from February 7th 00Z to 14th 00Z 1998. Units are $\mu g/m^3$ at ambient conditions. The black line is a best-fit line and the gray lines are 2:1, 1:1 and 1:2 model-to-observation ratio lines.

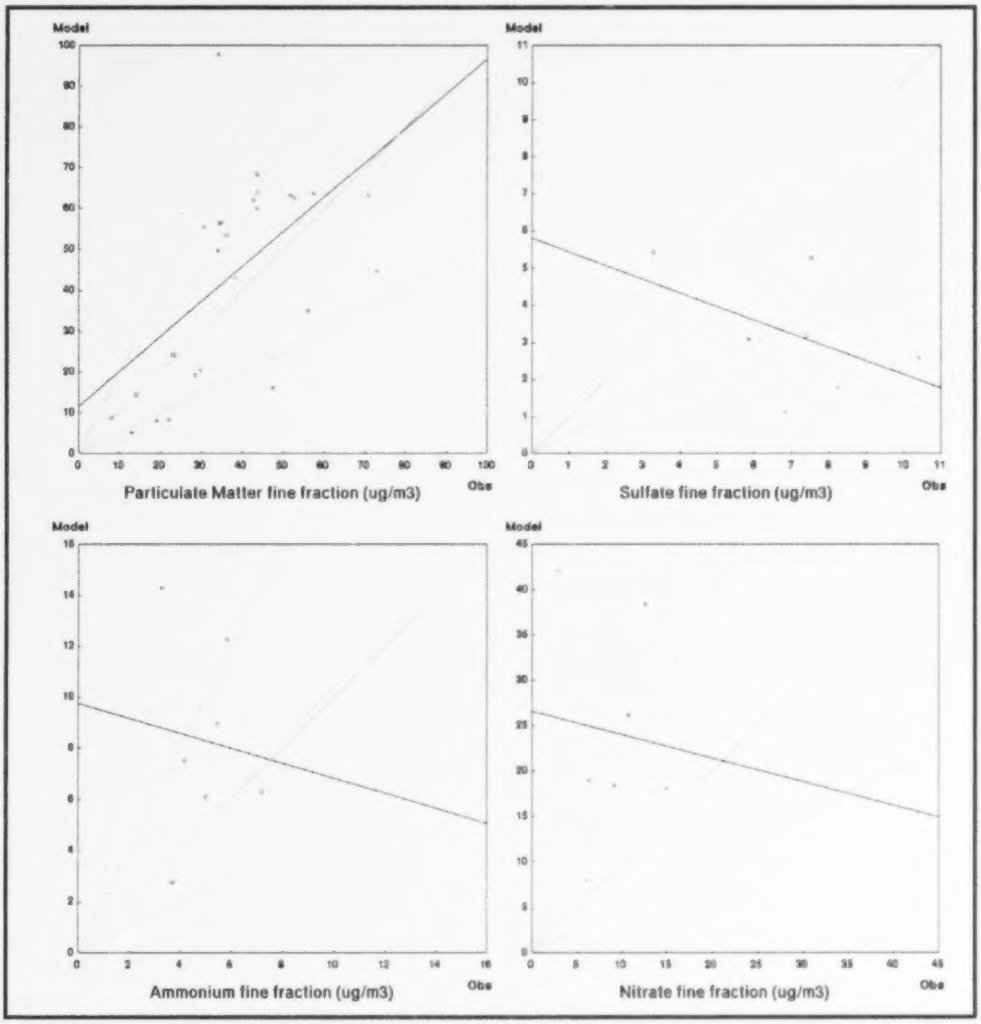

Figure A.6 - Same as Figure A.5 but for Canadian NAPS stations and µg/m³ at STP.

Table A.4 Performance statistics for $PM_{2.5}$ mass, $PM_{2.5}$ $SO_4^=$, $PM_{2.5}$ NH_4^+, and $PM_{2.5}$ NO_3^- concentrations at all available Canadian NAPS stations over the AURAMS domain for all days from February 7th 00Z to 14th 00Z 1998 (see Table A.2 for definitions)

Species	n	R^2	σ_{mod}*	σ_{obs}**	$\sigma_{mod\text{-}obs}$***	RMSE	NME	MB	NMB	curve fitting equation
$PM_{2.5}$ mass	27	0.33	563	252	215	20.5	43.3	6.0	16.0	mod = 0.85 obs + 11.62
$PM_{2.5}$ SO_4	7	0.24	2.3	4.1	-1.5	4.9	63.1	-3.9	-54.5	mod = -0.37 obs + 5.80
$PM_{2.5}$ NH_4	7	0.01	13	1.6	-0.5	5.2	78.4	3.6	67.9	mod = -0.29 obs + 9.76
$PM_{2.5}$ NO_3	7	0.01	126	15	-3.9	19.6	172.1	15.3	172.1	mod = -0.26 obs + 26.59

Legend: *variance of model data, **variance of observation data, ***covariance

A2.3 Model Evaluation for Summer 1995

Figure A.7 presents time series of modelled and observed ground-level ozone for two stations in the Windsor-Quebec City corridor for a ten-day period July 8^{th} to 17^{th}, 1995. The left panel is for a station in London, Ontario while the right panel is for a station at St-Anicet, Quebec, west of Montreal. This period includes both episodic and

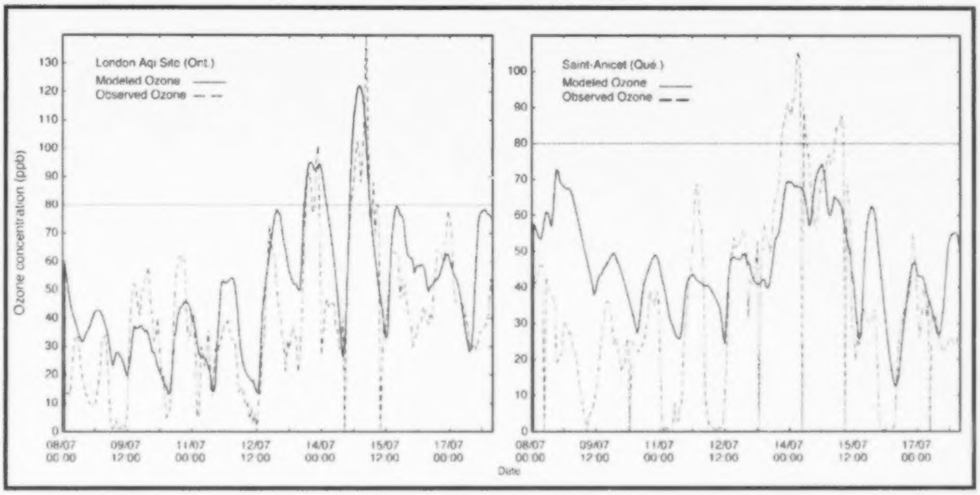

Figure A-7 - Time series of modelled and observed ozone for London, Ontario (left panel) and Saint-Anicet, Quebec (right panel) from July 8th to 16th 1995. Solid line: AURAMS prediction; dashed line: observations. All values in ppb.

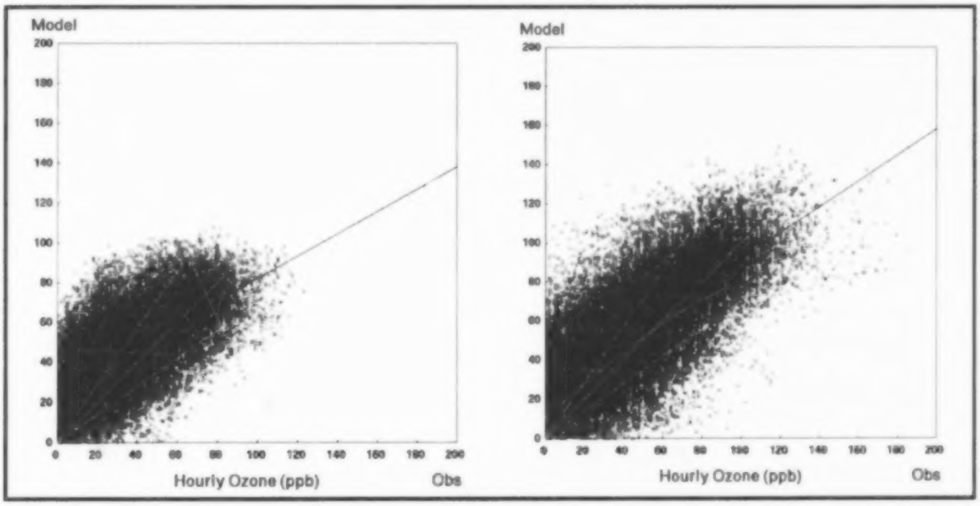

Figure A-8 - Scatter plots for ozone at all stations over the domain for all hours from July 8th to 11th 1995 (left panel) and from July 12th to 15th (right panel). Gray lines are 10:7, 1:1 and 7:10 model-to-observation ratio lines. All values in ppb.

Table A.5 Performance statistics for hourly ozone at all stations over the domain from July 8th to 11th and July 12th to 15th 1995. (see Table 2 for definitions)

Species	n	R^2	σ_{mod}*	σ_{obs}**	$\sigma_{mod\text{-}obs}$***	RMSE	NME	MB	NMB	curve fitting equation
Hourly O_3 (left)	40437	0.39	396	488	273	21.4	48.8	11.0	31.6	mod = 0.56 obs + 26.35
Hourly O_3 (right)	39913	0.50	745	849	561	23.8	40.3	9.9	21.1	mod = 0.66 obs + 25.91

Legend: *variance of model data, **variance of observation data, ***covariance

non-episodic conditions: ozone concentrations above 80 ppb were observed on July 13th and 14th at both stations. Both panels show that the ozone levels simulated by AURAMS during the worst days of the period (July 12th to 15th) are in better agreement with the observations than for the four preceding days. AURAMS over-predicts ozone at the beginning of the period but improves with time as the observed episode becomes more intense. This behaviour can also be seen in Figure A.8, which presents two scatter plots of modelled vs. observed ozone. The left panel covers the pre-episode period from July 7th to 11th while the right panel covers the period from July 12th to the 15th, the four days with the highest ozone concentrations. The two scatter plots are for all stations in the domain at all available hours. The slope of the best-fit line increases from 0.56 to 0.66 for the July 7-11 period vs. the July 12-15 period while the R^2 value between AURAMS-predicted and observed hourly ozone improves from 0.39 to 0.50. The complete set of performance statistics is provided in Table A.5. For the episode period, observed hourly ozone levels reach over 180 ppb and predicted levels reach about 150 ppb.

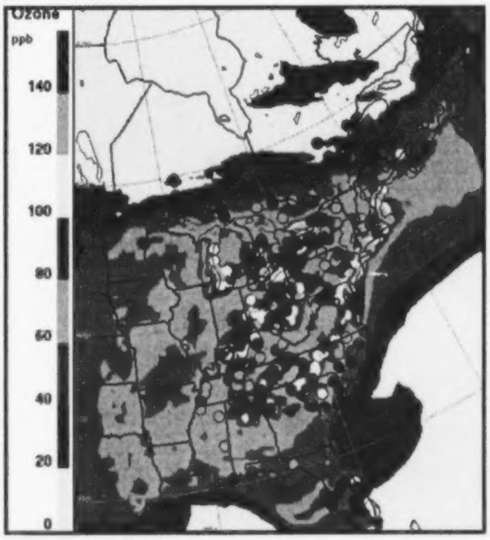

Figure A.9 - AURAMS simulated ground-level ozone for 2100 UTC (1700 EDT) on July 14th 1995. Observations valid for this hour are represented by the circles. Values are in ppb.

Figure A.9 shows an image of the AURAMS predicted ground-level ozone field for July 14th 1995 at 2100 UTC at the height of the episode with the observations for that time superimposed as colored circles at the measurement locations. In this figure, matching colours indicate good agreement with the measurements. There is generally good agreement between the model and the observations. Observed and modelled values are similar in the peak areas and we see the same patterns in the modelled field as in the observations. This figure is representative of the level of agreement between model and observations for the afternoon and early evening period. Figures A.7 and A.9 lead us to conclude that AURAMS reproduces the afternoon and evening portion of the diurnal cycle of ground-level ozone well but tends to over-predict during the night and morning hours.

Figures A.10 and A.11 show scatter plots comparing observed and predicted daily mass concentrations for $PM_{2.5}$ and its three inorganic chemical components for the eight-day period from July 8th to the 15th. As noted above, the number of measurements available for $PM_{2.5}$ comparisons is considerably less than that available for ozone, despite the fact that additional measurements

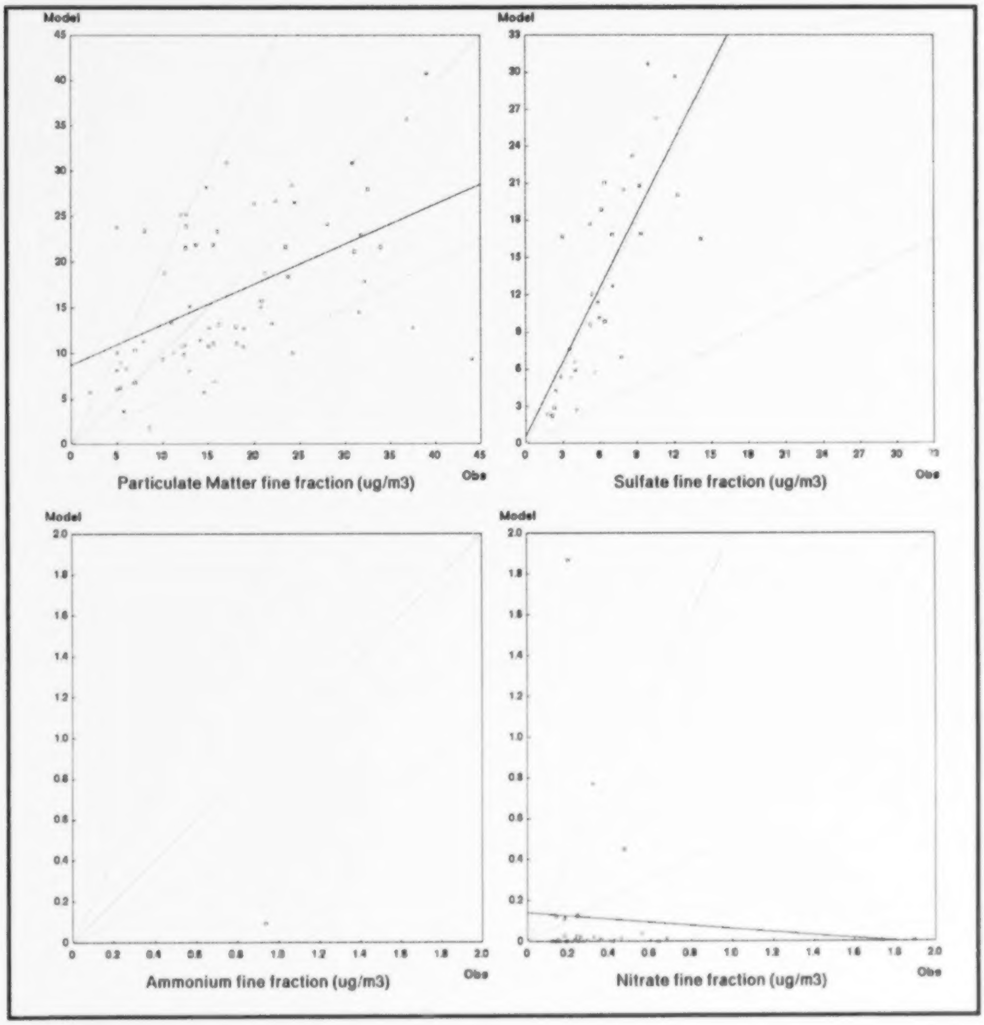

Figure A.10 - Scatterplots of daily (a) $PM_{2.5}$ mass, (b) $PM_{2.5}$ $SO_4^{=}$, (c) $PM_{2.5}$ NH_4^{+}, and (d) $PM_{2.5}$ NO_3^{-} concentrations at all available IMPROVE, GAViM and CAAMP stations over the AURAMS domain for all days from July 8th 00Z to July 16th 00Z, 1995. Units are μg/m^3 at ambient conditions. The black line is a best-fit line and the gray lines are 2:1, 1:1 and 1:2 model-to-observation ratio lines.

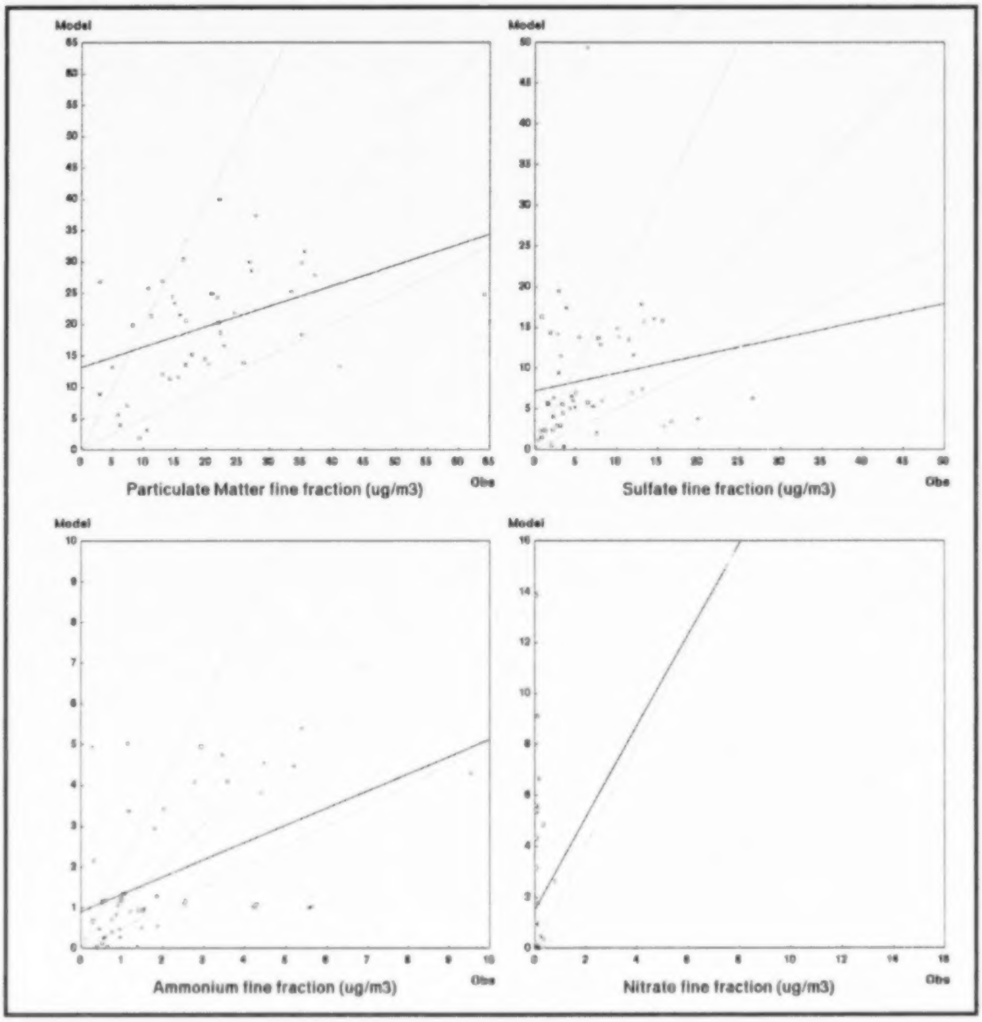

Figure A.11 - Same as Figure A.10 but for Canadian NAPS stations and μg/m³ at STP.

Table A.6 Performance statistics for $PM_{2.5}$ mass, $PM_{2.5}$ $SO_4^=$, $PM_{2.5}$ NH_4^+, and $PM_{2.5}$ NO_3^- concentrations at all available IMPROVE, GAViM and CAAMP stations over the AURAMS domain for all days from July 8th 00Z to 16th 00Z 1995. (see Table A.2 for definitions)

Species	n	R^2	σ_{mod}*	σ_{obs}**	$\sigma_{mod\text{-}obs}$***	RMSE	NME	MB	NMB	curve fitting equation
$PM_{2.5}$ mass	66	0.26	70	94	42	9.1	38.5	-1.0	-5.8	mod = 0.44 obs + 8.74
$PM_{2.5}$ SO_4	32	0.60	65	10	20	9.1	110.4	6.8	108.4	mod = 1.97 obs + 0.66
$PM_{2.5}$ NH_4	1	-	-	-	-	-	-	-	-	-
$PM_{2.5}$ NO_3	32	0.01	0.12	0.10	-0.01	0.5	105	-0.2	-65.6	mod = -0.08 obs + 0.14

Legend: *variance of model data, **variance of observation data, ***covariance

Table A.7 Performance statistics for $PM_{2.5}$ mass, $PM_{2.5}$ $SO_4^=$, $PM_{2.5}$ NH_4^+, and $PM_{2.5}$ NO_3^- concentrations at all available Canadian NAPS stations over the AURAMS domain for all days from July 8th 00Z to 16th 00Z 1995. (see Table A.2 for definitions)

Species	n	R^2	σ_{mod} *	σ_{obs} **	$\sigma_{mod\text{-}obs}$ ***	RMSE	NME	MB	NMB	curve fitting equation
$PM_{2.5}$ mass	42	0.19	80	141	46	11.4	41.8	-0.2	-0.9	mod = 0.33 obs + 13.17
$PM_{2.5}$ SO_4	51	0.02	62	33	6.9	9.2	85.2	2.1	31.2	mod = 0.21 obs + 7.28
$PM_{2.5}$ NH_4	51	0.24	2.7	3.6	1.5	1.8	59.5	-0.3	-13.1	mod = 0.42 obs + 0.91
$PM_{2.5}$ NO_3	39	0.01	9.2	0.02	0.03	3.4	1669	1.6	1622	mod = 1.80 obs + 1.53

Legend: *variance of model data, **variance of observation data, ***covariance

from the CAAMP network are available for this period. Model performance is similar to the winter case (cf. Figures A.5 and A.6), but in the summer AURAMS appears overall to over-predict SO_4 and under-predict NO_3, opposite behaviour to the winter case. Again, predictions of total $PM_{2.5}$ mass are not strongly biased.

The performance statistics corresponding to Figures A.10 and A.11 are provided in Tables A.6 and A.7. Although the agreement with NO_3^- measurements in the summer is poor, it should be noted that the NO_3^- measurements have a higher degree of uncertainty than those for particulate $SO_4^=$ and NH_4^+ due to the volatility of particulate NO_3^-. NAPS dichotomous NO_3^-data for 1995 in particular, are known to be biased low compare to other NO_3^- sampling methods by as much as 50% due to volatility problems (Brook and Dann, 1999), which may account for some of the discrepancies in Figure A.11d.

Finally, Figure A.12 compares a satellite visible image taken at 2308 UTC on July 10^{th} 1995 with the AURAMS predicted $PM_{2.5}$ concentration field at 15 m height at 2300 UTC. The zones highlighted on the satellite image correspond to locations where haze due to near-surface particles in suspension is visible. Qualitatively, we can see that the model reproduces the general patterns of the satellite image. Comparison to earlier and subsequent satellite images (not shown), display the same kind of general agreement throughout the episode.

A2.4 Summary of AURAMS performance evaluation

The evaluation presented above showed that AURAMS is able to simulate the main features of ozone and PM mass air concentrations under very different meteorological conditions. Generally AURAMS performed better for the winter case, although the increased amount of observed data for the winter case may introduce some bias.

During the summer case, AURAMS consistently over-predicted ozone concentrations in the lower range while under-predicting the peak values, a behaviour that is consistent with other oxidant models behavior during summer episodes (e.g. Byun and Dennis, 1995; MSC, 1997). Interestingly, AURAMS did not show the same tendency for the winter season when all observed values are in the same 0 to 50 ppbv range. This difference could be due to a combined effect of AURAMS spatial resolution (42 km) and a decrease in the regional representativeness of the measurement sites at night, during summertime events, when the stability close to the surface is strong. Further investigation is however needed to confirm this hypothesis.

AURAMS is able to reproduce the PM mass within a factor of two for both the winter and the summer case considered, but over-predicts particulate $SO_4^=$ and under-predicts $NO_3^-$and NH_4^+ in the summer case while exhibiting the opposite behaviour for the winter case. Based on the present comparisons with observations, AURAMS produces reasonable simulations of particulate $SO_4^=$ and NH_4^+, but the level of agreement for particulate NO_3^- is less satisfactory. As explained in the previous section, however, NO_3^- measurements also have a much higher degree of uncertainty, especially for periods as far back as 1995. However, AURAMS's ability to simulate the concentrations of the various inorganic PM components is also similar to what has been reported for other aerosol and oxidant models (e.g. Mebust et al., 2003), including the lower performance skill for particulate NO_3^-. Finally, it should be kept in mind that the evaluation of AURAMS was focused on two relatively short periods, therefore little to no averaging was done when comparing with observations.

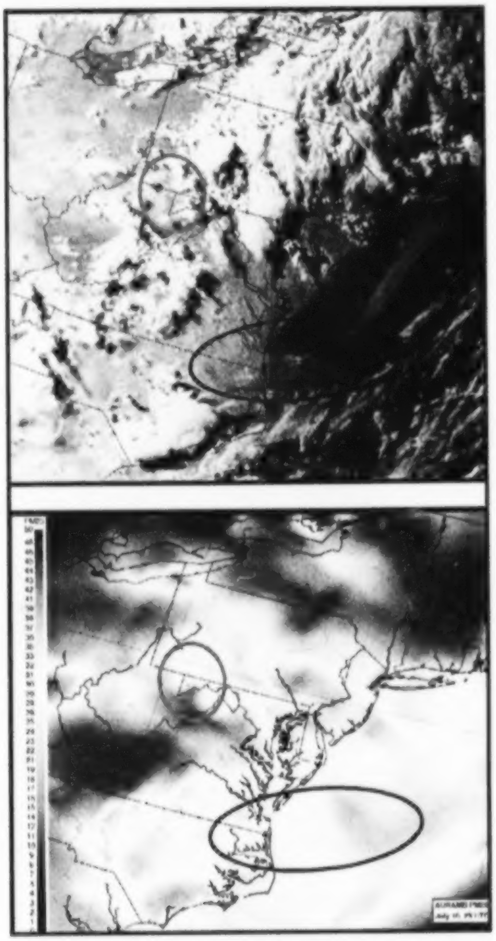

Figure A.12 - Comparison of AURAMS $PM_{2.5}$ output with satellite imagery. Top: Visible satellite image valid at 2308 UTC on July 10th 1995. Bottom: AURAMS $PM_{2.5}$ output in the lower levels valid at 2300 UTC.

The Subcommittee on Scientific Co-operation (Subcommittee 2), of the Canada-US Air Quality Committee deals with activities of scientific and technical cooperation under Annex II of the Air Quality Agreement (1991). The members of the Subcommittee are as follows:

CANADA

- Keith Puckett, Environment Canada, Co-Chair
  - Richard Bennett, B.C. Ministry of Water, Land and Air Protection
  - Lawrence Cheng, Alberta Environment
  - Fred Conway, Environment Canada
  - Chris Daly, Nova Scotia Environment and Labour
  - Tom Dann, Environment Canada
  - Dennis Herod, Environment Canada
  - Harry Hirvonen, Canadian Forest Service
  - Michel Jean, Environment Canada
  - Dean Jeffries, Environment Canada
  - Richard Leduc, Ministère de l'environnement du Québec
  - Ling Liu, Health Canada
  - Janet Mullins, Environment Canada
  - Carmelita Olivotto, Environment Canada
  - Neville Reid, Ontario Ministry of Environment

UNITED STATES

- William Russo, USEPA, Co-Chair
  - Robbins Church, USEPA
  - Robin Dennis, USEPA
  - Robert Devlin, USEPA
  - Neil Frank, USEPA
  - Rick Haeuber, USEPA
  - Robert Kotchenruther, USEPA
  - Rich Poirot, Vermont Department of Environmental Conservation
  - Mark Scruggs, National Park Service
  - Mary Striegel, National Center for Preservation Technology and Training
  - Joe Tikvart, USEPA
  - Borys Tkacz, USDA Forest Service
  - Jeff West, USEPA
  - William Wilson, USEPA